UNIVERSITY
OF MICHIGAN
JAN 25 1955
PHYSICS
LIBRARY

THE JOURNAL OF CHEMICAL PHYSICS

VOLUME 22 NUMBER 12

DECEMBER, 1954

Published by the

AMERICAN INSTITUTE OF PHYSICS

INCORPORATED

LANCASTER, PA., AND NEW YORK, N. Y.

THE JOURNAL OF CHEMICAL PHYSICS

BOARD OF EDITORS

CLYDE A. HUTCHISON, JR., *Editor*

Associate Editors

Term ending December 31, 1954	*Term ending December 31, 1955*	*Term ending December 31, 1956*
THEODORE H. BERLIN	RICHARD M. BADGER	BRYCE L. CRAWFORD, JR.
B. P. DAILEY	DAVID M. DENNISON	H. S. GUTOWSKY
HARALD H. NIELSEN	JOHN G. KIRKWOOD	WILLIAM N. LIPSCOMB
HARRISON SHULL	G. B. KISTIAKOWSKY	ELLIOTT W. MONTROLL
CHARLES P. SMYTH	A. W. LAWSON	GEORGE SCATCHARD
FRANK H. WESTHEIMER	S. S. PENNER	J. W. STOUT
	ROBERT L. SCOTT	GREGORY H. WANNIER

THE JOURNAL OF CHEMICAL PHYSICS is published monthly by the American Institute of Physics. Its purpose is to bridge a gap between journals of physics and journals of chemistry. The artificial boundary between physics and chemistry has now been in actual fact completely eliminated, and a large and active group is engaged in research which is as much the one as the other. It is to this group that the Journal is rendering its principal service and makes its greatest appeal, both as a prompt and efficient medium for publication of research and as a convenient and carefully edited assemblage of pertinent information.

Information for Contributors

Send **manuscripts** to Clyde A. Hutchison, Jr., Editor, *The Journal of Chemical Physics*, Institute for Nuclear Studies, University of Chicago, Chicago 37, Illinois. Unless otherwise stated submission of a manuscript is a representation that it has been neither copyrighted, published, nor submitted for publication elsewhere. Textual material (abstract, body of the paper, tabular material, references, and figure captions) must be in English, typewritten (except mathematical expressions) double spaced with wide margins on a durable, white paper, preferably letter size. The original copy, not the carbon, should be submitted. For general style, spellings, abbreviations, and form, consult recent issues of this journal. The authors' institutions are requested to pay a **publication charge** of $15.00 per page which, if honored, entitles them to 100 free reprints. Instructions will be sent with galley proofs.

An **abstract** must accompany each article. It should be adequate as an index and as a summary.

All but the simplest **mathematical expressions** should be carefully printed in by hand. Be sure to distinguish between capital and small letters. Indicate clearly superscripts and subscripts by inverted carets and carets, respectively. Avoid complicated superscripts and subscripts. Avoid repetition of a complicated expression by representing it by a symbol. Identify in the margin Greek letters and unusual symbols. Use fractional exponents instead of root signs. Use the solidus (/) for fractions wherever its use will save vertical space.

References should appear as footnotes, numbered consecutively. Literature citations of technical journals should be in the form indicated in the Style Manual of the American Institute of Physics and Chemical Abstracts (Chem. Abstracts 45, I-CCLV (1951)).

Tables may be typewritten on sheets separate from the running text. Each table must have a caption which will make the data in the table intelligible without reference to the text. Avoid complicated column headings.

Wherever possible **figures** should be planned for the width of a column (3 in.). A convenient reduction ratio is about 2:1 or 3:1. Lettering should be large enough on the original that when reduced it shall not be less than about $\frac{1}{16}$ in. (~1.5 mm). Line drawings must be in *india ink* on white paper or tracing cloth. Coordinate paper is not desirable but if used must be blue lined and the coordinate lines which are to show must be inked over. Pictures of apparatus, etc., should be glossy prints and should have maximum black and white contrast. Identify each original drawing or photograph on the back with the author's name and the figure number. Figures should be numbered consecutively. Captions should be typed on a separate sheet of paper.

A limited number of **alterations** in proof are unavoidable, but the cost of making extensive alterations after the article has been set in type will be charged to the author.

Proof and all correspondence concerning papers in the process of publication should be addressed to the Publication Manager, American Institute of Physics, 57 East 55 Street, New York 22, New York.

Subscription Price

	U. S. and Canada	Elsewhere
To members of the American Institute of Physics and Affiliated Societies	$12.00	$13.00
To all others	15.00	16.00

Back Number Prices

Yearly rate when complete year is available: $17.00.
Single copies: $1.50 each.

Subscriptions, renewals, and orders for single copies should be addressed to the American Institute of Physics, 57 East 55 Street, New York 22, New York.

Changes of address should be sent to the American Institute of Physics.

The Journal of Chemical Physics is published monthly at Prince and Lemon Streets, Lancaster, Pennsylvania.

Entered as second-class matter December 30, 1932, at the Post Office at Lancaster, Pa., under the Act of August 24, 1912. Acceptance for mailing at special rate of postage, provided for in paragraph (d-2), section 34.40, P. L. & R. of 1948, authorized February 5, 1933.

Copyright 1955 by the American Institute of Physics

THE JOURNAL
OF
CHEMICAL PHYSICS

VOLUME 22, NUMBER 12 DECEMBER, 1954

Force Constants for F_2CO and Thermodynamic Properties for F_2CO and FClCO

R. J. LOVELL, C. V. STEPHENSON,* AND E. A. JONES
Department of Physics and Astronomy, Vanderbilt University, Nashville, Tennessee
(Received June 2, 1954)

A set of force constants for F_2CO has been calculated using the observed fundamental frequencies and a potential function consisting of valence force interaction terms and an additional term involving an interaction between the oxygen and fluorine atoms. The large values obtained for the interaction constant and the angle deformation constants were related to interaction forces between the terminal atoms.
Also included in this paper are calculations of the thermodynamic properties of F_2CO and FClCO.

INTRODUCTION

RECENTLY there have been several investigations of the molecules carbonyl fluoride (F_2CO) and carbonyl chlorofluoride (FClCO). Included for both molecules are the infrared spectra of the gases from 2–15 microns and the Raman spectra of the liquids,[1] while in addition for F_2CO there are microwave studies,[2] electron diffraction measurements,[3] and grating studies.[4] There are in the literature, however, no calculations of force constants or of thermodynamic properties from either spectroscopic or calorimetric data. The general interest in the structure and properties of fluorine-bearing molecules and the scarcity of thermodynamic data on these molecules has prompted this effort to supply these data.

Both molecules are planar tetratomic with F_2CO belonging to the point group C_{2v} and FClCO to C_s. There are six nondegenerate vibrations for each molecule: $3\,A_1$, $2\,B_1$, and $1\,B_2$ for F_2CO and $5\,A'$ and $1\,A''$ for FClCO. The fundamental frequencies are compiled in Table I and the molecules are diagrammed in Fig. 1.

Since there are no microwave or electron diffraction data available for FClCO, the values given in Fig. 1 for the molecular parameters have been chosen from consideration of corresponding values for F_2CO[5] and Cl_2CO.[6]

NORMAL COORDINATE TREATMENT

In order to utilize the simplification of calculation for molecules with symmetry provided by group theory an orthonormal set of symmetry coordinates was formed from the internal coordinates. The internal coordinates are the changes in bond lengths and interbond angles. The symmetry coordinates are

$$\begin{aligned} A_1:&\quad R_1=(1/2)^{\frac{1}{2}}(\Delta d_1+\Delta d_2),\\ &\quad R_2=\Delta d_3,\\ &\quad R_3=(1/6)^{\frac{1}{2}}(2\Delta\gamma-\Delta\beta_1-\Delta\beta_2);\\ B_1:&\quad R_4=(1/2)^{\frac{1}{2}}(\Delta d_1-\Delta d_2),\\ &\quad R_5=(1/2)^{\frac{1}{2}}(\Delta\beta_1-\Delta\beta_2),\\ B_2:&\quad R_6=\Delta\delta. \end{aligned}$$

Redundant coordinate:

$$R_7=(1/3)^{\frac{1}{2}}(\Delta\gamma+\Delta\beta_1+\Delta\beta_2)\equiv 0.$$

It has been a matter of general experience that fluorine-bearing molecules cannot be described by ordinary valence or central force type potential functions. In order to describe the F_2CO molecule more realistically and at the same time keep within the number of independent force constants, potential functions were made up of terms containing the most important force constants, the valence constants, and

* Present address, Sandia Corporation, Albuquerque, New Mexico.
[1] Nielsen, Burke, Woltz, and Jones, J. Chem. Phys. **20**, 596 (1952).
[2] Smith, Tidwell, Williams, and Senatore, Phys. Rev. **83**, 485(A) (1951).
[3] Private communication from Dr. Robert Livingston, Chemistry Department, Purdue University.
[4] A. H. Nielsen, J. Chem. Phys. **19**, 98 (1951).
[5] Private communication from D. F. Smith, K-25 Laboratories, Oak Ridge, Tennessee.
[6] P. W. Allen and L. E. Sutton, Acta Cryst. **3**, 47 (1950).

other terms representing possible important interactions taken from the general potential function. It was not found possible to describe F_2CO by such a potential function. Direct interactions of the central force type between the terminal atoms were then investigated. It was found that a potential function consisting of the ordinary valence terms and one additional term representing a central force type interaction between the oxygen and fluorine atoms best described F_2CO. This interaction term has the effect of approximating several of the ordinary interaction terms, that of the C−F bonds and of the C−F bond with the F−C−F and F−C−O interbond angles. This potential function is

$$2V=k_1(\Delta d_1^2+\Delta d_2^2)+k_3\Delta d_3^2+k_\gamma d_1^2\Delta\gamma^2 +k_\beta d_1^2(\Delta\beta_1^2+\Delta\beta_2^2)+kD_{FO}^2+k_\delta d_1^2\Delta\delta^2,$$

where

$$D_{FO}=\frac{\Delta d_1(d_1-d_3\cos\beta)+\Delta d_3(d_3-d_1\cos\beta)+d_1d_3\sin\beta\Delta\beta}{(d_1^2+d_3^2-2d_1d_3\cos\beta)^{\frac{1}{2}}}$$

is the change in the O−F distance. Here k_1 and k_3 are the C−F and C−O stretching constants; k_β and k_γ are the O−C−F and F−C−F angle deformation constants; k_δ is the out-of-planar angle deformation constant; and k is the interaction constant.

From the potential energy matrix and the matrix of the coefficients of the symmetry coordinates one obtains the following F matrix elements:

A_1: $F_{11}=k_1+\dfrac{(d_1-d_3\cos\beta)^2}{d_{FO}^2}k,$

$F_{12}=\dfrac{2(2)^{\frac{1}{2}}(d_1-d_3\cos\beta)(d_3-d_1\cos\beta)}{d_{FO}^2}k,$

$F_{22}=k_3+\dfrac{(d_3-d_1\cos\beta)^2}{d_{FO}^2}k,$

$F_{13}=\dfrac{(-2/3^{\frac{1}{2}})d_1d_3(d_1-d_3\cos\beta)\sin\beta}{d_{FO}^2}k,$

$F_{23}=\dfrac{(-4/6^{\frac{1}{2}})d_1d_3(d_3-d_1\cos\beta)\sin\beta}{d_{FO}^2}k,$

$F_{33}=(2/3)d_1^2k_\gamma+1/3\left[d_1^2k_\beta+\dfrac{d_1^2d_3^2\sin^2\beta}{d_{FO}^2}k\right];$

B_1: $F_{44}=k_1+\dfrac{(d_1-d_3\cos\beta)^2}{d_{FO}^2}k,$

$F_{45}=\dfrac{2d_1d_3(d_1-d_3\cos\beta)\sin\beta}{d_{FO}^2}k,$

$F_{55}=d_1^2k_\beta+\dfrac{d_1^2d_3^2\sin^2\beta}{d_{FO}^2}k,$

B_2: $F_{66}=(d_1^2k_\delta),$

where $d_{FO}^2=(d_1^2+d_3^2-2d_1d_3\cos\beta)$.

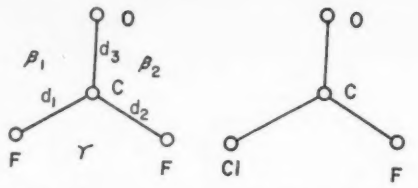

FIG. 1. Molecular parameters for F_2CO and FClCO.

d_1=C−F=1.32±0.02 A
d_3=C−O=1.17±0.02 A
$\gamma=\angle$F−C−F=112.5±0.6°

C−F=1.32 A
C−Cl=1.68 A
C−O=1.28 A
$\angle$Cl−C−O=122°
$\angle$F−C−O=122°

The inverse kinetic energy matrix, the G matrix, formed by Wilson's method, has these elements[7]

A_1: $G_{11}=\mu_F+(1+\cos\gamma)/\mu_C,$

$G_{12}=2^{\frac{1}{2}}\mu_C\cos\beta,$

$G_{22}=\mu_C+\mu_O,$

$G_{13}=-3^{\frac{1}{2}}\mu_C\sin\gamma/d_1,$

$G_{23}=6^{\frac{1}{2}}\mu_C\sin\beta/d_1,$

$G_{33}=3[\mu_F+(1-\cos\gamma)\mu_C]/d_1^2;$

B_1: $G_{44}=\mu_F+(1-\cos\gamma)\mu_C,$

$G_{45}=-2\mu_C(\sin\beta/d_3-\sin\beta\cos\beta/d_1),$

$G_{55}=\mu_F/d_1^2+2\mu_O/d_3^2 +2\mu_C(1/d_3^2-2\cos\beta/d_1d_3+\cos^2\beta/d_1^2);$

B_2: $G_{66}=(\mu_F/2)\cos^2(\gamma/2)d_1^2+\mu_O/d_3^2 +\mu_C\dfrac{[d_3+d_1\cos(\gamma/2)]^2}{d_3^2d_1^2\cos^2(\gamma/2)}.$

Substitution of the vibrational frequencies and molecular parameters into the secular determinant and subsequent expansion leads to the secular equations for F_2CO. The solution of the secular equations gives the set of force constants for carbonyl fluoride tabulated in Table II.[8] The force constants were reintroduced

TABLE I. The fundamental frequencies for F_2CO and FClCO (gaseous state) (see reference 1).

Assignment	F_2CO	FClCO
ν_1	965 cm^{-1}	776 cm^{-1}
ν_2	1928[a]	1868[a]
ν_3	626	501
ν_4	1249	1095
ν_5	584	415
ν_6	774	667

[a] Unperturbed values.

[7] E. Bright Wilson, Jr., J. Chem. Phys. 9, 76 (1941).

[8] The expression of the force constants to six significant figures was necessary in order to obtain the desired agreement between observed and calculated frequencies and, of course, does not imply that this degree of accuracy has been obtained for these constants.

TABLE II. Force constants for carbonyl fluoride.

Constant	Value	Constant	Value
k_1	4.83834×10^5 dynes/cm	k_β	1.31042×10^5 dynes/cm
k_2	14.38706×10^5	k	5.25724×10^5
k_γ	2.86763×10^5	k_δ	0.33383×10^5

into the secular equations and the frequencies calculated. The calculated and experimental frequencies agreed to within one-tenth of one percent.

The large value of the interaction constant k, even larger than the carbon-fluorine stretching constant, and the relatively large values of the angle deformation constants would seem to confirm the presence of large interaction forces between the oxygen and fluorine atoms.

THERMODYNAMIC PROPERTIES

The heat capacity, enthalpy, free energy, and entropy functions were computed at 273.16°K, 298.16°K, and at 100°K intervals from 300°K to 1500°K. The calculations were made using the rigid rotator, harmonic oscillator assumptions. Translational and rotational contributions were determined according to the equations from Mayer and Mayer,[9] and vibrational contributions were calculated using the tables in Taylor and Glasstone.[10] The physical constants were those of Birge.[11] The atomic weights of carbon, oxygen, fluorine, and chlorine were taken as 12.010, 16.000, 19.000, and 35.457, respectively.

TABLE III. Thermodynamic functions of F_2CO.

T°K	C_p^0 cal/deg mole	$\frac{H^0-H_0^0}{T}$ cal/deg mole	$\frac{-F^0-E_0^0}{T}$ cal/deg mole	S^0 cal/deg mole
273.16	10.79	8.72	52.18	60.90
298.16	11.29	8.91	52.91	61.82
300	11.33	8.93	52.96	61.89
400	13.08	9.75	55.65	65.40
500	14.45	10.56	57.90	68.46
600	15.50	11.31	59.90	71.21
700	16.29	11.96	61.70	73.66
800	16.91	12.55	63.33	75.88
900	17.39	13.05	64.82	77.87
1000	17.78	13.52	66.24	79.76
1100	18.08	13.91	67.55	81.46
1200	18.32	14.27	68.75	83.02
1300	18.53	14.59	69.92	84.51
1400	18.68	14.87	71.01	85.88
1500	18.83	15.14	72.04	87.18

F_2CO

The moments of inertia of F_2CO have been found from the microwave spectrum by Smith and reported by Nielsen[4] to be $I_a=69.98\times10^{-40}$ g cm², $I_b=71.70\times10^{-40}$ g cm², and $I_c=141.68\times10^{-40}$ g cm². The fundamental frequencies used are listed in Table I. Since the molecule belongs to the point group C_{2v}, it has a symmetry number $\sigma=2$. The values C_p^0, $(H^0-H_0^0)/T$, $-(F^0-E_0^0)/T$, and S^0 for F_2CO are listed in Table III. Electronic and nuclear spin contributions have been neglected and the pressure was assumed to be one atmosphere.

TABLE IV. Thermodynamic functions of FClCO.

T°K	C_p^0 cal/deg mole	$\frac{H^0-H_0^0}{T}$ cal/deg mole	$\frac{-F^0-E_0^0}{T}$ cal/deg mole	S^0 cal/deg mole
273.16	12.03	9.29	55.81	65.10
298.16	12.53	9.54	56.64	66.18
300	12.56	9.56	56.70	66.26
400	14.20	10.53	59.57	70.10
500	15.39	11.39	62.02	73.41
600	16.27	12.13	64.17	76.30
700	16.94	12.77	66.09	78.86
800	17.45	13.33	67.85	81.18
900	17.84	13.86	69.42	83.22
1000	18.15	14.21	70.87	85.08
1100	18.40	14.58	72.25	86.83
1200	18.61	14.92	73.53	88.45
1300	18.77	15.21	74.74	89.95
1400	18.91	15.48	75.91	91.39
1500	19.02	15.71	76.98	92.69

FClCO

With the molecular parameters given in Fig. 1 the principal moments of inertia for FClCO become $I_a=74.80\times10^{-40}$ g cm², $I_b=160.08\times10^{-40}$ g cm², and $I_c=233.1\times10^{-40}$ g cm². The fundamental frequencies used are listed in Table I. Since the molecule belongs to the point group C_s, it has a symmetry number $\sigma=1$. The values of the thermodynamic functions of FClCO are given in Table IV. Again electronic and nuclear spin contributions were neglected and the pressure was assumed to be one atmosphere.

[9] J. E. Mayer and M. G. Mayer, *Statistical Mechanics* (John Wiley and Sons, Inc., New York, 1940).

[10] M. S. Taylor and S. Glasstone, *Treatise on Physical Chemistry, I, Atomistics and Thermodynamics* (D. Van Nostrand Company, Inc., New York, 1942).

[11] R. T. Birge, Revs. Modern Phys. **13**, 233 (1941).

THE JOURNAL OF CHEMICAL PHYSICS VOLUME 22, NUMBER 12 DECEMBER, 1954

Sedimentation Potential and Velocity of Solid Spherical Particles

F. Booth
Wheatstone Laboratory, King's College, London, England
(Received April 10, 1951)

The electrical effects accompanying the steady fall of solid charged spherical particles under gravity in an electrolyte are examined theoretically. For a single particle falling in an infinite electrolyte, it is shown that, owing to fluid flow round the particle, the double layer field is modified. The effect in the double layer region is complicated, but outside this region a field is set up of the same form as that which would arise from a dipole fixed at the center of the particle with its axis vertical. A general expression is given for this dipole field in the case of nonconducting particles. The calculations extend previous work in that no restriction on the relative dimensions of the particle size and the double-layer thickness is imposed.

It is shown that the interaction between the charge on the particle and the modified field alters the sedimentation velocity of the particle. The calculations show that in practical cases the effect might, in favorable circumstances, reduce the velocity by a few percent.

The analysis is extended to suspensions containing a large number of particles uniformly distributed.

1. INTRODUCTION

IN the following paper the electrokinetic effect known as the sedimentation potential and also the sedimentation velocity of charged particles in electrolytes will be examined theoretically. The sedimentation field effect was discovered many years ago by Dorn,[1] and is sometimes known by his name. He observed that a vertical electric field developed in a suspension of glass beads in water when they were allowed to settle. Smoluchowski[2] gave the first theoretical estimate of the magnitude of the field. For a suspension of solid nonconducting spheres of radius a, immersed in an electrolyte of conductivity σ, dielectric constant ϵ, and with coefficient of viscosity η, he deduced that the sedimentation field should be

$$E=\epsilon\zeta g\Delta na^3/3\sigma\eta. \tag{1.1}$$

n denotes the number of particles per unit volume of suspension, ζ their zeta potential, Δ the difference in density between electrolyte and solid, and g is the usual acceleration of gravity. The formula applies only to the case where the double-layer thickness is small compared with the radius of the particles. More recently Hermans[3] has obtained the formula

$$E=\frac{7\epsilon\zeta g\Delta na^3(\sum_{i=1}^{s} n_i z_i^2\omega_i^{-1})}{36\eta(\sum_{i=1}^{s} n_i e z_i^2)^2}. \tag{1.2}$$

Here n_i, z_i, and ω_i refer to the s separate ionic species in the electrolyte. z_i denotes the valency of the ions of type i and ω_i their mobility; $(-e)$ is the electronic charge. n_i is the concentration of ions of species i at a point in the suspension sufficiently remote from the particles to be outside their ionic atmospheres. The other symbols of Eq. (1.2) have the same significance as in Eq. (1.1). If all of the ionic mobilities, ω_i, are set equal to one another, Eq. (1.2) reduces to Eq. (1.1) apart from the multiplying factor 7/12.

The sedimentation field has been studied experimentally by a considerable number of investigators. It seems difficult to obtain reliable results; for further details papers by Bull,[4] Quist and Washburn,[5] Rutgers,[6] and Elton[7] may be consulted.

Smoluchowski[2] also pointed out the existence of a closely related effect, namely the reduction of the sedimentation rate by the sedimentation field. Suppose we have a single spherical particle falling steadily in a very large volume of an electrolyte of uniform composition. Then if U_0 denotes the steady rate of fall when the surface of the particle is uncharged and U the steady rate when the particle carries a uniform surface charge so that it has a zeta potential ζ, U_0 and U are connected by the equation

$$U_0=U\left[1+\frac{1}{\eta\sigma}\left(\frac{\epsilon\zeta}{4\pi a}\right)^2\right]. \tag{1.3}$$

For Eq. (1.3) to apply the radius must be large compared with the double-layer thickness. Tiselius[8] tested this relation experimentally and found agreement as to order of magnitude.

In the following sections of the paper we shall investigate both effects in more detail than has been given hitherto; in particular we shall not limit the analysis to particles with a double-layer thickness which is negligible compared with the particle radius. The next section deals with the steady fall of a *single* charged particle through an infinite electrolyte. To determine the potential distribution in the neighborhood of the particle it is necessary to make a number of assumptions

[1] E. Dorn, Ann. Physik **3**, 20 (1878).
[2] M. v. Smoluchowski, *Graetz Handbuch der Elektrizität und des Magnetismus* (Leipzig, 1921), vol. II, p. 385.
[3] J. J. Hermans, Phil. Mag. (7) **26**, 650 (1935).
[4] H. B. Bull, J. Phys. Chem. **33**, 656 (1929); **38**, 401 (1934).
[5] J. D. Quist and E. R. Washburn, J. Am. Chem. Soc. **62**, 3169 (1940).
[6] A. J. Rutgers, Nature **157**, 74 (1946).
[7] G. A. H. Elton, Proc. Roy. Soc. (London) **A197**, 58 (1949).
[8] A. Tiselius, Kolloid-Z. **59**, 306 (1932).

about the conditions near the solid-liquid interface. We shall make exactly the same assumptions as in a previous paper on a closely related effect namely electrophoresis.[9] These are briefly, incompressibility of the electrolyte and uniformity of its dielectric constant ϵ, coefficient of viscosity η and ionic mobilities ω_i in the immediate neighborhood of the surface of the solid, no surface conduction, no variation in the surface charge density and no appreciable conduction through the body of the particle. With these assumptions it is found that, except for a region very near to the surface, the potential in the electrolyte is equivalent to that of a dipole at the center of the particle with its axis vertical. The effective dipole moment, μ may be expressed in the form of a power series in Q, where Qe is the total charge on the particle, or, alternatively as a power series in the zeta potential of the surface.

$$\mu=\sum_{\nu=1}^{\infty} a_\nu Q^\nu=\sum_{\nu=1}^{\infty} b_\nu(e\zeta/\mathbf{k}T)^\nu. \tag{1.4}$$

The coefficients a_ν and b_ν are very complicated functions involving the concentrations and mobilities of the ions present in the electrolyte and also the size of the particle. To solve our problem completely it would of course be necessary to find general formulas for both sets of coefficients and examine the limits of convergence of the series. The analysis to be given in the next section outlines a completely general procedure for calculating the coefficients in principle, but owing to the rapid increase in mathematical complexity as ν increases, it is not feasible to find more than the first few terms of either series explicitly, and quite impossible to arrive at general formulas. We shall, in fact, only determine a_1, a_2, b_1, and b_2 explicitly. This means that our results will only be of practical use for values of Q or ζ sufficiently small for the sum of all of the terms beyond the second of both series to be negligible compared with the sum of the first pair. It is obviously difficult to fix precisely the limitations that this imposes on Q or ζ. This question is discussed in some detail however and various criteria proposed. It will be demonstrated that the results have quite a wide range of practical use, although the series of Eq. (1.4) have not been carried very far.

The dipole field, which arises from the deviation of the ionic concentrations from their equilibrium values, modifies the sedimentation velocity in two ways. First, there is an additional force on the sphere due to the direct electrostatic interaction between the free ions and the surface charge. Secondly, the flow round the particle is modified, and this in turn alters the force on it caused by the surface stresses. The two effects work in opposite directions and the net result is a small reduction of the sedimentation velocity. For the usual values of the zeta potential the reduction amounts at most to a few percent. Physically the effect is exactly analogous to the relaxation effect in electrophoresis.[9] In both cases the rate of motion is modified in consequence of the loss of symmetry of the double-layer potential. The difference lies in the nature of the applied field causing the motion. Like the dipole moment, the alteration in the sedimentation velocity may be expanded in power series of Q or ζ.

$$U=U_0[1+\sum_{\nu=1}^{\infty} c_\nu Q^\nu]=U_0[1+\sum_{\nu=1}^{\infty} d_\nu(e\zeta/\mathbf{k}T)^\nu]. \tag{1.5}$$

U is the rate of sedimentation for a charge Q or zeta potential ζ, and U_0 the rate for zero charge or potential. The relevant calculations are given in Sec. 3, where c_1, c_2, d_1, and d_2 are calculated explicitly.

In Sec. 4, the extension of the analysis of Sec. 2 and 3, to the sedimentation of a collection of particles in a finite volume is discussed. The sedimentation field of a single particle is much too small to measure and in the usual experimental arrangements the cumulative effect of a large number is observed. Similarly it is customary to measure the sedimentation velocity of the boundary of a suspension. Unfortunately it is not possible to treat a suspension very exactly owing to the complicated hydrodynamic and electrostatic interaction between the particles and their double-layer fields; the boundary introduces further difficulties. Nevertheless it is possible to give a number of useful formulas for dilute suspensions.

Finally Sec. 5 contains a comparison with earlier work. It will be shown that under suitable conditions Smoluchowski's formulas, Eqs. (1.1) and (1.3), are retrieved.

In connection with experimental work the calculations may be of interest in two directions. Measurements of sedimentation potentials and velocities could be used to estimate zeta potentials and so form a useful check on other methods, for example electrophoresis measurements. Also they might be of use in applying corrections for electrical effects in estimations of the molecular weights of submicroscopic bodies from observation of sedimentation rates in the ultracentrifuge.[10] The possibility of double-layer effects upsetting the method has long been recognized; the usual practice is to add a fairly high concentration of electrolyte and then assume that electrical effects can be ignored. As we shall see this procedure is correct in principle but some numerical estimate of the possible correction would be desirable. Also addition of large excess of electrolyte may in some cases be ruled out; for example, it may not be feasible in some protein suspensions and a direct correction for the charge carried is the only possible technique.

[9] F. Booth, Proc. Roy. Soc. (London) **A203**, 514 (1950).

[10] T. Svedberg and K. O. Pedersen, *The Ultracentrifuge* (O.U.P.) (1940).

2. SEDIMENTATION OF A SINGLE PARTICLE IN A LARGE VOLUME OF ELECTROLYTE

In the absence of an ionic double-layer the steady velocity of fall of the particle would be given by the Stokes formula,

$$U_0=2ga^2\Delta/9\eta. \tag{2.1}$$

The various symbols have the same significance as in Eq. (1.1). This relation would still hold when the particle is charged if the double-layer were undisturbed by the motion; the double-layer however loses its spherical symmetry. It is not difficult to see physically how this arises. Suppose we consider the transfer of ions across an equatorial plane, horizontal, fixed with respect to the sphere, and passing through its center. When the sphere is falling freely, the velocity of the liquid across the plane will increase from zero at the surface, to the sedimentation velocity at large distances from the sphere, its direction being everywhere vertically upwards. Let us next suppose that the sphere is charged positively. The effect of the charge will be to reduce the number of ions of the same sign as the charge in the neighborhood of the sphere, and increase the number of ions of the opposite sign. Hence, instead of equal numbers of oppositely charged ions being swept into the region above the sphere by the fluid, as in the case when the sphere is uncharged, there will be an excess of negative ions carried above whereas positive ions will tend to accumulate in the region below the sphere. In this way an electrical field in the vertical direction is established. This will in its turn tend to redress the inequalities in the ionic concentrations. In the steady state the transfer of ions due to the fluid motion will just be counterbalanced by the flow arising from the sedimentation field and variations in the ionic concentrations.

To translate these ideas into exact results the equations of motion of the electrolyte and of the ions must be solved. A method of doing this has been given in two previous papers by the writer,[9,11] referred to hereafter by the symbols (*a*) and (*b*). When the sphere is held stationary in the liquid the potential near it can be expressed in terms of the total charge on its surface by the series

$$\psi_1(r)=\sum_{\nu=1}^{\infty} e^{2\nu-1}(\epsilon a)^{-\nu}(-\mathbf{k}T)^{1-\nu}Q^{\nu}\lambda_{\nu}(\chi r), \tag{2.2}$$

where

$$\chi^2=4\pi e^2\sum_{i=1}^{s} n_i z_i^2/\epsilon\mathbf{k}T. \tag{2.3}$$

The n_i are concentrations at infinity where ψ_1 vanishes and r is the distance from the center of the particle. In Eq. (2.2) it is presupposed that the charge is uniformly distributed over the surface or, at any rate, that it is legitimate to regard it as uniformly distributed. A general method of evaluating the functions $\lambda_\nu(\chi r)$ has been given in another paper.[12] For our present purpose however we only require the first *two* terms of series (2.2); the explicit expressions are set out in the Appendix. We have placed these, and other functions to be derived, in an appendix to avoid encumbering the text with complicated expressions. If $m_{1,i}$ denotes the concentration of the ion of type "i" at the point r, then $m_{1,i}$ and ψ_1 are connected by the Boltzmann equation,

$$m_{1,i}=n_i\exp(-ez_i\psi_1/\mathbf{k}T). \tag{2.4}$$

Now suppose that as a result of the motion of the sphere which is now allowed to fall freely and steadily under gravity, the potential referred to axes fixed in the sphere changes from ψ_1 to $\psi_1+\phi$ and the ionic concentrations from $m_{1,i}$ to $m_{1,i}+p_i$. The equations to determine the p_i and ϕ are

$$\nabla^2\phi=-4\pi e\sum_{i=1}^{s} z_i p_i/\epsilon, \tag{2.5}$$

$$\mathbf{k}T\nabla^2 p_i+ez_i\left(p_i\nabla^2\psi_1+\frac{\partial p_i}{\partial r}\cdot\frac{d\psi_1}{dr}\right)$$

$$+n_i ez_i\exp(-ez_i\psi_1/\mathbf{k}T)\left[\nabla^2\phi-\frac{ez_i}{\mathbf{k}T}\frac{\partial\phi}{\partial r}\cdot\frac{d\psi_1}{dr}\right]$$

$$=n_i\omega_i^{-1}\operatorname{div}(\mathbf{v}\cdot\exp(-ez_i\psi_1/\mathbf{k}T)). \tag{2.6}$$

The derivation of Eqs. (2.5) and (2.6) follows closely that of Eqs. (5.3) and (5.4) of paper (*b*) and so the detailed working will be omitted. $\mathbf{v}$ is the velocity of the fluid at any point in coordinates fixed with respect to the sphere. In Eq. (2.6) small terms involving products of the p_i with p_i, ϕ and $\mathbf{v}$ have been dropped.

Before proceeding to the solution of Eqs. (2.5) and (2.6) it is necessary to point out that merely by writing the equations for p_i and ϕ in this form we have introduced an important simplification. Equations (2.5) and (2.6) would be exact if we were dealing with a macroscopic flow problem as in ordinary fluid dynamics and could ignore the microscopic structure of the system. But in our case the potentials ψ_1 and ϕ, the concentrations $m_{1,i}$, p_i and also $\mathbf{v}$ are not fixed quantities but exhibit fluctuations owing to the Brownian motions of both particle and ions. An orthodox statistical mechanical treatment of the problem would require the determination of various relevant quantities like the p_i, not merely as distribution functions in *space* only, but in *time* also, on the lines for example of a recent theory of transport processes in liquids due to Kirkwood.[13] The relevant measurable physical quantities would then be obtained from the appropriate distribution functions by suitable time averaging. Such an analysis of a complicated problem of the present type would be extremely difficult, and so it is necessary to ignore

[11] F. Booth, Proc. Roy. Soc. (London) **A203**, 534 (1950).

[12] F. Booth, J. Chem. Phys. **19**, 821 (1951). Section 8.

[13] J. G. Kirkwood, J. Chem. Phys. **14**, 180 (1946).

fluctuations of the various variables in Eqs. (2.5) and (2.6).

It is difficult to estimate exactly how much error is introduced by neglecting fluctuations, but the following arguments indicate that it must be small, provided that the dimensions of the particle are much greater than those of the ordinary ions in the electrolyte. Eqs. (2.5) and (2.6) will be exact provided that, first the Brownian motion of the particle may be ignored, and secondly the fluctuations of the ionic concentrations at any point, fixed with respect to the particle, are small. As Overbeek[14] has pointed out recently, work on the conductivity of ordinary electrolytes can be used to justify to some extent neglect of the Brownian motion of the colloidal particles in theories of electrophoresis. Debye and Hückel[15] calculated the relaxation potential, which is analogous to our potential ϕ, near a particular ion which was, unlike the other ions, assumed to be moving with uniform velocity and not subject to Brownian motion. From the potential they calculated the relaxation force and hence the velocity of the ion and the specific conductivity. Later Onsager[16] found the relaxation force without ignoring the Brownian motion and obtained a somewhat different result. Since our method is analogous to that of Debye and Hückel rather than Onsager's it might be thought that this result invalidates our neglect of the Brownian motion of the sphere. The analogy is not quite correct however, since a single colloidal particle in an infinite electrolyte corresponds to a single foreign ion in an electrolyte. Bennewitz, Wagner, and Küchler[17] have calculated the relaxation force on ions present in small quantities in mixtures of electrolytes, both when the Brownian motion of the rare ion is taken into account and when it is not. They found that if R_D is the relaxation force on the Debye-Hückel model and R_0 the force on the Onsager model, then

$$R_D/R_0=1+\omega_r/\omega_e, \tag{2.7}$$

where ω_e is the mobility of the ions present in large amount and ω_r the mobility of the rare ion. Since the mobilities may be taken to be roughly proportional to the reciprocals of the ionic radii, we see that the two forces are nearly identical provided that the rare ion is very large compared with the others. In general the linear dimensions of colloidal particles are much greater than those of ordinary ions and so it is likely that the distinction between R_D and R_0 is of little importance in electrophoresis of colloids.

Turning to the problem in hand, since we are concerned with the relaxation effect in sedimentation, it seems reasonable to conclude that the same result holds in our case. Our problem differs in two respects from that of Bennewitz *et al.* In the first place it was tacitly assumed in their calculation that the thickness of the double-layer round the rare ion is large compared with the radius of that ion. This may not be true for colloidal particles. Also in our case the relaxation is due to the gravitational force acting effectively on a *single* particle only; in electrical conduction the external field gives rise to forces on all of the ions. In spite of these differences it seems likely that the Brownian motion of the sedimenting sphere can be ignored provided that it is large compared with the ordinary ions.

The second basic assumption implied in the use of Eqs. (2.5) and (2.6), namely that the fluctuations of the ionic concentrations may be ignored, is not peculiar to the problem in hand but is fundamental in the current theory of electrolytes based upon the Poisson-Boltzmann equation. So far it has only been rigorously justified under rather restricted conditions.[18] Recent work by Williams[19] however suggests that the solutions of the Poisson-Boltzmann equation for the potential near *plane* surfaces may not be seriously in error for zeta-potentials of less than 100 millivolts. Moreover there is an extensive amount of work based on the equation, which has been strikingly successful in explaining the main features of colloidal precipitation.[20] This suggests that neglect of ion fluctuation effects may not give results seriously in error in the present problem.

Now let us return to the solution of Eqs. (2.5) and (2.6). This can be effected formally by assuming expansions for ϕ, p_i, and v_r, the radial component of the fluid velocity $\mathbf{v}$, in powers of Q, like Eq. (2.2).

$$\phi=\sum_{\nu=0}^{\infty} e^{2\nu-1}(\epsilon a)^{-\nu}(\mathbf{k}T)^{1-\nu}Q^{\nu}\lambda_{\nu}^{*}, \tag{2.8}$$

$$p_i=\sum_{\nu=0}^{\infty} e^{2\nu-1}(\epsilon a)^{-\nu}(\mathbf{k}T)^{1-\nu}Q^{\nu}\pi_{i,\nu}, \tag{2.9}$$

$$v_r=U_0\sum_{\nu=0}^{\infty} e^{2\nu}(\epsilon a)^{-\nu}(\mathbf{k}T)^{-\nu}Q^{\nu}\beta_{\nu}. \tag{2.10}$$

The functions λ_ν^*, $\pi_{i,\nu}$, and β_ν will be functions of r and θ, the angle between the radius vector and the downward vertical. If we now substitute Eqs. (2.8) to (2.10) in Eqs. (2.5) and (2.6), and separate equations multiplying like powers of Q, we obtain a series of differential equations connecting the various unknown λ^*, π, and β functions. The successive equations can be solved by the method described in papers (*a*) and (*b*), each function of order ν being determinable provided those of lower order are known. In what follows we shall find the first *three* terms of series (2.8) only; this will enable us to find ϕ correct to the second power of ζ. The method is general however, and could easily be extended to give the terms of higher order.

[14] J. T. G. Overbeek, Advances in Colloid Sci. **3**, 113 (1948).
[15] P. Debye and E. Hückel, Physik. Z. **24**, 185, 305 (1923).
[16] L. Onsager, Physik. Z. **27**, 388 (1926); **28**, 277 (1928).
[17] Bennewitz, Wagner, and Küchler, Physik. Z. **30**, 623 (1929).
[18] J. G. Kirkwood, J. Chem. Phys. **2**, 767 (1934).
[19] W. E. Williams, Proc. Phys. Soc. (London) **A66**, 372 (1953).
[20] E. J. W. Vervey and J. T. G. Overbeek, *Theory of the Stability of Lyophobic Colloids* (Elsevier Publishing Company, London, 1948).

If we consider the part of Eq. (2.6) independent of Q,

$$\nabla^2(\mathbf{k}T\pi_{i,0}+n_iez_i\lambda_0^*)=0. \tag{2.11}$$

By methods similar to those of paper (*a*), it can be shown that, if the same boundary conditions at the solid-liquid interface are assumed, then

$$\lambda_0^*=\pi_{i,0}=0, \quad \text{all } i. \tag{2.12}$$

The coefficient of Q in Eq. (2.6) gives

$$\nabla^2(\mathbf{k}T\pi_{i,1}+n_iez_i\lambda_1^*)=-\frac{n_iez_iU_0\beta_0}{\omega_i\mathbf{k}T}\cdot\frac{d\lambda_1}{dr}. \tag{2.13}$$

From the Stokes theory

$$\beta_0=-\left[1-\frac{3a}{2r}+\frac{a^3}{2r^3}\right]\cos\theta. \tag{2.14}$$

$\pi_{i,1}$ and λ_1^* are now expanded in series of spherical harmonics

$$\pi_{i,1}=\sum_{n=0}^{\infty}\pi_{i,1,n}(r)P_n(\cos\theta), \tag{2.15}$$

$$\lambda_1^*=\sum_{n=0}^{\infty}\lambda_{1,n}(r)P_n(\cos\theta), \tag{2.16}$$

where now the $\pi_{i,1,n}$ and $\lambda_{1,n}$ are functions of r only. From the boundary conditions

$$\lambda_{1,n}=\pi_{i,1,n}=0 \quad \text{all } i, \text{ and all } n, \text{ if } \quad n\neq 1. \tag{2.17}$$

For n equal to 1,

$$\Delta_1^{(r)}(\mathbf{k}T\pi_{i,1,1}+n_iez_i\lambda_{1,1})=\frac{n_iez_iU_0}{\omega_i\mathbf{k}T}\left(1-\frac{3a}{2r}+\frac{a^3}{2r^3}\right)\cdot\frac{d\lambda_1}{dr}, \tag{2.18}$$

where

$$\Delta_n^{(r)}=\frac{d^2}{dr^2}+\frac{2}{r}\frac{d}{dr}-\frac{n(n+1)}{r^2}. \tag{2.19}$$

Integrating by the usual methods, we get

$$\mathbf{k}T\pi_{i,1,1}+n_iez_i\lambda_{1,1}=A_{i,1}r+\frac{B_{i,1}}{r^2}-\frac{n_iez_iU_0}{\chi\omega_i\mathbf{k}T}F_1(b,x), \tag{2.20}$$

where

$$b=\chi a, \quad x=\chi r. \tag{2.21}$$

$A_{i,1}$ and $B_{i,1}$ are integration constants and $F_1(b,x)$ will be found in the Appendix (Eq. (6.4)). Since both $\pi_{i,1,1}$ and $\lambda_{1,1}$ must vanish at infinity

$$A_{i,1}=0. \tag{2.22}$$

$B_{i,1}$ is determined from the condition that there is no net flow of ions to the surface. Using Eq. (2.5) of paper (*a*) and remembering that the radial component of the fluid velocity must vanish on the surface of the sphere, we have

$$\mathbf{k}T\left.\frac{d\pi_{i,1,1}}{dr}\right|_a+n_iez_i\left.\frac{d\lambda_{1,1}}{dr}\right|_a=0. \tag{2.23}$$

Using Eq. (2.20), this gives

$$B_{i,1}=-a^3n_iez_iU_0F_1'(b,b)/2\omega_i\mathbf{k}T. \tag{2.24}$$

Multiplying Eq. (2.20) by $4\pi ez_i/\epsilon\mathbf{k}T$, summing over all i, and using Eq. (2.5), we finally get the following differential equation for $\lambda_{1,1}$.

$$(\Delta_1^{(x)}-1)\lambda_{1,1}=\frac{4\pi e^2U_0\sum_{i=1}^{s}n_iz_i^2\omega_i^{-1}}{\chi^3\epsilon(\mathbf{k}T)^2}\times\left[F_1(b,x)+\frac{b^3}{2x^2}F_1'(b,b)\right]. \tag{2.25}$$

On integration this yields

$$\lambda_{1,1}=C_{1,1}e^{b-x}\left(\frac{1}{x}+\frac{1}{x^2}\right)+D_{1,1}e^{b+x}\left(\frac{1}{x}-\frac{1}{x^2}\right)+\frac{4\pi e^2U_0\sum_{i=1}^{s}n_iz_i^2\omega_i^{-1}}{\chi^3\epsilon(\mathbf{k}T)^2}\left[F_2(b,x)-\frac{b^3}{2x^2}F_1'(b,b)\right], \tag{2.26}$$

where $C_{1,1}$ and $D_{1,1}$ are constants of integration and $F_2(b,x)$ is given by Eq (6.5). Since $\lambda_{1,1}$ must vanish at infinity, $D_{1,1}$ must be zero. The other constant is fixed by the condition that the surface charge remains unaltered in sedimentation. It follows that

$$\epsilon d\lambda_{1,1}/dx|_b-\epsilon_s\lambda_{1,1}(b)/b=0, \tag{2.27}$$

which gives

$$C_{1,1}=\frac{2\pi e^2U_0a^3\sum_{i=1}^{s}n_iz_i^2\omega_i^{-1}[2\epsilon b(F_2'(b,b)+F_1'(b,b))+\epsilon_s(bF_1'(b,b)-2F_2(b,b))]}{\epsilon bk^2T^2[\epsilon(2+2b+b^2)+\epsilon_s(1+b)]}. \tag{2.28}$$

Now let us consider the behavior of $\lambda_{1,1}$ as a function of x. For large x, $F_2(b,x)$ can be written in the form

$$F_2(b,x)=\frac{be^{b-x}}{(1+b)}\left[-\frac{1}{2}+\frac{3b}{4x}\log x+O\left(\frac{1}{x}\right)\right]. \tag{2.29}$$

This decays to zero as e^{-x} for x or r sufficiently large, just like the potential in the double-layer in the steady equilibrium state. It follows that outside the double layer region the only part of $\lambda_{1,1}$ which is of importance is the part involving $F_1'(b,b)$ in the third term of Eq.

(2.26), which varies as $\cos\theta/r^2$. This corresponds to the field of an electrical dipole at the center of the sphere with its axis vertical. From Eq. (2.26) it is easy to find its equivalent moment; comparing with Eq. (1.3), we find for the coefficient of Q in the series for μ,

$$a_1=ga^2e\Delta q_3^*S_3(b)/\epsilon kT\sum_{i=1}^{s}n_iz_i^2. \tag{2.30}$$

q_m^* is a convenient dimensionless parameter defined as in paper (*a*) by

$$q_m^*=\epsilon kT\sum_{i=1}^{s}n_iz_i^{m-1}\omega_i^{-1}/e^2\pi\eta\sum_{i=1}^{s}n_iz_i^2, \tag{2.31}$$

and $S_3(b)$ is given in the Appendix, Eq. (6.9). The moment in terms of the zeta potential is easily found from series (2.2); for the first coefficient of the second series of Eq. (1.3), we find

$$b_1=ga^3\Delta q_3^*S_3^*(b)/e\sum_{i=1}^{s}n_iz_i^2, \tag{2.32}$$

where $S_3^*(b)$ is given by Eq. (6.18). In deriving Eq. (2.32) we have used the fact that the potential ζ is simply $\psi_1(a)$. The functions $S_3(b)$ and $S_3^*(b)$ are plotted in Fig. 1. Both tend to the value 1/18 for b zero; for b very large $S_3(b)$ tends to zero whereas $S_3^*(b)$ tends to 1/12. This completes our determination of the coefficients a_1 and b_1 and we can now proceed to evaluate a_2 and b_2.

The coefficient of Q^2 in Eq. (2.6) gives

$$\nabla^2(kT\pi_{i,2}+n_iez_i\lambda_2^*)=-z_ikT\left[\pi_{i,1}\nabla^2\lambda_1+\frac{\partial\pi_{i,1}}{\partial r}\cdot\frac{d\lambda_1}{dr}\right]$$
$$+n_iez_i^2\left[\lambda_1\nabla^2\lambda_1^*+\frac{\partial\lambda_1^*}{\partial r}\cdot\frac{d\lambda_1}{dr}\right]$$
$$+\frac{n_iez_iU_0}{\omega_ikT}\left[\beta_0\left(\frac{d\lambda_2}{dr}+z_i\lambda_1\frac{d\lambda_1}{dr}\right)-\beta_1\frac{d\lambda_1}{dr}\right]. \tag{2.33}$$

All the quantities on the right-hand side of this equation are known except β_1; to find this we must examine the motion of the electrolyte. It is easy to obtain the additional retarding force on the particle caused by the alteration of the potential from ψ_1 to $\psi_1+\phi$, provided that ϕ can be written in the form

$$\phi=\Phi(r)\cos\theta, \tag{2.34}$$

where $\Phi(r)$ is a function of r only. The exact equation for the rate of fall U is

$$4\pi a^3g\Delta/3=6\pi a\eta U+\epsilon a\int_a^\infty\xi(r)dr, \tag{2.35}$$

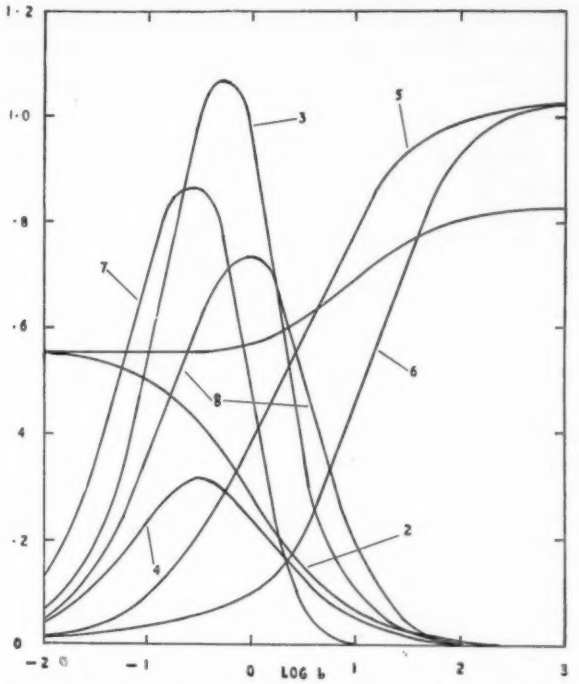

FIG. 1. S_n, S_n^*, V_n and V_n^* as functions of $\log_{10}b$. Curve 1. $10\times S_3^*(b)$, 2. $10\times S_3(b)$, 3. $5\times10^2S_{2,3}(b)$, 4. $-10^3\times S_4(b)$, 5. $10^2\times S_{2,3}^*(b)$, 6. $-10^2\times S_4^*(b)$, 7. $-5\times10^2V_3(b)$, 8. $-2\times10^2V_3^*(b)$. The functions are multiplied by the various factors merely to facilitate plotting on the same scale.

where

$$\xi(r)=\frac{1}{3}\int_r^\infty\left[\frac{d\psi_1(z)}{dz}\cdot\Delta_1^{(z)}\Phi(z)-\Phi(z)\cdot\frac{d(\Delta_0^{(z)}\psi_1(z))}{dz}\right]\left(\frac{z^2}{r^2}-\frac{r}{z}\right)dz. \tag{2.36}$$

The derivation of Eq. (2.35) follows so closely the calculation given in paper (*a*) that we shall merely sketch how it can be obtained. The effect of altering the potential from ψ_1 to $\psi_1+\phi$ is to give an additional force on the particle due to the interaction between the field of ϕ and charge on the surface, and to the modification of the fluid stresses. To find the latter the general expressions for the velocity components in the electrolyte must be obtained. The calculation gives results similar to Eqs. (6.13) and (6.14) of paper (*a*). The total force arising from the viscous stresses follows easily from the velocity components. The electrostatic force on the sphere is obtained by the method of Sec. 7 of paper (*a*), the only change being that in Eq. (7.7), E must be deleted. Substituting for $\Phi(r)$ from Eq. (2.8) and for ψ_1 from Eq. (2.2) we see immediately from Eq. (1.3) that

$$c_1=d_1=0. \tag{2.37}$$

It follows that

$$\beta_1=0. \tag{2.38}$$

Using series expansions for $\pi_{i,2}$ and λ_2^* of the same form as Eq. (2.15) and (2.16) for $\pi_{i,1}$ and λ_1^*, Eq.

(2.33) separates into a set of differential equations for the $\pi_{i,2,n}$ and $\lambda_{2,n}$. We find as before that for n not equal to unity,

$$\lambda_{2,n}=\pi_{i,2,n}=0. \tag{2.39}$$

For n equal to 1, the analysis follows closely the treatment of Eq. (2.18), and we have after integration

$$\mathbf{k}T\pi_{i,2,1}+n_iez_i\lambda_{2,1}=A_{i,2}r+B_{i,2}r^{-2}+n_iez_i^2\lambda_{1,1}\lambda_1+B_{i,1}z_i\chi^2F_5(b,x)+\frac{n_iez_iU_0}{\chi\omega_i\mathbf{k}T}[z_iF_3(b,x)+q_2F_4(b,x)], \tag{2.40}$$

where $A_{i,2}$ and $B_{i,2}$ are constants of integration and the functions $F_3(b,x)$, $F_4(b,x)$, and $F_5(b,x)$ are given in Eqs. (6.6) to (6.8) and q_2 by Eq. (6.3). Since the potential $\lambda_{2,1}$ must vanish at infinity, $A_{i,2}$ must vanish. The condition of no flow of ions to the surface gives

$$\mathbf{k}T\left.\frac{d\pi_{i,2,1}}{dx}\right|_b+n_iez_i\left.\frac{d\lambda_{2,1}}{dx}\right|_b=n_iez_i^2\left.\frac{d\lambda_{1,1}}{dx}\right|_b-z_i\mathbf{k}T\pi_{i,1,1}(b)\left.\frac{d\lambda_1}{dx}\right|_b. \tag{2.41}$$

This relation serves to determine $B_{i,2}$ which is found to be

$$B_{i,2}=\frac{n_iez_iU_0a^3}{2\omega_i\mathbf{k}T}\Big[q_2F_4'(b,b)+z_i\Big(F_3'(b,b)-\frac{b^3}{2}F_5'(b,b)F_1'(b,b)+\tfrac{1}{2}F_1'(b,b)+\frac{1}{b}F_1(b,b)\Big)\Big]. \tag{2.42}$$

Multiplying Eq. (2.40) by $4\pi ez_i/\epsilon\mathbf{k}T$ and summing over all i, we get a differential equation like Eq. (2.25) to determine $\lambda_{2,1}$. The analysis is exactly analogous to that used for Eq. (2.25) and so the details will be omitted and we shall merely set down the final expression for a_2 in series (1.4).

$$a_2=gae^3\Delta[q_2q_3^*S_{2,3}(b)+q_4^*S_4(b)]/(\epsilon kT)^2\sum_{i=1}^{s}n_iz_i^2. \tag{2.43}$$

The values of $S_{2,3}(b)$ and $S_4(b)$ in terms of the $F_n'(b,b)$ are given in the appendix, and they are also plotted in Fig. 1. Both functions vanish for b very small or very large and have single turning points for b approximately equal to 0.4.

For b_2 we have

$$b_2=ga^3\Delta[q_2q_3^*S_{2,3}^*(b)+q_4^*S_4^*(b)]/e\sum_{i=1}^{s}n_iz_i^2. \tag{2.44}$$

$S_{2,3}^*(b)$ and $S_4^*(b)$ are given in the appendix and plotted out in Fig. 1; they differ from $S_{2,3}(b)$ and $S_4(b)$ in that both steadily increase from zero to the same limiting value as b goes from zero to infinity.

This completes the calculation of a_2 and b_2. Clearly we could continue the procedure and, by examining the part of Eq. (2.6) multiplying Q^3, obtain a_3 and b_3. Unfortunately the next stage becomes extremely complicated and so we shall not go further than a_2 and b_2. In view of this, the question naturally arises as to how good is an approximation consisting of *two* terms only of series (1.4). Clearly the approximation is better the smaller Q or ζ, but some more precise numerical criteria are needed than this qualitative remark.

Some estimate can be formed in the following way. For each value of b we can determine a critical value of the zeta potential so that the second term of the series (1.4) for μ in powers of $(e\zeta/kT)$ just equals a chosen fraction, say f, of the first.

$$\zeta_c(b)=kT[q_2q_3^*S_{2,3}^*(b)+q_4^*S_4^*(b)]^{-1}fq_3^*S_3^*(b)/e. \tag{2.45}$$

If we now make the reasonable assumption that for the higher terms of the series each term is approximately equal to f times its predecessor, then we have, if μ_2 denotes the value of μ computed from the first two terms of Eq. (1.4) then

$$|\mu-\mu_2/\mu|\leqslant f^2,\quad \zeta\leqslant\zeta_c(b). \tag{2.46}$$

Thus if we fix the ratio f to be 0.1, we might reasonably expect the error of μ_2 to be of the order of one percent.

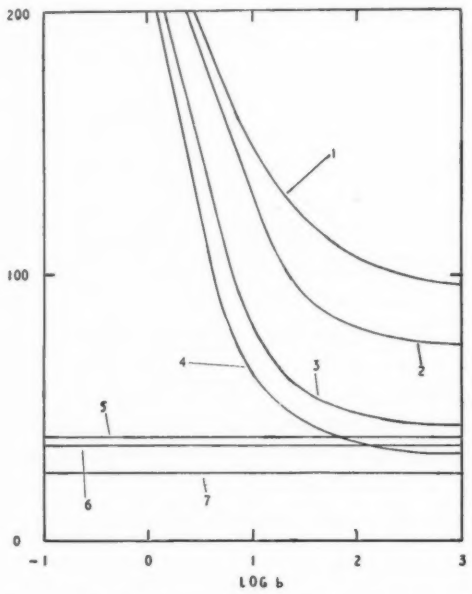

FIG. 2. Critical zeta potentials for various electrolytes: ζ_c in millivolts as functions of $\log_{10}b$. Curve 1. NaCl, 2. H_2O, 3. KOH, 4. NaOH. Curves 5, 6, and 7 represent *minimum* values of ζ_c. 5. $CaCl_2$, 6. $CuCl_2$, 7. $Ca(OH)_2$. For KCl $\zeta_c>1000$ millivolts, and for Na acetate $\zeta_c>200$ millivolts.

In Fig. 2 we have plotted ζ_c as a function of b for T equal to 298°K and f equal to 0.1 for various electrolytes. The relevant q_m and q_m^* are tabulated in Table I. The curves for any other chosen fraction, say f', can be found by multiplying each ordinate by f'/f. For monovalent electrolytes the slopes of the curves are everywhere negative and the minima lie at the limit for b large. For the unsymmetrical electrolytes we have chosen, the behavior is rather complicated since b_2 changes sign as b varies. Owing to this we have simply indicated the *minimum* values of ζ_c. Generally the critical potentials for the higher valency electrolytes are lower than for the simpler electrolytes; in practice of course lower zeta potentials usually accompany electrolytes of high valency.

Before leaving the sedimentation field and considering the velocity, it is of interest to see how dependent are our results on the boundary conditions chosen. It is of importance to notice that both the form and magnitude of the dipole field depend only on the condition that there is no conduction through the particle and not upon the more speculative condition that the surface charge remains unchanged. This can be seen immediately from Eq. (2.26). Thus if we postulate that the potential not the charge remains unaltered at the surface, we merely change the coefficient $C_{1,1}$ to

$$C_{1,1}=\frac{4\pi e^2U_0b^2\sum_{i=1}^{s}n_iz_i^2\omega_i^{-1}}{\chi^3\epsilon k^2T^2(1+b)}\left[\frac{b}{2}-F_1'(b,b)-F_2(b,b)\right], \quad (2.47)$$

and a_1 is unaltered. This point is of interest since it seems very likely that both the charge and the potential at the surface may in fact alter in sedimentation.

This concludes our analysis of the sedimentation potential of a single particle and we can now examine the velocity.

3. THE SEDIMENTATION VELOCITY

The coefficients c_ν and d_ν of series (1.5) are easily found from the work of Sec. 2 and Eqs. (2.35) and (2.36). It is merely necessary to substitute series (2.8) for ϕ and series (2.2) for ψ_1 and compare coefficients of like powers of Q.

We have immediately that

$$c_1=d_1=0, \quad (3.1)$$

and so there is no correction of order ζ to the sedimentation velocity. For c_2 we have

$$c_2=q_3^*e^4V_3(b)/(\epsilon a\mathbf{k}T)^2, \quad (3.2)$$

where

$$V_3(b)=\frac{1}{18}\int_b^\infty\int_x^\infty\frac{d\lambda_1(y)}{dy}\left[F_1(b,y)+\frac{b^3}{2y^2}F_1'(b,b)\right]\times\left(\frac{y^2}{x^2}-\frac{x}{y}\right)dxdy. \quad (3.3)$$

TABLE I. q_m and q_m^* values for various electrolytes at 25°C.

Electrolyte	q_2	q_3^*	q_4^*
H_2O	0	0.304	−0.0843
NaCl	0	1.270	0.263
KCl	0	1.026	0.0193
NaOH	0	0.961	0.573
KOH	0	0.717	0.329
Na acetate	0	1.707	−0.173
$CaCl_2$	1	2.058	3.109
$Ca(OH)_2$	1	1.852	3.315
$CuCl_2$	1	2.233	3.459

The full expression for $V_3(b)$ after integration is given in the appendix and it is plotted out in Fig. 1. As b increases from zero to infinity, $V_3(b)$ decreases from zero to a simple minimum at b equal to 0.25, and then increases to zero again.

For d_2 we have

$$d_2=q_3^*V_3^*(b). \quad (3.4)$$

V_3^* behaves like $V_3(b)$ but has a minimum at b equal to 1.0.

Further terms c_3, d_3, c_4, etc., can be obtained but their form is very complicated, and as will be seen when numerical values are examined, it does not appear likely that they are of much importance in practical cases.

4. SEDIMENTATION OF A SUSPENSION

Now let us examine the sedimentation of a cloud of particles distributed uniformly through a volume of electrolyte with a density of n particles per unit volume. The problem is much more difficult than that discussed in Sec. 2 since it is necessary to take into account the effects of the motions and fields of the particles on one another.

We must first notice that the behavior of the suspension depends materially on the relative magnitudes of the double-layer thickness of a single particle, if no other particles were present, and the mean separation of the particles. The simplest case is when this double-layer thickness is much greater than the separation, that is, for

$$\chi^3\ll n. \quad (4.1)$$

The suspension may then be regarded as an ordinary electrolyte, the spheres being merely exceptionally large and highly charged ions. If a suspension of this type is mixed thoroughly so that all the concentrations are initially uniform throughout, and then allowed to settle, at first there will be no sedimentation field. Since the rate of sedimentation of the particles is much greater than that of the ions however, the concentrations will tend to become nonuniform. This will in turn give rise to a vertical electric field. The steady state will be given by the condition that there must be no net flow of charge across any fixed horizontal cross section drawn in the suspension. The effect has been examined by

various writers[21] and so we shall merely state the results in our notation. For the sedimentation field we have

$$E=\frac{2gna^2Q\Delta}{9\eta e\sum_{i=1}^{s} n_i\omega_i z_i^2}=\frac{2gna^3\zeta\epsilon\Delta}{9\eta e^2\sum_{i=1}^{s} n_i\omega_i z_i^2}, \tag{4.2}$$

and for the sedimentation velocity

$$U=U_0\left[1-\frac{nQ^2}{6\pi\eta a\sum n_i z_i^2\omega_i}\right]$$

$$=U_0\left[1-\frac{na\zeta^2\epsilon^2}{6\pi\eta e^2\sum n_i z_i^2\omega_i}\right]. \tag{4.3}$$

In deriving Eqs. (4.2) and (4.3) it is assumed that the volume of the particles is small compared with the total volume of the suspension since only in this case is the Stokes theory valid for the fluid flow round the individual particles. Thus formulas (4.2) and (4.3) require the condition

$$n\ll a^{-3}, \tag{4.4}$$

in addition to (4.1). In addition all effects of the boundaries of the suspension on the motion are ignored.

Although formulas (4.2) and (4.3) are often applied indiscriminately, conditions (4.1) and (4.4) are so restrictive that it seems unlikely that Eqs. (4.2) and (4.3) can apply very rarely, if at all, to real suspensions. Thus Eq. (4.1) means that the separation must be much less than, at the most 10^{-4} or 10^{-5} cm. On the other hand Eq. (4.4) requires that the particle radius must be much less than this mean separation. Hence (4.2) and (4.3) can only apply to extremely fine particles.

When the double-layer thickness is of the same order or less than the mean separation of the particles, the above formulas break down. This follows, since near the particles there is an excess of ions of charge opposite in sign to that on the particles, but the liquid near the particles tends to be carried along with the solid matter. Hence, the net transfer of charge resulting from sedimentation alone is less than obtains in the derivation of Eqs. (4.2) and (4.3).

A complete analysis for the general case when (4.1) and (4.4) are not followed is impossible since it would be necessary to work out the motion of the particles and of the electrolyte for the whole suspension in detail. Some progress can be made however when (4.4) together with the *reverse* of Eq. (4.1) hold; that is, when the double-layer thickness is small compared with the mean separation.

$$\chi^3\gg n. \tag{4.5}$$

This condition means that if the particles were held stationary, the potential near any given particle would still be given by Eq. (2.2) and the effect of the charges and ionic atmospheres of neighboring particles could be ignored.

Consider now what happens when a suspension satisfying these conditions is first thoroughly mixed so that the ionic and particle concentrations are uniform throughout, and then allowed to settle. Strictly the theory of Sec. 2 cannot be used, since the boundary condition that ϕ tends to zero as r tends to infinity does not necessarily follow. But, provided that the sedimentation has not proceeded for a time sufficiently long to produce large scale variations in the ionic concentrations, we would expect each particle to be surrounded by a dipole potential as in Sec. 2. The problem of determining the average field due to such a system of dipoles is a well-known one in the theory of dielectrics. The potential at any point P in the suspension is

$$\phi^\dagger(P)=n\int(\mathfrak{y}(P)\cdot\mathrm{grad}(1/PQ))dV, \tag{4.6}$$

where dV is a volume element drawn round the point Q. The integration is over the whole volume of the suspension. Any field due to polarization of the containing vessel is neglected. ϕ^+ like ϕ may be expanded in powers of Q or ζ. If we confine attention to the part depending on the first power of Q or ζ, and distinguish this by the suffix 1, we have

$$\phi_1^\dagger(P)=3v_0\zeta g\Delta\gamma(P)q_3^*S_3^*/4\pi kT\sum_{i=1}^{s} n_i z_i^2, \tag{4.7}$$

where

$$\gamma(P)=\int_S(\mathbf{e}\cdot\mathbf{n})/PR\cdot dS. \tag{4.8}$$

$\mathbf{e}$ is a unit vector drawn vertically downwards. v_0 is the total volume of solid matter in unit volume of the suspension; $\mathbf{n}$ is a unit vector along the outward normal to the element of surface dS drawn round the point R on the boundary surface S of the suspension. The factor γ depends only on the geometry of S and the position of P. For an infinite sheet with horizontal plane surfaces $\gamma(P)$ is $4\pi h$ where h is the distance measured downwards from an arbitrary point; for a sphere $\gamma(P)$ is $4\pi h/3$. In more complicated cases, for example a cylinder with horizontal ends, $\gamma(P)$ is easily calculated from Eq. (4.8).

So much for the sedimentation field; now consider the sedimentation velocity. Clearly the method of Sec. 3 can still be used provided a term ϕ^*, which represents a contribution due to all the particles in the suspension but excluding the dipole field of the particular sphere being studied, is added to the potential ϕ of Eq. (2.7). For the calculation of the potential ϕ^* standard texts on dielectric theory may be consulted. For two cases, suspensions in the form of a sphere or an infinite hori-

[21] Reference 10, p. 23.

zontal sheet, the analysis is particularly simple.

$$\phi^*=\beta n\mu\cos\theta\left(r+\frac{a^3}{2r^2}\right), \tag{4.9}$$

where β equals $8\pi/3$ for the thin horizontal sheet and zero for a spherical form. Instead of Eq. (3.4) we now have

$$d_2=q_3^*(V_3^*(b)-81\beta v_0 S_3^{*2}(b)b^{-2}). \tag{4.10}$$

The correction to d_2 tends to zero for b large. On the other hand as b decreases the correction apparently increases indefinitely, since $S_3^*(b)$ remains finite as b tends to zero. But the condition that the double-layers do not overlap must be preserved. For values of b less than some limit it would be necessary to reduce the concentration of particles for condition (4.6) to remain satisfied.

When the shape of the boundary of the suspension is different from the two cases we have just examined, the field derived from the potential ϕ^+ will not in general be uniform throughout the suspension. Consequently the rate of sedimentation will depend on the position of the particle in the suspension. It is quite easy to show for example that for a suspension in the form of a thin cylinder with vertical walls and horizontal upper and lower surfaces, the sedimentation rate is still given by Eq. (4.10), but the coefficient β now depends on the height of the particle. Near the upper and lower surfaces, β equals $2\pi/3$; in intermediate positions its value is less, being at a minimum at a point midway between the upper and lower surfaces. For a very long thin suspension this minimum value would be $-4\pi/3$.

5. DISCUSSION

With the calculations completed it is now of interest to see what is the order of magnitude of the fields and velocity corrections they predict. The order of magnitude of μ is easily estimated from Eqs. (2.30) and (2.32). For ζ equal to 100 millivolts, a 10^{-1} cm, Δ equal to 1 and pure water for electrolyte we find that μ is of the order 5×10^{-4} volt cm^2. This would give a potential difference of about 1 millivolt between two points, one a centimeter above, the other a centimeter below the particle. Usually the moment will be much less than this estimate owing to the factors a^2 or a^3 in the numerators, and the concentrations n_i in the denominators of the right-hand sides of Eqs. (2.30) and (2.32); for example, for a $N/100$ solution of potassium chloride we find that μ is only 1.6×10^{-10} volt cm^2. These low values indicate that it seems unlikely that the field arising from sedimentation round a *single* particle will be detected experimentally.

On the other hand for suspensions quite appreciable fields might be set up If we set v_0 equal to 0.01 in Eq. (4.7) and all other quantities as in the case of pure water examined above, we find that the sedimentation field is about 0.2 v/cm.

Now let us examine the order of magnitude of the corrections to the sedimentation velocity. From Eq. (3.4) we see that for a given zeta potential and concentration of electrolyte, the correction to U_0 depends on the parameter b only through the function $V_3^*(b)$. For the temperature 25°C and for b chosen so that $V_3^*(b)$ has its greatest negative value, we find

$$U=U_0[1-.0037q_3^*(e\zeta/kT)^2+0(\zeta^3)]. \tag{5.1}$$

Hence for ζ equal to 100 millivolts, the correction varies from 2 percent for pure water to 15 percent for cupric chloride, among the selection of electrolytes listed in Table I. Using Eq. (4.10) it is easily verified that the formula corresponding to Eq. (5.1) for a *suspension* is

$$U=U_0[1-q_3^*(0.0037+0.23\beta v_0)(e\zeta/kT)^2+0(\zeta^3)]. \tag{5.2}$$

From this result it will be seen that unless β is very small or the suspension very dilute the term involving v_0 may well be of comparable or greater importance than the first part of the correction.

Next let us consider the limiting forms of μ for the extremes of b very small and b very large. The first corresponds to a double-layer thickness much greater than the radius. In terms of ζ we find

$$\mu=\frac{ga^3\Delta}{e\sum_{i=1}^{s}n_iz_i^2}\left[\frac{q_3^*}{18}\left(\frac{e\zeta}{kT}\right)+b\left(\frac{q_2q_3^*}{72}-\frac{q_4^*}{216}\right)\left(\frac{e\zeta}{kT}\right)^2+0(\zeta^3)\right]. \tag{5.3}$$

At first sight it might appear from this formula that we could increase μ indefinitely simply by increasing a and reducing the ionic concentrations n_i, since the q_m and q_m^* for a given temperature, depend only on the ionic valencies and mobilities. But it must be remembered that it is not possible to reduce the ionic concentrations below the hydroxyl and hydrogen ion concentrations in pure water. Moreover the condition that b must be very small limits the radius to about 10^{-6} cm.

For the double-layer thickness much less than the radius we find

$$\mu=\frac{ga^3\Delta}{12e\sum_{i=1}^{s}n_iz_i^2}\left[q_3^*\left(\frac{e\zeta}{kT}\right)+\frac{(q_2q_3^*-q_4^*)}{8}\left(\frac{e\zeta}{kT}\right)^2+0(\zeta^3)\right]. \tag{5.4}$$

It is easy to derive Eq. (5.4) independently by simple arguments, thus providing a useful check on the rather complicated calculations of Sec. 2. As explained in the introduction, in the steady state the flow of ions across

the equatorial plane through the center of the sphere due to the sedimentation field just compensates the flow past the surface due to the fluid motion. From Sec. 2 we would expect that the quantity $(kTp_i+n_iez_i\phi)$ should have a functional dependence on r and θ of dipole form, except in the double-layer region very close to the sphere; hence we may write

$$kTp_i+n_iez_i\phi=d_i\cos\theta/r^2. \tag{5.5}$$

The rate of transfer of ions of type i from below to above the equatorial plane is therefore

$$t_i=2\pi\omega_i d_i/a. \tag{5.6}$$

But this must equal the transfer in the double-layer region due to the fluid flow.

$$t_i=2\pi\int_a^\infty v_\theta|_{\pi/2}(m_i-n_i)r\,dr. \tag{5.7}$$

From the Stokes theory

$$v_\theta|_{\pi/2}=-U_0\left(1-\frac{3a}{4r}-\frac{a^3}{4r^3}\right), \tag{5.8}$$

and m_i is given by Eq. (2.4). Carrying through the integrations of Eq. (5.8) which simplify considerably in view of the condition $b\gg1$, we find

$$t_i=-\frac{3\pi U_0 n_i}{\chi^2}\left[z_i\left(\frac{e\zeta}{kT}\right)+\frac{(z_iq_2-z_i^2)}{8}\left(\frac{e\zeta}{kT}\right)^2+0(\zeta^3)\right]. \tag{5.9}$$

t_i is next eliminated between Eqs. (5.6) and (5.9) and from the resulting formula for d_i and its definition (5.5), expression (5.4) for the dipole moment is readily retrieved.

Finally it is of interest to verify that our results reduce to those of Smoluchowski under the appropriate special conditions. Suppose we confine attention to terms in μ of order ζ, and let b be very large so that the double-layer is very thin. In addition let us suppose that all of the ionic mobilities are equal; then if σ is the specific conductivity of the electrolyte

$$\sigma=e^2(\sum_{i=1}^{s}n_iz_i^2)^2/\sum_{i=1}^{s}n_iz_i^2\omega_i^{-1}. \tag{5.10}$$

For the dipole moment we now find

$$\mu=\epsilon\zeta a^3g\Delta/12\pi\eta\sigma, \tag{5.11}$$

which is the result found by Smoluchowski. For the sedimentation field of a suspension we find

$$E=n\epsilon\zeta a^3g\Delta\gamma(P)/12\pi\sigma\eta, \tag{5.12}$$

which reduces to Eq. (1.1) for the case when $\gamma(P)$ equals 4π. For the sedimentation velocity, we have from Eq. (6.32),

$$V_3^*(b)=-1/4b^2. \tag{5.13}$$

Hence from Eq. (3.4), if the ionic mobilities are again set equal

$$U=U_0\left[1-\frac{1}{\eta\sigma}\left(\frac{\epsilon\zeta}{4\pi a}\right)^2+0(\zeta^3)\right], \tag{5.14}$$

which is equivalent to Eq. (1.3).

ACKNOWLEDGMENTS

My thanks are due Dr. A. B. Lidiard for checking the calculations of the formulas listed in the Appendix, and to The Central Research Fund of the University of London for the loan of a calculating machine. I am also grateful to the British Empire Cancer Campaign for financial support.

6. APPENDIX

(a) $\lambda_n(x)$ Functions

$$\lambda_1(x)=\frac{b}{1+b}\cdot\frac{e^{b-x}}{x}. \tag{6.1}$$

$$\lambda_2(x)=-\frac{q_2}{4x}\left(\frac{b}{1+b}\right)^2\left[e^{2b-x}(E_i(b)-E_i(x))+\left(\frac{b-1}{b+1}\right)(e^{4b-x}E_i(3b)+e^{2b+x}E_i(3x))\right], \tag{6.2}$$

where

$$q_2=\sum_{i=1}^{s}n_iz_i^3/\sum_{i=1}^{s}n_iz_i^2. \tag{6.3}$$

(b) $F_n(b,x)$ Functions

$$F_1(b,x)=\frac{be^{b-x}}{(1+b)}\left[\frac{1}{x^2}+\frac{1}{x}+b\left(-\frac{1}{x^2}-\frac{1}{4x}+\frac{1}{4}-\frac{x}{4}e^xE_i(x)\right)+b^3\left(\frac{1}{8x^3}-\frac{1}{24x^2}+\frac{1}{48x}-\frac{1}{48}+\frac{xe^xEi(x)}{48}\right)\right]. \tag{6.4}$$

$$F_2(b,x)=\frac{be^{b-x}}{(1+b)}\left[-\frac{3}{4x^2}-\frac{3}{4x}-\frac{1}{2}+b\left(\frac{5}{4x^2}-\frac{1}{4x}-\frac{1}{4}+\frac{3}{4}\log x\left(\frac{1}{x}+\frac{1}{x^2}\right)+\frac{xe^x}{4}Ei(x)+\frac{3}{4}\left(\frac{1}{x^2}-\frac{1}{x}\right)e^{2x}Ei(2x)\right)+b^3\left(\frac{1}{12x^2}+\frac{1}{48x}+\frac{1}{48}-\frac{xe^x}{48}Ei(x)\right)\right]. \tag{6.5}$$

$$F_3(b,x)=\frac{b^2e^{2b-2x}}{(1+b)^2}\Big[\frac{1}{2x^3}+\frac{3}{4x^2}+b\Big(-\frac{1}{2x^3}-\frac{1}{12x^2}+\frac{1}{3x}-\frac{1}{6}$$
$$-\Big[\frac{1}{4x^2}+\frac{1}{4x}+\frac{1}{4}\Big]e^xEi(x)+\frac{x}{3}e^{2x}Ei(2x)\Big)$$
$$+b^3\Big(\frac{7}{80x^4}-\frac{1}{30x^3}-\frac{1}{180x^2}-\frac{11}{720x}-\frac{1}{90}$$
$$+\Big[\frac{1}{x^2}+\frac{1}{x}+1\Big]\frac{e^xEi(x)}{48}+\frac{x}{45}e^{2x}Ei(2x)\Big)\Big]. \quad (6.6)$$

$$F_4(b,x)=\frac{b^2}{(1+b)^3}[(b+1)e^bEi(b)+(b-1)e^{3b}Ei(3b)]e^{b-x}$$
$$\times\Big[-\frac{1}{4x^2}-\frac{1}{4x}+b\Big(\frac{1}{4x^2}+\frac{1}{16x}-\frac{1}{16}+\frac{xe^x}{16}Ei(x)\Big)$$
$$+b^3\Big(-\frac{1}{32x^3}+\frac{1}{96x^2}-\frac{1}{192x}+\frac{1}{192}-\frac{xe^x}{192}Ei(x)\Big)\Big]$$
$$+\frac{b^2e^{2x-2x}}{(1+b)^2}\Big[-\frac{1}{4x^2}+\Big(\frac{1}{4x^2}+\frac{1}{4x}\Big)e^xEi(x)$$
$$+\Big(-\frac{1}{4x^2}+\frac{1}{4x}\Big)e^{3x}Ei(3x)$$
$$+b\Big(-\frac{1}{8}+\Big[-\frac{1}{4x^2}-\frac{1}{16x}+\frac{1}{16}\Big]e^xEi(x)$$
$$-\frac{xe^{2x}}{32}Ei^2(x)+\Big[\frac{1}{2x^2}+\frac{x}{4}\Big]e^{2x}Ei(2x)$$
$$+\Big[-\frac{1}{4x^2}+\frac{1}{16x}+\frac{1}{16}\Big]e^{3x}Ei(3x)$$
$$+\frac{x}{16}\int_x^\infty\frac{e^xEi(3x)}{x}dx\Big)$$
$$+b^3\Big(\frac{1}{144x^2}-\frac{1}{144x}+\frac{7}{288}$$
$$+\Big[\frac{1}{32x^3}-\frac{1}{96x^2}+\frac{1}{192x}-\frac{1}{192}\Big]e^xEi(x)$$
$$+\frac{x}{384}e^{2x}Ei^2(x)-\frac{7x}{144}e^{2x}Ei(2x)$$
$$-\Big[\frac{1}{32x^3}+\frac{1}{96x^2}+\frac{1}{192x}+\frac{1}{192}\Big]e^{3x}Ei(3x)$$
$$-\frac{x}{192}\int_x^\infty\frac{e^xEi(3x)}{x}dx\Big)\Big]. \quad (6.7)$$

$$F_5(b,x)=\frac{be^{b-x}}{(1+b)}\Big[-\frac{1}{2x^3}-\frac{1}{6x^2}+\frac{1}{12x}$$
$$-\frac{1}{12}+\frac{xe^x}{12}Ei(x)\Big]. \quad (6.8)$$

(c) $S_n(b)$ Functions

$$S_3(b)=-b^2F_1'(b,b)/36. \quad (6.9)$$

For b small we have very nearly

$$S_3(b)\simeq 0.05556-0.05556b$$
$$+0.05903b^2-0.05960b^3. \quad (6.10)$$

For b large

$$S_3(b)\simeq 0.08333b^{-1}-0.3333b^{-2}+2.417b^{-3}. \quad (6.11)$$

$$S_{2,3}(b)=b^2F_4'(b,b)/36 \quad (6.12)$$
$$\simeq 0.01389b-0.02778b^2+0.04167b^3-0.05883b^4$$
$$+e^{2b}Ei(2b)[-0.02778b^2$$
$$+0.05556b^3-0.08333b^4]$$
$$+e^{3b}Ei(3b)[0.02778b^2-0.08333b^3$$
$$+0.1713b^4], \quad b\ll 1. \quad (6.13)$$
$$\simeq 0.02430b^{-2}-0.1557b^{-3}+1.103b^{-4},$$
$$b\gg 1. \quad (6.14)$$

$$S_4(b)=b^2\Big[F_3'(b,b)-\frac{b^3}{2}F_1'(b,b)F_5'(b,b)$$
$$+\frac{1}{2}F_1'(b,b)+\frac{1}{b}F_1(b,b)\Big]\Big/36, \quad (6.15)$$
$$\simeq -0.004633b-0.003067b^2$$
$$+0.009259b^3-0.01860b^4$$
$$+e^bEi(b)[0.01389b^2-0.01389b^3$$
$$+0.01678b^4], \quad b\ll 1, \quad (6.16)$$
$$\simeq -0.01042b^{-2}+0.1302b^{-3}-1.260b^{-4}. \quad (6.17)$$

(d) $S_n^*(b)$ Functions

$$S_3^*(b) = -b^2(1+b)F_1'(b,b)/36, \tag{6.18}$$

$$\simeq 0.05556 + 0.00347b^2 - 0.00579b^3, \quad b \ll 1, \tag{6.19}$$

$$\simeq 0.08333 - 0.25b^{-1} + 2.083b^{-2}, \quad b \gg 1. \tag{6.20}$$

$$S_{2,3}^*(b) = b^2(1+b)^2\left[F_4'(b,b) + \frac{b^2 e^{3b} Ei(3b)}{2(1+b)^2} F_1'(b,b)\right] \Big/ 36, \tag{6.21}$$

$$\simeq 0.01389b - e^{2b}Ei(2b)0.02778b^2 - e^{3b}Ei(3b)0.001630b^4, \quad b \ll 1, \tag{6.22}$$

$$\simeq 0.01041 - 0.04691b^{-1} + 0.3919b^{-2}, \quad b \gg 1. \tag{6.23}$$

$$S_4^*(b) = b^2(1+b)^2\left[F_3'(b,b) - \frac{b^3}{2}F_1'(b,b)F_5'(b,b) + \frac{1}{2}F_1'(b,b) + \frac{1}{b}F_1(b,b)\right] \Big/ 36, \tag{6.24}$$

$$\simeq -0.004633b - 0.01233b^2 - 0.001508b^3 - 0.003149b^4 + e^b Ei(b)[0.01389b^2 + 0.01389b^3 + 0.002890b^4], \quad b \ll 1. \tag{6.25}$$

$$\simeq -0.01042 + 0.1094b^{-1} - 1.010b^{-2}, \quad b \gg 1. \tag{6.26}$$

(e) $V_3(b)$ and $V_3^*(b)$ Functions

$$V_3(b) = \frac{1}{(1+b)^2}\left[\frac{1}{48} - \frac{b}{16} + \frac{61b^2}{1440} - \frac{b^3}{480} - \frac{b^4}{1080} + \frac{b^5}{1080} - \frac{b^6}{540} + e^b Ei(b)\left(-\frac{b^2}{24} + \frac{b^4}{288}\right) + e^{2b}Ei(2b)\left(\frac{b^2}{6} - \frac{b^3}{12} + \frac{b^7}{240}\right)\right] + \frac{F_1'(b,b)}{(1+b)}\left[\frac{b^2}{96} - \frac{5b^3}{288} - \frac{b^4}{576} + \frac{b^5}{576} + e^b Ei(b)\left(\frac{b^4}{48} - \frac{b^6}{576}\right)\right], \tag{6.27}$$

$$\simeq -0.02778b + 0.10009b^2 - 0.17362b^3 + e^b Ei(b)[-0.04167b + 0.04167b^2 - 0.04080b^3 + 0.043406^4] + e^{2b}Ei(2b)[0.16667b^2 - 0.41667b^3 + 0.6667b^4], \quad b \ll 1. \tag{6.28}$$

$$\simeq -0.25b^{-4} + 3.969b^{-5} - 46.16b^{-6}, \quad b \gg 1. \tag{6.29}$$

$$V_3^*(b) = V_3(b)(1+b)^2, \tag{6.30}$$

$$\simeq -0.02778b + 0.04453b^2 - 0.00122b^3 + e^b Ei(b)[-0.04167b - 0.04167b^2 + 0.00087b^3 + 0.00347b^4] + e^{2b}Ei(2b)[0.16667b^2 - 0.08333b^3], \quad b \ll 1 \tag{6.31}$$

$$\simeq -0.25b^{-2} + 3.469b^{-3} - 38.49b^{-4}, \quad b \gg 1. \tag{6.32}$$

THE JOURNAL OF CHEMICAL PHYSICS VOLUME 22, NUMBER 12 DECEMBER, 1954

Statistical Interpretations of Unimolecular Reaction Rates

HAROLD S. JOHNSTON AND JAMES R. WHITE
Department of Chemistry, Stanford University, Stanford, California

(Received March 4, 1954)

Consistency theorems are derived from the general Lindemann theory of unimolecular reaction rates; one can make several general statements about the signs of the slopes and curvatures of plots of observed rate constants against a function of the pressure. Observed rate constants and simple combinations of observed rate constants are interpreted in terms of Tolman's distribution function, the distribution of molecules which react. Moments of the ratio of rate constant for decomposition to that for deactivation by collision, c_i/b_i, can be found at any pressure. By means of Schwarz's inequality one can find several dimensionless quantities which provide consistency tests with respect to the statistical interpretations and which provide a check against a wrong assignment of the high- or low-pressure limit. These methods are used to examine the data for cyclobutane, cyclopropane, nitrogen pentoxide, and nitrous oxide. Previous interpretations given to the data on the last two cases are revised. The average detailed rate constants for molecules which react are estimated using an approximate relation.

INTRODUCTION

As we obtained experimental data on the unimolecular decomposition of nitrogen pentoxide (in the presence of nitric oxide) the data were interpreted and presented in terms of the general Lindemann theory instead of in terms of any of the detailed theories which use the same general mechanism.[1] It was felt that if a set of data could not fulfill the requirements of the general theory, there was no use in employing the data to test detailed theories (as originally obtained,[1] the data appeared to be in strong contradiction with Rice-Ramsperger-Kassel theory). Considerations of this kind led to the development of certain statistical interpretations and consistency tests, based primarily on the extremes of pressure, that is, either the high-pressure limit or the low-pressure limit. With these theorems we become suspicious of our early work at low pressures, and a reinvestigation revealed a systematic error, partial heterogeneity at very low pressures.[2] Using the general Lindemann theory, Kassel[3] has recently deduced several powerful consistency theorems and general interpretations; some of these theorems apply to all pressures and some are restricted to the middle region of pressure. Kassel found that our previous interpretations, based on the extremes of pressure, were inconsistent with the same data at the middle region of pressure. Kassel concluded (and we agree) that there must be some systematic error in the high-pressure region for nitrogen pentoxide and that certain slopes we were looking for[4] could not be found because of the masking effect of experimental error. These examples illustrate the power of the general theory in uncovering experimental error and faulty interpretations. Also it is obvious that consistency tests based on all the data are much better than those restricted to a limited portion. The present article extends our previous approach and that of Kassel to all pressures. The emphasis is on consistency tests so far as the raw data are concerned, statistical interpretations of various combinations of observable terms, and finally consistency tests on these statistical interpretations.

CONSISTENCY TESTS FOR RATE DATA

An abbreviated[4] yet adequate form of the general Lindemann mechanism is

$$\begin{aligned} A+M &\xrightarrow{a_i} A_i^*+M, \\ A_i^*+M &\xrightarrow{b_i} A+M, \\ A_i^* &\xrightarrow{c_i} \text{products}. \end{aligned} \tag{1}$$

The general expression for the first-order constant is

$$k=\sum_i \frac{a_i c_i [M]}{b_i [M]+c_i}. \tag{2}$$

From the nature of the problem a_i, b_i, c_i, and $[M]$ are all positive numbers or zero. Derivatives of k with respect to $[M]$ are

$$\frac{dk}{d[M]}=\sum_i \frac{a_i c_i^2}{(b_i[M]+c_i)^2}, \tag{3}$$

$$\frac{d^2k}{d[M]^2}=-\sum_i \frac{2a_i b_i c_i^2}{(b_i[M]+c_i)^3}. \tag{4}$$

One sees from these simple considerations that a plot of k *vs* $[M]$ has positive slope and negative curvature everywhere; there can be no inflection points. The inflection points reported by Hinshelwood and coworkers indicate that the reaction under consideration is one of a chemically complex mechanism and not an elementary unimolecular reaction;[5] the appeal to two

[1] R. L. Mills and H. S. Johnston, J. Am. Chem. Soc. **73**, 938 (1951).
[2] H. S. Johnston and R. L. Perrine, J. Am. Chem. Soc. **73**, 4782 (1951).
[3] L. S. Kassel, J. Chem. Phys. **21**, 1093 (1953).
[4] H. S. Johnston, J. Chem. Phys. **20**, 1103 (1952).
[5] Stubbs, Ingold, Spall, Danby, and Hinshelwood, Proc. Roy. Soc. (London) **A214**, 20 (1952).

modes of decomposition does not alter this conclusion since each must be of the form of (2). Similarly a plot of log k *vs* log $[M]$ has positive slope, varying from one to zero. A plot of k *vs* $1/[M]$ has negative slope and positive curvature everywhere, and it has a finite intercept at zero $1/[M]$. A plot of $1/k$ *vs* $1/[M]$ has positive slope and negative curvature. A plot of k', or $k/[M]$, *vs* $[M]$ has negative slope and positive curvature everywhere, and it has a finite intercept at $[M]=0$. A plot of log k' *vs* log $[M]$ has everywhere a negative slope varying from zero to one. These statements are valid whether the sum in (2) contains one term, more than one, or even an infinite number, and regardless of the actual or relative magnitudes of a_i, b_i, and c_i.

STATISTICAL INTERPRETATIONS

It is of interest to distinguish between three different distribution functions over the reacting states i, and these are: (i) the Maxwell-Boltzmann, $P_i=[A_i^*]_{eq}/[A]$; (ii) the actual or steady state, $Q_i=[A_i^*]/[A]$; and (iii) "the distribution function for molecules which react per unit time" or Tolman's[6] distribution function $T_i'=Q_ic_i$. The normalized Tolman distribution function T_i is given by $T_i=T_i'/k$. In terms of the Lindemann mechanism (1) the three distribution functions have the form

$$P_i=a_i/b_i, \tag{5}$$

$$Q_i=a_i[M]/(b_i[M]+c_i), \tag{6}$$

$$T_i'=kT_i=a_ic_i[M]/(b_i[M]+c_i), \tag{7}$$

$$=a_ic_i/(b_i+c_im), \tag{8}$$

where $m=1/[M]$. In previous articles we have substituted (5) into (2) and interpreted the expansion parameters at high and low pressures as averages over P_i.[2,4] These interpretations involved the difficulty of separating out intercepts and slopes from curvature for data of rather poor precision, and they were limited to a very narrow range of pressure. In the present article all interpretations are based on the normalized "distribution function for molecules which react," and the interpretations are based on closed algebraic expressions which are valid at all pressures. Even so, it is convenient to collect here several relations at the extremes of pressure. Define $X_i=c_i/b_i$, and define the nth moment of c_i/b_i over Tolman's distribution function as $\nu_n=\langle c^n/b^n\rangle_{Av}{}^T$. At $m=0$ or at infinite pressure, $T_i=T_i^\infty=a_ic_i/b_ik_\infty$. At $[M]=0$ or zero pressure, $T_i=T_i^0=a_i[M]/k_0=a_i/k_0'$. Expansion of (8) and (7), respectively, about $m=0$ and $[M]=0$ and summation over i gives[7]

$$k_H/k_\infty=1-\nu_1{}^\infty m+\nu_2{}^\infty m^2-\nu_3{}^\infty m^3+\cdots, \tag{9}$$

$$k'/k_0'=1-\nu_{-1}{}^0[M]+\nu_{-2}{}^0[M]^2-\nu_{-3}{}^0[M]^3+\cdots. \tag{10}$$

One is now prepared to use the definitions above to derive relations giving statistical interpretations to certain combinations of observable kinetic data. From definitions one may write down expressions valid at all pressures

$$k_\infty T_i^\infty/k=(1+X_i/[M])T_i, \tag{11}$$

$$k_0'T_i^0/k'=(1+[M]/X_i)T_i. \tag{12}$$

Multiply (11) and (12) by $X_i{}^n$ and sum over all states i, and obtain a recursion formula for the moments of c_i/b_i

$$\nu_{n+1}=(k_\infty\nu_n{}^\infty-k\nu_n)/k' \tag{13}$$

and a recursion formula for the negative moments of c_i/b_i, that is, moments of b_i/c_i

$$\nu_{n-1}=(k_0'\nu_n{}^0-k'\nu_n)/k. \tag{14}$$

When $n=0$, $\nu_n=1$, and thus is obtained a starting point for (13) and (14). In this case one obtains the interesting relations

$$\nu_1=\langle c/b\rangle_{Av}{}^T=(k_\infty-k)/k', \tag{15}$$

$$\nu_{-1}=\langle b/c\rangle_{Av}{}^T=(k_0'-k')/k. \tag{16}$$

These relations provide an upper limit on the range of validity of (9) and (10). When $k=k_\infty/2$, the average $\langle c/b[M]\rangle_{Av}{}^T$ is unity; the expansion (9) depends on the condition that $b_i[M]>c_i$ for all i; and thus it is clear that (9) represents a region of "falloff" of the first order constant of far less than 50 percent. Similarly it is seen that (10) represents a "falloff" of the second-order constant of far less than 50 percent.

For this paragraph only, the discussion will be less general than (1) which has three completely general and unspecified functions a_i, b_i, and c_i. We make the usual assumption about b_i, namely that it may be adequately approximated by the kinetic collision constant, and thus with the assignment of a kinetic collision diameter b may be computed. To this degree of approximation (15) and (16) taken on interpretations of considerable physical interest, that is, the average rate constant with respect to decomposition from the reacting states and the mean life with respect to decomposition of the molecules which react

$$\langle c\rangle_{Av}{}^T=(k_\infty-k)b/k', \tag{17}$$

$$\langle 1/c\rangle_{Av}{}^T=(k_0'-k')/bk. \tag{18}$$

[6] R. C. Tolman, J. Am. Chem. Soc. **42**, 2506 (1920); **47**, 2652 (1925). Tolman interpreted the energy of activation as the difference in the average energy of the molecules which react and the average energy of all molecules. His distribution function, "the molecules which react in unit time," is simply the product of the steady-state probability of a state Q_i times the rate constant for decomposition from that state c_i. Even more general than the Lindemann mechanism itself are the relations

$$-\frac{1}{[A]}\frac{d[A]}{dt}=k=\sum_i Q_ic_i=\sum_i T_i'.$$

From this relation it is seen that the first-order rate constant is the normalization constant for the distribution function T_i'.

[7] Since $\nu_{-1}{}^0=\langle b/c\rangle_{Av}{}^0$, one must worry about the convergence of (10). One could certainly find mathematical functions for a_i, b_i, and c_i which would lead to divergence of (10). The mere occurrence of zeros in c_i does not cause this difficulty, although from (10) it would appear to do so. $T_i'=Q_ic_i$ is zero if c_i is zero, and thus such terms are absent from the sum giving k and are not included in the expansion giving (10).

The term c_i is strictly a mechanical (not a statistical) quantity, the probability of decomposition per unit time of an isolated molecule in the quantum state i. The change of $\langle c\rangle_{Av}{}^T$ and $\langle 1/c\rangle_{Av}{}^T$ with pressure is due entirely to a change in the distribution of molecules over the states which react, and it is of great interest to note the reflection of this changing distribution on the values of these averages.

The value of $(k_\infty - k)/k'$ assumes the indeterminate form of 0/0 at infinite pressure; however, from (9) it can be seen to converge to the finite value $\nu_1{}^\infty$. Thus from kinetic data one plots ν_1 *vs* $1/[M]$ (or $1/\nu_1$ *vs* $1/[M]$) to zero to get $\nu_1{}^\infty$. If this extrapolation is valid, one may use (13) to compute the second moment or $\langle c^2/b^2\rangle_{Av}{}^T$ as a function of pressure. From this one finds the variance $\mu_2 = \nu_2 - \nu_1{}^2 = \langle (X-\nu_1)^2\rangle_{Av}{}^T$. It should be emphasized that the values of ν_2 contain the accumulated errors of k, k_∞, ν_1, and $\nu_1{}^\infty$, and even the second moment requires excellent experimental data. If the precision of the data justify it, one may extrapolate ν_2 to zero $1/[M]$ to get $\nu_2{}^\infty$ and thus ν_3, and similarly to build up to ν_4. If one had four such moments, one could evaluate the statistical parameters giving the mean, spread, asymmetry, and kurtosis of a plot of T_i *vs* X_i at every pressure. However repeated use of (13) causes an accumulation of experimental error, and even with the best data available at present, no more than two (or at most three) moments are reliable, as will be shown below. In an exactly parallel manner one may use (14) to build up a series of moments of b_i/c_i if one has the low-pressure second-order limit. Here, too, because of experimental error only a small number, one or at most two, are accessible at present.

TESTS FOR THE CONSISTENCY OF THESE STATISTICAL INTERPRETATIONS

For a given set of data it is certain that (13) and (14) must eventually break down because of experimental error. It is very easy in a case like this to overinterpret the data. Fortunately, there exist stringent inequality relations among moments which check gross abuses of this sort. By use of Schwarz' inequality one may write down various relations, one of the most interesting being

$$J = \left(\frac{k_\infty - k}{k}\right)\left(\frac{k_0' - k'}{k'}\right) = \nu_1\nu_{-1} \geq 1. \qquad (19)$$

At the high concentration limit J reduces to the quantity F previously defined,[4] and at the low limit J becomes G.[4] Furthermore, if J has the limiting value of unity, (19) becomes

$$\frac{1}{k} = \frac{1}{k_\infty} + \frac{1}{k_0'[M]}, \qquad (20)$$

which is referred to as Hinshelwood's first theory, that is, the case of only one term in the summation (2). Other relations based on Schwarz' inequality are

$$L = \nu_2/\nu_1{}^2 \geq 1, \qquad (21)$$

$$H = \nu_{-2}/\nu_{-1}{}^2 \geq 1. \qquad (22)$$

TABLE I. Cyclobutane at 449°C.

M m/cc×10⁸	k sec⁻¹×10⁴	ν_1 m/cc×10⁸	$(\mu_2)^{\frac{1}{2}}$ m/cc×10⁸	L
∞	5.06	2.91	(3.2)	(2.2)
178	4.98	2.91	···	
113	4.94	2.80	···	
42.2	4.78	2.49	···	
34.2	4.68	2.79	···	
21.3	4.49	2.71	···	
11.5	4.24	2.23	3.1	2.9
2.44	3.30	1.30	2.5	4.6
1.73	3.15	1.05	2.3	5.7
1.49	3.00	1.02	2.2	5.6
1.24	2.91	0.92	2.1	6.1
0.93	2.67	0.84	1.9	5.2
0.49	2.26	0.61	1.6	7.9

TABLE II. Cyclopropane, corrected to 500°C.

M m/cc×10⁸	k sec⁻¹×10⁴	ν_1 m/cc×10⁸	$(\mu_2)^{\frac{1}{2}}$ m/cc×10⁸	L
	6.17	60.1	71	2.4
	Pritchard, Sowden, and Trotman-Dickenson			
200	4.90	51.8	46	1.8
88.9	4.61	30.0	60	5.0
88.6	4.43	34.8	56	3.6
88.2	4.48	33.3	57	4.0
35.0	3.72	23.0	46	5.0
26.2	3.67	17.8	43	6.8
16.2	3.23	14.7	37	7.5
15.2	3.19	14.2	37	7.7
14.5	3.30	12.6	36	9.1
11.9	3.17	11.3	34	9.9
7.81	2.66	10.3	30	9.5
6.90	2.48	10.3	29	9.2
5.83	2.48	8.68	27	11
4.95	2.28	8.45	26	11
4.06	2.25	7.07	24	13
3.26	2.14	6.14	22	14
3.05	2.01	6.31	22	14
2.34	1.80	5.68	21	14
2.05	1.69	5.43	20	15
1.51	1.51	4.66	18	17
1.35	1.41	4.56	18	17
1.18	1.29	4.46	18	17
0.885	1.19	3.70	16	20
0.848	1.13	3.78	16	19
0.710	0.995	3.69	16	19
0.581	1.01	2.97	14	24
0.529	0.960	2.87	14	25
0.446	0.840	2.83	14	24
0.405	0.795	2.74	14	25
0.362	0.760	2.58	13	26
0.319	0.686	2.55	13	26
0.286	0.640	2.47	13	27
0.245	0.656	2.06	12	33
0.224	0.577	2.17	12	31
0.160	0.500	1.81	11	36
	Chambers and Kistiakowsky			
1460	5.94	55.3	86	3.4
780	5.76	56.3	57	2.0
402	5.51	48.2	73	2.5
218	5.11	45.2	62	2.9
112	4.77	33.0	63	4.6
76.3	4.58	26.5	59	5.9
51.7	4.12	25.8	52	5.0
29.5	3.78	18.6	45	6.7

TABLE III. Nitrogen pentoxide in the presence of nitric oxide at 27°.

M m/cc×10⁸	k sec⁻¹	ν_1 m/cc×10⁵	ν_{-1} cc/m×10⁻⁶	J
0		0.11	16	18
1	0.0023	0.12	14	17
2	0.0041	0.14	14	20
3	0.0054	0.16	15	24
5	0.0076	0.18	14	27
7	0.0093	0.21	14	29
10	0.0117	0.24	12	30
20	0.0175	0.31	10	31
30	0.0217	0.37	8.8	32
50	0.0285	0.46	7.2	33
70	0.0342	0.52	6.2	33
100	0.041	0.61	5.4	33
200	0.057	0.86	4.1	35
300	0.077	0.94	3.4	32
500	0.088	1.2	2.8	32
700	0.104	1.2	2.4	30
1000	0.123	1.4	2.0	28

$k_\infty = 0.29$ sec⁻¹ $k_0' = 2.62\times10^5$ cc mole⁻¹ sec⁻¹

At the low-pressure limit L reduces to F, and at the high-pressure limit H becomes G. Thus one has the consistency tests $J_\infty = L_0$, $J_0 = H_\infty$. Other terms which must be equal to or greater than one are

$$\nu_1\nu_3/\nu_2^2, \quad \nu_2\nu_4/\nu_3^2, \quad \text{etc.} \tag{23}$$

As one goes up a sequence of terms $\nu_n\nu_{n+2}/(\nu_{n+1})^2$, one notes that the high-pressure limit of one such term is the low-pressure limit of the next higher term. Similar relations apply for negative moments. We have noted that when (13) or (14) is pushed too far, the values of terms such as (23) become less than one. Also when one extrapolates a plot of $1/k$ *vs* $1/[M]$ too far, the nominal value of k_∞ and the slope produce unsatisfactory values of L, H, and the terms in (23). Likewise a wrong assignment of k_0' produces impossible values of L, H, etc. The value of J is relatively insensitive to a wrong choice of k_∞ and k_0'.

APPLICATION TO EXPERIMENTAL DATA

Cyclobutane

The data of Walters and co-workers[8] on cyclobutane provide an excellent case of a precise detailed study of the falloff of the rate constant with pressure in the high-pressure region. From one apparatus to another there may be a difference of 2 or 3 percent, but in one apparatus the precision seems to be good almost to one percent. The work in one bulb from 90 to 742 mm clearly shows that the first-order rate constant has its high-pressure value. The work from 0.2 to 80 mm gives a detailed falloff below this value. The data do not approach the low-pressure limit which probably occurs around 10^{-4} mm. Thus these data provide an excellent test of (13), (15), (17), and L, but they cannot be used for the corresponding low-pressure values nor for J. The successive extrapolations to the high-concentration intercept were made as $1/k$ *vs* $1/[M]$. The values of the various terms are listed in Table I.

One of the most impressive features of this table is the large magnitude of the spread. At infinite pressure the spread $(\mu_2)^{\frac{1}{2}}$ is slightly larger than the mean, and since all quantities are non-negative, this demonstrates asymmetry. At lower pressures the average ν_1 decreases faster than k, but the spread decreases slower than k. Thus at 2.4×10^{-8} m cc⁻¹, the standard deviation is twice the mean, implying a highly asymmetrical distribution function. At the lowest pressures this trend has continued, the relative spread and asymmetry increased as pressure decreased. The dimensionless number L, which would be unity if (2) had only one value of c_i/b_i, increases as pressure decreases, and it is substantially larger than one throughout.

An effort was made to calculate the third and fourth moments. The third moments did not lead to any contradiction with Schwarz' inequality but the fourth one did, and this casts doubt on the validity of the third one also. Although the numerical values of the third moment are probably of no real significance, the trend was in the direction of increasing asymmetry as the pressure decreased.

Cyclopropane[9]

The data for cyclopropane are more extensive than those for cyclobutane. The high concentration limit is covered in detail, and although a very considerable region of "falloff" is covered, the data do not give the low concentration limit. The data of Pritchard, Sowden, and Trotman-Dickenson were corrected to 500°C to

TABLE IV. Nitrogen pentoxide in the presence of nitric oxide at 50.1°.

M m/cc×10⁸	k sec⁻¹	ν_1 m/cc×10⁵	ν_{-1} cc/m×10⁻⁶	J
0			14	
0.64	0.0141	0.24	13	31
1.45	0.0283	0.28	15	42
1.89	0.0330	0.31	19	59
2.69	0.0512	0.28	9	26
3.13	0.0630	0.27	6	16
3.68	0.0597	0.33	13	42
3.82	0.0578	0.36	15	54
3.96	0.0627	0.34	13	43
4.59	0.0655	0.38	14	55
4.64	0.0643	0.39	15	60
5.44	0.0676	0.44	17	73
5.76	0.0763	0.41	14	57
6.14	0.0781	0.42	14	60
6.41	0.0824	0.42	13	57
6.08	0.0817	0.40	13	51
7.01	0.0770	0.49	17	82
7.06	0.0834	0.46	14	66
7.80	0.0856	0.49	15	74
8.50	0.0913	0.50	14	73

$k_\infty = 5.5$ sec⁻¹ $k_0' = 23.8\times10^5$ cc mole⁻¹ sec⁻¹

[8] Genaux, Kern, and Walters, J. Am. Chem. Soc. **75**, 6196 (1953); and private communication from Professor Walters.

[9] Pritchard, Sowden, and Trotman-Dickenson, Proc. Roy. Soc. (London) **A217**, 563 (1953); and private communication from Trotman-Dickenson. T. S. Chambers and G. B. Kistiakowsky, J. Am. Chem. Soc. **56**, 399 (1934).

correspond with the conditions of Chambers and Kistiakowsky. The values of the moments are given in Table II.

Exactly the same pattern of trends is seen here as for cyclobutane. At high pressures the distribution function for molecules which react is only slightly asymmetrical, when plotted against c_i/b_i, and it has a very broad spread. At lower pressures the spread decreases but relative to the mean it increases, and the asymmetry increases enormously. The value of L at low pressures is more than thirty, and since at zero pressure it becomes F, one sees that the low-pressure limit lies far below the lowest pressure attained. Since observations already include a range of 10^4 in $[M]$, this conclusions confirms that based on nitrous oxide and on nitrogen pentoxide that the pressure range from high to low limits is something like 10^5 or 10^6 or more.

Nitrogen Pentoxide

The experimental error for this case is much greater than that of the two previous cases. The values of k_0' are fairly well known and that of k_∞ is known approximately at one temperature. Thus values of ν_1, ν_{-1} and J can be computed, but higher moments are inaccessible from these data. In this laboratory we have obtained over 800 runs on the decomposition of nitrogen pentoxide in the presence of nitric oxide, and for this presentation a drastic condensation is necessary. The equivalent concentration[10] was computed for all of Mills' runs[1] with pure reactants, nitrogen, carbon dioxide, and argon and for all of Perrine's runs[2] at 27°, and a plot was made of log k *vs* log[**M**]. A smooth curve was drawn in and points from this curve are given in Table III. A set of unsmoothed data is given in Table IV for runs made at low pressures at 50.1°.

From these tables it appears that J may be almost constant over a wide range of intermediate pressures, but it falls off at very low pressures. The values of J at 27° are about 20 to 30, whereas the end values deduced by the previous method[4] was 11 and 3. In the present method J is evaluated from a closed exact formula, but the previous method relied on separating out slopes from curvature in regions of large experimental error. Thus we agree with Kassel[3] that the slopes at the extremes of pressure are not known from these data and the older values of F and G are invalid. The values of ν_{-1} at very low pressures are the same within experimental error at 27° and 50°. This confirms the previous[4] belief that at low pressures the average of $1/c_i$ is dominated by the lowest value of c_i, and thus the average $\langle 1/c \rangle$ is very nearly equal to the reciprocal of the minimum value of c and is thus temperature independent. The values of ν_1 and of J increase with temperature, and thus comparison from one molecule to another is complicated by the temperature effect.

TABLE V. Nitrous oxide at 615°C.

M m/cc×10⁴	k sec⁻¹×10⁴	ν_1 m/cc×10⁴	ν_{-1} cc/m×10⁻⁴	J
0	...	...	7	...
0.005	0.0695	0.53	8.6	4.6
0.010	0.136	0.54	6.6	3.6
0.025	0.328	0.54	4.2	2.3
0.050	0.506	0.69	8.6	6.0
0.100	0.830	0.80	7.5	6.0
0.250	1.21	1.3	8.0	10.4
0.500	1.86	1.5	5.8	8.7
1.00	2.62	1.8	4.5	8.4
2.50	3.92	2.3	3.3	7.5
5.00	5.19	2.2	2.6	5.7

TABLE VI. Average rate constants for molecules which react at high pressures.

Molecule	Temp. °K	E_c/RT	$\langle c \rangle_{Av}{}^T$ sec⁻¹×10⁻⁸	Atoms in molecule
Cyclobutane	722	43	0.03	12
Cyclopropane	773	42	0.60	9
	743	44	0.48	
Nitrogen pentoxide	300	37	14	7
Nitrous oxide	888	35	200	3

Nitrous Oxide

The data for nitrous oxide are even worse than those for nitrogen pentoxide. By means of the consistency tests outlined in this article, we believe that both k_∞ and k_0' are in doubt, though a rough estimate has been made for each. We believe that these data should not be used for a close test of reaction rate theories. For purposes of rough comparisons, the interpolated points[11] at 888°K are given in Table V with ν_1, ν_{-1}, and J. Again one concludes that J_0 and J_∞ based on slopes at the extremes of pressure[3,4] are invalid. In other respects these data agree with those for nitrogen pentoxide within experimental error, although the apparent decrease in J at high pressures is probably not real.

Using (19) to evaluate the average value of c_i (or to give its upper limit if deactivation does not occur at every collision), one finds the values given in Table VI. In spite of the fact that E_c/RT differ slightly, in spite of the crudity of the assumption behind (19), and in spite of experimental error, Table VI shows a strong correlation between molecular complexity and average rate constant for these four molecules. It is seen that as the number of atoms decreases, the average rate constant increases rapidly. To this same degree of approximation every value of ν_1 in the preceding tables becomes a value of $\langle c \rangle_{Av}{}^T$ if multiplied by 10^{14} cc mole^{-1} sec^{-1}.

[10] H. S. Johnston, J. Am. Chem. Soc. **75**, 1567 (1953).

[11] H. S. Johnston, J. Chem. Phys. **19**, 663 (1951).

Hybridization and Ionic Character in CH_3Cl*

PAUL N. SCHATZ
Metcalf Chemical Laboratories, Brown University, Providence, Rhode Island
(Received April 12, 1954)

The quadrupole coupling constant and dipole moment of the CH_3Cl molecule have been investigated as functions of the hybridization and ionic character. It is found that somewhat different results are obtained if one includes the effect of overlap in calculating the quadrupole coupling constant. The inclusion of overlap is contrary to the usual assumption that the quadrupole coupling constant arising from a purely covalent chlorine p bond is the same as the quadrupole coupling constant of a free chlorine atom. The results suggest that more s hybridization of the chlorine bonding wave function occurs than is assumed by Townes and Dailey and there is some indication of the occurrence of an appreciable amount of $3d$ character in this function. No precise assignment of values for the ionic character and hybridization appeared feasible.

INTRODUCTION

QUADRUPOLE coupling constants have been used quite extensively, in a semiquantitative way, to determine the character of bonds in a variety of simple molecules.[1,2] For example, Townes and Dailey have tentatively concluded that the C—Cl bond in CH_3Cl is an 80 percent covalent 20 percent ionic hybrid with the chlorine bonding orbital containing about 18 percent s character.[1] Similar reasoning led to the conclusion that the bonding orbitals in Cl_2 are essentially pure p in character.[3] However, it has recently been shown[4] that if one includes the overlap integral between the two bonding orbitals, then the formation of the Cl—Cl bond distorts the charge distribution sufficiently so that roughly 17 percent s hybridization is needed to account for the measured quadrupole coupling constant. In the case of HCl, the inclusion of overlap gives rise to a quadrupole coupling constant of about -128.5 Mc[5] for a purely covalent p bond rather than -110.4 Mc (the quadrupole coupling constant of a free Cl^{35} atom). Such calculations involve the assumption that the inclusion of overlap terms will, in fact, improve the agreement between calculated and experimental quadrupole coupling constants. Since the wave functions used in such calculations are quite approximate, it is not possible to ascertain with certainty the validity of this assumption. However, it would certainly seem to be of interest to explore the effect of ionic character and hybridization on the quadrupole coupling constant of other simple molecules without neglecting the overlap terms. This paper reports some results obtained for CH_3Cl. In an attempt to fix more than one parameter, it seemed desirable to examine the effect of these same parameters on the dipole moment although the simple model employed in this work may be inadequate for this purpose because of the extreme sensitivity of the dipole moment to small shifts in the charge distribution.

* Supported by the Office of Naval Research under Contract N6ori-88, Task Order 1.

[1] C. H. Townes and B. P. Dailey, J. Chem. Phys. **17**, 782 (1949).
[2] B. P. Dailey, J. Phys. Chem. **57**, 490 (1953).
[3] R. Livingston, J. Chem. Phys. **19**, 803 (1951); J. Phys. Chem. **57**, 496 (1953).
[4] P. N. Schatz, J. Chem. Phys. **22**, 755 (1954).
[5] P. N. Schatz, J. Chem. Phys. **22**, 695 (1954).

CALCULATIONS AND RESULTS

The threefold axis of CH_3Cl was chosen to coincide with the z axis of a Cartesian coordinate system. The carbon atom is at the origin with the chlorine atom along the positive z direction. The three tetrahedral carbon orbitals bonded respectively to hydrogens 1, 2, and 3 (h_1, h_2, and h_3) are labelled C_1, C_2, and C_3. Orbital C_4 is bonded to the chlorine atom whose bonding orbital is labelled Cl_b.

The CH_3Cl molecule has been described by the following wave function

$$\Psi=\psi_{\text{covalent}}+\lambda\psi_{\text{ionic}}. \tag{1}$$

Eight electrons have been explicitly considered in these wave functions corresponding to the four valence bonds formed by the carbon atom. ψ_{covalent} was formed in the usual way.[6] Simonetta and Schomaker[7] have discussed the modifications in the covalent wave function which are necessary in order to describe an ionic structure. In the present work, the ionic wave function used corresponds to the structure

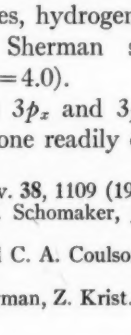

The following atomic orbitals were used; for the hydrogen atoms, hydrogen $1s$ wave functions with the screening constant equal to 1.10; for the carbon atom, tetrahedral orbitals employing carbon $2s$ and $2p$ functions given by Duncanson and Coulson;[8] for the chlorine $3s$, $3p_z$, and $3d_z$ states, hydrogen-like wave functions with Pauling and Sherman screening constants[9] ($Z_s=8.4$, $Z_p=6.5$, $Z_d=4.0$).

Assuming that the $3p_x$ and $3p_y$ chlorine electrons remain unperturbed, one readily obtains the following

[6] J. C. Slater, Phys. Rev. **38**, 1109 (1931).
[7] M. Simonetta and V. Schomaker, J. Chem. Phys. **19**, 649 (1951).
[8] W. E. Duncanson and C. A. Coulson, Proc. Roy. Soc. Edinburgh **62A**, 37 (1944).
[9] L. Pauling and J. Sherman, Z. Krist. **81**, 1 (1932).

expression for the dipole moment (in Debye units),

$$\mu=[4.2917A-8\bar{Z}_b-2\bar{Z}_{nb}]e. \quad (2)$$

Here $\bar{Z}_b$ is the average value of the Z coordinate of a bonding electron in A and $\bar{Z}_{nb}$ is the same quantity for a nonbonding electron. (In the case of zero hybridization this nonbonding pair is just the $3s$ electron pair. When hybridization occurs this pair will in general be an $s-p_Z$ hybrid[10]). $e=4.802\times10^{-10}$ esu. The structural parameters used were taken from some recent microwave work reported by Townes *et al.*[11] $\mu=-1.87d$[12] (chlorine negative end of dipole). The bonding and nonbonding wave functions were respectively of the form

$$\psi_{Cl_b}=a\psi_{3s}+b\psi_{3p_Z}+c\psi_{3d_Z}, \quad (3)$$

$$\psi_{Cl_{nb}}=a'\psi_{3s}+b'\psi_{3p_Z}. \quad (4)$$

In order that these functions be normalized and orthogonal, it follows that $a^2+b^2+c^2=a'^2+b'^2=1$; $a'a+b'b=0$.

TABLE I. Molecular integrals. $S_{ab}\equiv\int\psi_a^*\psi_b d\tau$, $M_{ab}\equiv\int\psi_a^*Z\psi_b d\tau$. Two-center integrals are evaluated with the carbon atom as origin. The one-center integrals are evaluated with the center in question as the origin.

Two-center				One-center	
$S_{h_1h_2}$ =	0.217	$M_{h_1h_2}$ =	−0.07605A	$M_{C_sC_{p(Z)}}$ =	0.4732A
$S_{C_1h_1}$ =	0.688	$M_{C_1h_1}$ =	−0.1870A	$M_{Cl_sCl_{p(Z)}}$ =	0.5031A
$S_{C_4Cl_s}$ =	0.315	$M_{C_4Cl_s}$ =	0.3580A	$M_{Cl_pCl_d}$ =	0.5366A
$S_{C_4Cl_p}$ =	0.476	$M_{C_4Cl_p}$ =	0.3320A	$M_{Cl_sCl_d}$ =	0
$S_{C_4Cl_d}$ =	0.356	$M_{C_4Cl_d}$ =	0.1823A	$M_{C_1C_1}$ =	−0.1366A
$S_{C_4h_1}$ =	0.121	$M_{C_4h_1}$ =	−0.00068A	$M_{C_1C_2}$ =	−0.1366A
$S_{C_2h_1}$ =	0.121	$M_{C_2h_1}$ =	−0.00068A	$M_{C_4C_4}$ =	0.4098A
$S_{C_1Cl_s}$ =	−0.004	$M_{C_1Cl_s}$ =	0.0078A	$M_{C_1C_4}$ =	0.1366A
$S_{C_1Cl_p}$ =	0.077	$M_{C_1Cl_p}$ =	0.01562A		
$S_{C_1Cl_d}$ =	0.158	$M_{C_1Cl_d}$ =	−0.02526A		
$S_{h_1Cl_s}$ =	0.049	$M_{h_1Cl_s}$ =	0.07886A		
$S_{h_1Cl_p}$ ≈	0.125	$M_{h_1Cl_p}$ ≈	0.07696A		
$S_{h_1Cl_d}$ ≈	0.17	$M_{h_1Cl_d}$ ≈	−0.00265A		

The values of the various molecular integrals are listed in Table I. Most of these integrals were evaluated using Mulliken's tables of overlap integrals.[13] Some use was also made of a table published by Jaffe.[14] Although these tables of integrals are tabulated for Slater functions, the integrals occurring in the present work could be expressed as appropriate linear combinations of Slater functions most of which were tabulated in the tables. In the few cases where it was necessary to explicitly evaluate integrals, the usual methods were used.[13] The values of the integrals $S_{h_1Cl_p}$, $S_{h_1Cl_d}$, $M_{h_1Cl_p}$, and $M_{h_1Cl_d}$ are only approximate.

The chlorine quadrupole coupling constant may be considered as arising from three separate factors: (1) the bonding electrons, (2) the pairs of $3p_x$ and $3p_y$ electrons, (3) the nonbonding pair, which makes a nonzero contribution whenever $s-p_Z$ hybridization occurs. All other contributions are considered negligible.[1,15] Proceeding in the same manner as for HCl[5] and using the same notation, one obtains the following expression for the total quadrupole coupling constant

$$eq_rQ=[q_b-2q_{p_Z}+q_{nb}]eQ, \quad (5)$$

or

$$eq_rQ=110.4\text{ Mc}[\alpha+2b'^2-2], \quad (6)$$

where α is defined by the equation

$$q_b=\alpha q_{p_Z}. \quad (7)$$

The following experimental relationship has been used throughout:

$$eQ\int\psi_{3p_Z}^2[3\cos^2\theta-1/r^3]d\tau\equiv eQq_{p_Z}=110.4\text{ Mc}^1. \quad (8)$$

The results of the calculations are shown in Figs. 1–3. Figure 1 shows the calculated quadrupole coupling constant as a function of ionic character for various

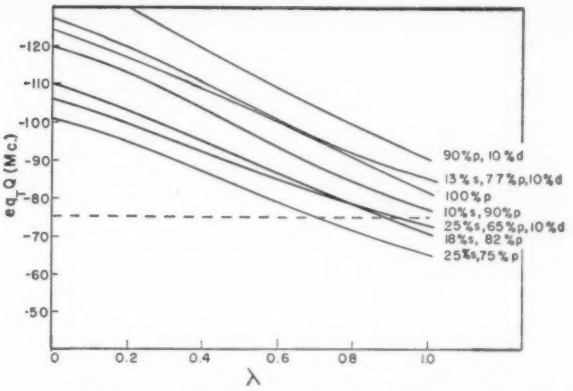

FIG. 1. Quadrupole coupling constant of CH_3Cl as a function of ionic character for various states of hybridization of the chlorine atom. The dotted line is the experimental value.

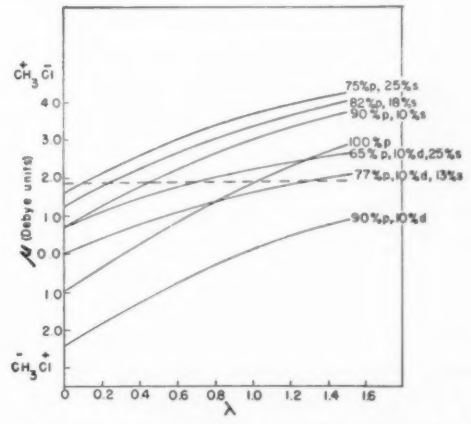

FIG. 2. Dipole moment of CH_3Cl as a function of ionic character for various states of hybridization of the chlorine atom. The dotted line is the experimental value.

[10] D. Z. Robinson, J. Chem. Phys. **17**, 1022 (1949).
[11] Miller, Aamodt, Dousmanis, Townes, and Kraitchman, J. Chem. Phys. **20**, 1112 (1952).
[12] Shulman, Dailey, and Townes, Phys. Rev. **78**, 145 (1950).
[13] Mulliken, Rieke, Orloff, and Orloff, J. Chem. Phys. **17**, 1248 (1949).
[14] H. H. Jaffe and G. O. Doak, J. Chem. Phys. **21**, 196 (1953).
[15] C. H. Townes and B. P. Dailey, J. Chem. Phys. **20**, 35 (1952).

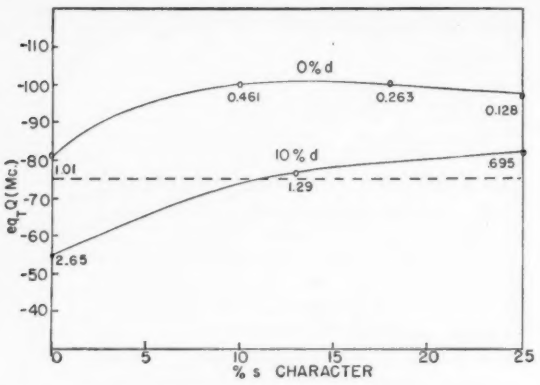

FIG. 3. Quadrupole coupling constant of CH_3Cl for various states of hybridization of the chlorine atom. The value of λ, indicated at various points by the numbers along the curves, was chosen in all cases to give the experimental dipole moment. The dotted line is the experimental value of the CH_3Cl quadrupcle coupling constant.

hybridizations, and Fig. 2 shows a similar plot of the calculated dipole moment. Figure 3 shows the calculated quadrupole coupling constant at various hybridizations, the coefficient of the ionic wave function (λ) having been chosen so that the experimentally observed dipole moment is obtained by using Eq. (2). Values of λ are indicated by numbers at various points along the curves.

In all cases, the dotted horizontal lines represent the experimental results.

CONCLUSIONS

The curves in Fig. 1 show the behavior one would expect. For any particular value of λ one obtains a lower quadrupole coupling constant as the s hybridization is increased. If one assumes a value of λ in the vicinity of 0.5 to be reasonable, then Fig. 1 indicates the occurrence of a large amount of hybridization (i.e., >25 percent s character). It will be observed that the introduction of d character at any given value of λ raises the quadrupole coupling constant. This was pointed out by Townes and Dailey.[1]

Whereas the usual method of interpretation[1] assumes the quadrupole coupling constant of a purely covalent chlorine p bond ($\lambda=0, b=1$) to be -110.4 Mc, Fig. 1 indicates a value of about -127 Mc. So once again, as in the cases of HCl[5] and Cl_2[4], the neglect of the effect of overlap makes a considerable difference.

Figure 2 shows the same qualitative features found by Robinson for HCl[10]. The dipole moment is a sensitive function of both the ionic character and the state of hybridization, and it is not possible to specify either parameter with any great precision. At any given value of λ the introduction of d character decreases the dipole moment.

Figure 3 represents an attempt to account simultaneously for both the experimental dipole moment and the experimental quadrupole coupling constant. The upper curve indicates that if the chlorine bonding function is an $s-p$ hybrid, then there is no way of adjusting simultaneously both the hybridization and the ionic character of this very simple description to account for both experimental quantities. The predicted quadrupole coupling constant is close to the experimental value only at very small hybridizations, but the amount of ionic character required then seems unreasonably large.

The lower curve in Fig. 3 shows the results of a calculation in which it has been assumed that the chlorine bonding wave function is an spd hybrid containing 10 percent d character. It has also been assumed that the nonbonding wave function remains an $s-p$ hybrid in view of the very large promotion energy which would be involved if d_z character were included. The nonbonding wave function is kept orthogonal to the bonding wave function.

This calculation gives better agreement with the experimental quadrupole coupling constant and with a more reasonable value of λ if a large amount of hybridization is used (i.e., >25 percent s). But it remains to be seen whether such a description is reasonable in view of the neglect of possible polarization of the $3p_x$ and $3p_y$ electrons.

The fact that it is difficult to fit both the dipole moment and quadrupole coupling constant is not too surprising. As Townes and Dailey have pointed out,[1] it is possible to change the dipole moment quite substantially even by polarization effects which change the quadrupole coupling constant very little.

In conclusion, the present results suggest that more s hybridization occurs than is assumed by Townes and Dailey[1] (or there is a much larger contribution from ionic structures than is ordinarily supposed). There is also some indication of an appreciable amount of d character in the chlorine bonding function. However, any precise assignment of values for the ionic character and hybridization would be quite arbitrary and no such assignment has been attempted. The situation is further complicated by the possible occurrence of an appreciable amount of polarization of the $3p_x$ and $3p_y$ electron pairs. Such polarization would lower the calculated quadrupole coupling constant thus necessitating smaller amounts of hybridization and ionic character to obtain agreement with experiment.

Finally, it might be noted that the distinction between the existence of $s-p$ hybridization and ionic character is somewhat artificial since both effects result physically in an over-all shift of electronic charge toward the chlorine atom. This is emphasized particularly by the upper curve of Fig. 3 which is quite flat over a considerable range of hybridization. In that case, a whole range of values of λ and percent s character lead to approximately the same calculated quadrupole coupling constant and dipole moment.

I would like to thank Professor D. F. Hornig for numerous helpful suggestions.

THE JOURNAL OF CHEMICAL PHYSICS VOLUME 22, NUMBER 12 DECEMBER, 1954

Studies on a Group of Silicon Carbide Structures

RICHARD S. MITCHELL*
Mineralogical Laboratory, University of Michigan, Ann Arbor, Michigan
(Received May 10, 1954)

Morphological and structural details of silicon carbide type 141*R* are given. This polymorph, having a structure represented by the zigzag sequence 3333333333333332, is a member of the '3...2' rhombohedral series proposed by Ramsdell [Am. Mineralogist **32**, 64 (1947)].

A detailed study of the '3...2' series is undertaken, resulting in an empirical mechanism which can be used for the direct determination of the structure of any member of this series. Using this means the structure of the new polymorph 393*R* is suggested.

INTRODUCTION

WITH the discovery of each new polymorph of silicon carbide it becomes more evident that there is no limit to the possible modifications of this substance. Up to the present time, the structures of 15 types have been established. The largest structure of this group is 87*R*.[1] Types consisting of a larger number of layers have also been reported, but no satisfactory analysis of their structures has so far been advanced. Some of these types are ~270*R*,[2] 594*R*[3]; 141*R*, 168*R*, 192*R*,[4] and recently the writer has also identified 120*R*, 393*R*, 33*H*, 48*H*, and three specimens of 78*H*. In this paper a structure for type 141*R* is proposed which is in good agreement with the observed data. Upon the basis of this new structure as well as from previously known structures, the writer suggests a mechanism for the direct determination of the structures of an evidently common group of silicon carbide polymorphs. Using this means the structure of type 393*R* is proposed. Much work has also been done on the structures of some of the other types listed above, but at present no definite results can be reported.

DISCOVERY AND IDENTIFICATION OF 141*R*

Two specimens of silicon carbide 141*R* have been encountered at this laboratory. The first of these (No. 109), upon which all the structural work was based, was discovered in 1950. Though the presence of this form was first noticed on Weissenberg films, its exact identity was not determined until later by the use of the Laue method. The second specimen (No. 169) was discovered recently during an investigation, with the Laue method, of a number of silicon carbide crystals showing growth spirals. The x-ray patterns of these two specimens are identical.

Both specimens of silicon carbide 141*R* are coalesced with type 6*H*. The 6*H* Laue spots are valuable reference points in the identification of this new rhombohedral form. In any rhombohedral type (*xR*), the *range* from 10·0 to 10·*x* for *xR* coincides exactly with the range 10·0 to 10·6 for 6*H*. One must remember, however, that the 10·*l* reflections of the rhombodhedral *xR* are missing when $l-1\neq 3n$. It also follows that the range between two adjacent 6*H* reflections, e.g., 10·1 to 10·2, coincides exactly with 1/6 of the 10·0 to 10·*x* range of *xR*. Thus, if 6*H* spots were present on a film with unknown *xR* spots, one could identify the *xR* type by multiplying by 6 the number of spaces between the *xR* 10·*l* reflections that lie between any two adjacent 6*H* 10·*l* spots, counting, of course, the spaces between the missing reflections caused by the rhombohedral lattice. On the x-ray films 23.5 of these spaces lie between the known 10·1 and 10·2 6*H* reflections. The number of layers in the unknown type would, therefore, be $6\times 23.5=141$. A synthetic Laue pattern of silicon carbide 141*R* was also constructed according to the method previously described.[5] This corresponded exactly with the 10·*l* spots on the Laue film.

THE STRUCTURE OF 141*R*

Those 141*R* 10·*l* reflections which coincide most closely with 6*H* 10·*l* positions are of stronger intensity. This intensity coincidence is an indication of the presence of many 33 units, which characterize 6*H*, in the zigzag sequence of 141*R*. Assuming that many 33 units are necessary because of this intensity distribution, and also that the only numbers found in zigzag sequences are 2, 3, and 4,[6] the only possible way to complete the 141*R* cell is the arrangement 3333333333333332. The calculations for this sequence gave satisfactory agreement with the observed intensities of the films. Table I compares the calculated and observed intensities for this sequence. Other evidence supporting the validity of this sequence for the 141*R* structure is presented in a later section.

This new rhombohedral polymorph has the following (hexagonal) cell dimensions:

$$a_0=3.073\ kX,\dagger \quad c_0=354.33_3\ kX, \quad Z=141$$

* Present address: Department of Geology, University of Virginia, Charlottesville, Virginia.

[1] L. S. Ramsdell, Am. Mineralogist **32**, 64 (1947).

[2] G. S. Zhdanov and Z. V. Minervina, J. Exptl. Theoret. Phys. **17**, 3 (1947).

[3] Honjo, Miyake, and Tomita, Acta Cryst. **3**, 396 (1950).

[4] L. S. Ramsdell and R. S. Mitchell, Am. Mineralogist **38**, 56 (1953).

[5] R. S. Mitchell, Am. Mineralogist **38**, 60 (1953).

[6] L. S. Ramsdell and J. A. Kohn, Acta Cryst. **5**, 215 (1952).

† These dimensions are given in *kX* units to agree with the earlier published data which, although reported as Angstrom units, were really in *kX* units.

or, for rhombohedral axes,

$$a_{rh}=118.12_4\,kX,\quad \alpha=1°30',\quad Z=47.$$

The space group for 141*R* is *R3m*, as in the other known rhombohedral polymorphs. The zigzag sequence 3333333333333332, which must be repeated three times to give the complete unit cell, results in the following atomic positions:

47 *Si* at 0, 0, *rz*
47 *C* at 0, 0, *rz*+*p*
47 *Si* and 47 *C* at 1/3, 2/3, 2/3+the above coordinates
47 Si and 47 *C* at 2/3, 1/3, 1/3+the above coordinates.
r=0, 2, 6, 8, 12, 14, 18...48; 51, 54, 57, 60...93; 97, 99, 103, 105, 109, 111, 115...139.
z=1/141
p=(3/4) (1/141).

TABLE I. Comparison of observed and calculated intensities for some of the reflections of type 141*R*.

(10.*l*)	I_{calc}	I_{obs}	(10.*l*)	I_{calc}	I_{obs}
10.1	0.8	vvw?	10.$\bar{35}$	0.4	a
4	0.9	vvw?	$\bar{38}$	3.2	a
7	2.0	vvw	$\bar{41}$	1.5	a
10	1.2	vvw	$\bar{44}$	0.1	a
13	8.0	vw	$\bar{47}$	1000.0	vvs
16	6.5	vw	$\bar{50}$	2.1	a
19	21.9	w	$\bar{53}$	2.4	a
22	190.3	ms	$\bar{56}$	0.0	a
25	129.9	ms	$\bar{59}$	5.0	a
28	30.0	mw	$\bar{62}$	0.0	a
31	23.9	w	$\bar{65}$	1.7	vvw
34	25.9	w	$\bar{68}$	18.3	w
37	12.0	w	$\bar{71}$	685.8	vs
40	17.0	w	$\bar{74}$	19.2	w
43	52.5	m	$\bar{77}$	0.1	vw
46	740.4	vs	$\bar{80}$	5.7	vw
49	139.3	ms	$\bar{83}$	12.9	vw
52	21.9	w	$\bar{86}$	5.2	vvw
55	14.9	vw	$\bar{89}$	14.1	w
58	2.9	vw	$\bar{92}$	78.0	m
61	6.4	vw	$\bar{95}$	221.3	ms
64	4.5	w	$\bar{98}$	14.5	w
67	19.5	w?	$\bar{101}$	9.0	vw
70	744.9	vs	$\bar{104}$	6.0	vw
73	31.2	mw	$\bar{107}$	0.4	vw
76	7.9	vw	$\bar{110}$	0.4	vvw
10.$\bar{2}$	0.8	a	$\bar{113}$	7.9	vw
$\bar{5}$	0.4	a	$\bar{116}$	61.1	m
$\bar{8}$	0.5	a	$\bar{119}$	39.6	m
$1\bar{1}$	1.2	a	$\bar{122}$	4.9	vvw
$\bar{14}$	2.0	a	$\bar{125}$	0.7	vvw
$\bar{17}$	3.3	a	$\bar{128}$	13.4	vw
$\bar{20}$	7.9	...	$\bar{131}$	5.4	vvw
$\bar{23}$	479.6	s	$\bar{134}$	0.0	vvw
$\bar{26}$	27.0	w	$\bar{137}$	0.9	vvw
$\bar{29}$	3.0	vvw	$\bar{140}$	0.9	vvw
$\bar{32}$	1.4	a			

THE MORPHOLOGY OF 141*R*

Because two examples of 141*R* have been discovered it will be necessary to give separate descriptions of each of the specimens.

Crystal No. 109 is blue-gray in color and transparent; it measures about 1.00 mm long, 0.75 mm wide, and 0.25 mm thick. It is tabular parallel to (0001), the two pinacoids being the largest and best developed faces present.

Of the six trigonal pyramid zones, only four have measurable faces, giving goniometer signals of varying quality. There is a striking resemblance between the character of the pyramid faces as observed in the optical goniometer and the reflections of the corresponding 10.*l* planes that exist on x-ray films. In fact a photograph of a series of these goniometer signals would give a fair picture of the 10.*l* reflections observed on a Buerger precession film. Table II is a summary of the various forms observed on the crystal. The quality of the goniometer signal is divided into the two components, intensity and amount of lateral blurring. In attempting a comparison of these data with the x-ray data of Table I or Fig. 1, one should consider the more intense reflections in the cases where two intensities are reported. The goniometer reflections which are much blurred, compare, in general, with the regions on the x-ray film where whole groups of weak or very weak reflections occur. These correspond also with the *clusters* of reflections lying around points *F'*, *B*, and *C* in the graph of calculated 141*R* intensities shown on Fig. 1. The faces which are sharper and of a higher intensity correspond, in general, to reflections on the

TABLE II. Morphological data for SiC type 141*R*.

Form	No. times observed	Quality *I*	Quality Amt. blurred	Angle between form and base Observed	Angle between form and base Calculated[a]
00.1	2	s	none	0°	0°
10.$\bar{1}\bar{2}\bar{2}$	1	vw	much	~47°	47°30′
10.$\bar{1}\bar{1}\bar{9}$	2	w	much	48°16′	48°13′
10.$\bar{1}\bar{1}\bar{6}$	1	vw	much	~48°50′	48°56′
10.$\bar{9}\bar{5}$	2	mw-vvw	some	~54°–54°52′	54°30′
10.$\bar{7}\bar{1}$	3	ms-vvw	none to some	61°45′–62°0′	61°56′
10.$\bar{4}\bar{7}$	3	ms-vvw	some	70°38′–70°52′	70°33′
10.$\bar{2}\bar{6}$?	1	vvw	much	~79°	78°57′
10.$\bar{2}\bar{3}$	3	ms-vvw	some to much	80°0′–80°5′	80°12′
10.$1\bar{1}$	1	vw	some	84°57′	85°17′
10.$\bar{8}$	1	vw	much	~85°53′	86°34′
10.0 / 10.1	4	w-vw	much	89°48′–~90°	90°00′ / 89°34′
10.4?	1	vw	some	88°14′	88°17′
10.16	1	vvw	much	~83°	83°09′
10.19	3	m-vw	much	~82°	81°53′
10.22	3	m-vw	v. much	~80°41′	80°37′
10.25	3	m-vw	some to much	~79°40′	79°22′
10.28	3	vvw	much	~78°	78°07′
10.31	1	vvw	much	~77°	76°54′
10.43	2	vw	some to much	72° 1′–72°7′	72°6′
10.46	4	mw-w	some to much	70°44′–70°53′	70°56′
10.49	2	w-vvw	much	69°38′–~70°	69°48′
10.52	1	vvw	much	68°42′	68°40′
10.70	4	ms-w	none to some	62°15′–62°30′	62°16′
10.73	2	vvw	some	~59°30′	61°16′
10.94	3	ms-mw	some	54°30′–54°53′	54°47′
10.118	1	vw	some	48°15′	48°27′

[a] Calculated from the theoretical axial ratio for a 141 layer cell.

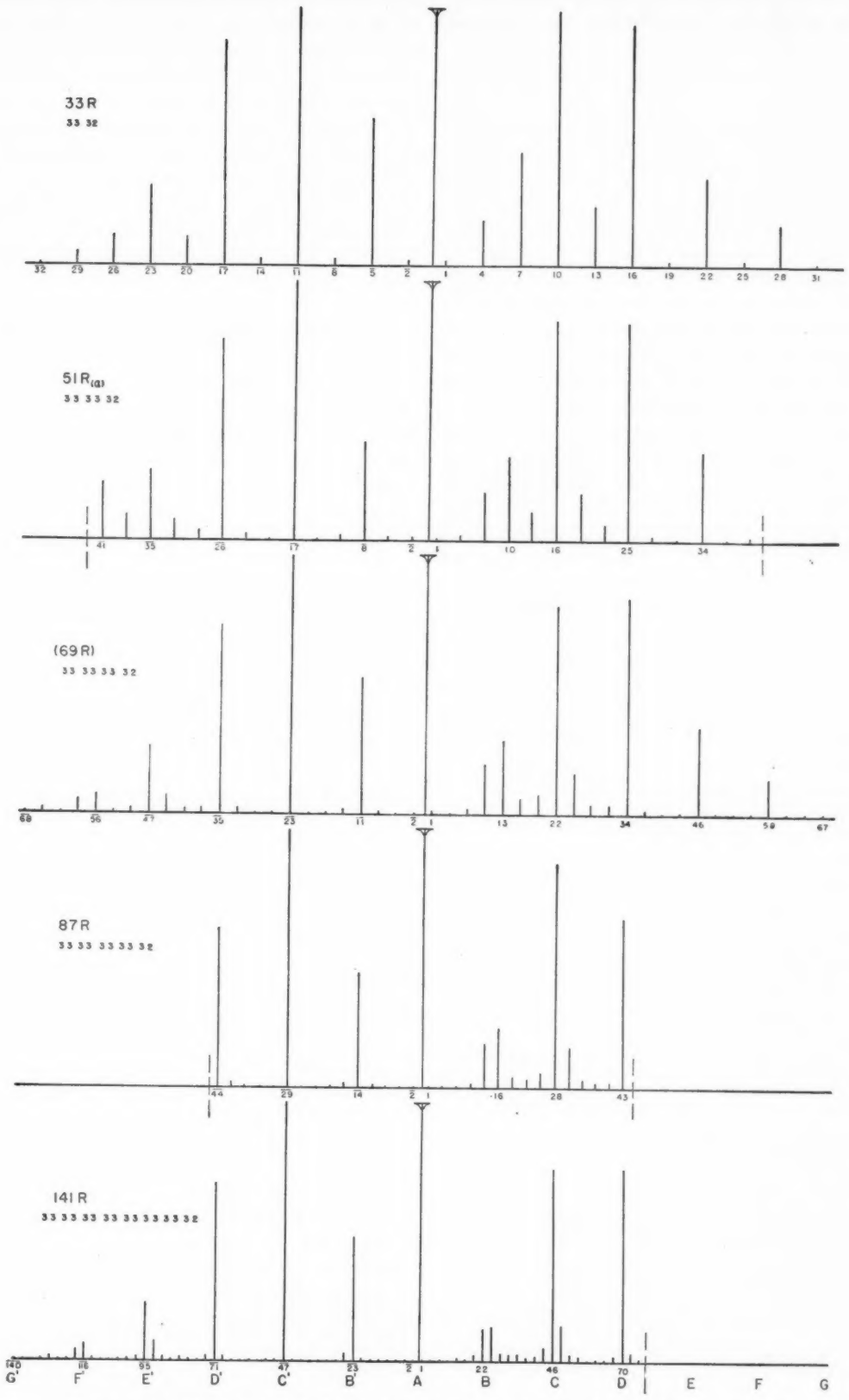

FIG. 1. Comparison of the calculated 10·*l* reflections for five members of the '3. . .2' series.

x-ray film which are medium strong to very very strong. A study of the morphology revealed that the coalesced $6H$ portion was very minor. Only one pyramid zone showed faces which could definitely be distinguished from the $141R$ faces.

Crystal No. 169 is dark blue in color, translucent, and about 2.5 mm long, 1.5 mm wide, and 0.5 mm thick. It is tabular parallel to (0001). Attached to the edge of this crystal is another silicon carbide plate of about the same size. These two crystals do not appear to be related by twinning. Their c axes are inclined to each other by an angle of about 68°18′ and none of the other axes are parallel. This attached crystal is a combination of types $6H$, $15R$, $33R$ plus a new type which is in the general vicinity of $400H$, if hexagonal, or $1200R$, if rhombohedral. Polymorph $141R$ is also coalesced with $6H$. Of the six trigonal pyramid zones, only four have measurable faces. The measured faces of three of these zones are of very good quality and have angular values indicating pure $6H$. The fourth zone, whose reflections appeared to result from a thinner plate coalesced with the predominant $6H$ portion of the crystal, gave blurred reflections exactly the same in character as those for crystal No. 109 which were summarized above in Table II. It thus appears from the morphology of the crystal that $141R$ is a separate crystal plate syntactically coalesced with a thicker crystal of $6H$.

Crystal No. 169 is also interesting from the point of view that it displays a visible growth spiral. The spiral radiates counterclockwise from the center of the pinacoid on that surface of the crystal which was determined above as being $141R$. Verma[7] who has done considerable work measuring the step heights of the spirals on silicon carbide crystals, has shown that these heights are of a magnitude equal to either fractions or multiples of actual unit cells. The step height of the spiral on $141R$ has not yet been determined. The writer has noticed visible spirals on numerous other specimens of silicon carbide which have giant c_0 values. With the exception of $168R$, he has so far been unable to exactly identify these. Perhaps most crystals of this substance which display spirals visible to the naked eye, possess giant c_0 values. This point definitely warrants further investigation.

TABLE III. The relationship of $6H$ positions to xR $10{\cdot}l$ reflections.

$6H$ $10{\cdot}l$	Fractional relationship	Value of l for the xR $10{\cdot}l$ reflections
$10{\cdot}0$	2/6 way between xR $10{\cdot}1$ and $10{\cdot}\bar{2}$	
$10{\cdot}1$	3/6 way between xR $10{\cdot}l$ and $10{\cdot}l+3$	$l=1+3n$
$10{\cdot}2$	2/6 way between xR $10{\cdot}l$ and $10{\cdot}l+3$	$l=1+3(2n+1)$
$10{\cdot}3$	1/6 way between xR $10{\cdot}l$ and $10{\cdot}l+3$	$l=1+3(3n+2)$
$10{\cdot}4$	Coincides with xR $10{\cdot}l$	$l=1+3(4n+3)$
$10{\cdot}5$	5/6 way between xR $10{\cdot}l-3$ and $10{\cdot}l$	$l=1+3(5n+4)$
$10{\cdot}6$	4/6 way between xR $10{\cdot}l-3$ and $10{\cdot}l$	$l=1+3(6n+5)$
$10{\cdot}\bar{1}$	1/6 way between xR $10{\cdot}l$ and $10{\cdot}l-3$	$l=-(2+3n)$
$10{\cdot}\bar{2}$	Coincides with xR $10{\cdot}l$	$l=-(2+3(2n+1))$
$10{\cdot}\bar{3}$	5/6 way between xR $10{\cdot}l+3$ and $10{\cdot}l$	$l=-(2+3(3n+2))$
$10{\cdot}\bar{4}$	4/6 way between xR $10{\cdot}l+3$ and $10{\cdot}l$	$l=-(2+3(4n+3))$
$10{\cdot}\bar{5}$	3/6 way between xR $10{\cdot}l+3$ and $10{\cdot}l$	$l=-(2+3(5n+4))$
$10{\cdot}\bar{6}$	2/6 way between xR $10{\cdot}l+3$ and $10{\cdot}l$	$l=-(2+3(6n+5))$

[7] A. R. Verma, Nature **168**, 431 (1951); Z. Elektrochem. **56**, 4, 268 (1952).

141R AND OTHER SIMILAR SILICON CARBIDE STRUCTURES

The $141R$ zigzag sequence falls into the '3...2' rhombohedral series proposed by Ramsdell,[1] where the ratio of 33's to 32's in this case is 7:1. The following extension of the Ramsdell series includes this new form:

		Ratio of 33 to 32
$15R$	32	0:1
$33R$	3332	1:1
$51R_{(a)}$	333332	2:1
$(69R)$‡	33333332	3:1
$87R$	3333333332	4:1
$(105R)$‡	333333333332	5:1
$(123R)$‡	33333333333332	6:1
$141R$	3333333333333332	7:1
$6H$	33333333333333333...∞	1:0

These sequences must be repeated three times to give the complete unit cell, since the last layer must be directly above the initial layer. Each member of this series (xR) will have

$$x=3(6n+5) \qquad (1)$$

where x=number of layers in the polymorph, n is any whole number, $6=3+3$, and $5=3+2$.

Ramsdell[1] has pointed out that major "blocks" of the larger cells have the $6H$ structure because of the increasing number of successive 33 units in the zigzag sequence, and thus the larger cells in the series become increasingly more like $6H$. $6H$ is the limiting case of this series. Because of the abundance of the 33 units in the many-layered rhombohedral structures, the intensities of the rhombohedral $10.l$ reflections lying near $6H$ $10.l$ positions should be greater.

Because every polymorph of silicon carbide has the same a axis and a c axis whose length is an exact multiple of a common unit ($d=2.513$ kX), there is a coincidence of the rows of $10.l$ reflections of all silicon carbide types. Moreover, the *range* from 10.0 to $10.x$ for every xR or xH type will be equal on a film. This distance corresponds to the reciprocal of the basic unit. This relationship between $6H$ and $141R$ was used above to identify the $141R$ form. In the following discussion

‡ These types have not yet been discovered.

xR 10.l reflections which fall in this *range* will simply be called xR reflections. The 6H 10.l reflections will be designated 6H positions since we are only interested in their position on the films in relationship to actual xR reflections.

It was stated above that the rhombohedral 10.l reflections lying near 6H 10.l positions should be of greatest intensity. In order to determine which xR reflections are most influenced by these 6H positions it is necessary to determine which of the 10.l reflections for the members of the '3...2' series are most closely related to these 6H positions. Table III summarizes the relationship of 13 6H 10.l positions to their two neighboring xR 10.l reflections. The value n, used in determining l for the 10.l reflections, can be found from $n=(x-15)/18$, a rearrangement of Eq. (1) above. In Table III it is easily observed that the 6H positions are related to the xR reflections in a limited number of ways. The 6H position can either coincide with a xR reflection or be 1/6, 2/6, 3/6, 4/6, or 5/6 the way between two of the xR reflections. The importance of these different fractions will be discussed in more detail later using 141R as an example.

The general effect of the 6H positions of the xR reflections is easily observed in Fig. 1 which is a graph showing a comparison of the calculated 10.l reflections for 5 members of the '3...2' series. A, B, C, D, E, F, and G are the locations of the 6H positions 10.0, 10.1, 10.2, etc. respectively, and B', C', D', E', F', and G' are the locations of the 6H positions $10.\bar{1}$, $10.\bar{2}$, etc., respectively.

Those calculated intensity values plotted in Fig. 1 for type 141R are the same as those listed in Table I. The values for 33R, 51$R_{(a)}$, 87R§ were taken from Ramsdell.[1,8] Type 69R has not yet been discovered, so no intensity values for this structure have previously been published. The complete *ranges* of 10.l reflections for 51$R_{(a)}$, 87R, and 141R have not been calculated. For this reason the extent of their calculation is indicated by the light vertical dashed lines in the figure. The darkest 10.l reflections, which in each case have l equal to 1/3.x of the xR form were arbitrarily made equal for each of the types.

The intensity of a xR reflection is not only conditioned by its promixity to a 6H 10.l position, but also depends upon the intensity of the 6H reflection that falls at this position. In other words a xR reflection falling near a very intense 6H reflection position should itself be of a high intensity, and a xR reflection next to a weak 6H reflection position should itself be weak.

In order to show more clearly the dual importance of the proximity as well as the intensity of a 6H position, the relative intensities of the 6H positions are compared to the relative intensities of the neighboring 141R reflections in Table IV. For convenience the intensities for 6H $10.\bar{2}$ and 141R $10.\overline{47}$ were made equal, because they are the most intense reflections for both polymorphs and coincide with each other in position. On this basis their magnitudes are in such good agreement, that a good comparison is possible.

TABLE IV. Intensities of 6H reflections compared to adjoining 141R reflections.

6H 10.l	6H intensity	Adjoining 141R reflections	141R intensity	Fractional distance of 6H between 141R
10.0	0.0	10.1 $-10.\bar{2}$	0.8–0.8	2/6
10.1	478.1	10.22 –10.25	190.3–129.9	3/6
10.2	1000.0	10.46 –10.49	740.4–139.3	2/6
10.3	640.5	10.70 –10.73	744.9–31.2	1/6
10.4	311.2	10.94	not calc.	coincides
10.5	129.5	10.115–10.118	not calc.	5/6
10.6	0.0	10.139–10.142	not calc.	4/6
$10.\bar{1}$	478.1	$10.\bar{2}3$ $-10.\bar{2}6$	479.6–27.0	1/6
$10.\bar{2}$	1000.0	$10.\overline{47}$	1000.0	coincides
$10.\bar{3}$	640.5	$10.\bar{6}8$ $-10.\bar{7}1$	18.3–685.8	5/6
$10.\bar{4}$	311.2	$10.\bar{9}2$ $-10.\bar{9}5$	78.0–221.3	4/6
$10.\bar{5}$	129.5	$10.\overline{116}$–$10.\overline{119}$	61.1–39.6	3/6
$10.\bar{6}$	0.0	$10.\overline{140}$–$10.\overline{143}$	0.9–not calc.	2/6

It is easily noticed that in the cases where a 6H position is 1/6 or 5/6 the way between two 141R reflections (e.g., 6H $10.\bar{1}$), the intensity of that 141R reflection nearest the 6H position is the greater by a large ratio. Its intensity is close to the intensity of the 6H reflection its neighbors. When a 6H position is 2/6 or 4/6 the way between two 141R reflections (e.g., 6H $10.\bar{4}$) the intensity of that 141R reflection nearest the 6H position is the greater, but by a smaller ratio than for the 1/6 or 5/6 case. Also its intensity is considerably less than that of the neighboring 6H reflection. When the 6H position is 3/6 way between two 141R reflections (e.g., 6H $10.\bar{5}$ and 10.1) both of these reflections will have an intensity much less than the 6H intensity and will differ from each other by a very small ratio. In the cases where a 141R reflection lies in the same position as a possible 6H reflection (e.g., 141R $10.\overline{47}$) it will have an intensity nearly equal to that corresponding 6H reflection. The intensities of the other 141R reflections neighboring this case (e.g., 141R $10.\overline{44}$ and $10.\overline{50}$) are much smaller.

In the discussion above, only the influences of the 6H positions upon two neighboring xR reflections were considered. These effects can be somewhat more generalized in considering the other xR reflections. If one temporarily disregards the reflections of high intensity discussed above and considers the remaining reflections (Fig. 1), it will be noticed that in the regions between G' and D' and also between A and D, there are *clusters* of reflections of a higher intensity compared to the remaining regions. More specifically, they lie as *clusters* around 6H $10.\bar{5}$, $10.\bar{4}$, 10.1, and 10.2. These are regions where the 6H positions are related to xR reflections by 2/6, 3/6, and 4/6 as was discussed earlier. When the 6H

§ Upon recalculation it was shown that $10.\overline{29}$ for 87R should be more intense than the 10.28 reflection. The reverse condition had previously been reported.

[8] L. S. Ramsdell, Am. Mineralogist **30**, 519 (1945).

positions superimpose, or are very close to xR reflections, e.g., by 1/6 or 5/6, the adjoining neighbors are very low in intensity or nearly absent. An example of this is the neighbors of $141R$ $10.\overline{47}$ in Fig. 1. The xR reflections in regions corresponding to the $6H$ missing reflections 10.0, 10.6, and $10.\overline{6}$ are themselves usually very weak or absent.

Another important relationship exists between the members of the series in discussion. As the number of layers in the form increases the ratio between the intense reflections near $6H$ positions and those *clusters* of less intense reflections also increases. This is easily understood when one recalls that in the larger cells of the series the number of 33 units in the zigzag sequence increases, making the structure more like $6H$ in character. As the structure approaches this limiting case, the reflections near $6H$ positions will become more intense while other reflections become less intense. When $6H$ is reached only the $6H$ positions are present. As a result of this fact it is obvious that above a certain point the many-layered forms in the series would have no distinguishing characteristics. Only reflections next to $6H$ positions would be noticeable on the film. This increasing ratio between the more intense reflections and the less intense reflections makes intensity evaluation very difficult in the many-layered forms. Those intense reflections near $6H$ positions have to be greatly overexposed before the less intense *clusters* of reflections can be observed or evaluated. These facts were considered in the evaluation of the $141R$ intensities in Table I.

In résumé it may be said that all xR forms belonging to the '3...2' series have the following characteristics: (a) x must equal $3(6n+5)$. (b) $10.l$ reflections lying next to $6H$ positions have the greatest intensity. In general, the intensity of these depends upon the exact proximity of the $6H$ position and upon the intensity of the possible $6H$ $10.l$ at that position. (c) All of the remaining xR reflections follow a characteristic pattern, in that they fall as *clusters* of reflections of medium intensity around the $6H$ $10.\overline{5}$, $10.\overline{4}$, 10.1, and 10.2 positions. (d) As the number of layers in the form increases there is an increasing ratio between the intensity of the reflections near $6H$ positions and the intensity of the *clusters* of less important reflections.

It seems logical to conclude that any new type which fits all of the above conditions would belong to this series.

SILICON CARBIDE TYPE 393R

Silicon carbide type $393R$, which was discovered during the course of the writing of this paper, serves as an excellent example of the usefulness of the above study of the '3...2' series. The fact that the crystal was coalesced with type $6H$ permitted its unambiguous identification using Laue photographs.

Of great importance is the fact that this type fits the condition $x=3(6n+5)$, where $n=21$. Buerger precession films showed the characteristic intensity distribution for the '3...2' series. As was to be expected, the reflections next to $6H$ positions were so intense, compared to the minor *clusters* of reflections, that at first glance the crystal appeared to be pure $6H$. Closer inspection, however, showed the presence of those less intense *clusters* of reflections in the regions characteristic for them in this series.

Consequently, on the basis of empirical reasoning, it seems quite certain that $393R$ is a member of the '3...2' series. Its zigzag sequence is 3333333333333333-33333333333333333333333333332, where the ratio of 33's to 32's is 21:1. There is no point in listing the coordinates of the 786 atoms in the unit cell of this form, since they can easily be derived from the above zigzag sequence.

This new rhombohedral polymorph has the following (hexagonal) cell dimensions:

$$a_0=3.073\ kX,\quad c_0=987.60_9\ kX,\quad Z=393,$$

or, for rhombohedral axes,

$$a_{rh}=329.20_8\ kX,\quad \alpha=0°32',\quad Z=131.$$

The space group for $393R$ is $R3m$, as in the other rhombohedral polymorphs.

The crystal is dark blue in color, almost opaque, and about 2.5 mm long, 1.5 mm wide, and 1.0 mm thick. X-ray data show that it is syntactically coalesced with $6H$. An unusual feature of the crystal is the fact that it is also coalesced with another $6H$ crystal in such a manner that their c axes are parallel but their a axes have an angle between them of about 3°19'. The crystal is also randomly attached to other bits of various silicon carbide crystals which have not been identified. One basal pincoid of $393R$ shows a pattern of concentric scalloped-circles. It was because of this unusual surface feature that the crystal was initially investigated. Four of the six trigonal pyramid zones have measurable faces. The measured angles showed no appreciable departure from the corresponding $6H$ angles. This is to be expected since the structure is so closely related to $6H$. Most of the reflections were of good quality. Because of the very close similarity of this crystal to $6H$ it does not seem necessary to include a table of morphological data.

CONCLUSION

Virtually this study provides an empirical mechanism for the direct determination of the structures of an evidently common group of silicon carbide polymorphs. Perhaps from now on the tedious calculations involved in the determination of the intensities of the many-layered forms of the '3...2' series can be eliminated. Similar studies of other series of silicon carbide zigzag sequences might prove as equally useful in the solution of the structures of other many-layered types.

ACKNOWLEDGMENTS

This investigation was carried out through the financial assistance of the U. S. Office of Naval Research.

The writer wishes to thank Professor L. S. Ramsdell of the Mineraological Laboratory, University of Michigan, for his many helpful suggestions during the progress of the study. Special mention is also due Dr. J. A. Kohn, U. S. Bureau of Mines, Electrotechnical Laboratory, Norris, Tennessee, who began the study of type 141*R* in 1950. The following, of the University of Michigan, should also be acknowledged for their help with the intensity calculations: W. B. Fauser, Jr., J. Funkhouser, A. A. Giardini, and E. L. Hastings.

THE JOURNAL OF CHEMICAL PHYSICS VOLUME 22, NUMBER 12 DECEMBER, 1954

Vibrational Spectra of $CF_2=CHD$ and $CF_2=CD_2$*

WALTER F. EDGELL AND CASPER J. ULTEE†
Department of Chemistry, Purdue University, Lafayette, Indiana

(Received May 14, 1954)

A method has been devised to prepare $CF_2=CD_2$ and $CF_2=CHD$. The infrared spectra of the gaseous compounds and the Raman spectra of the liquids have been determined. The observed frequencies have been assigned to the fundamental modes of vibration and to overtones and combinations. The torsional frequency has been estimated as *ca* 720 and *ca* 520 cm^{-1} in $CF_2=CH_2$ and $CF_2=CD_2$, respectively. The overtone of the torsional frequency interacts with the CH_2 or the CD_2 deformation fundamental and this is the cause of the anomalous results with the product rule.

INTRODUCTION

THE infrared spectrum of $CF_2=CH_2$ was first studied by Torkington and Thompson in 1945.[1] Edgell and Byrd reported the Raman spectrum of liquid $CF_2=CH_2$ in 1949 and assigned the fundamentals.[2] At about the same time Smith, Nielsen, and Claassen published the results of their investigation of the Raman and infrared spectrum of gaseous $CF_2=CH_2$.[3] In general, there is good agreement between the last two investigations, except for the assignment of the A_1 CH_2 deformation frequency and the A_2 torsion.

This laboratory has been studying the coupling between the (hypothetical) group and skeletal motions during the actual fundamental vibrations of some simple molecules. $CF_2=CH_2$ is quite interesting from this point of view. However, isotopic species are needed for a complete analysis. These and other reasons have prompted us to investigate the spectra of $CF_2=CD_2$ and $CF_2=CHD$. It was also hoped that such a study might remove the uncertainties in the $CF_2=CH_2$ assignment. No previous references to these molecules have been found.

PREPARATION OF SAMPLES

The $CF_2=CD_2$ was prepared by the following reactions:

(1) $CF_3CD_2OH+ClSO_2$—⟨⟩—$CH_3\rightarrow$

$CF_3CD_2OSO_2$—⟨⟩—CH_3+HCl;

(2) $CF_3CD_2OSO_2$—⟨⟩—$CH_3+NaI\rightarrow$

$CF_3CD_2I+NaOSO_2$—⟨⟩—CH_3;

(3) $CF_3CD_2I+Mg\rightarrow CF_2=CD_2+MgIF$.

The CF_3CD_2OH was prepared by the method of Henne *et al.* using $LiAlD_4$ instead of $LiAlH_4$,[4] and following the procedure of Edgell and Borneman.[5] The alcohol was converted to the *p*-toluenesulfonic acid ester, a typical preparation of which is given below:

50 g (0.5 mole) of CF_3CD_2OH were mixed with 105 g (0.55 mole) of $ClSO_2$—⟨⟩—CH_3 in a 1-liter flask provided with a reflex condenser, stirrer, and dropping funnel. The flask was cooled in an ice bath and 80 g (~1 mole) of pyridine were added slowly. The reaction mixture was stirred overnight at a temperature of 0°C. The resulting mixture was poured on ice and neutralized with dilute HCl. The ester was filtered off, washed with water, recrystallized from petroleum ether, and

---

* Abstracted from the Ph.D. thesis of C. J. Ultee, Purdue University, April, 1954.

† Purdue Research Foundation Fellow, 1952–1953 and Standard Oil Foundation, Inc., Fellow 1953–1954.

[1] P. Torkington and H. W. Thompson, Trans. Faraday Soc. **41**, 236 (1945).

[2] W. F. Edgell and W. E. Byrd, J. Chem. Phys. **17**, 740 (1949); **18**, 892 (1950).

[3] Smith, Nielsen, and Claassen, J. Chem. Phys. **18**, 326 (1950).

[4] Henne, Alm, and Smook, J. Am. Chem. Soc. **70**, 1968 (1948).

[5] W. F. Edgell and E. H. Borneman, to be published. See also E. H. Borneman, Ph.D. thesis, Purdue University, 1952.

vacuum dried. Yield was 115 g (90 percent); m.p. was 40.5°C.

The $CF_3CD_2OSO_2$⟨⬡⟩CH_3 was reacted with NaI using β-β'-dihydroxyethyl ether as a solvent. 100 g (0.40 mole) of $CF_3CD_2OSO_2$⟨⬡⟩CH_3, 75 g (0.5 mole) of NaI, and 300 ml of $(HOCH_2CH_2)_2O$ were mixed in a 1-liter flask, provided with a short column. The mixture was heated to 100–150°C. CF_3CD_2I distilled off at 52°C (uncorrected). The crude product was washed with water and dried with drierite. Yield was 75–80 g (~90 percent).

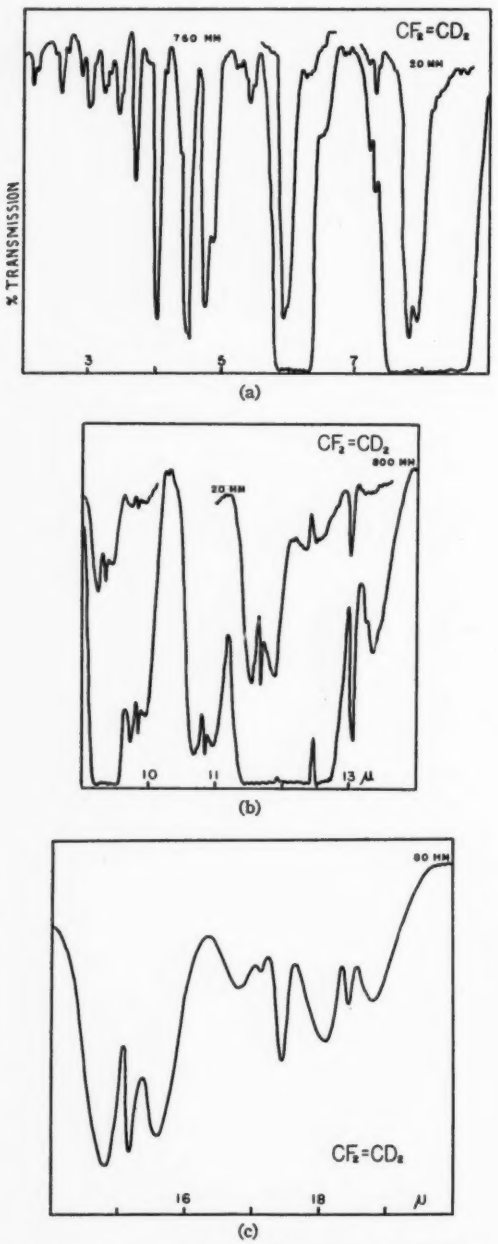

FIG. 1. Infrared spectrum of gaseous $CF_2=CD_2$ in the region 2 to 20 μ.

Finally, $CF_2=CD_2$ was prepared by the reaction of CF_3CD_2I with Mg.[6] 50 g (~0.2 mole) of CF_3CD_2I were mixed with an equal volume of ether and dried over drierite. Carefully washed and dried Mg (10 g) and a small crystal of I_2 were placed in a dry 200-ml 3-neck flask provided with stirrer, dropping funnel, and dry ice-triclene condenser. The flask was slightly heated to disperse the I_2 and, after cooling, 10 ml of anhydrous ether were added to the Mg. The CF_3CD_2I-ether mixture was then introduced drop by drop. No heating was necessary to start or maintain the reaction. The $CF_2=CD_2$ was collected in a liquid N_2 trap and purified by repeated distillations. Yield was ~75 percent.

The $CF_2=CHD$ was prepared from CF_3CHDOH which was obtained by the following reactions:

$$(1)\ CF_3COOH+LiAlH_4 \xrightarrow{0^0C} CF_3CHO\cdot H_2O+CF_3CH_2OH;$$

$$(2)\ CF_3CHO\cdot H_2O+\text{conc. } H_2SO_4 \xrightarrow{\triangle} CF_3CHO;$$

$$(3)\ CF_3CHO+LiAlD_4 \rightarrow CF_3CHDOH.$$

The first and second steps were carried out as described by Husted and Ahlbrecht.[7] The CF_3CHO was distilled bulb to bulb three times to remove any CF_3CH_2OH. The third step was carried out as follows: 9 g (~0.25 mole) of $LiAlD_4$ were added to 1 liter anhydrous ether in a 2-liter 3-neck flask provided with a gas inlet tube, a stirrer, and a dry-ice, reflux condenser. 100 g (~1 mole) of CF_3CHO were slowly passed into the flask. After the CF_3CHO was added, the excess $LiAlD_4$ (very little) was carefully decomposed with H_2O. The resulting slurry was poured into a mixture of 800-g ice and 50-ml concentrated H_2SO_4. The ether layer was separated, and the water layer extracted once with additional ether. The CF_3CHDOH was separated from the ether by fractionation. B.p. was 75° (uncorrected); yield was 80 g (81 percent). The remaining steps of the preparation are identical with those of $CF_2=CD_2$.

PURITY OF SAMPLES

The purity of $CF_2=CD_2$ was checked by mass spectrographic analysis, which showed an average atom percent H of 2.6.‡ The percent of $CF_2=CHD$ is 5.3 ± 0.1 based on the C_2FHD/C_2FD_2 and $C_2F_2HD/C_2F_2D_2$ ion ratios. The spectrum also showed a CF_3 ion fragment resulting from an impurity probably present in 1 to 2 percent. This substance is most likely CF_3CD_2H for which the mass spectrum shows some supporting

[6] H. G. Gilman and R. G. Jones, J. Am. Chem. Soc. **65**, 2037 (1943).

[7] D. R. Husted and A. H. Ahlbrecht, J. Am. Chem. Soc. **74**, 5422 (1952).

‡ Thanks are due Dr. F. W. McLafferty of the Dow Chemical Company, and Mr. N. Mumbach of the Linde Air Products Company, who performed the analyses.

evidence. The presence of $CF_2=CHD$ in the $CF_2=CD_2$ sample is also shown by the appearance of weak bands at 10.8 and 13.0 μ in its infrared spectrum, and the weak lines at 922, 1710, 2323, and 3130 cm^{-1} in the Raman spectrum. The above values for the amount of this impurity has been substantiated by infrared measurements in which $CF_2=CHD$ was placed in the reference beam of the double-beam spectrometer.

The purity of the $CF_2=CHD$ sample was also determined by mass-spectrographic analysis. The main impurity was $CF_2=CH_2$ at about 2 percent, as could be expected from the results on $CF_2=CD_2$. The spectrum also showed evidence of about 0.4 percent $CF_2=CD_2$ and 0.3 percent of a CF_3 impurity, probably CF_3CH_2D. In the infrared spectrum, one band at 803 cm^{-1} has been assigned to $CF_2=CH_2$. The Raman spectrum showed no lines which could be interpreted as arising from $CF_2=CH_2$.

INSTRUMENTATION

The infrared spectra were obtained with a Perkin Elmer Model 21 double-beam spectrophotometer, equipped with NaCl, CaF_2, and KBr optics. A spectrometer built around a Perkin Elmer Model 99 double-pass monochrometer was also used in the CsBr and LiF regions. The various spectral regions were calibrated with air (CO_2 and H_2O), C_2H_2, NH_3, HBr, HCl, CH_4, and CO. Sample pressures up to 800 mm were used in 10-cm gas cells. The infrared spectrum of $CF_2=CD_2$ is shown in Fig. 1 and the observed bands are listed in Table I. Figure 2 shows the infrared spectrum of $CF_2=CHD$; the observed bands are listed in Table II.

The Raman spectra were obtained with an Applied Research Laboratories Spectrometer. This instrument has a camera aperture ratio of $f/3.5$ and a reciprocal dispersion of 15 A/mm at 4358 A. The exitation unit consists of two "Toronto" type low pressure mercury arcs, operating on 220 v, dc and 10 amp each. The intensity of the exciting radiation is enhanced by a cylindrical reflector coated with a silicone resin pigmented with TiO_2. The samples were kept at about −100°C by a cryogenic unit which has been described previously.[8] A solution of Rhodamine 5 DGN Extra in water was used in the cooling jacket to reduce the general background. The Raman spectra were recorded on Eastman Tri-X Pan film using slit widths from 150 to 300 μ and exposures from 2 to 10 hr. A reference spectrum of argon was used to calculate the Raman shifts by means of a graphical method.[9] Semiquantitative relative intensities and depolarization ratios were measured photoelectrically. In addition, depolarization measurements were made photographically. The polarization data were obtained with polaroid cylinders.[10,11] Two runs were made, one with a polaroid cylinder in which the electric vector was oriented parallel to the axis of the Raman tube and the other with a cylinder which orients the electric vector perpendicular to the Raman tube.

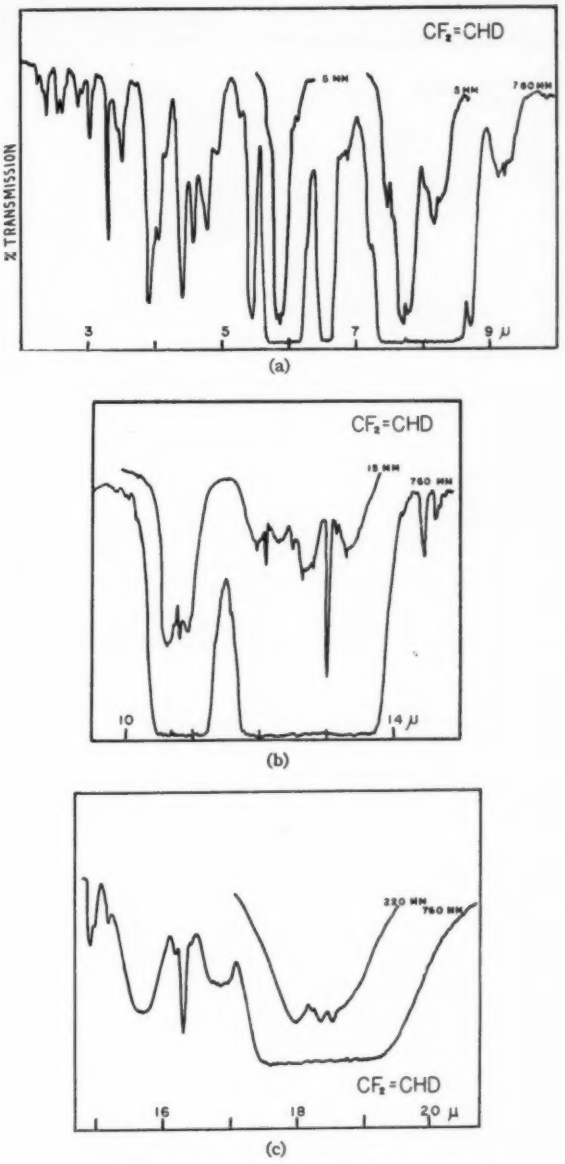

FIG. 2. Infrared spectrum of gaseous $CF_2=CHD$ in the region 2 to 20 μ.

Densitometer tracings were made of the photographic films and the readings corrected for the nonlinearity of the relation between peak height and intensity, and for the background. The depolarization ratios thus obtained must be corrected for instrumental polarization. This correction was obtained by determining

[8] W. F. Edgell and C. E. May, to be published; C. E. May, Ph.D. Thesis, Purdue Univ., June, 1953.
[9] C. E. May, Ph.D. thesis, Purdue University, 1953.
[10] J. T. Edsall and E. B. Wilson, Jr., J. Chem. Phys. 6, 125 (1938).
[11] F. F. Cleveland and M. J. Murray, J. Chem. Phys. 7, 396 (1939).

TABLE I. The infrared spectrum of gaseous $CF_2=CD_2$.

Band, cm^{-1}	Intensity[a]	Band type	Assignment
374	m		B_1 fundamental
531 543 556	s	*A*	A_1 fundamental
556 572 575 582 592	s	*C*	B_2 fundamental
617	vw		$CF_2=CHD$ impurity
641 660 677	vs	*C*	B_2 fundamental
749 770 791	m	*C*	$CF_2=CHD$ impurity
801 814	vs	*B*	B_1 fundamental
829	vw		$CF_2=CHD$ impurity
845 853 858 867	vs	*A*	A_1 fundamental
917 929 942	s	*A*	$CF_2=CHD$ impurity
989 999	wsh		Impurity?
1010 1021 1033	s	*A*	2×520
1064 1076 1087	s	*A*	A_1 fundamental
1166	s		2×575
1181 1198 1226	s	*C*?	543+660; $CF_2=CHD$?
1238	s		575+660
1283 1292	vs	*B*	B_1 fundamental
1332 1346 1357	w		2×660; 543+807
1401 1409	w		543+858
1528 1538 1552	w	*A*	2354–807; $CF_2=CHD$ impurity?
1598 1611 1621	s	*A*	2×807
1646 1652 1663	s	*A*	374+1284; 707+858
1692 1705 1714	vs	*A*	A_1 fundamental
1750 1758 1764	w	*A*?	543+575+660
1800	vw		2×575+660
1869	vw		575+1284
1877	vw		2×660+543
1922 1933 1943	vw	*A*	858+1076
2080 2089 2101	m	*A*	808+1284
2135 2146 2156	m	*A*	2×1076; 858+1284
2263 2270 2274 2284	s	*A*	A_1 fundamental
2323	w		$CF_2=CHD$ impurity
2350 2358	w	*B*	B_1 fundamental
2372	w		660+1705
2448 2463	vvw		374+807+1284
2551 2563	m	*A*	858+1705; 2×1284
2621 2628 2638	w	*A*	543+807+1284
2765 2773 2782	m	*A*	1076+1705
2921	w		575+2354
2989	w		1284+1705
3067 3083	vvw		807+2274
3119	vvw		858+2274
3173	vvw		807+2354
3190	vvw		858+2354
3322	vvw		2×807+1705
3394	vvw		2×1705
3455	vvw		1076+2354
3561	vvw		1284+2274
3619	vvw		1284+2354
3820	vvw		3×1284
3964	vvw		1705+2274
4065	vvw		1705+2354

[a] s = strong, m = medium, w = weak, v = very, and sh = shoulder.

TABLE II. The infrared spectrum of gaseous $CF_2=CHD$.

Band, cm^{-1}	Intensity	Band type	Assignment
392	m		A' fundamental
533			
541			
544	s	A–B	A' fundamental; 925–392?
556			
593			
617	s	C	A'' fundamental
637			
660			
670	vvw		1298–617
689			1227–542
694			
751			
754			
764			
770	vs	C	A'' fundamental
775			
783			
787			
793			
803	s	C	$CF_2=CH_2$ impurity
811			
816			
829			
833	vs	A	A' fundamental
840			
917			
929	vs	A	A' fundamental
943			
988			
998	vvw		impurity?
1008			
1019	vvw		392+617
1080			
1092	vw	A	2×542
1100			
1160			
1170	m	B?	617+542; 770+392
1216			
1224	vs	A	A' fundamental
1234			
1234			
1242	vs	A	2×617
1245			
1290	vs	B	A' fundamental
1312			
1335	msh	B?	392+929
1344			
1391	w		617+770
1399			
1467			
1479	vvw	A	452+929
1486			
1527			
1538	s	A	2×770
1550			
1561	vw		392+542+617

Band, cm^{-1}	Intensity	Band type	Assignment
1607			
1611	w	A?	392+1224
1619			
1639			
1652	s	A	2×829
1664			
1706			
1716	vs	A	A' fundamental
1728			
1758	m		829+929
1767			
1847			
1858	s	A	2×929
1866			
2053			
2067	vw	A	829+1224
2076			
2111			
2126	m	A	829+1298
2134			
2155			
2166	w	A	929+1224
2177			
2221	m		929+1298
2228			
2258	vvw		545+1715
2276			
2312			
2325	s	A	A' fundamental
2334			
2440			
2451	vw	A	2×1224
2458			
2522	m		1224+1298
2774	vvw		452+929+1298
2886	vvw		542+2325
2934	vw		1298+1715
3117			
3133	m	A	A' fundamental
3139			
3254	vvw		929+2325
3418	vvw		2×1715
3547	vvw		1224+2325
3636	vvw		1298+2325
3660	vvw		3×1224
3948	vvw		829+3133
4037	vvw		1712+2325
4338	vvw		1224+3133
4413	vvw		1298+3133
4591	vvw		545+1715+3133

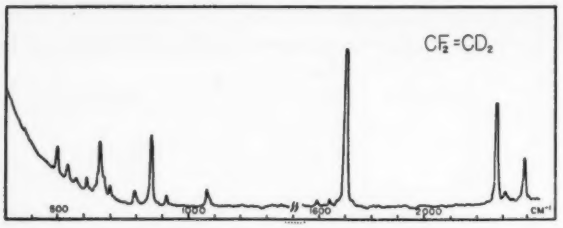

FIG. 3. Raman spectrum of liquid $CF_2=CD_2$ with photoelectric recording.

the depolarization ratios for CCl_4 and toluene photoelectrically and comparing these with the data in the literature. The data for $CF_2=CD_2$ were obtained photographically and also photoelectrically for the stronger lines. Improvement in the amplification system of the spectrograph made it feasible to obtain all the depolarization ratios for $CF_2=CHD$ photoelectrically. It should be noted that the depolarization factors for the weaker lines and for those lines close to the exciting mercury line are susceptible to considerable error. The observed Raman lines and depolarization factors are listed in Tables III and IV. Photoelectric tracings of the Raman spectra are shown in Figs. 3 and 4.

The Raman spectra warrant some discussion. Most lines were observed with excitation by both the 4358 A and 4047 A mercury lines. Some of the strong lines also were observed from the 4077 A mercury line. In the spectrum of $CF_2=CD_2$ there are several lines for which more than one explanation is possible. A line of medium intensity was observed at 618 cm^{-1} if excited by 4358 A. This frequency shift has been explained as the 2386 cm^{-1} line excited by the 4047 A mercury line, although there is a weak infrared band at 618 cm^{-1}. A similar difficulty exists for a rather strong line observed at 508 cm^{-1}. It has been explained as the 2276 cm^{-1} line excited by the 4047 A line. No band was observed in the infrared at this frequency. This interpretation is supported by the fact that the intensity of these lines is decreased when the Raman tube is wrapped in a Wratten 2B filter. Such a filter decreases the intensity of the 4047 A exciting line, while leaving the 4358 A line relatively unchanged.

The Raman spectrum of $CF_2=CHD$ presents similar problems. Lines at 545 and 557 cm^{-1} are observed as if excited by both the 4358 and 4047 A mercury lines.

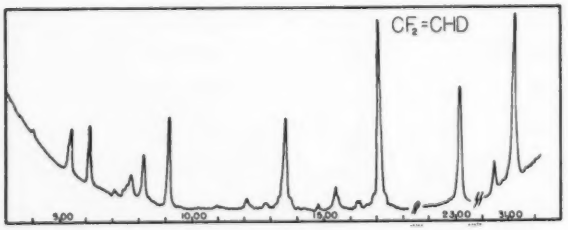

FIG. 4. Raman spectrum of liquid $CF_2=CHD$ with photoelectric recording.

TABLE III. The Raman spectrum of liquid $CF_2=CD_2$.

Line	Relative intensity[a]	ρ[b]	Assignment
373 cm^{-1}	...[c]	...	B_1 fundamental
538	10	0.9	A_1 fundamental
574	5	...	B_2 fundamental
660	38	0.9	B_2 fundamental
803	10	0.9	B_1 fundamental
853	45	0.37	A_1 fundamental
1071	10	0.47	A_1 fundamental
1270	...	...	B_1 fundamental
1321	...	...	2×660
1600	5	...	2×803
1695	100	0.28	A_1 fundamental
2276	67	0.30	A_1 fundamental
2385	30	0.9	B_1 fundamental
922	5	...	$CF_2=CHD$
1710	...	...	$CF_2=CHD$
2323	5	...	$CF_2=CHD$
3130	...	...	$CF_2=CHD$

[a] From photoelectric recording.
[b] ρ = depolarization factor, measured photographically.
[c] Observed photographically only.

The 557 cm^{-1} line is of medium intensity, the 545 cm^{-1} line is somewhat weaker. In a Wratten-filter run the 545 cm^{-1} from the 4047 A line was not observed, while the same shift from 4358 A was relatively undiminished in intensity. It was concluded that a line at this frequency exists in the Raman spectrum. In contrast, the line displaced 557 cm^{-1} from the 4047 A mercury line was definitely observable in the Wratten-filter run although its intensity was decreased; the same shift from the 4358 A line was also substantially diminished in intensity. The line found at 557 cm^{-1} from the 4047 A, is interpreted as the weak mercury line at 4140 A, while the line displaced the same amount from the 4358 mercury line is interpreted as the 2325 cm^{-1} line excited by the 4046 A line. This same line is also observed excited by 4077 A, as indeed are several of the strong Raman lines.

TABLE IV. The Raman spectrum of liquid $CF_2=CHD$.

Line	Relative intensity[a]	ρ[b]	Assignment
399 cm^{-1}	...[c]	...	A' fundamental
545	24	0.50	A' fundamental
612	28	0.85	A'' fundamental
774	11	0.83	A'' fundamental
822	20	0.38	A' fundamental
921	46	0.16	A' fundamental
1209	7	0.76	A' fundamental
1230	...	...	2×612
1287	3	0.70	A' fundamental
1643	5	0.72	2×822
1710	100	0	A' fundamental
1749	3	...	822+921
2323	59	0.28	A' fundamental
3127	81	0.15	A' fundamental

[a] From photoelectric recording.
[b] ρ = depolarization factor; measured photoelectrically.
[c] Observed photographically only.

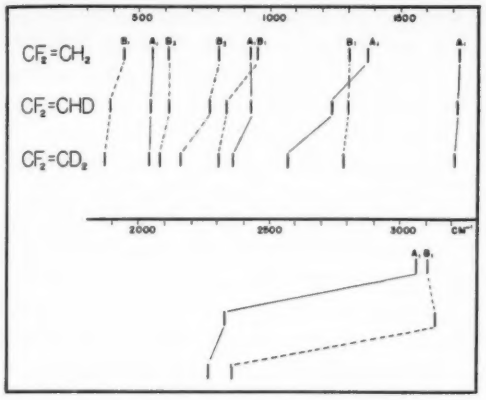

FIG. 5. Fundamental frequencies of $CF_2=CH_2$, $CF_2=CHD$, and $CF_2=CD_2$.

ASSIGNMENT OF THE FUNDAMENTALS

Recent spectroscopic[2,3,12] and electron diffraction[13] work on $CF_2=CH_2$ has shown that this molecule is planar, thus having the symmetry C_{2v}. It is assumed that $CF_2=CD_2$ has the same molecular parameters and symmetry. According to group theory, the normal vibrations divide themselves into the following types: $A_1(5)$, $A_2(1)$, $B_1(4)$, and $B_2(2)$. All fundamentals are Raman active; the vibrations belonging to type A_1 are polarized. The A_1, B_1, and B_2 fundamentals are infrared active and give rise to type A, B, and C bands for which the theory of Badger and Zumwalt[14] predicts P-R separations of 24, 11, and 40 cm^{-1}, respectively. The observed band envelopes are in excellent agreement with this prediction. The A_1 vibrations can be classified roughly as the symmetrical CD_2, CF_2, and C=C stretching vibrations and the CD_2 and CF_2 deformation vibrations. The A_2 vibration is the torsional mode. The antisymmetrical CD_2 and CF_2 stretchings and the rocking of the CF_2 and the CD_2 groups make up the B_1 vibrations. The two B_2 vibrations are the in- and out-of-phase wagging motions of the CF_2 and the CD_2 groups.

The $CF_2=CHD$ molecule has the symmetry C_s. The 12 normal vibrations can be divided into two types: $A'(9)$ and $A''(3)$. Both types are allowed in both the Raman and infrared. The A'' vibrations give rise to type C bands. The A' vibrations will give rise to type

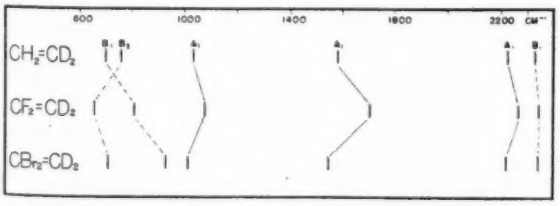

FIG. 6. Characteristic frequencies of the $C=CD_2$ group.

[12] A. Roberts and W. F. Edgell, J. Chem. Phys. **17**, 742 (1949).
[13] I. L. Karle and J. Karle, J. Chem. Phys. **18**, 963 (1950).
[14] R. M. Badger and L. R. Zumwalt, J. Chem. Phys. **6**, 711 (1938).

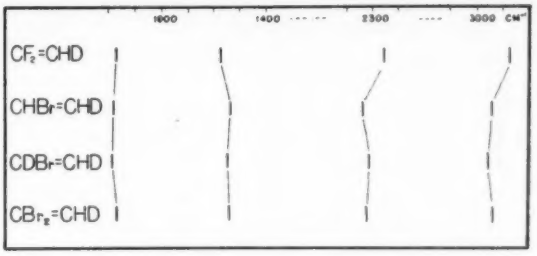

FIG. 7. Characteristic frequencies of the C=CHD group.

A bands if the dipole moment change is along the axis of smallest moment of inertia and to type B bands if along the intermediate axis of inertia. In general the dipole moment change will have components along both these axes and hence the observed band will be of a hybrid type. The infrared spectrum shows bands with contours very similar to those observed in $CF_2=CH_2$ and $CF_2=CD_2$. The description of the vibrations is similar to that of $CF_2=CD_2$; the A_1 and B_1 vibrations of the latter go over into the A' vibrations of $CF_2=CHD$, and the A_2 and B_2 vibrations transform into the class A''.

It will be instructive in making the assignments to consider several series of molecules. The correlations of the $CF_2=CH_2$, $CF_2=CHD$, and $CF_2=CD_2$ fundamentals are shown in Fig. 5, while the CD_2 and CHD frequencies are compared with those in similar molecules in Figs. 6 and 7.

In $CF_2=CD_2$, the CD_2 stretching frequencies are found at 2276 and 2385 cm^{-1} in the Raman effect. The former line is strong, sharp, and polarized while the latter line is of medium strength and has a depolarization factor of 0.9. Thus, the line at 2276 cm^{-1} has been assigned to the A_1 and the 2385 cm^{-1} line to the B_1 stretching vibration of CD_2. The infrared spectrum in this region contains four bands (see Fig. 1) with intensities of the same order of magnitude. The problem is further complicated by the possibility of substantial liquid-vapor shifts. Upon examining this region under the higher resolution available with the LiF prism in the double-pass instrument all these bands have typical type A structures. The band at 2274 cm^{-1} (4.4 μ), whose contour is shown in Fig. 8, has been assigned to the symmetric CD_2 stretching vibration on the basis of its

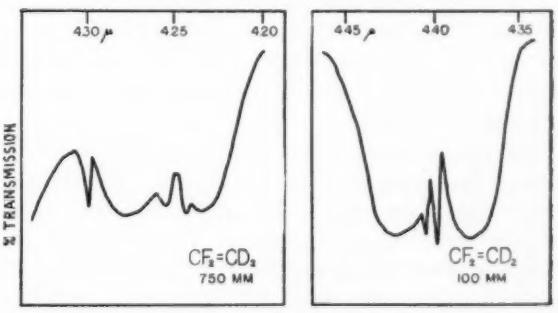

FIG. 8. The CD_2 stretching vibrations in $CF_2=CD_2$.

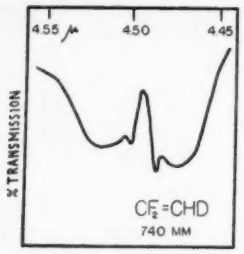

FIG. 9. The 4.5 μ band in $CF_2=CHD$.

relative intensity and the close numerical agreement with the value found in the Raman effect. This band is overlapped by a weaker band of either type *A* or type *C* structure, centering at 2270 cm^{-1}, which may be the type *C* combination 1705+575 cm^{-1}. The bands at 2551, 2146, and 2089 cm^{-1} are assigned to the combinations 858+1705, 858+1284, and 808+1284 cm^{-1}, all of which involve strong fundamentals. The band at 4.4 μ has a weak shoulder at higher pressures which may be separated under greater resolution into the band shown in Fig. 8 at 2354 cm^{-1} (4.25 μ). It is overlapped by a type *A* band at 4.30 μ arising from the $CF_2=CHD$ impurity. The 4.25 μ band is clearly of type *B* and since no other band of this type appears in this region it is assigned to the antisymmetrical stretching vibration.

In $CF_2=CHD$, strong polarized lines are found at 3127 and 2323 cm^{-1} in the Raman effect. These lines have been assigned to the CH and CD stretching vibrations, respectively. In the infrared there is a strong band at 3133 cm^{-1}, clearly showing type *A* structure. On the basis of its intensity and band envelope, it has been assigned to the CH stretching vibration. In the CD stretching vibration region the infrared spectrum shows bands at 2325, 2225, and 2126 cm^{-1}. The band at 2325 cm^{-1} shows a type *A* structure and is assigned to the CD stretching vibration. The band at 2224 cm^{-1} (see Fig. 9) has a type *B* structure as modified by a modest difference in moment of inertia between the ground and excited states. It is assigned to the combination 929+1298 cm^{-1}. The type *A* band at 2126 cm^{-1} is assigned to 829+1298cm^{-1}.

The C=C vibration generally comes around 1600 cm^{-1} in hydrocarbons, but has been shown to shift to substantially higher frequencies in fluorinated molecules by Edgell and Byrd,[2] J. R. Nielsen and co-workers,[3] and others. The strong type *A* infrared bands at 1715 and 1705 cm^{-1} in $CF_2=CHD$ and $CF_2=CD_2$, respectively, are assigned to this vibration. The corresponding Raman lines found at 1710 and 1695 cm^{-1} are intense and highly polarized.

The symmetrical CF_2 stretching vibration is somewhat coupled to the motion of the $CH_2(CHD,CD_2)$ group and gives rise to strong, type *A* bands in the infrared and strong, polarized lines in the Raman effect. These lines are found at 926, 929, and 858 cm^{-1} in the infrared and at 915, 921, and 853 cm^{-1} in the Raman effect of $CF_2=CH_2$, $CF_2=CHD$, and $CF_2=CD_2$, respectively. The antisymmetrical CF_2 stretching vibration gives rise to very intense type *B* bands in the infrared spectrum at 1288 and 1301 cm^{-1} and to very weak Raman lines at 1270 and 1287 cm^{-1}, respectively, in $CF_2=CD_2$ and $CF_2=CHD$.

The rocking, the deformation, and wagging vibrations of the CF_2 group may be expected to have values similar to those found for $CF_2=CH_2$. They are found at 373, 538, and 574 cm^{-1} in the Raman effect and at 374, 543, and 575 cm^{-1} in the infrared for $CF_2=CD_2$. The last two bands have type *A* and type *C* structures as required; no structure was resolvable in the first band because of the wide slits necessary to obtain sufficient energy to record the spectrum. The corresponding Raman lines of $CF_2=CHD$ are found at 399, 545, and 612 cm^{-1}, with infrared bands at 392, 542, and 617 cm^{-1}. Here the latter has a clear-cut type *C* structure while the band at 542 cm^{-1} has a hybrid *A-B* structure.

The remaining motions are primarily concerned with the H and D atoms. The CD_2 rocking vibration gives rise to a type *B* infrared band at 808 cm^{-1} and a moderately intense, depolarized Raman line at 803 cm^{-1}. The CHD rocking vibration is found at 829 cm^{-1} in the infrared and at 822 cm^{-1} in the Raman effect. This vibration has the largest component of its dipole moment along the axis of minimum moment of inertia as indicated by the fact that its band is nearly a type *A* structure. The CD_2 and CHD wagging vibrations are easily recognized by the type *C* structure of their infrared bands and are found at 660 and 770 cm^{-1}, respectively. The corresponding depolarized Raman lines are found at 660 and 774 cm^{-1}.

A major uncertainty in the $CF_2=CH_2$ assignment was the CH_2 deformation vibration. Edgell and Byrd[2] favored the value at 1359 cm^{-1} found with medium intensity in the Raman spectrum of the liquid at −110°C. Although Smith, Nielsen, and Claassen[3] observed this line as weak and sharp at 1358.7 cm^{-1} in the Raman spectrum of the gas at room temperature, they assigned a weak, diffuse line at about 1405 cm^{-1} to this vibration. The infrared spectrum[3] shows a type *A* band of moderate intensity at 1414 cm^{-1} and a weak yet apparently sharp shoulder at 1361 cm^{-1} which may possibly arise from either an *A* or a type *C* band. The

TABLE V. Application of the product rule to $CF_2=CH_2$, $CF_2=CD_2$.

Type	No. vibrations	CH_2 def.	CD_2 def.	Observed	Calculated	Discrepancy (%)
B_2	2	...	...	1.293	1.298	0.4
B_1	4	...	...	1.853	1.835	1.0
A_1	5	1414	1076	1.959	1.968	0.4
		1414	1021	2.065	1.968	4.9
		1361	1076	1.886	1.968	4.2
		1361	1021	1.987	1.968	1.0
		(1380)	(1060)	1.941	1.968	1.4

band at 1414 cm^{-1} may be explained as the combination 803+611, on the one hand, while that at 1361 cm^{-1} may be 550+803, a type *C* band. In the Raman spectrum of $CF_2=CD_2$ there remains unassigned a line of moderate intensity at 1071 cm^{-1} and weak lines at 1321 and 1600 cm^{-1}. The last two are outside the region expected for this vibration and are assigned to the overtones 2×660 and 2×803 cm^{-1}. The infrared spectrum shows strong type *A* bands at 1076 and 1021 cm^{-1}. The former band might be explained as 2×543, but the corresponding combination is absent in $CF_2=CH_2$ and present only very weakly in $CF_2=CHD$. On the other hand there seems to be no combination of bands already assigned which can account for the 1201 cm^{-1} band. It does not seem reasonable however to find an overtone as strong or stronger than its fundamental in both the Raman and infrared spectrum, and for this reason we assign the Raman line 1071 cm^{-1} and the infrared band at 1076 cm^{-1} to the CD_2 deformation fundamental (as combined with torsion; see below).

In the Raman spectrum of $CF_2=CHD$ there remain unassigned lines at 1209, 1230, 1643, and 1749 cm^{-1}. The last two are outside the region in question and correspond to 2×822 and 921+822 cm^{-1}. The very weak Raman line at 1230 cm^{-1} is assigned to the combination 2×612. The remaining line of moderate intensity is interpreted as the deformation vibration of the CHD group. Figure 2 shows a strong infrared band of uncertain envelope at this point. Examination of this region under high resolution shows two overlapping type *A* bands of nearly equal intensities with *Q* branches at 1224 and 1242 cm^{-1}. These are interpreted as the CHD deformation fundamental and the overtone 2×617, with the possibility of some mixing as a consequence of Fermi resonance.

The assignment of the CH_2, CHD, and CD_2 deformation frequencies has presented similar difficulties in each respective molecule, in that in each case a choice had to be made between a number of different frequencies. The choice has to a large degree been determined by the presence and the intensities of the Raman lines. The application of the Teller-Redlich product rule to the problem of the deformation frequencies is quite suggestive. The results may be seen in Tables V through VII. Consider first the molecules $CF_2=CH_2$ and $CF_2=CD_2$. The assignment for the B_1 and B_2 vibrations is straightforward and we see the expected good agreement between the experimental frequency ratio and that predicted by theory. The two candidates for the uncertain deformation frequency in each of the molecules make possible four different assignments. It is seen that the 1414–1076 combination and the 1361–1021 combination give good agreement with the theoretical value. However, these assignments exclude one strong band or Raman line for either the $CF_2=CH_2$ or the $CF_2=CD_2$ molecule and hence are less likely from an experimental viewpoint. The 1414–1021 assignment involves the combination of the weak bands or Raman lines and its unfavorable product rule ratio should exclude it as a possibility. Unfortunately, the 1361–1076 assignment, which involves the strong bands or Raman lines, results in no better agreement with the product rule. A discrepancy of 4 percent is not to be expected from the zero-order theory plus the usual anharmonicities. On the other hand, deviations from the product rule will be caused by Fermi resonance, Coriolis coupling between different frequencies, and indeed by any effect which may substantially combine and modify the zero-order frequencies. One would not expect such complications on the basis of the frequencies already assigned and hence one is led to suspect that they have their origin in the yet undiscussed torsional frequency.

TABLE VI. Application of the product rule to $CF_2=CD_2$, $CF_2=CHD$.

Type	No. vibrations	CD_2 def.	CHD def.	Observed	Calculated	Discrepancy (%)
$A'(A_1,B_1)$	9	1076	1242	1.859	1.884	1.3
		1076	1224	1.836	1.884	2.5
		1021	1242	1.959	1.884	4.0
		1021	1224	1.935	1.884	2.7
		(1060)	1224	1.857	1.884	1.3

TABLE VII. Application of the product rule to $CF_2=CH_2$, $CF_2=CHD$.

Type	No. vibrations	CH_2 def.	CHD def.	Observed	Calculated	Discrepancy (%)
$A'(A_1,B_1)$	9	1414	1242	1.953	1.924	1.5
		1414	1224	1.977	1.924	2.8
		1361	1242	1.880	1.924	2.3
		1361	1224	1.903	1.924	1.1
		(1380)	1224	1.934	1.924	0.5

The work of Arnett and Crawford[15] yields a value of $k=0.269\times10^{-11}$ erg/radian^2 for the torsional force constant in ethylene. The recent work of Mann, Acquista, and Plyler[16] on tetrafluoroethylene indicates a value of $k=0.245\times10^{-11}$ erg/radian^2. If one uses a force constant of this order of magnitude, one can calculate the torsional frequency in $CF_2=CH_2$ as *ca* 720 cm^{-1} and in $CF_2=CD_2$ *ca* 520 cm^{-1}.

It is interesting to note that Edgell and Byrd observed a very weak Raman line at 714 cm^{-1} in $CF_2=CH_2$ which they, quite tentatively, assigned to this mode. Our data do not positively exclude the presence of a weak Raman line at about 508 cm^{-1} in $CF_2=CD_2$. However, since a Raman line has been observed at 508 cm^{-1} from 4358 A only, and this is satisfactorily accounted for experimentally as the 2276 cm^{-1} fundamental excited by the 4046 A (see under

[15] R. L. Arnett and B. L. Crawford, Jr., J. Chem. Phys. **18**, 118 (1950).

[16] Mann, Acquista, and Plyler, J. Research Natl. Bur. Standards **52**, 67 (1954), RP 2474.

TABLE VIII. The fundamental frequencies of $CF_2=CH_2$, $CF_2=CHD$, and $CF_2=CD_2$.

$CF_2=CH_2$ Description[a]		$CF_2=CHD$ Description		$CF_2=CD_2$ Description	
A_1: CH_2 str.	3060 cm^{-1}	A': CH str.	3133 cm^{-1}	A_1: CD_2 str.	2274 cm^{-1}
C=C str.	1728	C=C str.	1715	C=C str.	1705
CH_2 def.	(*ca* 1380)	CHD def.	1224	CD_2 def.	(*ca* 1060)
CF_2 str.	926	CF_2 str.	929	CF_2 str.	858
CF_2 def.	550	CF_2 def.	542	CF_2 def.	543
B_1: CH_2 str.	3103	CD str.	2325	B_1: CD_2 str.	2354
CF_2 str.	1302	CF_2 str.	1298	CF_2 str.	1284
CH_2 rock.	955	CHD rock.	829	CD_2 rock.	807
CF_2 rock.	438	CF_2 rock.	392	CF_2 rock.	374
B_2: CH_2 wag.	803	A'': CHD wag.	770	B_2: CD_2 wag.	660
CF_2 wag.	611	CF_2 wag.	617	CF_2 wag.	575
A_2: torsion	(*ca* 714)	torsion	...	A_2: torsion	(*ca* 520)

[a] Str. = stretching, def. = deformation, rock. = rocking, wag. = wagging.

Experimental Section), we cannot conclude that such a frequency has in fact been observed. No infrared band has been observed at these frequencies as is expected from the selection rules.

On the other hand, the overtone of the torsional frequency is of species A_1 and hence allowed in both the Raman and infrared spectra. The overtone frequencies would be expected, very roughly, near 1400 and 1030 cm^{-1} in $CF_2=CH_2$ and $CF_2=CD_2$. It is hard to escape the suggestion that these overtones have combined with the CH_2 and the CD_2 deformation fundamentals in Fermi resonance. This is allowed, of course, by the selection rules and would account for the discrepancy in the product rule values for the A_1 frequencies, as discussed above. The experimental data on the intensities suggest that the unperturbed overtone may lie above the unperturbed deformation fundamental in $CF_2=CH_2$ and below this fundamental in $CF_2=CD_2$. Moreover such an explanation simultaneously removes the difficulties in the product rule calculations (see Tables V to VII).

On the basis of these considerations, we tentatively assign the torsional frequency in $CF_2=CH_2$ to *ca* 714 cm^{-1} and *ca* 520 cm^{-1} in $CF_2=CD_2$. The unperturbed deformation vibrations are tentatively taken as *ca* 1380 and *ca* 1060 cm^{-1}, respectively. No value is assigned to the torsional frequency in $CF_2=CHD$.

The fundamentals of $CF_2=CH_2$, $CF_2=CHD$, and $CF_2=CD_2$ are compared in Fig. 5. It should be noted that the correlation is good. In Fig. 7, a comparison is found of the frequencies involving the CHD group for the molecules $CF_2=CHD$, $CHBr=CHD$, $CDBr=CHD$, and $CBr_2=CHD$.[17] The good correlation found indicates that the assignment is essentially correct. The fundamentals of $CF_2=CD_2$ involving the $C=CD_2$ portion of the molecule are compared with those of $CH_2=CD_2$[18] and $CBr_2=CD_2$[17] in Fig. 6. It is interesting to note that all the A_1 fundamentals of $CF_2=CD_2$ shown here are shifted to higher frequencies than one might expect from this correlation. This is believed to be the consequence of the coupling of the frequencies characteristic of an "isolated" CF_2 group with those of the "isolated" CD_2 group and the C=C bond, as opposed to any substantial increase in force constants pertaining to these bonds. How this may occur can be seen as follows: In the C=C vibration, there is a tendency for the deuterium atoms to move with the carbon atom because of their substantially lighter mass. Now fundamental modes of vibrations must be orthogonal and this requires that the double bond be stretched somewhat during the vibrations of the CD_2 group. To what degree the CF_2 end of the molecule participates in these vibrations depends upon the extent that the CF_2 frequencies are coupled to the C=C stretching. That this takes place to a considerable degree is shown by the fact that the C=C vibration appears more than 100 cm^{-1} higher than one might expect it. Thus we find both the CD_2 stretching and deformation vibrations shifted to higher frequencies. Again the correlation supports the validity of the assignments. The fundamental frequencies have been collected in Table VIII. On the basis of these fundamentals all the other frequencies observed in the infrared and Raman spectra are explained as indicated in Tables I–IV. It should be noted that in general the agreement between calculated and observed values is good. Moreover, no unlikely combinations are involved.

ACKNOWLEDGMENT

The authors are indebted to the U. S. Atomic Energy Commission for financial support of this work. One of us (C.J.U.), wishes to thank the Purdue Research Foundation and the Standard Oil Foundation, Inc. for fellowships during the course of this work.

[17] de Hemptinne, Velghe, and van Riet, Bull. Acad. Roy. Belg. **30**, 40 (1944).

[18] Lancaster, Inskeep, and Crawford, J. Chem. Phys. **19**, 661 (1951).

Effect of Intermolecular Interactions between CH Frequencies on the Infrared Spectra of *N*-Paraffins and Polythene*

R. S. STEIN, *Department of Chemistry, University of Massachusetts, Amherst, Massachusetts*

AND

G. B. B. M. SUTHERLAND, *Department of Physics, University of Michigan, Ann Arbor, Michigan*

(Received May 14, 1954)

A systematic study has been made of the infrared absorption band near 725 cm^{-1} which arises from the rocking vibration of methylene groups in *n*-paraffins and in polyethylene. In unoriented crystals of *n*-paraffins, this band exhibits two components of equal intensity below the transition point; above the transition temperature and in the liquid state only the higher frequency component is found. In solid cold-drawn polyethylene the two components are of unequal intensity, the low frequency component being the stronger; in liquid polyethylene only the lower frequency component is found. Studies were made of polyethylene in various states of crystallinity and orientation, using both polarized and unpolarized radiation. The results obtained can be consistently interpreted, if the higher frequency component is attributed to crystallites in the polyethylene and the lower frequency component is assumed to be due partly to the crystalline and partly to the amorphous form of the polyethylene. It is concluded that the doubling of this frequency arises from some interaction between methylene groups which is peculiar to the crystalline state of long chain *n*-paraffins below their transition points.

INTRODUCTION

THERE are three main regions of intense absorption in the infrared spectrum of any *n*-paraffin and of polythene between 1 and 15μ. These are centered near 3.3μ (2920 cm^{-1}), 6.9μ (1470 cm^{-1}), and 13.8μ (725 cm^{-1}). The first two have long been known to be associated with internal modes of vibration of the CH_2 groups while the third has recently been proved[1,2] to be due to a deformation motion of the CH_2 groups as units which may be roughly described as a twisting of this group about the C-C-C skeletal axis. It was noticed by Thompson and Torkington[3] that this last band showed a doublet structure in solid polythene which disappeared when the polythene became molten. This phenomenon was further investigated by Elliott, Ambrose, and Temple,[4] who confirmed this finding. Using polarized radiation, they reported that when the incident radiation was polarized perpendicular to the chain axis (in stretched, partially oriented polythene) the doublet was present, but when the radiation was polarized parallel to the chain only a single broad band was observed. They attributed the higher frequency component (referred to as component *B*), which disappeared on changing the direction of polarization, to the mode of vibration mentioned above and remarked that the origin of the other component was obscure, suggesting that it might be due to amorphous regions in the material.

More recently King, Hainer, and McMahon[5] have studied the behavior of this band with unpolarized radiation as polythene is cooled to 77°K and 4°K. The higher frequency component sharpens very considerably and moves about 4 cm^{-1} to shorter wavelengths; the lower frequency component (component *A*) remains broad and moves only about 1 cm^{-1} in the same direction. The explanation offered by these workers is that component *B* arises from chains in the *gauche* configurations in the crystalline portions while component *A* is due to chains in the *cis* configuration in amorphous portions of the polythene.

The effect of heating on this doublet was also studied by Robert and Favre.[6] Rugg, Smith, and Atkinson[7] discuss the effect of cold drawing of polythene on the intensity of the components and indicate that they are affected by the degree of strain of the polythene crystallites.

One object of the present investigation was to try to elucidate this phenomenon, it being considered important to have a complete understanding of the spectrum of polythene which may, in many senses, be regarded as the basic polymer. Since the phenomenon was clearly related to orientation and crystallinity, it was desirable to study pure crystalline *n*-paraffins of varying chain length above and below the melting point. It was also desirable to see whether corresponding changes took place in any of the other CH frequencies. In the case of the internal deformation mode of the CH_2 groups at 1470 cm^{-1}, such changes were found, but time did not permit a careful examination of the CH stretching frequencies near 2920 cm^{-1}.[8] It was also desirable to investigate deuterated paraffins to see whether

* R. S. Stein and G. B. B. M. Sutherland, J. Chem. Phys. **21**, 370 (1953). This work was conducted while both authors were at the Department of Colloid Science, Cambridge, England.

[1] N. Sheppard and G. B. B. M. Sutherland, Nature **159**, 739 (1947).

[2] G. B. B. M. Sutherland and A. Vallance Jones, Nature **160**, 567 (1947).

[3] H. W. Thompson and P. Torkington, Proc. Roy. Soc. (London) **184A**, 3 (1945).

[4] Elliott, Ambrose, and Temple, J. Chem. Phys. **16**, 877 (1948).

[5] King, Hainer, and McMahon, J. Appl. Phys. **20**, 599 (1949).

[6] Louis Robert and Jean Favre, Compt. rend. **234**, 2270 (1952).

[7] Rugg, Smith, and Atkinson, J. Polymer Sci. **9**, 579 (1952).

[8] Private communication from Dr. Gilbert W. King.

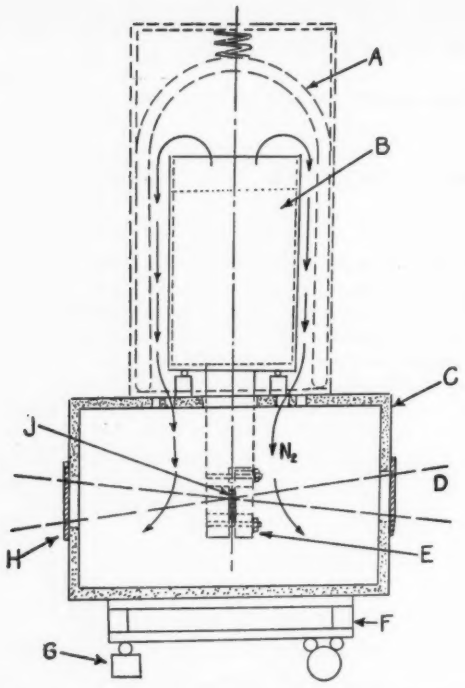

FIG. 1. The low-temperature unit: (A) removable Dewar flask; (B) copper cup containing liquid nitrogen; (C) insulated box; (D) path of infrared radiation; (E) cylindrical copper rod; (F) carriage which rides on the track (G); (H) silver chloride window; and (J) sample or silver chloride liquid cell.

the effects could be attributed to vibrations involving only the hydrogen (or deuterium) atoms and were not due to combination frequencies involving vibrations of the carbon skeleton. It was hoped that investigations along these lines, in addition to throwing light on the polythene phenomenon, might give help in understanding changes in the infrared spectra of compounds in going from the solid crystalline state through a partially ordered solid state to the liquid state.

EXPERIMENTAL PROCEDURE

The experiments described here were mainly carried out with a Perkin-Elmer Model 12B Spectrometer using automatic recording. The measurements with polarized radiation were made using a 5-plate selenium pile transmission polarizer which was placed immediately in front of the entrance slit. The resolving power at 725 cm^{-1} was approximately 3 cm^{-1}. Measurements

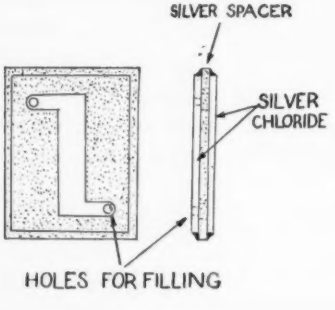

FIG. 2. The silver chloride liquid cell.

on polymer films at elevated temperatures were made by holding the sample between two rock salt plates in an electrically heated cell, the temperature of the sample being obtained by means of a thermocouple between the plates.

Measurements at liquid nitrogen temperatures were made in a special low temperature unit designed and constructed by Dr. A. V. Jones[9] (Fig. 1). The sample was held between silver chloride plates which were bolted between semicylinders of copper at the lower end of the copper rod (*E* of Fig. 1). Corrosion of the silver chloride by the copper was prevented by a covering of silver metal. Condensation of water on the silver chloride windows was prevented by flushing with a stream of dry nitrogen from the evaporating liquid nitrogen. Measurements by Dr. Jones indicated that the temperature of the sample was within 10°C of

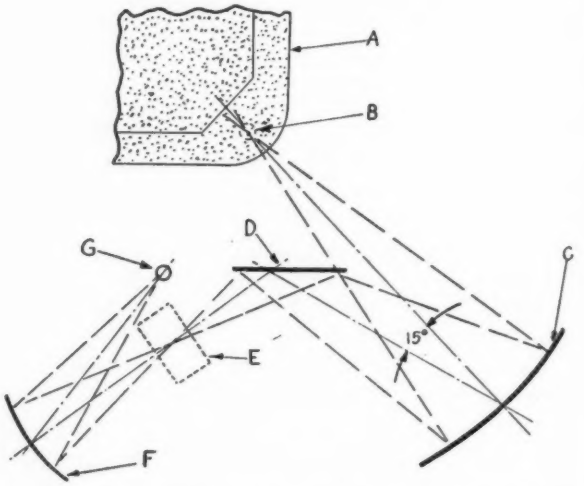

FIG. 3. The modified optical system: (A) the Perkin-Elmer spectrometer; (B) the former location of the globar; (C) a 15 cm diameter, 38 cm focal length front surface aluminized spherical mirror; (D) plane mirror; (E) sample cell; (F) 20 cm focal length front surface aluminized spherical mirror; and (G) the globar.

liquid nitrogen temperature, and that heating of the sample due to energy absorption from the infrared beam did not amount to more than 3° or 4°C.

Measurements on materials which were liquid at room temperature but solid at low temperatures were made by using the silver chloride transmission cell (Fig. 2) which was placed between the copper blocks *E*. The spacer was made of silver and the cell was bolted together. Arrangements were such that the cell could be filled after it was mounted on the copper rod. It was not possible to obtain a completely uniform layer of solid upon freezing the liquid and consequently impossible to obtain quantitative intensity measurements under these conditions.

In order to make room for the low temperature unit, it was necessary to have an extra focus in the radiation

[9] A. Vallance Jones, Ph.D. dissertation, Cambridge University (1949).

path. This was done as shown in Fig. 3, the low temperature unit being mounted on a sliding platform which could be moved in and out from the optical path without upsetting alignments.

The polythene samples studied were both solvent cast and extruded samples of du Pont polythene† and ICI polythene.‡ The solid pure *n*-paraffin samples studied were mostly those used in the investigations of Dr. Alex Müller[10–17] and were kindly made available to us by Professor Sir. E. K. Redeal, then at the Royal Institution. The remaining samples of *n*-paraffins were kindly supplied by Dr. J. W. Oldham of the Royal Institution and by the Anglo-Iranian Oil Company.

EXPERIMENTAL RESULTS

(a) Polythene

The effect of melting on the polythene doublet near 725 cm^{-1} was first reinvestigated using unpolarized radiation. At room temperature, the doublet consists of two peaks, one at 720 cm^{-1} (A) and the other at about 730 cm^{-1} (B) (Fig. 4). In all cases, the intensity of the lower frequency component (A) was observed to be greater than that of the higher frequency one (B). A general observation was that the more highly crystalline the sample, the more nearly were the two peaks equal in intensity. As the temperature was increased, the intensity of component *B* decreased continuously until at the melting point it had completely disappeared. Component *A* became lower and broader during this process, but the integrated extinction coefficient remained essentially constant. Upon cooling, the bands reversibly assumed their original shapes. No shift in the frequency of maximum absorption for either of the bands was observed.

An attempt was made to divide a plot of the extinction coefficient (Fig. 5) into two bands. This was done assuming (a) that the extinction coefficients of the bands are additive, (b) that the bands are symmetrical about their maxima, (c) that the loss in radiation due to scattering by the solid may be determined by interpolating from transmission measurements made on either side of the doublet where no absorption is believed to occur, and (d) that there is not an appreciable part of the absorption which is included in a long low tail extending far from the center of the band. The areas under the two bands were determined by measurement with a planimeter and were corrected for the finite slit width of the spectrometer using the method of Hardy and Young.[18] In making this correction, it was assumed that the bands had the shape described by the well-known Lorenz equation (1).

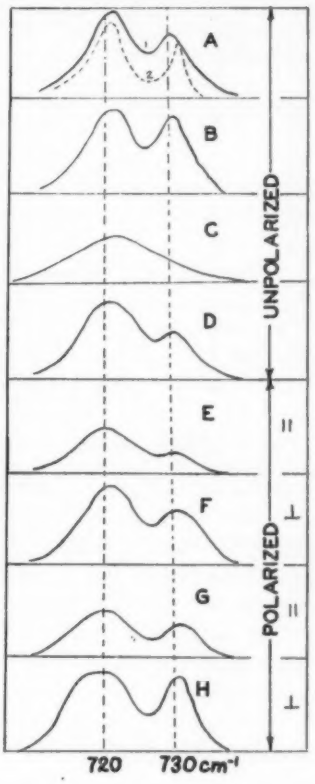

FIG. 4. The behavior of the 13.8μ doublet of polythene under various conditions: (A) general appearance at (1) room temperature and (2) −185°C; (B) appearance with a highly crystalline sample of polythene at room temperature; (C) at the melting point of polythene (about 110°C); (D) sample corresponding to (A) which has been stretched 500 percent at room temperature; (E) the preceding sample with radiation polarized parallel to the direction of stretching, and (F) perpendicular to the direction of stretching; (G) the preceding sample after annealing at a temperature slightly below the melting point with parallel polarization, and (H) with perpendicular polarization.

$$\ln\frac{I_0}{I}=\frac{c}{(\nu-\nu_0)^2+b^2}. \tag{1}$$

The correction factor was

$$\text{percent error}=\frac{\ln(I_0/I)_{\max}}{11.08}\frac{a^2}{S^2}, \tag{2}$$

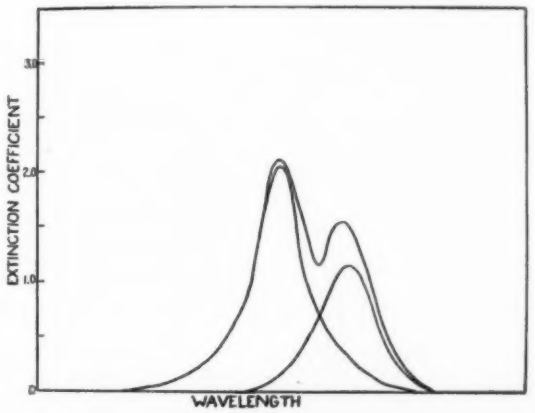

FIG. 5. The resolution of the doublet into two bands.

† Supplied through Dr. J. H. Dillon through the courtesy of Dr. F. F. Signaigo. E. I. du Pont de Nemours and Company, Rayon Department, Pioneering Research Station, Buffalo, New York.

‡ Supplied through the courtesy of Dr. R. B. Richards, Imperial Chemical Industries, Ltd., Alkali Division, Winnington, Northwich, Cheshire, England.

[10] A. Müller, Proc. Roy. Soc. (London) **A124**, 317 (1929).
[11] A. Müller, Proc. Roy. Soc. (London) **A127**, 417 (1930).
[12] A. Müller, Proc. Roy. Soc. (London) **A138**, 514 (1939).
[13] A. Müller, Nature **129**, 436 (1932).
[14] A. Müller, Proc. Roy. Soc. (London) **A154**, 624 (1936).
[15] A. Müller, Proc. Roy. Soc. (London) **A158**, 403 (1937).
[16] A. Müller, Proc. Roy. Soc. (London) **A178**, 227 (1941).
[17] A. Müller and K. Lonsdale, Acta Cryst. **1**, 129 (1948).
[18] A. C. Hardy and F. M. Young, J. Opt. Soc. Am. **39**, 265 (1949).

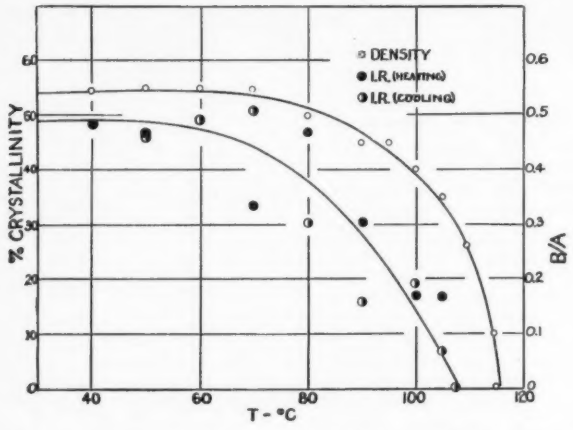

FIG. 6. A comparison of the ratio of the intensity of peak B to that of peak A with temperature with the variation of crystallinity (as determined by density methods).

where S is the half-width of the band and a that of the spectrometer slit. In no case did this correction amount to more than 10 percent.

The ratio of the integrated extinction coefficient under band B to that under A is plotted as a function of temperature in Fig. 6. For comparison, a typical plot of the crystallinity of polythene as a function of temperature[19] is also included. It is apparent that the relative integrated extinction coefficients and the degree of crystallinity are closely related.

A sample of the du Pont polythene 20μ thick was cold drawn as much as possible without tearing (about 500 percent) and spectra were determined. It was found that when stretched and examined with unpolarized radiation, band B became considerably weaker (Figs. 4a and 4d). For example, in the unstretched state the ratio of the extinction coefficient at the maximum of band B to that of A was about 0.7, while in the stretched state it appeared to be about 0.4. (These figures are rough because of the overlap of the bands.) With polarized radiation, band A gave a dichroism D

$$(\text{where } D=[\ln(I_0/I)_{\max\perp}]/[\ln(I_0/I)_{\max\parallel}])$$

of 6.5, while band B gave about 100. This indicates that whatever structural feature is responsible for band B is much more sensitive to orientation than that responsible for band A.

TABLE I. Transition points of C_nH_{2n+2}.

n	Melting point (This work)	(Müller)	(SPK)	Transition point (This work)	(Müller)	(SPK)
18	30°C	···	28.3°C	···	···	26.8°C
19	33°C	···	31.4°C	15°C	···	···
21	43°C	···	40.4°C	30°C	···	···
23	44°C	···	47.0°C	28°C	28–40°C	···
24	50°C	51.2°C	50.6°C	40°C	40–41°C	47.9°C
26	58°C	58.0°C	55.8°C	48°C	45–46°C	48.8°C
29	65°C	61.4°C	63.2°C	56°C	56.7–57.1°C	57.1°C
34	69°C	72.8°C	···	68°C	67–68.9°C	···
54	90°C (gradual)	···	···	80–92°C (gradual)	···	···

[19] R. B. Richards, Trans. Faraday Soc. 41, 127 (1945).

On annealing by heating for 1 hour at the melting point (without being held stretched) and then recooling quickly (5 minutes), the dichroism of each band was lost, and the intensity of band B relative to A regained its original value. There was, however, some indication that the relative intensities were restored at a lower temperature than that at which the dichroism vanished.

(b) Pure Hydrocarbons

In order to eliminate the complications arising from the coexistence of amorphous and crystalline components, the spectra of pure crystalline hydrocarbons were next studied. The latter were melted and crystallized on rock salt plates. It was found that for n-paraffins above $C_{16}H_{34}$, a doublet was present at temperatures well below their melting points, closely resembling that found for polythene except that the two peaks had equal intensity. However, on heating, peak B was observed to disappear sharply several degrees below the melting point, the transition range being less than a degree (Fig. 7). On cooling, the peak reappeared sharply at the same temperature. The transition temperature at which the peak disappeared is given for a series of n-paraffins in Table I. The melting points given in Table I were obtained by observing the temperature at which the edges of a small crystal of the material began to melt when placed on an electrically heated block on the stage of a polarizing microscope. These are compared with the values given by Müller[11] and Seyer, Patterson, and Keays (SPK).[20]

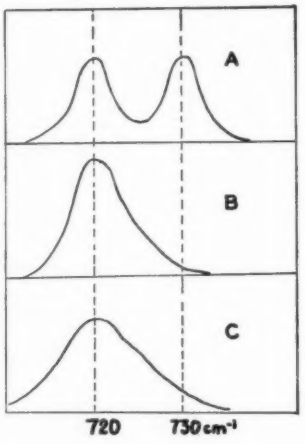

FIG. 7. The behavior of the 13.8μ doublet of n-paraffins at the transition point: (A) ½°C below the transition point; (B) ½°C above the transition point; and (C) above the melting point.

The transition temperatures may be compared (Table I) with transition temperatures ascribed to these same samples by Müller,[11] who observed a discontinuous change in the nature of the x-ray diffraction pattern. The transition points determined by Seyer, Patterson, and Keays came from discontinuities in the slope of the density-temperature curve. It is apparent that the various transition points are related to the same phenomenon. There seems little doubt that these transi-

[20] Seyer, Patterson, and Keays, J. Am. Chem. Soc. 66, 179 (1944).

tions are due to changes in crystal structure. The x-ray patterns indicate that on passing the transition point the longitudinal order of the chains in the crystal is preserved, but that there is an expansion of the unit cell perpendicular to the crystal symmetry in this plane. There appears to be some evidence to indicate that above the transition there is rotational disorder about the long axes of the chains.

(c) Deuteration

In a fully deuterated paraffin wax the absorption near 725 cm^{-1} is shifted to about 520 cm^{-1}.[1] Attempts to examine the behavior of this band on melting the deuterated paraffin led to inconclusive results because of lack of resolving power. However, this band was examined for us in another laboratory§ and the doublet separation in the solid phase was determined as 6 cm^{-1}, the individual peaks being at 518 cm^{-1} and 524 cm^{-1}. On heating to the melting point, the band at 524 cm^{-1} gradually disappears, as does the corresponding high-frequency component of this band in a normal paraffin wax.

The ratio of a hydrogenic frequency in an H compound to the corresponding frequency of the D compound should be approximately $\sqrt{2}$, and this same factor would be expected for doublet separations unless the doublet arises from combination with a low lattice mode due entirely to the nonhydrogenic atoms. The predicted separation for the doublet near 520 cm^{-1} would, therefore, be close to 7 cm^{-1} if the doubling phenomenon has no connection with the carbon vibrations. The observed value of 6 ± 1 cm^{-1} proves that the cause of the doubling must be sought entirely in motions of the hydrogen atoms.

The analog of the 1470 cm^{-1} band in n-paraffins is near 1090 cm^{-1} in the deuterated paraffin. This band is clearly a doublet in the original spectrum of Sheppard and Sutherland.[1] The maxima were carefully redetermined to be at 1086 cm^{-1} and 1093 cm^{-1}. On melting, the doublet disappears and is replaced by a single peak at an intermediate frequency.

(d) Splitting of Other Frequencies

The fact that the internal deformation frequency of the CD_2 group in solid deuterated paraffin is so clearly split at 1090 cm^{-1} led us to reexamine the band due to the corresponding frequency in CH_2 groups at 1470 cm^{-1} in C_{24}, C_{26}, C_{34}, and C_{54} n-paraffins. Although the fine structure of the atmospheric water vapor is troublesome in this region, it was possible to establish two peaks in the solid state close to 1464 cm^{-1} and 1473 cm^{-1}. On melting, these are replaced by a single broader peak centered near 1466 cm^{-1}. We understand that this same splitting has more recently been observed by King[8] in polythene, where he also finds evidence for splitting in the CH stretching frequencies near 3.4μ.

§ We are much indebted to the late Dr. H. P. Koch of the British Rubber Producers Research Association for making these observations for us.

TABLE II. Absorption bands obtained with n-paraffins in the vicinity of 13.8μ at approximately liquid nitrogen temperature.

n	Frequencies of absorption maxima (cm^{-1})
Above 18	720 (strong), 733 (strong)
18	720
16	720 (strong), 733 (fairly strong)
15	720 (strong), 728 (very weak), 733 (fairly strong)
11	720 (strong), 728 (weak), 733 (fairly strong)
10	720 (strong), 730 (strong)
9	720 (strong), 737 (strong)
6	720 (strong), 733 (weak)

(e) Effect of Low Temperatures

A sample of polythene was cooled to within 10 °C of the liquid nitrogen temperature. It was found that the component B became appreciably sharper and shifted a little towards higher frequencies (about 3 cm^{-1}). Band A exhibited a similar but much smaller shift (about 0.5 cm^{-1}) and remained diffuse. This is in agreement with the observations of King, Hainer, and McMahon.[5]

(f) Stearic Acid and Paraffin Wax

The 13.8μ band is present in any compound containing a paraffinic chain $-(CH_2)_nCH_3$ where $n>3$. Observations were made on stearic acid ($n=17$) and a similar doubling was observed at room temperature. The high-frequency component disappeared on melting. In solution in CS_2 it was also found that only the lower-frequency component was present. Similar results were obtained for ordinary paraffin wax. Cole and Jones[21] have observed the dichroic doublet for single crystals of $C_{19}H_{39}COOH$.

(g) Multiple Splittings

Paraffins below C_{18} which were normally liquid at room temperature were solidified by cooling to within 10°C of liquid nitrogen temperature in a silver chloride cell. Most of these exhibited splitting of the 13.8μ band, but not always in the simple manner found with the higher paraffins.

The results of these experiments are summarized in Table II. The resolving power was not so high in these cases as with the preceding measurements because of the scattering of the material and because of the difficulty of forming a uniform film of the solid.

It would be interesting to see whether these anomalies can be correlated with irregularities in crystal structure.

DISCUSSION OF RESULTS

In both of the explanations previously advanced for the doubling of the 13.8μ band in polythene[4,5] it was

[21] A. R. H. Cole and R. N. Jones, J. Opt. Soc. Am. 42, 348 (1952).

assumed that the two components of the doublet were quite independent of one another. There was agreement that component B at 730 cm^{-1} must be due to the rocking frequency of the CH_2 group in the oriented crystalline portions of the polymer, while component A at 720 cm^{-1} was attributed solely to the amorphous part of the polymer. The experimental work described above shows that the components of the doublet are not independent of one another. The most important new fact is that in several purely crystalline n-paraffins the intensities of the components are equal. It is only reasonable to conclude that in polythene the crystalline portion must also contribute to the intensity of component A of the doublet. Confirmation of this conclusion comes from our polarization data which show that A does possess the same type of dichroism as B, but much less pronounced. Additional support is given by our observation that the more crystalline the sample of polythene, the more nearly equal are the intensities of A and B. We may now consider in some detail some of the consequences of this conclusion.

Let A_c be the integrated extinction coefficient for band A due to the crystalline material, B_c the contribution of the crystals to band B, and let A_a represent the contribution of the amorphous material to band A, and A_T and B_T the total integrated extinction coefficients, respectively, of bands A and B. It follows that

$$A_c = B_c, \tag{3}$$

$$A_T = xA_c + (1-x)A_a, \tag{4}$$

and

$$B_T = xB_c, \tag{5}$$

where x is the weight fraction of crystalline material in the sample. Let ρ be the ratio of the extinction coefficients for amorphous to crystalline material, i.e.,

$$\rho = A_a/A_c.$$

Then

$$\frac{B_T}{A_T} = \frac{x}{x+(1-x)\rho}. \tag{6}$$

It is clear that as x decreases with increasing temperature, the ratio (B_T/A_T) will decrease in a corresponding manner. In fact, if ρ can be determined, it would be possible to determine x from a measurement of (B_T/A_T).

In this connection, it should be mentioned that some observations were made on the intensity of the 13.8μ bands in crystalline $C_{21}H_{44}$ above and below the transition temperature. It was found that the total integrated intensity of the two bands observed below the transition temperature was equal to the integrated intensity of the single band observed above that temperature. From such an observation one might conclude that the value of ρ should be 2. However, it could be argued that A_a should be derived from measurements above the melting point. This is not easy to do experimentally as the scattering of radiation is so different on the two sides of the melting point. Exploratory experiments seem to indicate that there is a decrease in the integrated extinction coefficient on melting which would reduce ρ to about 1.4.

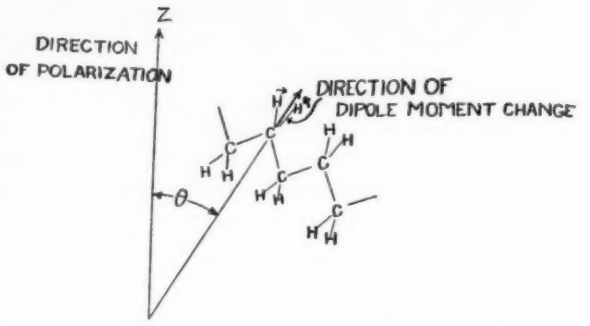

FIG. 8. The orientation of dipole moment change associated with the symmetrical CH_2 deformation frequency.

The CH_2 rocking motion causes a varying component of dipole moment only perpendicular to the chain axis. Therefore, in a completely oriented crystalline paraffin, absorption due to this vibration occurs only with radiation polarized perpendicular to these axes. Assume for simplicity that no double orientation occurs upon stretching and let the extinction coefficient per CH_2 group for light polarized along the direction of maximum varying dipole be a. If the angle between this direction for a CH_2 group and the actual direction of the incident electric vector is θ (Fig. 8), the extinction for this CH_2 group is $a\cos^2\theta$. The total extinction coefficient for radiation polarized parallel to the z axis for a sample of polythene containing n CH_2 groups per cm^3 will be

$$E_{\parallel} = a\sum_i n_i \cos^2\theta_i \tag{7}$$

where n_i of the CH_2 groups are oriented at angle θ_i. If the sample is unoriented, all orientations are equally likely and

$$E_{\parallel} = \tfrac{1}{3}na, \tag{8}$$

since $\cos^2\theta = \frac{1}{3}$ averaged over a sphere. Similarly for an unoriented sample

$$E_{\perp} = \tfrac{1}{3}na \tag{9}$$

and thus for unpolarized radiation

$$E = E_{\parallel} + E_{\perp} = \tfrac{2}{3}na. \tag{10}$$

Now suppose the sample is completely oriented with the chain axis lying along the z axis and with the a and b axes randomly oriented in a direction perpendicular to this; clearly

$$E_{\parallel} = 0, \tag{11}$$

while for $E_{\perp}$, θ may assume any value around a circle with equal probability giving

$$E_{\perp} = \frac{na\int_0^{2\pi}\cos^2\theta d\theta}{2\pi} = \tfrac{1}{2}na \tag{12}$$

and, for unpolarized radiation,

$$E=\tfrac{1}{2}na. \tag{13}$$

It follows, therefore, that for unpolarized radiation, the extinction coefficient E will be less for an oriented sample than for an unoriented sample. Now band B is due entirely to the crystalline material, which orients quite highly on stretching.[22] This accounts qualitatively for the reduction in absorption for this band on stretching (Fig. 4). Band A is due to both amorphous and crystalline contributions. The amorphous material does not orient nearly so well as does the crystalline; consequently, the reduction in intensity for this band will not be so great. Thus the ratio (B/A) should decrease on stretching in agreement with observation (Fig. 4). There is some evidence that the reduction may be even greater than one would expect from this consideration, and that a further decrease in band B may occur as a result of a factor such as crystal deformation. However, better intensity measurements are necessary to establish this point.

The conclusion that in polythene component A is due partly to amorphous and partly to crystalline material, whereas component B is due entirely to crystalline material, also gives a satisfactory explanation of the behavior of these bands at very low temperatures. The considerable sharpening of band B is probably due to the depopulation of higher energy lattice modes, combination with which can be an important factor in broadening this band at room temperature. The increase in the B frequency at very low temperatures is also to be expected since the lattice contracts as the temperature is lowered. The doublet separation which is presumably due to the crystalline field is, therefore, increased. On the other hand, the greater width of component A at all temperatures may be attributed mainly to the amorphous polythene. It probably arises from two causes: (a) the configuration of the polymer molecule is very variable in the amorphous state and (b) the field in which the CH_2 groups oscillate is also very variable.[5] Both factors could be expected to cause small changes in the rocking frequency. Since these conditions persist at low temperatures the width and position of this band will be rather insensitive to temperature.‖

We conclude that the splitting of certain frequencies in the infrared spectra of n-paraffins and of polythene in the solid form arises only when these materials are in a certain crystalline state. The exact manner in which the crystalline field causes the observed splittings is discussed in a following paper.[23]

ACKNOWLEDGMENT

The authors wish to thank Dr. A. Vallance Jones for valuable advice and assistance in parts of the experimental work and Dr. N. Sheppard for helpful discussion. One of us (R.S.S.) is indebted to the U. S. National Research Council for a fellowship during the tenure of which the major portion of this work was accomplished.

[22] C. W. Bunn, *Advances in Colloid Science* (Interscience Publishers, Inc., New York, 1940), Vol. 2, p. 146.

‖ Some recent observations by S. Krimm (J. Chem. Phys. **22**, 568 (1954)) demonstrate that the polarization of the components A and B is dependent upon the orientation of the a and b axes of the crystallites. This is further confirmation of the above observations, and is in agreement with predictions based upon an analysis of coupled vibrations within the crystal (see reference 23).

[23] R. S. Stein (to be published).

Vibrational Spectrum and Structure of Nitryl Chloride

RAYMOND RYASON* AND M. KENT WILSON
Mallinckrodt Chemical Laboratory, Harvard University, Cambridge, Massachusetts

(Received May 17, 1954)

An investigation of the infrared spectrum of gaseous NO_2Cl and the Raman spectrum of liquid NO_2Cl results in the following assignment of fundamental frequencies:

$\nu_1(a_1) = 1293\ cm^{-1}$, $\nu_4(b_1) = 1685\ cm^{-1}$,
$\nu_2(a_1) = 794\ cm^{-1}$, $\nu_5(b_1) = 367\ cm^{-1}$,
$\nu_3(a_1) = 651\ cm^{-1}$, $\nu_6(b_2) = 411\ cm^{-1}$.

The structural implications of the data are discussed, and it is concluded that the structure is .

However, it is not possible to say whether the molecule is planar or pyramidal.

INTRODUCTION

MULLER[1] prepared nitryl chloride in 1862, and examined its absorption in the visible region of the spectrum. Although he reported the absorption spectrum of NO_2Cl to be identical with that of NOCl, subsequent work[2] has shown NO_2Cl to be a colorless gas at room temperature, whereas NOCl is a reddish-brown gas. In the years following the initial researches on nitryl chloride, little work has been done to determine the structure of this acid chloride.[3] The chemical evidence is ambiguous as to whether there is an N—Cl or an O—Cl bond and has afforded no information as to the over-all geometry of the molecule.[4,5] A preliminary report on the infrared spectrum is contained in a communication concerned with the stability of nitryl chloride.[6] Strong bands were observed near 1700, 1340, 1275, and 795 cm^{-1}. The present paper reports a more extensive investigation of the vibration spectrum of this substance and discusses the structural implications.

EXPERIMENTAL

The reaction of anhydrous nitric acid with chlorosulfonic acid[7] proved to be a convenient method of synthesizing the nitryl chloride used in this investigation. The crude reaction product was frozen in a trap cooled with liquid nitrogen as rapidly as it was produced, and then purified by suitable bulb-to-bulb distillations.

The infrared absorption spectrum of gaseous NO_2Cl was obtained on a Baird Associates spectrophotometer equipped with NaCl optics, and a Perkin-Elmer Model 12C spectrometer, modified for double-pass operation, with NaCl, CaF_2, KBr, and CsBr prisms. Cells 4 cm, 5 cm, and 10 cm in length were used with three different window materials: NaCl single crystals, KCl pressed powder,[8] and polythene cut from wash bottles. The polythene windows were used from about 600 cm^{-1} to 300 cm^{-1}. An attempt to use KBr windows met with small success as gaseous NO_2Cl reacts with solid KBr to form an opaque white coating on the exposed surface. The corrosive action of this acid chloride on mercury necessitated the use of a spoon gauge for the pressure measurements.

The Raman spectrum was investigated, using a grating instrument[9] equipped with a Toronto mercury arc source.[10,11] When attempts to obtain the Raman spectrum of the gas were unsuccessful, a cold cell similar to that described by Lord and Nielsen[12] was constructed, and attempts were made to obtain the Raman spectrum of the liquid at −40°C. With a Wratten 2A filter the liquid NO_2Cl underwent only slight photodecomposition, but because of the very high absorption coefficient of the NOCl[13] formed only one Raman line was obtained. This was a very wide diffuse line centered at about 360 cm^{-1}.

The observed frequencies, assignments (assuming C_{2v} symmetry) and qualitative descriptions of the band shapes of the infrared bands of NO_2Cl are summarized in Table I. The numbering of the frequencies follows that suggested by Herzberg.[14] The observed spectrum of NO_2Cl, replotted on a linear frequency scale, is exhibited in Fig. 1.

* Present address: California Research Corporation, Richmond, California.

[1] R. Muller, Ann. Chem. Justus Liebigs **122**, 1 (1862).

[2] D. M. Yost and H. Russell, *Systematic Inorganic Chemistry* (Prentice-Hall, Inc., New York, 1946), p. 46.

[3] See reference 2, p. 48.

[4] M. Schmeisser and E. Gregor-Haschke, Z. anorg. u. allgem. Chem. **225**, 33 (1947).

[5] H. H. Batey and H. H. Sisler, J. Am. Chem. Soc. **74**, 3408 (1952).

[6] R. A. Ogg and M. K. Wilson, J. Chem. Phys. **18**, 900 (1950).

[7] See Schechter, Conrad, Daulton, and Kaplan, J. Am. Chem. Soc. **74**, 3052 (1952).

[8] R. Ryason, J. Opt. Soc. Am. **43**, 928 (1953).

[9] W. E. Brown, Ph.D. thesis, Harvard University (1948).

[10] Walsh, Crawford, and Scott, J. Chem. Phys. **16**, 97 (1948).

[11] The authors wish to thank Professor D. F. Hornig and his research group at Brown University for instructive discussions concerning the Toronto mercury arcs.

[12] R. C. Lord and E. Nielsen, J. Opt. Soc. Am. **40**, 655 (1950).

[13] See C. F. Goodeve and S. Katz, Proc. Roy. Soc. (London) **A172**, 432 (1939).

[14] G. Herzberg, *Infrared and Raman Spectra of Polyatomic Molecules* (D. Van Nostrand Company, Inc., New York, 1945), p. 272.

DISCUSSION

Although the strong bands at 367 cm^{-1}, 795 cm^{-1}, and 1685 cm^{-1} can immediately be assumed to be fundamentals, it would hardly be expected that both the strong bands at about 1300 cm^{-1} would be fundamentals. However, if the band at 651 cm^{-1} is assumed to be a fundamental, then the 1265 cm^{-1} and 1318 cm^{-1} bands can be accounted for by assuming Fermi resonance between a fundamental at *ca.* 1300 cm^{-1} and the first harmonic of the 651 cm^{-1} band. From a knowledge of the relative intensities of the bands making up the Fermi doublet one may obtain the unperturbed levels by use of the relation[15]

$$\frac{I_A}{I_B}=\frac{W-\Delta}{W+\Delta},$$

where I_A and I_B are the two intensities, W is the absolute value of the difference in frequency of the observed bands, and Δ is the absolute value of the difference between the unperturbed levels. In the derivation of this relation the intensity of the unperturbed overtone is neglected in comparison with that of the fundamental. The observed difference in frequency is 53 cm^{-1} and if the intensity ratio is estimated as 1.4 the difference in the unperturbed levels is calculated to be 9 cm^{-1}. Assuming no anharmonicity, the unperturbed level of the first overtone of the 651 cm^{-1} band would lie at 1302 cm^{-1}, and therefore the unperturbed fundamental is calculated to be at 1293 cm^{-1}. Thus, because of their intensity the bands near 367, 651, 794, 1293, and 1685 cm^{-1} are considered available for assignment to fundamental modes.

TABLE I. Infrared absorption bands of NO_2Cl.

Frequency (cm^{-1})	Assignment	Band structure
	Fundamentals	
1293	$\nu_1(a_1)$	*PQR*
794	$\nu_2(a_1)$	*PQR*
651	$\nu_3(a_1)$	*PQR*
1685	$\nu_4(b_1)$	*PR*
367	$\nu_5(b_1)$	Double *Q* branch
411	$\nu_6(b_2)$	...
	Overtone and combination bands	
732	$2\nu_5(A_1)$	...
822	$2\nu_6(A_1)$	*PQR*
1160	$\nu_2+\nu_5(B_1)$	Double *Q* branch
1318	$2\nu_3(A_1)$	*PQR*
2055	$\nu_4+\nu_5(A_1)$ / $\nu_1+\nu_2(A_1)$	*PQR*
2110	$\nu_2+2\nu_3(A_1)$	*PQR*
2517	$2\nu_1(A_1)$	*PQR*
2569	$\nu_1+2\nu_3(A_1)$	*PQR*
2666	$4\nu_3(A_1)$	*PQR*
2943	$\nu_1+\nu_4(B_1)$	*PR*
2990	$\nu_4+2\nu_3(B_1)$	*PR*
3343	$2\nu_4(A_1)$	...

[15] A. Langseth and R. C. Lord, Jr., Kgl. Danske Videnskab. Selskab. Mat-fys. Medd **16**, 6 (1948).

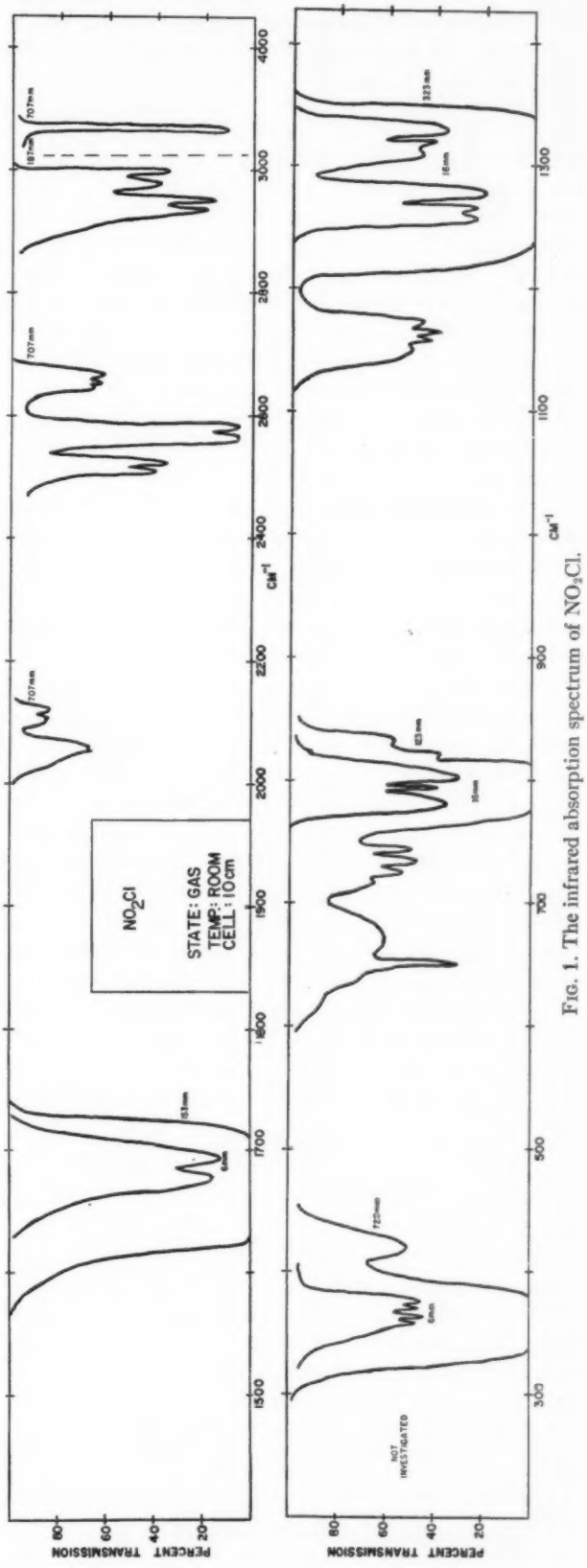

FIG. 1. The infrared absorption spectrum of NO_2Cl.

Nitryl chloride has the same number of valence electrons as the planar nitrate ion, so an assignment of

fundamentals on the basis of a planar model of C_{2v} symmetry will be attempted. The assignment of the bands at 1293 and 1685 cm^{-1} to the symmetric and antisymmetric N−O stretching modes, respectively, and the 795 cm^{-1} frequency to the NO_2 in-plane bend follows from the observation that in NO_2 the corresponding bands appear at 1322.5, 1616.0, and 750.9 cm^{-1}.[16] In NOCl[17] the vibration involving the N−Cl stretch is observed at 592 cm^{-1} and the deformation frequency is 332 cm^{-1}. Thus, we assign the 367 cm^{-1} band in NO_2Cl to the in-plane chlorine bending vibration and the absorption at 651 cm^{-1} to the N−Cl stretching mode. The remaining frequency, $\nu_6(b_2)$, is the out-of-plane bend and judging from the series F_2CO, Cl_2CO,[18] and Cl_2CS[19] in which ν_6 is, respectively, 774 cm^{-1}, 440 cm^{-1}, and 200 cm^{-1}, ν_6 in nitryl chloride must be at about 400 to 450 cm^{-1}. There is a weak absorption band very close to the strong absorption at 367 cm^{-1}; the maximum is at 410 cm^{-1}. If it is assumed that there are two fundamentals in this region, one, ν_5 at 367 cm^{-1}, and the other, ν_6 at *ca.* 411 cm^{-1}, the assignment of fundamentals is completed. The assumption of a band near 411 cm^{-1} also explains, in a qualitative manner, the shapes of the absorptions at 367 and 732 cm^{-1}, both of which are rather unusual for this molecule.

On the basis of this assignment, the remaining bands can be accounted for as combinations and overtones of these fundamentals. The details of this interpretation are presented in Table I. A few observed bands are not reported because they all changed intensity on purification, and coincided in frequency with known absorption bands of NO_2, NOCl, and NO.

Some further comments concerning the assignment of the bands at 794 and 651 cm^{-1} are necessary. In nitric acid, Cohn, Ingold, and Poole[20] assign to the NO_2 bending motion a frequency of 680 cm^{-1} which is observed in the Raman effect, but not in the infrared. These authors further assign a medium strength infrared band at 765 cm^{-1}, which does not occur in the Raman effect, as the out-of-plane bending mode of the NO_3 group. In nitromethane the NO_2 deformation is given as 647 cm^{-1}.[21] It is also reported that the symmetrical oxygen-chlorine stretching frequency in ClO_2[22] occurs at 954 cm^{-1} and the vibration corresponding to the O−Cl stretch in HOCl[23] is 739 cm^{-1}. Taken alone these assignments would indicate that in NO_2Cl the 651 cm^{-1} band is assigned as the NO_2 bend and the 794 cm^{-1} band as an O−Cl stretch in a model not possessing C_{2v} symmetry. However, the data on NO_2 and N_2O_4,[24] supplemented by our observation in NO_2F of a band at 826 cm^{-1} which is very similar in contour to the 794 cm^{-1} band observed in NO_2Cl, strengthens the assignment of this band to the NO_2 bend and suggests that the assignment in HNO_3 should be interchanged. Further, the 651 cm^{-1} band observed in NO_2Cl agrees very well with the N−Cl stretching frequency reported in NCl_3.[25]

A comparison of the observed band shapes in NO_2Cl with those calculated for various asymmetric top models by Badger and Zumwalt[26] yields additional tentative conclusions concerning the structure of nitryl chloride. Assuming NO_2Cl to be a planar molecule of C_{2v} symmetry, it is clear that vibrations of symmetry a_1 give rise to type *A* bands, vibrations of symmetry b_1 give rise to type *B* bands, and vibrations of symmetry b_2 lead to type *C* bands. To compare directly with Badger and Zumwalt's calculated band shapes, moments of inertia were calculated for five assumed structures of the NO_2Cl molecule. The N−O distance was assumed to be 1.16 A, the N−Cl distance 1.98 A, and the O−N−O angle 130°. Four of the structures were obtained by allowing the angle between the N−Cl bond and the O−N−O plane to vary from 180° to 140°. The fifth was obtained by assuming a planar molecule of C_{2v} symmetry with the above distances, and $\angle$O−N−O equal to 180°. The resulting moments were then used to calculate the asymmetry parameters of Badger and Zumwalt. Although a rather long extrapolation is required (the calculated parameters ranged from $\rho=1.16$ and $s=-0.53$ to $\rho=11.65$ and $s=-0.98$), it would seem that all five of the above structures lead to the conclusion that type *A* and type *C* bands should have strong *Q* branches, and type *B* bands should have two maxima. Thus, except for ν_5 and ν_6—the contour of ν_6 is uncertain—all the above structures correctly predict the observed band shapes for this assignment of the fundamentals. Therefore, it is not possible to distinguish between the planar and the pyramidal models for nitryl chloride from the shapes of the infrared absorption bands. However, the zigzag model

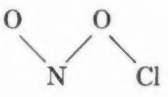

can be excluded for this model predicts that the bands at 1293, 794, and 651 cm^{-1} should be of type *B* and that at 1685 cm^{-1} should be a type *A* band. This is contrary to observation. An exactly similar argument excludes

[16] G. E. Moore, J. Opt. Soc. Am. **43**, 1045 (1953).
[17] W. G. Burns and H. J. Bernstein, J. Chem. Phys. **18**, 1669 (1950).
[18] Nielsen, Burke, Woltz, and Jones, J. Chem. Phys. **20**, 596 (1952).
[19] H. W. Thompson, J. Chem. Phys. **6**, 748 (1938).
[20] Cohn, Ingold, and Poole, J. Chem. Soc. 4273 (1952).
[21] A. J. Wells and E. B. Wilson, Jr., J. Chem. Phys. **9**, 314 (1941).
[22] K. Hedberg, J. Chem. Phys. **19**, 509 (1951).
[23] K. Hedberg and R. M. Badger, J. Chem. Phys. **19**, 508 (1951).
[24] W. D. Perkins and M. K. Wilson, Phys. Rev. **85**, 755 (1952).
[25] G. E. Moore and R. M. Badger, J. Am. Chem. Soc. **74**, 6076 (1952).
[26] R. M. Badger and L. R. Zumwalt, J. Chem. Phys. **6**, 711 (1938).

the highly unlikely model with the oxygen and nitrogen atoms on a line with the chlorine attached to one of the oxygen atoms and off the axis. Thus, the spectroscopic data obtained in this investigation support a structure for nitryl chloride in which a chlorine atom is bonded to an NO_2 group through the nitrogen atom.

ACKNOWLEDGMENTS

One of the authors (RR) wishes to thank the Harvard Graduate School of Arts and Sciences for predoctoral fellowships. We also wish to thank the Mallinckrodt Chemical Works for financial assistance covering a portion of this investigation.

THE JOURNAL OF CHEMICAL PHYSICS VOLUME 22, NUMBER 12 DECEMBER, 1954

Nuclear Magnetic Resonance in Liquids under High Pressure*

G. B. BENEDEK† AND E. M. PURCELL
Harvard University, Cambridge, Massachusetts

(Received May 21, 1954)

The work reported here is an application of free precession or "spin echo" techniques in nuclear magnetic resonance to a study of the properties of liquids under high pressure. The proton relaxation time T_1 was measured as a function of pressure, over the range 1 to 10 000 atmospheres, for six liquids: water, *n*-pentane, *n*-hexane, toluene, ethyl iodide, and methyl iodide. In addition to the relaxation time, the normalized values $D(P)/D(1)$ of the self-diffusion constant were measured as a function of pressure for water and methyl iodide.

In each liquid T_1 decreases with increasing pressure. However, comparison of the observed variation of T_1 with pressure with Bridgman's data on the variation of viscosity η with pressure shows in all cases (except that of methyl iodide for which no viscosity data are available) that T_1 is not simply proportional to $1/\eta$, but instead $T_1\eta$ increases with pressure. Similarly, for water and methyl iodide, the diffusion constant D varies in such a way that T_1/D increases with pressure. For water the Stokes-Einstein relation $D\eta=cT$ is obeyed within the errors of observation. The behavior of T_1 can be understood if one assumes that the dominant relaxation mechanism involves intramolecular fields, whose correlation time is determined by the rotational freedom of the molecule, and that compression of the liquid inhibits migrational freedom more drastically than rotational freedom.

The necessity of making the present measurements has led to the discovery that BeCu, a heat treatable alloy, makes a very satisfactory high pressure, non-magnetic bomb which might well be used for other magnetic investigations under high pressure.

INTRODUCTION

IT is well established that molecular motion plays a dominant role in the process of nuclear relaxation in ordinary (diamagnetic) liquids. Previous investigations[1] have revealed a fairly close relation between the nuclear relaxation time in a liquid and the macroscopic viscosity of that liquid. In those investigations a change in viscosity was brought about by changing the temperature or by changing the proportions of the components in a solution of two liquids. The experiments described here were undertaken to investigate the effect of high pressure on the nuclear relaxation time T_1 in several liquids. High pressure is known[2] to cause relatively large changes in viscosity. Observations of T_1 were made on the proton resonance in several liquids up to pressures as high as 10 000 atmospheres. Free precession ("spin echo") techniques[3-6] were used to determine the nuclear relaxation times. Since these spin echo techniques also provide a means of determining simply and accurately[3,6] the molecular translational self-diffusion constant D for a limited class of liquids, measurements of D as a function of pressure were made on two of the liquids studied.

EXPERIMENTAL EQUIPMENT AND PROCEDURES

(a) Spin Echo Aspects

In the free precession techniques of nuclear magnetic resonance, the sample is placed in a strong dc magnetic field and is surrounded by a coil whose axis is perpendicular to the direction of the dc field. A short pulse of current oscillating at the nuclear resonance (Larmor) frequency of the sample is passed through the coil producing a pulsed magnetic field oscillating at the nuclear resonance frequency. The magnetization vector of the nuclear spin system is nutated by this pulse to an extent which is determined by the product of the amplitude of the rf field and its time of duration. The nutating effect of a pulse can be used to specify the pulse; thus a pulse which nutates the spin system say 90° is called a "90° pulse." To measure the relaxation time T_1, a "180° pulse" is first applied to the sample

* This work was supported in part by the joint program of the Office of Naval Research and the U. S. Atomic Energy Commission.

† Now at the Lincoln Laboratory, M.I.T.

[1] Bloembergen, Purcell, and Pound, Phys. Rev. **73**, 679 (1948).
[2] P. W. Bridgman, Proc. Am. Acad. Arts. Sci. **61**, No. 3 (1926).
[3] E. L. Hahn, Phys. Rev. **80**, 580 (1950).
[4] E. L. Hahn, Phys. Today **6**, No. 11 (1953).
[5] H. Y. Carr, thesis, Harvard University (1952).
[6] H. Y. Carr and E. M. Purcell, Phys. Rev. **94**, 630 (1954).

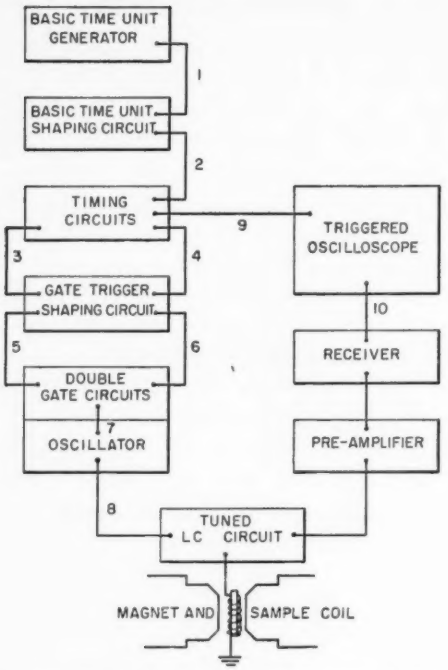

FIG. 1. Block diagram of electronic equipment.

(inverting the polarization vector) and then, at some later time, a 90° pulse is applied. Immediately after the latter pulse a signal is observed which is induced by the precessing nuclear magnetization, from the intensity of which one can infer the extent of the relaxation which has occurred since the initial pulse. To measure diffusion, one applies first a 90° pulse, then a 180° pulse, and observes the subsequent "spin echo." The intensity of the echo, under suitable conditions, is largely controlled by the incoherence resulting from diffusion of the precessing nuclei in the inhomogeneous magnetic field, and from the behavior of the echo intensity and a knowledge of the field gradient the diffusion constant can be deduced. Detailed explanations of these spin echo methods have been published in references 3, 4, 5, and 6.

It is to be noted that the spin echo techniques are suited to a determination of the self-diffusion constant D only for those liquids whose resonant nuclei are all in equivalent chemical environments. The presence of nonequivalent protons in a molecule gives rise to chemical shift and indirect spin-spin interaction[7,8] effects which make the determination of D difficult. As a result, in the present work D was measured as a function of pressure for only the liquids methyl iodide and water. Further, it must be noted that the measurement of D depends upon the presence of a magnetic field that varies linearly in magnitude along the sample. If the absolute value of the field gradient along the sample is known then the absolute value of D can be found. Experimentally a linear gradient can be produced at the sample by means of the magnetic field set up by two long, straight, current-carrying wires parallel to and equidistant from the sample. In the present experiments, emphasis is on the pressure dependence of the self-diffusion constant. As a result a serious effort to determine experimentally the exact value of the field gradient at the sample was not made. Thus, only normalized values of the diffusion constant $[D(P)/D(1)]$ (the ratio of D at pressure P to D at atmospheric pressure) are reported as a function of pressure.

The spin echo equipment which was used in this experiment has been described in detail in reference 5 and reference 9. The function of the various pieces of electronic equipment can be understood with the aid of the block diagram of Fig. 1. The basic time unit generator produces a characteristic signal (square wave or sinusoid) which is repeated periodically with a period

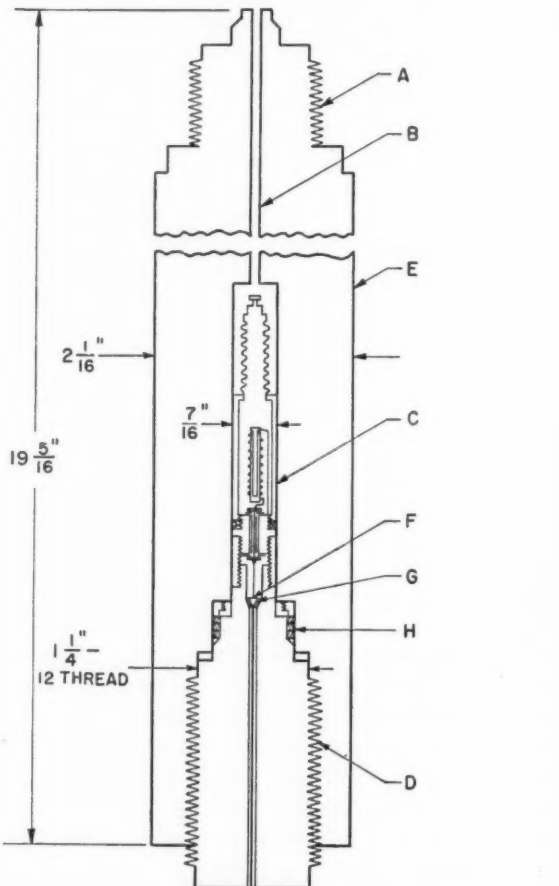

FIG. 2. Cross section diagram of bomb assembly.

[7] E. L. Hahn and D. E. Maxwell, Phys. Rev. **88**, 1070 (1953).
[8] Gutowsky, McCall, and Slichter, J. Chem. Phys. **21**, 279 (1953).

[9] G. B. Benedek, thesis, Harvard University (1953). A limited number of copies of this thesis are available for loan to those who may need more detailed information on the experimental equipment.

called the basic time unit (Btu). The Btu shaping circuit converts these signals into sharp trigger pulses which are then arranged into groups of 1000 triggers§ by the timing circuits. The timing circuit produces a square pulse at $t=0$ and at any chosen one of the following 1000 triggers and repeats this two pulse sequence in each succeeding group of 1000 Btu. After shaping, these two pulses are capable of triggering two separate gating circuits which in turn are capable of turning on a 30-Mc oscillator when triggered and turning it off at any time later. Thus the output of the oscillator consists of two 30-Mc rf pulses at $t=0$ and $t=N$ Btu, each of which has a pulse width which is variable independently of the other. The two rf pulses are then fed into an LC circuit tuned to the frequency of the oscillator which in turn is adjusted, by varying the strength of the dc magnetic field, to be the resonant or Larmor frequency for the nuclei of the sample. The inductive arm of the LC circuit serves as the coil enclosing the sample. The pulse width settings were adjusted so that one of the gates produced "90° pulses" and the other produced "180° pulses." A typical value for the 90° pulse width was 20 microseconds and H_1, the rf field amplitude during the pulse was about 3 gauss. The pulse widths available were in the range from 2 to 200 microseconds. The power output of the oscillator was of the order of 1 watt. Both the rf pulses and the nuclear signals that result from them are fed directly into an rf preamplifier, thence to a broad band receiver. Finally the detected driving pulses and nuclear signals are presented on an oscilloscope with a long persistence screen whose sweep is triggered at time $t=0$.

(b) High Pressure Aspects

One of Professor Bridgman's presses[10,11] capable of attaining pressures of 12 000 kg/cm² was used to produce the required pressure changes. The necessity of immersing the liquid test sample in a large dc magnetic field has led to the discovery that the nonmagnetic alloy beryllium-copper can be used as a high pressure bomb for pressures at least up to 10 000 kg/cm². The beryllium content of the alloy ranges from 1.7 to 2 percent depending upon the exact properties desired. The copper content is roughly 98 percent, and a trace of cobalt is included. Beryllium copper hardens by precipitation, and heat treatment hardens it all the way through. High strength Berylco No. 25 was obtained from the Beryllium Corporation of Reading, Pennsylvania, in the solution quenched form. In this form the alloy is soft, rather homogeneous in its interior and easily machinable. After machining the cylinder was hardened by heating it at 600°F for four hours and then quenching it to room temperature in water.

§ The timing circuit was capable of many operations. Only those operations used in measuring T_1 and D are described here.

[10] P. W. Bridgman, Proc. Am. Acad. Arts Sci. 49, 627 (1914).

[11] P. W. Bridgman, *The Physics of High Pressures* (G. Bell and Sons, Ltd., London, 1949).

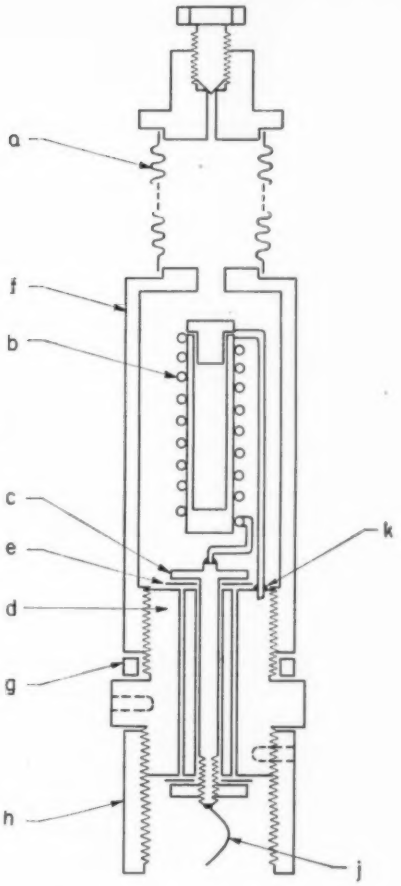

FIG. 3. Coil and sample holder assembly.

A cross section diagram of the BeCu high pressure bomb with the sample assembly and high pressure electrical plug in place is shown in Fig. 2. The bomb (E) is connected at (A) to the bottom of the high pressure press by means of a pipe connection of the unsupported area type. The pressure-transmitting fluid is led into contact with the sample holder assembly (C) via a long $\frac{1}{8}$ in. diameter hole (B).

Since the sample liquids had to be separated from the pressure transmitting fluid, an easily disassembled, leakproof rf coil and sample holder was developed. This holder, constructed of BeCu, is indicated crudely in Fig. 2 as (C) but is shown in detail in Fig. 3. Referring to Fig. 3 it will be observed that the loss in volume resulting from the compression of the sample fluid is taken up by the collapse of a metal sylphon (a) on the container. The rf coil (b) is grounded on one side at (k). Rf current is led out on a metal stem (c) which is insulated from the base section (d) by a mica washer (e) which was flat to within 1 ten thousandth of an inch. This washer also prevents leakage of the sample fluid past the stem (c). The container is sealed by screwing the case (f) tightly against a flat gold washer (g). The relative incompressibility of gold compared to BeCu insured that as the pressure increased this seal would tighten. The entire container was screwed onto a

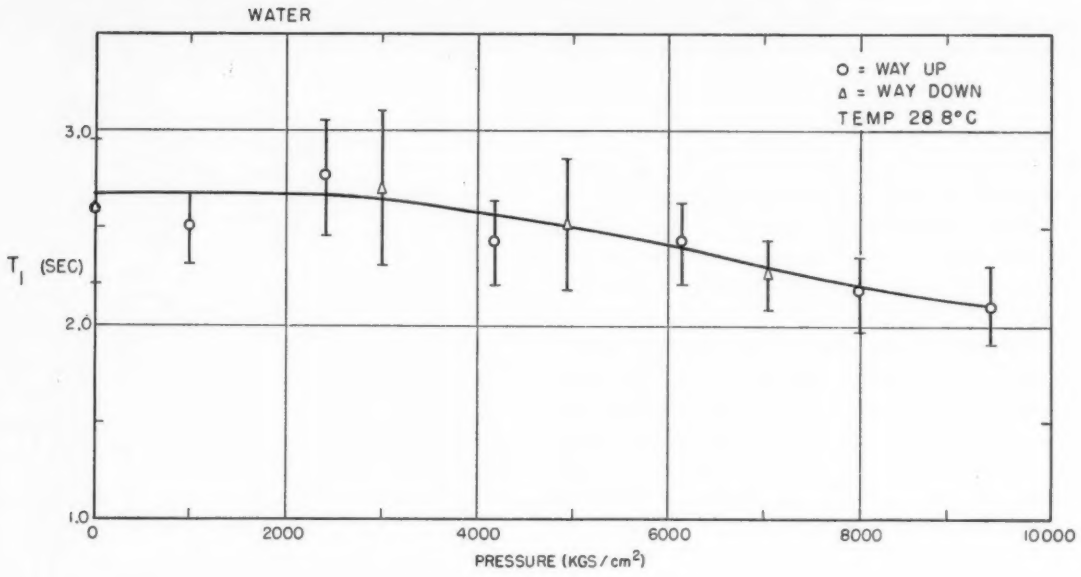

FIG. 4. T_1 *versus* pressure for water.

collar (*h*) whose other end was screwed onto the high pressure electrical plug *D* shown on Fig. 2. A flexible braided wire (*j*) was soldered between the rf coil and the electrical terminal on the plug *D*. Teflon spacers which were inserted in the sample holder to keep the sample fluid away from areas in which the driving field H_1 had a value different from its value inside the coil are not shown for the sake of clarity.

Returning to Fig. 2, it is seen that rf current is led in and out of the bomb by means of the high pressure BeCu electrical plug *D*. This plug contains as its electrical lead out element a cone type stem *F* insulated from its seat by a pipestone sleeve *G*. Leakage around the plug is prevented by the usual unsupported area type packing *H*. The washers used for this packing were constructed of lead and half hardened BeCu or copper.

Pressure was measured with a manganin wire gauge[11] connected to a Carey-Foster bridge. The gauge was calibrated against the freezing pressure of mercury at 0°C (7640 kgs/cm²).

All the high pressure equipment, including two low pressure pumps and the Carey-Foster bridge, was mounted on a movable platform which supported a scaffold from which the high pressure press and BeCu bomb were suspended. The lower end of the bomb could

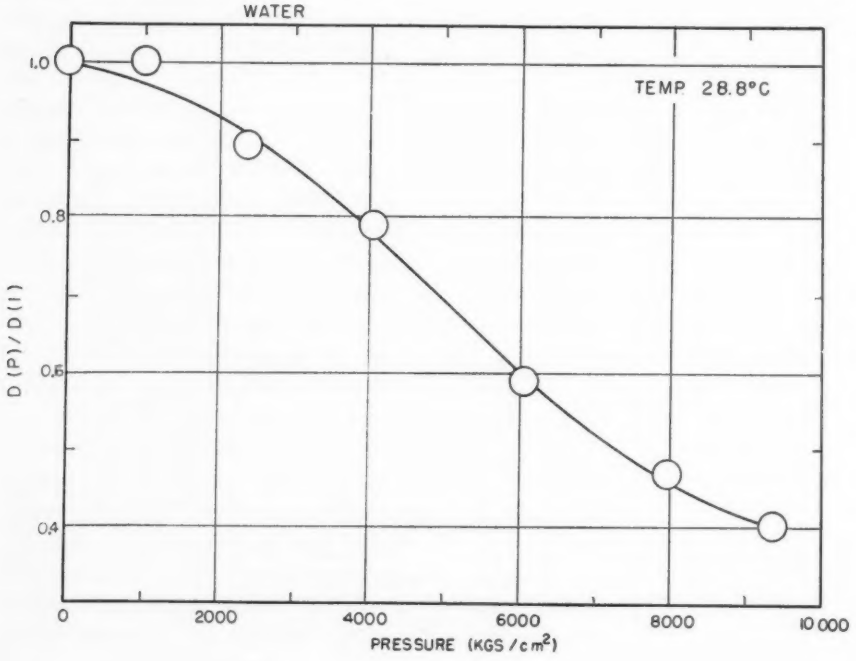

FIG. 5. Normalized diffusion constant *versus* pressure for water.

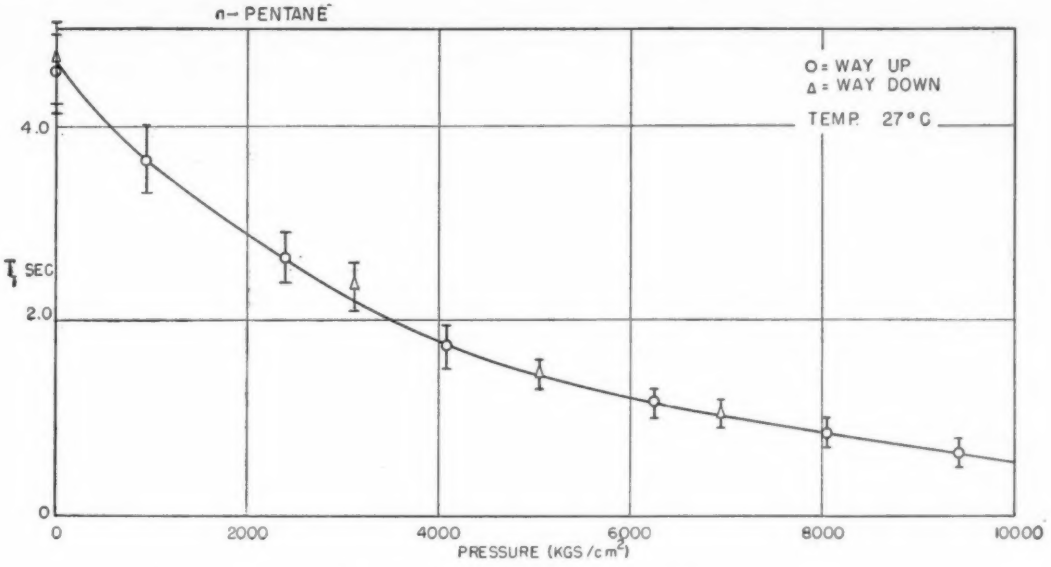

FIG. 6. T_1 *versus* pressure for *n* pentane.

thus be brought into the gap of an electromagnet which had a pole diameter of 8 inches and a pole separation of $2\frac{1}{8}$ inches. When work had to be performed on the press, the entire assembly could easily be wheeled away from the magnet into a clear area.

EXPERIMENTAL RESULTS

(a) Water (H_2O)

The water used was doubly distilled. The second stage of distillation took place in glass and included passage of the water vapor through an ion exchange column. An attempt to remove dissolved paramagnetic oxygen was made by boiling the water in an atmosphere of nitrogen and then sealing off the water in a vessel in which there was a nitrogen atmosphere. Figure 4 is a plot of T_1 *versus* pressure for H_2O. Points were taken both on the increase and on the decrease of pressure. The vertical line at each point indicates what is believed to be the limit of error. The small change in T_1 for water is a reflection of the relatively small viscosity variation in water as a function of pressure. Figure 5 is a plot of the ratio of the diffusion constant at pressure P, $D(P)$ to the diffusion constant at one atmosphere $D(1)$. This ratio will be called the normalized diffusion constant $D(P)/D(1)$.

(b) *n* pentane: $CH_3(CH_2)_3CH_3$

The pentane was obtained from Matheson, Coleman, and Bell. The sample was 99 percent pure *n* pentane, the principal impurity being isopentane. Figure 6 shows T_1 *versus* pressure again for points both on the increase and decrease of pressure.

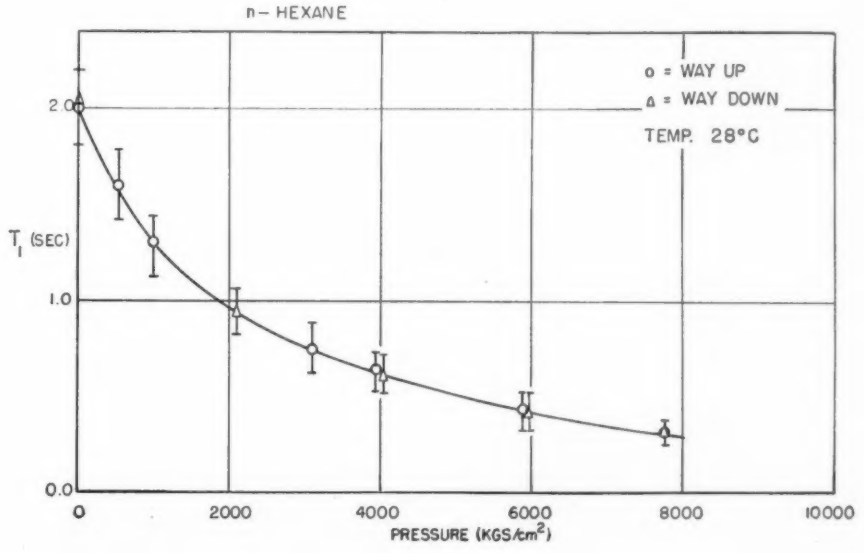

FIG. 7. T_1 *versus* pressure for *n* hexane.

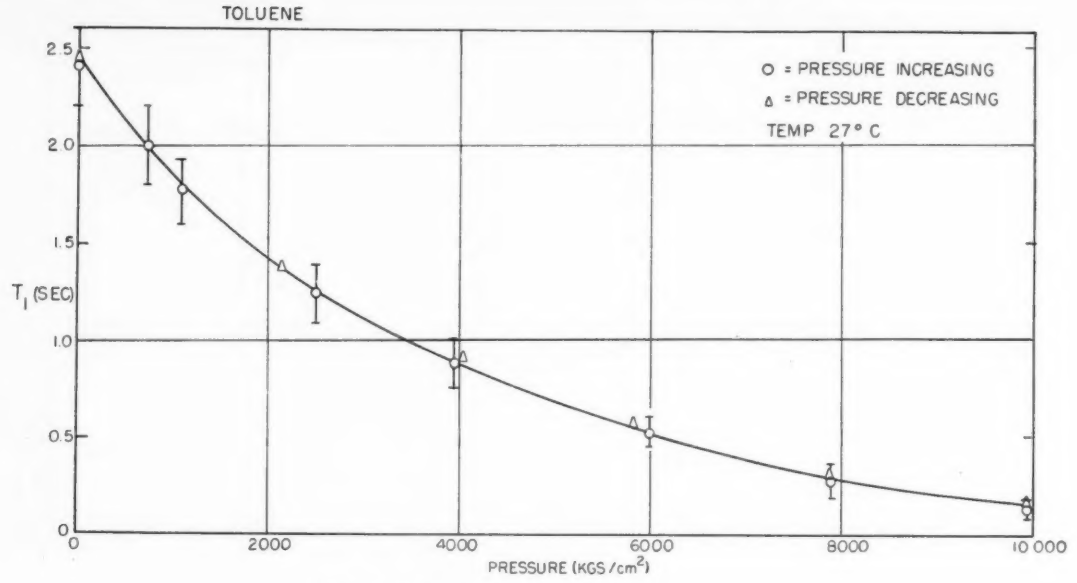

FIG. 8. T_1 *versus* pressure for toluene.

(c) *n* hexane: $CH_3(CH_2)_4CH_3$

Matheson, Coleman, and Bell supplied the *n* hexane. The sample was at least 99 percent *n* hexane, the most probable impurity being methyl cyclopentane. Figure 7 shows T_1 *versus* pressure.

(d) Toluene: $C_6H_5CH_3$

The purity of the toluene was in excess of 99 percent and it was free of unsaturates. Figure 8 shows T_1 *versus* pressure for toluene.

(e) Ethyl Iodide: CH_3CH_2I

The sample used was at least 99 percent pure. Figure 9 shows T_1 *versus* pressure for ethyl iodide.

(f) Methyl Iodide: CH_3I

The methyl iodide used was Eastman Kodak white label grade. Since the freezing pressure of CH_3I at room temperature was not known, the pressure was not increased beyond 7000 kg/cm² for fear of freezing the

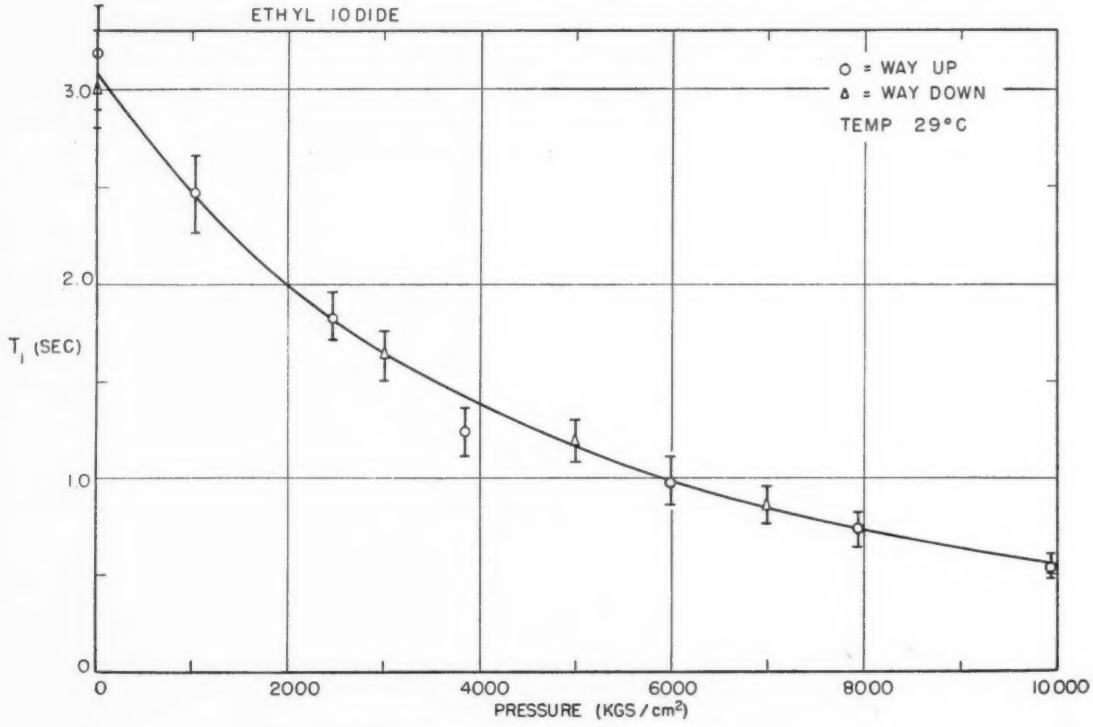

FIG. 9. T_1 *versus* pressure for ethyl iodide.

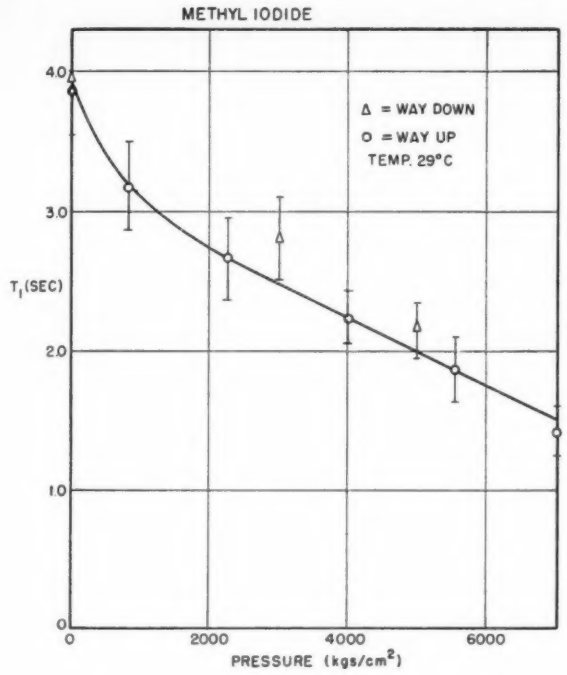

FIG. 10. T_1 *versus* pressure for methyl iodide.

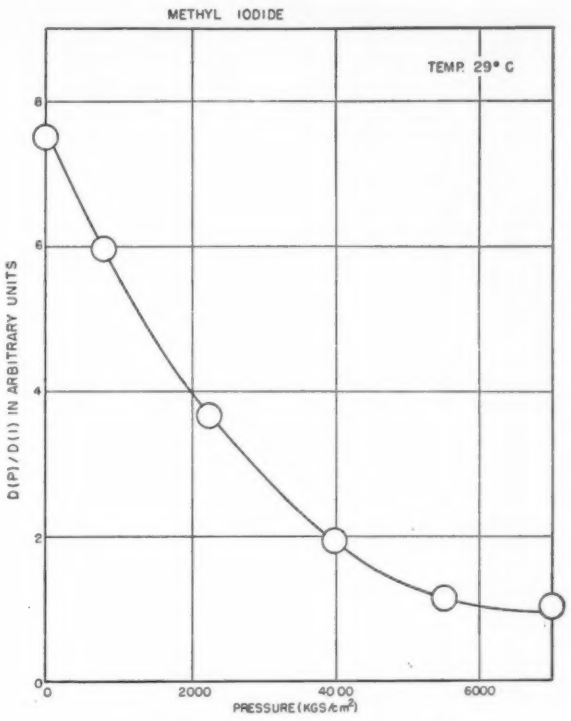

FIG. 11. Normalized diffusion constant D *versus* pressure for methyl iodide.

liquid and damaging the sample holder. T_1 *versus* pressure is shown in Fig. 10. The absence of modulation on the echo envelope made possible the determination of the variation of D with pressure. This is shown in Fig. 11.

COMPARISON WITH THE THEORY

A general theory of the mechanism of nuclear relaxation has been developed by Bloembergen, Purcell,

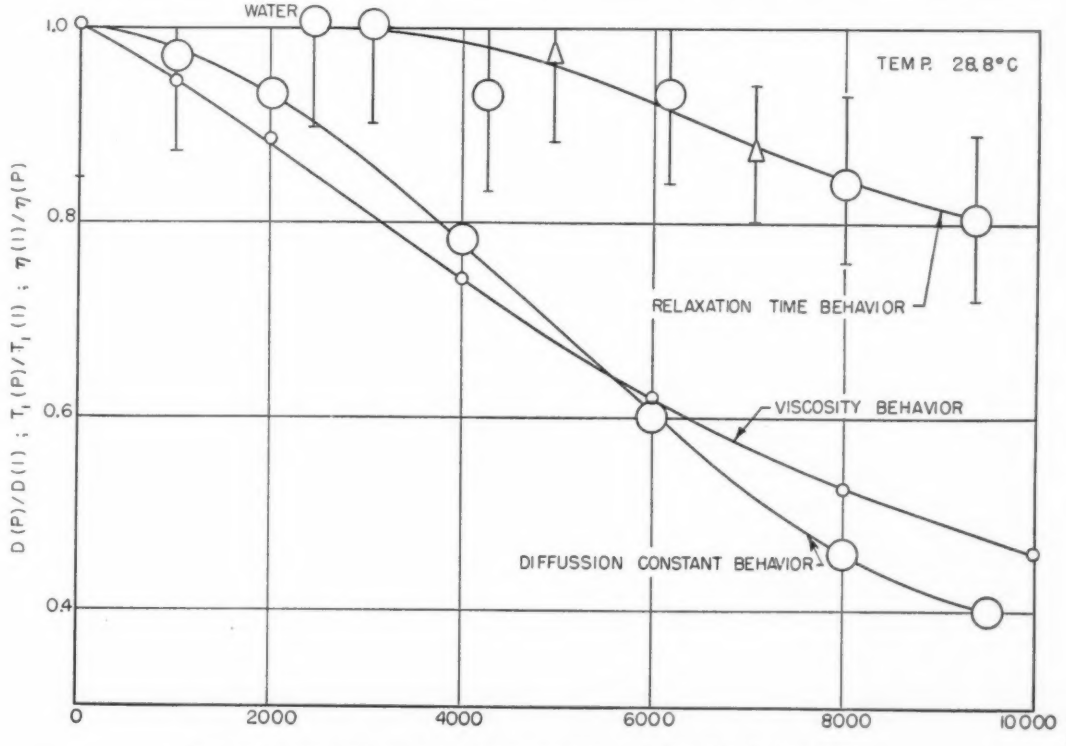

FIG. 12. Normalized relaxation time, reciprocal of normalized viscosity and normalized diffusion constant *versus* pressure.

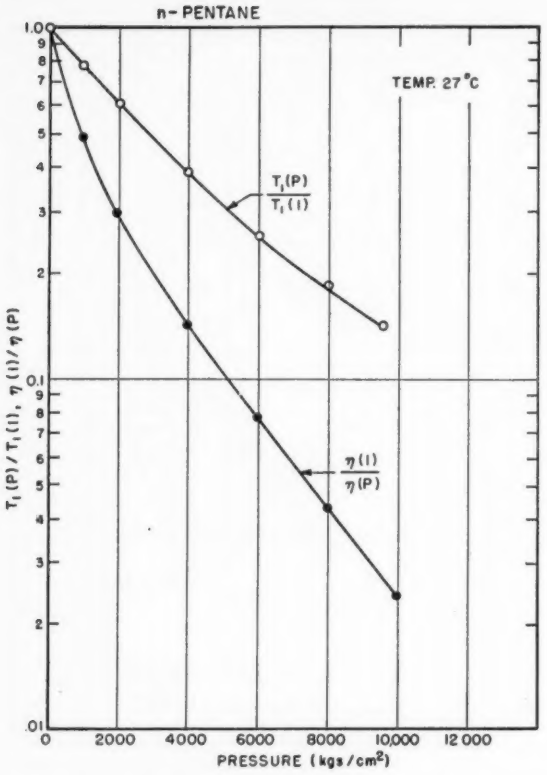

FIG. 13. Normalized T_1 and reciprocal of normalized viscosity *versus* pressure for *n* pentane.

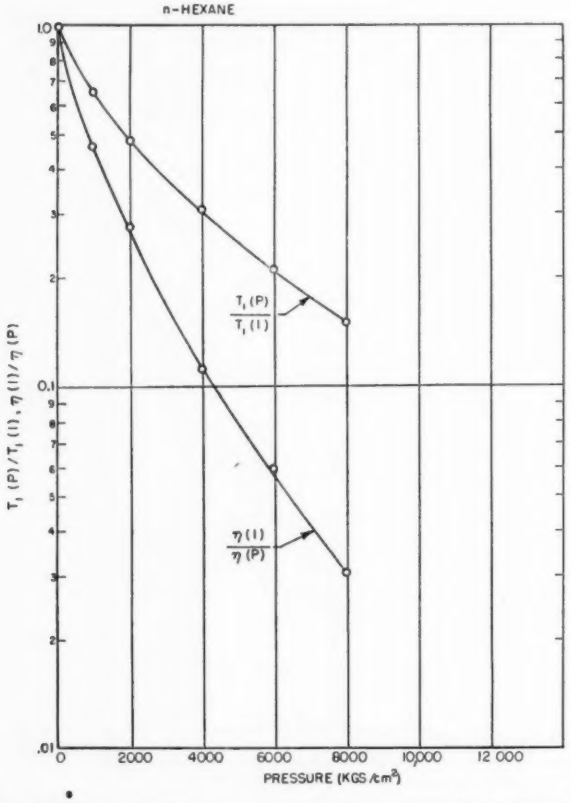

FIG. 14. Normalized T_1 and reciprocal of normalized viscosity *versus* pressure for *n* hexane.

and Pound.[1] By applying this theory to the case of the water molecule they were able to derive the following equation relating the relaxation time T_1 to the motion of the water molecules in the liquid:

$$\frac{1}{T_1}=\frac{9}{10}\frac{\gamma^4\hbar^2\tau_c}{b^6}+\frac{3\pi}{10}\frac{\gamma^4\hbar^2N}{aD}. \tag{1}$$

In Eq. (1), γ is the gyromagnetic ratio of the proton, b the internuclear distance in a water molecule, N the number of molecules per cm³, D the molecular diffusion constant, and a is the molecular radius. The first term on the right describes an *intra*molecular effect which depends on the random rotation or reorientation of the molecule. The quantity τ_c, defined more precisely in reference 1, is the correlation time for molecular rotation. The second term on the right expresses an *inter*molecular effect; the relaxation caused by fluctuating fields arising from protons in neighboring molecules. The field fluctuation is here mainly determined by the motion of the neighboring molecules relative to a given molecule, that is, by molecular diffusion. The correlation time of these fluctuations, which does not appear explicitly in the term as written, is of the order of magnitude a^2/D. Both this quantity and τ_c are assumed in Eq. (1) to be small compared to a nuclear Larmor period.

On the hypothesis that the molecule can be treated as a macroscopic sphere in a viscous liquid, τ_c in the

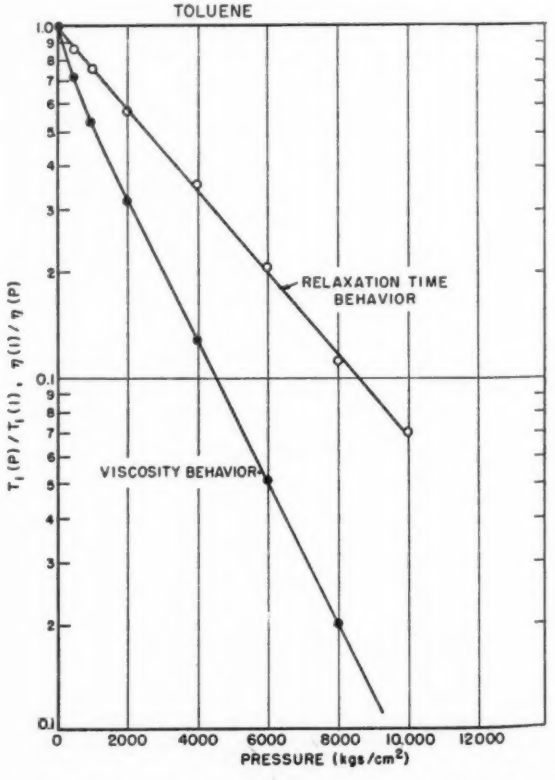

FIG. 15. Normalized T_1 and reciprocal of normalized viscosity *versus* pressure for toluene.

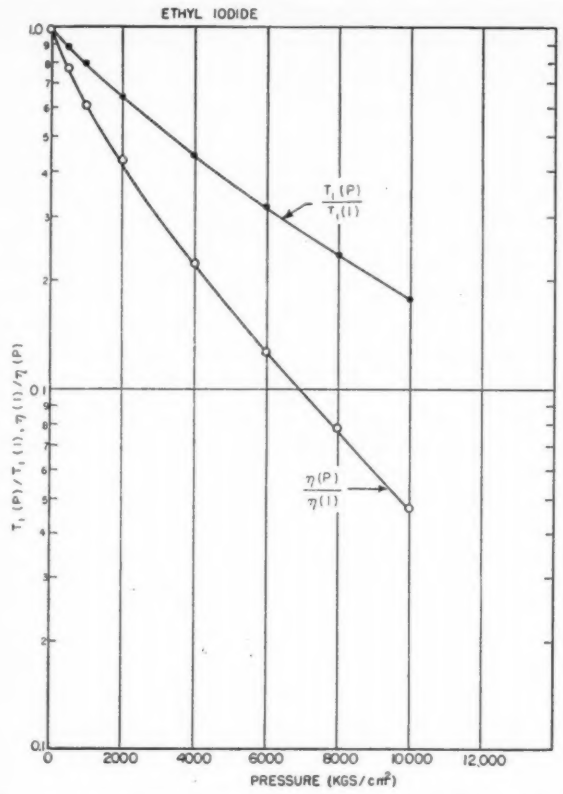

FIG. 16. Normalized T_1 and reciprocal of normalized viscosity *versus* pressure for ethyl iodide.

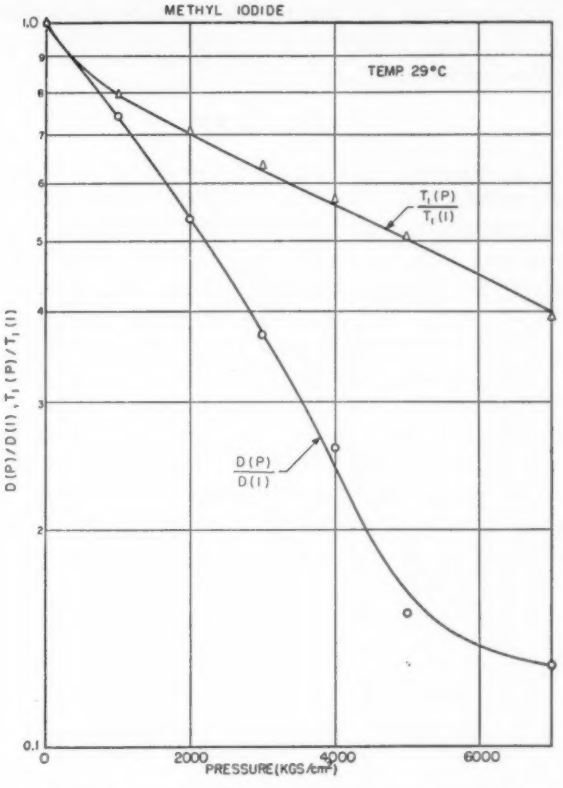

FIG. 17. Normalized diffusion constant and normalized T_1 for methyl iodide.

first term of Eq. (1) can be expressed[1] in terms of the macroscopic viscosity η as

$$\tau_c = (4\pi\eta a^3/3kT). \tag{2}$$

A similar hypothesis leads to the Stokes-Einstein relation between η and D, namely,

$$D = (kT/6\pi\eta a). \tag{3}$$

Using Eqs. (2) and (3), the expression for T_1 can be written in terms of the viscosity η as

$$\frac{1}{T_1} = \frac{\gamma^4\hbar^2}{5}\left[\frac{6\pi a^3}{b^6} + 9\pi^2 N\right]\frac{\eta}{kT}. \tag{4}$$

Generalizing the theory to apply to molecules containing several protons does not change the form of Eq. (4). Indeed the generalized expression for T_1 can be written simply as

$$(1/T_1) = (\alpha + \beta N)(\eta/T), \tag{5}$$

where α and β are constants independent of temperature and pressure and T is the absolute temperature.

Ignoring the relatively minor effect of pressure on N, we should thus expect, if relations (2) and (3) are valid, that T_1 would vary inversely with η as the pressure is changed at constant temperature. This prediction can be tested by comparing the observed variation of T_1 with pressure with Bridgman's data[2] on the variation of viscosity with pressure. In Figs. 12 to 16 are plotted the normalized relaxation time $T_1(P)/T_1(1)$ as well as the reciprocal of the normalized viscosity $\eta(1)/\eta(P)$ as functions of P.

The variation of T_1 is evidently not proportional to the variation in $1/\eta$. Instead the product ηT_1 increases significantly as the pressure is raised. If one were to take into account the variation of N, the disagreement with Eq. (5) would be even greater. This is scarcely worth while as the density change (at most 25 percent) is relatively small compared to the change in η.

In the case of methyl iodide no viscosity data are available, but we were able to measure the normalized molecular diffusion constant D, $(D(P)/D(1))$ as a function of pressure. Comparing the effect of pressure on D with the pressure variation of T_1 (Fig. 17), one observes that the change in D is much greater than the change in T_1. This too is in disagreement with the implication of Eqs. (3) and (5).

Finally, by using Bridgman's viscosity data in conjunction with the present measurements on the variation of the diffusion constant for water, the form of the Stokes-Einstein relation [Eq. (2)] can be checked. This is done in Fig. 12 wherein is plotted the inverse normalized viscosity $\eta(1)/\eta(P)$ and the normalized diffusion constant $D(P)/D(1)$ *versus* pressure. The closeness with which these two curves are in agreement can be taken as proof of the validity of the Stokes-

Einstein relation for water. The absence of viscosity data on methyl iodide made it impossible to check the Stokes-Einstein relation for this liquid.

CONCLUSIONS

It is apparent that the experimental results are in disagreement with Eq. (5). A natural explanation for this discrepancy can be found by examining the assumptions underlying Eq. (2). This equation relates the *reorientation* correlation time τ_c to the macroscopic viscosity η. Through the Stokes-Einstein relation (3), τ_c is further related to the molecular diffusion constant. It has been assumed, in effect, that the time required for the reorientation of a molecule is under all circumstances proportional to the time required for a translational diffusion jump. In the case that the temperature of the liquid is changed, this assumption is reasonable for an increase in temperature provides more thermal energy for the surmounting of both the rotational and translational barriers. This expectation was indeed confirmed in the case of glycerine[1] which showed over a wide range of η, a good correlation between η and $1/T_1$.

However, if the free volume of the liquid is reduced by compressing the liquid, it is altogether plausible that the freedom to migrate will be more drastically affected than the freedom to rotate. This is obviously true for spherical molecules and must hold true, in some degree, for molecules of any fairly compact form. Thus it is to be expected that τ_c, the correlation time for molecular reorientation, will not change as drastically with pressure as is implied by Eq. (2). As a result, the *intra*molecular contribution to T_1 will not fall off as rapidly with pressure as the *inter*molecular contribution. Since the intramolecular contribution is generally larger than the intermolecular term, it will therefore dominate the situation, and, as is observed, T_1 will be longer than would be expected from Eq. (5). We may say, therefore, that the present results are in harmony with the view that reduction of free volume in a liquid restricts the molecular migration more drastically than the molecular rotation.

ACKNOWLEDGMENTS

The authors wish to acknowledge with thanks the help of Professor P. W. Bridgman who suggested the use of beryllium copper as a nonmagnetic high pressure bomb, and who kindly lent us one of his high pressure presses. We thank also Dr. H. Y. Carr who designed and built the 90°–180° pulse spin echo equipment.

Microwave Determination of the Structure of Pyridine

BØRGE BAK, LISE HANSEN, AND JOHN RASTRUP-ANDERSEN
Chemical Laboratory of the University of Copenhagen, Copenhagen, Denmark
(Received May 20, 1954)

2-, 3-, and 4-mono-deutero-pyridine have been prepared and the microwave spectra recorded. For each of the isotopic species 11–12 transitions (*Q*- and *R*-branch lines) were localized, a number of which could be identified by their Stark effect. For all three species rotational constants of high precision were calculated. The material so provided in connection with known rotational constants for ordinary pyridine is insufficient for a complete determination of the ten geometrical parameters of the molecule. Seven models with a choice of C−H distances close to the correct value (1.075–1.085 A) were considered one of which was shown to be consistent with electron-diffraction work and current valence theory. In this model $d(N-C(2))=1.340\pm0.005$; $d(C(2)-C(3))=1.390\pm0.005$; $d(C(3)-C(4))=1.400\pm0.005$ A. The valence angles in the aromatic ring (starting with the C(6)−N−C(2) angle) are: 116° 42′; 124° 00′; 118° 36′; 118° 06′.

I. INTRODUCTION

THE problem of contributing to our knowledge of the configuration of pyridine by means of microwave measurements was simultaneously attacked by two groups of investigators.[1,2] While two of the present authors (B.B. and J.R.-A.) were unsuccessful in getting satisfactory agreement between the observed and the calculated spectrum, McCulloh and Pollnow[2] presented a very convincing analysis, partially based on their demonstration of the somewhat unexpected fact that the axis of *least* moment of inertia coincides with the dipole moment vector, the N−C(4) direction. By studies of the Stark effect for an authentic 1→2 transition this important property of the pyridine molecule was affirmed.[3]

McCulloh and Pollnow showed that pyridine is planar with a twofold axis of symmetry, and they calculated the principal moments of inertia. However, the magnitude of *ten* geometrical parameters must be known for a complete description of the geometry of the molecule. Therefore, determinations of the principal moments of inertia of several isotopic species, in addition to those of pyridine itself, must be made. In principle, the seven isotopic molecules derived from pyridine by isotopic substitution of one of the atoms N, C(2), C(3), C(4), H(2), H(3), and H(4) must be investigated. It is the purpose of the present paper to give data for the microwave spectra of the three monodeuterated pyridines. Although not complete, the picture of the pyridine molecule so obtained has so many interesting details, not subject to change as a result of possible exhaustive studies of the microwave spectra of a further number of isotopic pyridines that it seemed worth while to publish the present result.

[1] B. Bak and J. Rastrup-Andersen, J. Chem. Phys. **21**, 1305 (1953).
[2] K. E. McCulloh and G. F. Pollnow, J. Chem. Phys. **21**, 2082(L) (1953); **22**, 681 (1954).
[3] Bak, Hansen, and Rastrup-Andersen, J. Chem. Phys. **22**, 565 (1954).

II. EXPERIMENTAL PART

A. Preparation of Materials

No methods for the preparation of the partially deuterated pyridines can be found in the literature (pyridine-d_5 has recently been prepared[4]). Preparation from the corresponding halogen derivatives may be possible by means of a modified Grignard technique[5] (although certainly very difficult). The following simple method for conversion of a monohalogenated pyridine into the corresponding monodeutero derivative of high purity was finally found: 0.0085 mole of highly purified 4-chloro-, 3-bromo-, or 2-bromopyridine was dissolved in 25-cc $2n$ D_2SO_4 (0.05 equivalents) in a 150-cc flask fitted with reflux condenser. 1.31-g Zn dust (0.05 mole) was added and the mixture was kept at 100°C for 100 minutes under exclusion of atmospheric moisture. The amount of (excess) deuterium evolved corresponded very closely to the simultaneous occurrence of the reactions $Zn+D_2SO_4\rightarrow ZnSO_4+D_2$ and $C_5NH_4X+D_2\rightarrow C_5NH_4D+DX$ (X being a halogen atom), i.e. the pyridine is for example not converted to piperidine (which was found to happen in the reaction $C_5NH_4Cl(4)+HJ$[5] also investigated by us). After cooling of the reaction mixture the D_2O solution was separated from excess Zn dust by filtering. 10–15 cc of the deuterium oxide was distilled off at room temperature *in vacuo* into a receiver in which a mixture of dried $HgCl_2$ (5.5 g) and NaCl (1.5 g) had been placed in advance. The resulting salt solution was added to the contents of the distilling flash under vigorous shaking. After cooling to 0°C the white precipitate formed was filtered off, washed twice with ice-cooled alcohol and three times with dry ether and finally dried *in vacuo* over conc. H_2SO_4. The corresponding pyridine complex has first been described by Ladenburg[6] and its formula proved to be Py, HCl, $2HgCl_2$ (m.p. 179°).

In preliminary experiments with pyridine we found that the complex formed by us had the correct melting point but only approximately the composition given by

[4] Corrsin, Fax, and Lord, J. Chem. Phys. **21**, 1170 (1953).
[5] M. Proost and J. P. Wibaut, Rec. trav. chim. **59**, 971 (1940).
[6] A. Ladenburg, Ann. Chem. Justus Liebigs **247**, 1 (1888).

TABLE I. Yields of *D*-pyridines from 0.0085-mole halopyridine and their main infrared absorption lines in the 670–1300 cm^{-1} region (NaCl optics, Beckmann I.R.2 spectrophotometer). The strongest lines are in italics.

Compound	Ladenb. complex	*D*-pyridine	Infrared absorption places
2*D*-pyridine	4.35 g	0.40 g	*749*, *816*, 903, 995, 1031, 1062, 1113, 1154, 1214, 1300
3*D*-pyridine	3.25—	0.35—	*718*, 747, *824*, 849, 938, 979, 1034, 1087, 1109, 1128, 1198, 1272
4*D*-pyridine	4.50—	0.50—	709, 743, *864*, 991, *1016*, 1071, 1088, 1120, 1218, 1280
Pyridine			*703*, *749*, 991, 1031, 1069, 1149, 1217
Pyridine-d_5			762, 798, *823*, 833, 886, 908, *963*, 1011, 1043, 1143, 1228, *1302*

TABLE II. Observed and calculated microwave absorption frequencies of mono deutero pyridines in the 18 000–27 000 MHz region.

	2*D*-pyridine		3*D*-pyridine		4*D*-pyridine	
Transition	Observed	Calcul.	Observed	Calcul.	Observed	Calcul.
$1_{10}\rightarrow 2_{11}$	19537.4[a]	19537.1	19523.6[a]	19523.0	19116.5[a]	19115.6
$1_{01}\rightarrow 2_{20}$	25989.0[c]	25988.2	25949.0[c]	25948.5	26199.3[a]	26200.0
$2_{21}\rightarrow 3_{22}$	25260.5[c]	25261.1	25238.6[c]	25239.3	24827.8[c]	24827.5
$2_{11}\rightarrow 3_{12}$	26135.7[c]	26136.8	26098.0[c]	26097.4	26204.2[a]	26204.5
$2_{12}\rightarrow 3_{13}$	20019.5[c]	20020.3	19993.5[c]	19994.8	19950.7[a]	19950.8
$2_{02}\rightarrow 3_{03}$	20050.4[c]	20049.2	20022.3[c]	20022.4	20039.6[a]	20039.8
$9_{64}\rightarrow 9_{63}$	18704.5[b]	18704.6	18751.5[b]	18751.2		(15188)
$7_{44}\rightarrow 7_{43}$	19631.7[b]	19631.9	19628.8[b]	19628.9	18322.2[b]	18322.2
$6_{34}\rightarrow 6_{33}$	19843.5[b]	19843.3	19828.8[b]	19828.6	19186.0[b]	19186.2
$9_{54}\rightarrow 9_{73}$	20160.8[b]	20160.9	20116.7[b]	20116.6	21847.6[b]	21847.0
$10_{64}\rightarrow 10_{83}$	20439.5[b]	20439.7	20372.0[b]	20372.5	23734.0[b]	23734.4
$11_{74}\rightarrow 11_{93}$	20943.0[a]	20943.1	20838.4[c]	20838.1	26634.1[b]	26633.6

[a] Lines unambigously identified by their Stark effect.
[b] *Q* lines identified by the graphical method.
[c] Lines identified in spite of the presence of adjacent lines.

Ladenburg. Since, however, for our purpose the complex only acts as a suitable "multiplicator" of the small amount of *D*-pyridine formed (0.3–0.5 g) we did not care too much for its exact characterization. After the drying the complex was mixed with 2.0-g pulverized NaOH in a 40-cc glass tube which was afterwards evacuated, sealed off, and heated for one hour on a steam bath in order to liberate the deuterated pyridine. After cooling in liquid air the tube was opened and connected to a vacuum line. The *D*-pyridine formed was distilled off at 10°C yielding a product contaminated with about 5 percent of water judging from the infrared absorption curve of the liquid.

Three further distillations from vessels with 0.5, 0.2, and 0.1-g pulverized NaOH sufficed to remove all the water. The infrared spectra taken served to show that the procedure followed here resulted in the production of pure samples, not contaminated with pyridine, isomeric monodeuterated derivatives, or higher deuterated pyridines. The same conclusion could later be drawn from the microwave spectra. Table I gives numerical data in connection with the preparations.

B. Measurements of Microwave Absorption Frequencies and Identification of the Lines

The microwave spectrograph used was of the ordinary Stark-modulation type with a pen-and-ink recorder. Only rough estimates of the line intensities are possible. The built-in frequency standard was repeatedly calibrated against spectral lines of well-known frequency by recording these lines on the paper with the same tuning rate for the klystron as applied at the pyridine experiments. The frequency standard showed great stability, so that the frequencies measured by us are thought to be good to 0.1 MHz. Wherever possible the identity of the lines was secured by studies of their Stark effect, but it must be mentioned that there are serious limitations to the application of this principle for "large" molecules such as pyridine. At approximately every ten MHz a spectral line is found so that little space (if any) is left for the full "development" of the Stark pattern. For 1→2 and 2→3 transitions, however, it was often possible to carry through a Stark analysis in spite of the presence of adjacent lines. Most of these low-J, R-branch lines have a comparatively large Stark effect which, in the first place, means that they may be observed at low square-wave field intensity (150 volts/cm) where many of the remaining lines do *not* appear, and secondly, that their Stark components move rather vividly around between possible neighboring lines as a function of the square-wave voltage applied. When two or three of these R-branch lines had been identified a good estimate of the asymmetry parameter κ could usually be made. This enabled us to start looking for Q lines which could be picked out between candidates by plotting $(A-C)/2$ as a function of κ. Curves intersecting in a point common to a bunch belong to Q-type transitions. Table II gives the observed *and* identified lines for the three monodeuterated pyridines together with the calculated values based on the interpretation given. We are

TABLE III. Rotational constants (A,B,C) in MHz, asymmetry parameter (κ), and principal moments of inertia (I_a,I_b,I_c) in amu A^2 of pyridine and deuterated pyridines together with the quantum defect (Q.D.) of all four species.

	2*D*-pyridine	3*D*-pyridine	4*D*-pyridine	Pyridine
A	5900.80±0.14	5889.12±0.12	6038.90±0.13	6039.13±0.03
B	5558.47±0.14	5554.96±0.16	5419.93±0.13	5804.70±0.03
C	2861.76±0.14	2858.02±0.12	2855.78±0.13	2959.25±0.03
κ	0.77471±0.00002	0.77951±0.00004	0.61109±0.00002	0.84777±0.00001
I_a	85.663±0.002	85.833±0.002	83.704±0.002	83.701±0.001
I_b	90.939±0.002	90.996±0.002	93.263±0.002	87.081±0.001
I_c	176.633±0.008	176.864±0.007	177.002±0.008	170.814±0.002
Q.D.	0.061±0.012	0.035±0.011	0.035±0.012	0.032±0.004

aware of the disadvantage of not giving a full list of the observed frequencies. Such a list would, however, comprise between 500 and 1000 lines for *each* of the isotopic molecules in the 18 000–30 000 MHz interval investigated.

All observed frequencies were corrected for centrifugal stretching using the constants derived by McCulloh and Pollnow from their observations on pyridine. In principle the constants to be applied for the deuterated pyridines are a trifle different, but since the corrections are small (0.1–1.2 MHz) no significant error is committed by using the pyridine constants.

III. CALCULATION OF THE ROTATIONAL CONSTANTS

The rotational constants of the various deuterated pyridines were calculated by first reading $(A-C)/2$ and κ from the plot of the Q-type transitions. With 2D-pyridine as an example we found that intersection of the curves took place between $[(A-C)/2, \kappa]$ $=[1519.58, 0.77462]$ and $[1519.50, 0.77475]$. Hence we concluded that $(A-C)/2=1519.52\pm0.02$ and κ $=0.77471\pm0.00002$ ("probable" errors). These values were now inserted in the relationships below together with the experimental values of the frequencies (corrected for centrifugal distortion). This gave 6 different values of $A+C$, given in the column beside the frequency relations.

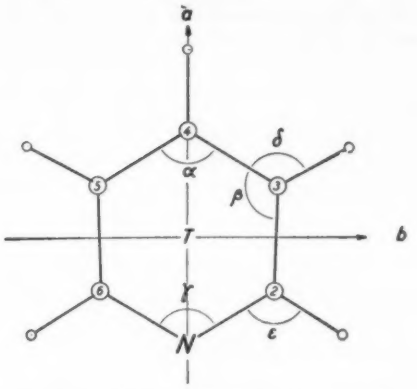

FIG. 1. Showing positions of pyridine atoms in relation to the principal axes of inertia and the center of mass, $T(0,0,0)$, of the entire molecule. Definition of the angles α, β, γ, δ, and ϵ.

	$A+C$
$\nu(1_{10}\rightarrow2_{11})=2(A+C)+(A-C)/2[3\kappa-1]$	8762.63
$\nu(1_{01}\rightarrow2_{20})=2(A+C)+(A-C)/2[\kappa+1+2(\kappa^2+3)^{\frac{1}{2}}]$	8762.95
$\nu(2_{21}\rightarrow3_{22})=3(A+C)+(A-C)/2[3\kappa-3]$	8762.37
$\nu(2_{11}\rightarrow3_{12})=3(A+C)+(A-C)/2[\kappa+3-2(4\kappa^2-6\kappa+6)^{\frac{1}{2}}]$	8762.18
$\nu(2_{12}\rightarrow3_{13})=3(A+C)+(A-C)/2[\kappa+3-2(\kappa^2+15)^{\frac{1}{2}}]$	8762.29
$\nu(2_{02}\rightarrow3_{03})=3(A+C)+(A-C)/2[3\kappa-3+2(\kappa^2+3)^{\frac{1}{2}}-2(4\kappa^2+6\kappa+6)^{\frac{1}{2}}]$	8762.97
	8762.56 ± 0.23

We concluded from this that $(A+C)/2=4381.28$ ±0.12. The known values of $(A-C)/2$ and $(A+C)/2$ result in the rotational constants $A=5900.80\pm0.14$ and $C=2861.76\pm0.14$. From the definition of κ as a function of A, B, and C we then calculated $B=5558.47\pm0.14$.

Table III gives the rotational constants for the three monodeuterated species. Since the rotational constant A refers roughly to the N−C(4)-line, the constant B to a line in the plane of the molecule perpendicular to the A axis and through the center of mass, and C to the principal axis perpendicular to the plane of the molecule, the qualitative significance of the rotational constants is easy to visualize.

IV. CALCULATION OF THE MOLECULAR MODEL

Based on the moments of inertia given in Table III our first task is to calculate the positions of the hydrogens. All coordinates refer to a Cartesian coordinate system (a,b,c) with its origin in the center of mass of pyridine and coinciding with the principal axes of inertia of that molecule. All moments of inertia and masses with a prime refer to monodeuterated molecules, those without to pyridine itself. Defining

$$k=\frac{M'}{M(m_D-m_H)}=1.00610\ \text{amu}^{-1},$$

where M is the mass of pyridine, we can write:

$$a^2=\frac{k}{4(I_b-I_a)}\cdot[(I_c'-I_c)-(I_a'-I_a)+(I_b'-I_b)]\times[(I_b'+I_b)-(I_c'-I_c)-(I_a'+I_a)],$$

$$b^2=\frac{k}{4(I_b-I_a)}\cdot[(I_c'-I_c)+(I_a'-I_a)-(I_b'-I_b)]\times[(I_b'+I_b)+(I_c'-I_c)-(I_a'+I_a)].$$

By insertion we get the results of Table IV.

If we let small letters refer to the coordinates of the hydrogens, capital letters to the coordinates of the ring atoms (N(A_1,B_1), C(A_i,B_i), where $i=2, 3, 4, 5, 6$), the molecule being placed as shown in Fig. 1, it is easy to

TABLE IV. Calculated positions of the hydrogen atoms in pyridine (a,b) (A.U.); moments of inertia of the hydrogens (I^H) and the carbon-nitrogen ring ($I^{5C,N}$) (amu A^2).

	H(2)	H(3)	H(4)
a	-1.276 ± 0.004	1.205 ± 0.004	2.493 ± 0.004
a^2	1.630 ± 0.010	1.453 ± 0.010	6.213 ± 0.020
b	2.056 ± 0.004	2.153 ± 0.004	
b^2	4.225 ± 0.020	4.634 ± 0.020	
I_a^H		17.86 ±0.08	
$I_a^{5C,N}$		65.84 ±0.08	
I_b^H		12.48 ±0.06	
$I_b^{5C,N}$		74.60 ±0.06	

TABLE V. Survey of carbon-hydrogen distances (d(C(i)−H)) (A) assumed at the calculation of molecular models I–VII.

d(C(2)−H)	1.075	1.080	1.085	1.075	1.085	1.075	1.085
d(C(3)−H)	1.075	1.080	1.085	1.080	1.080	1.085	1.075
d(C(4)−H)	1.075	1.080	1.085	1.085	1.075	1.085	1.075
Model no.	I	II	III	IV	V	VI	VII

derive that

$$m_N A_1^2+m_C(2A_2^2+2A_3^2+A_4^2)=I_b-I_b^H=I_b^{5C,N}, \quad (1)$$

$$m_C(2B_2^2+2B_3^2)=I_a-I_a^H=I_a^{5C,N}, \quad (2)$$

$$m_N A_1+m_C(2A_2+2A_3+A_4)=-m_H(2a_2+2a_3+a_4), \quad (3)$$

where (3) expresses, that b is an axis through the center of mass.

These three equations contain six unknowns. It is exactly at this point that some experimental material from, say, $C_4{}^{12}C^{13}NH_5$ would be useful. However, for lack of such data we have decided to proceed as follows:

Since we know the location of the hydrogens we may draw circles, centered in the hydrogen positions and with radii ($=d_{CH}$) equal to supposed C−H distances. We have considered the possibilities of Table V because preliminary calculations had revealed that taking $d_{CH}=1.07$ A gave $d_{CN}=1.29$ A, which is certainly too low, while $d_{CH}=1.09$ A gave $d_{CN}\gtrsim d_{CC}=1.38$ A, which is also highly improbable. The variation in the C−H distances considered corresponds approximately to the experimental error in the coordinates of the hydrogens. In what follows the middle position of the hydrogen atoms (Table IV) are taken as "mathematical" points, the experimental uncertainty in these coordinates being approximately included in the range of d_{CH} values considered. The experimental error in the *right-hand* sides of (1), (2), and (3) is of course still taken into account.

Taking for example model I in Table V we have:

$$(B_2-2.056)^2+(A_2+1.276)^2=1.075^2, \quad (4)$$

$$(B_3-2.153)^2+(A_3-1.205)^2=1.075^2, \quad (5)$$

$$A_4=a_4-1.075=2.493-1.075=1.418. \quad (6)$$

This is seen to give three additional equations by the aid of which a complete set of the variables (A_1,A_2,A_3,A_4,B_2,B_3) can be obtained. The results are given in Table VI together with the resulting bond distances and bond angles.

V. CONCLUSIONS AND DISCUSSION

Each of the three dominant methods for determination of molecular structure of gases and vapors, the spectroscopic, the electron-interferometric, and the quantum-mechanical calculation procedure contributes to the picture of pyridine that can now be given.

What may be concluded from *spectroscopy* is included in Table VI. It is noted that irrespective of the choice of C−H distance the two different C−C *distances* are about equal to the C−C distance in benzene (1.395 A) as found by Raman technique[7] (1.396–1.401 A) and electron-diffraction experiments[8] (1.393±0.005 A). However, all the valence *angles* in pyridine deviate distinctly from 120° so that the pure sp^2-hybridization present in benzene is slightly disturbed.

Electron-diffraction work[9] gave d(C(2)−C(3)) indistinguishable from d(C(3)−C(4))=1.39±0.02 A and d(N−C(2))=1.37±0.03 A, leaving the question of the magnitude of the valence angles partially unanswered.

We shall now try to see which structural features for pyridine may be predicted by means of the so-called valence-bond method from quantum mechanics, restricting ourselves to statements of comparative character.

TABLE VI. Calculated values of pyridine ring-atom coordinates (A_1,A_2,A_3,A_4,B_2,B_3), carbon-carbon distances (d(C(i)−C(j))), carbon-nitrogen distance (d(N−C(2))), the C(5)−C(4)−C(3) angle α, the C(4)−C(3)−C(2) angle β, the C(2)−N−C(6) angle γ, the C(4)−C(3)−H(3) angle δ, and the N−C(2)−H(2) angle ϵ as functions of assumed C−H distances (A) (models I–VII).

	I	II	III	IV	V	VI	VII
A_1	−1.370	−1.390	−1.412	−1.388	−1.395	−1.396	−1.388
A_2	−0.713	−0.698	−0.679	−0.701	−0.691	−0.694	−0.699
A_3	0.706	0.703	0.701	0.708	0.699	0.705	0.700
A_4	1.418	1.413	1.408	1.408	1.418	1.408	1.418
B_2	1.140	1.144	1.150	1.148	1.142	1.152	1.137
B_3	1.201	1.197	1.192	1.194	1.199	1.190	1.204
d(C(2)−C(3))	1.420	1.402	1.381	1.410	1.391	1.400	1.401
d(C(3)−C(4))	1.396	1.392	1.386	1.384	1.398	1.382	1.402
d(N−C(2))	1.316	1.337	1.364	1.338	1.342	1.349	1.329
α	118° 40′	118° 40′	118° 40′	119° 14′	118° 06′	118° 52′	118° 22′
β	118° 12′	118° 30′	118° 55′	118° 31′	118° 36′	119° 01′	118° 04′
γ	120° 06′	117° 40′	114° 58′	118° 12′	116° 42′	117° 18′	117° 34′
δ	121° 40′	121° 38′	121° 39′	122° 13′	121° 07′	122° 00′	121° 10′
ϵ	118° 28′	116° 28′	114° 06′	116° 45′	115° 44′	115° 53′	116° 40′

[7] B. Stoicheff, J. Chem. Phys. **21**, 1410 (1953).
[8] I. L. Karle, J. Chem. Phys. **20**, 65 (1952).
[9] V. Schomaker and L. Pauling, J. Am. Chem. Soc. **61**, 1769 (1939).

Figure 2 gives the eight dominant bond structures for pyridine together with their relative weights x, y, z, and s ($2x+3y+2z+s=1$). It is seen that the double-bond character (DBC) of the C(3)−C(4) bond is measured by $x+y+z$, the sum of the weights of the structures in which the bond has been formulated as double. Correspondingly, the DBC of the C(2)−C(3) bond is $x+y+z+s$. Hence we conclude that the latter bond must be shorter than the former. It is seen that this condition is only obeyed by models such as III, V, and VII in Table VI.

Furthermore we want to compare the DBC of the C−C distance in benzene with the DBC's of the carbon-carbon bonds in pyridine. Since ionic structures may be ignored for benzene, the DBC for the C−C bond must be measured by $(x+y)(2x+3y+2z+s)/(2x+3y)=x+y+(2z+s)(x+y)/(2x+3y)$. Here, we have assumed that the ratio of the weights of a Kekulé and a Dewar bond structure is the same for benzene and for pyridine. Since $x\sim 5.5y$, $(x+y)/(2x+3y)$ is close to 0.5, which means that the DBC for the carbon-carbon bond in benzene is measured by $x+y+z+\frac{1}{2}s$. Therefore, the bond length in the benzene ring is predicted to fall approximately halfway between the two different C−C bonds in pyridine. This is only compatible with models like V and VII.

Finally, we shall ask for the DBC of the N−C(2) bond. It is measured by $x+y$. Now, it is highly probable that $z\sim s$. To the extent to which this is true we see that the decrease in DBC from the C(2)−C(3) bond to the C(3)−C(4) bond is the same as the decrease from C(3)−C(4) to N−C(2). Therefore, the increase in N−C bond length caused by the presence of ionic structures as compared with a pure Kekulé-Dewar pyridine model approximately equals the difference in lengths between the two unequal C−C bonds. From

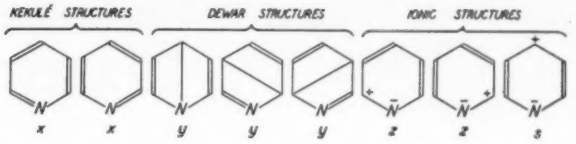

FIG. 2. Dominant bond structures for pyridine. x, y, z, and s are the weights of the corresponding structures ($2x+3y+2z+s=1$).

Table VI we see that this difference is 0.007 and 0.001 A for models V and VII, respectively. The error in these numbers resulting from experiment amounts to about 0.006 A. If we make the reasonable assumption that the bond-order *versus* bond-distance curves for C−C and C−N distances are almost parallel as exemplified by C_2H_6(C−C=1.54), CH_3NH_2(C−N=1.47), and H_2C_2(C≡C=1.21), CH_3CN(C≡N=1.158) with a mutual distance at about 0.06 A near the double-bond point, we conclude that the C−N distance in a Kekulé-Dewar pyridine model would have to be 1.335 A. In the "true" pyridine molecule this distance must be about 0.01 A larger (the approximate magnitude of the difference between the two C−C bonds), i.e. 1.345 A. This happens to fit well with the model V which also had the correct C−C distances.

A C−N distance=1.345 A in pyridine is just barely consistent with the electron-diffraction measurements. The result of future studies of the pyridine structure by means of electron-diffraction technique must be awaited with great interest.

To summarize, a model like V can be pointed out which is consistent with the microwave spectrum and valence theory aspects and not inconsistent with earlier electron-diffraction work. The pyridine molecule pictures in Fig. 1 has the relative dimensions of model V.

Shock-Tube Measurements of Vibrational Relaxation*

EDWARD F. SMILEY AND ERNST H. WINKLER
U. S. Naval Ordnance Laboratory, White Oak, Maryland

(Received May 21, 1954)

Vibrational relaxation times at temperatures between 400°K and 1500°K have been measured in chlorine and carbon dioxide with a shock tube. The approach toward equilibrium vibrational excitation behind the shock wave is obtained from the density profile of the transition region using an optical interferometer. The measurements were made with a relatively narrow shock tube in order to avoid errors caused by optical distortions. The accuracies of the measured relaxation times are estimated to be from 20 percent to 50 percent.

INTRODUCTION

IN a report entitled "Deviation from Thermal Equilibrium in Shock Waves," Bethe and Teller[1] extend the shock wave theory to the general case in which the specific heat changes with temperature and relaxation phenomena occur. In an earlier note[2] it has been proposed that the approach to equilibrium behind a shock front could be evaluated to obtain relaxation times which might supplement acoustical data at high temperatures. The shock wave is produced in a shock tube, and a Mach-Zehnder interferometer gives the density profile in the transition region.

For a temperature range behind the shock front in which dissociation and electronic excitation are absent, Bethe and Teller showed that, on the high pressure side of the shock front, equilibrium of the translational and rotational degrees of freedom is established within a few collisions, while the vibrational degrees of freedom may need many collisions before equilibrium is reached. Within such a transition region the temperature, as defined by the translational and rotational energies behind the shock front, decreases, and the density and pressure increase (Fig. 1). In the general case the solution of the integral equations is obtained by numerical integration. For small changes of the temperature in the transition region, for which the relaxation time can be considered constant and the vibrational energy a linear function of the temperature, the equations can be integrated in closed form. The vibrational energy and the temperature then change exponentially with the distance from the shock front, and the other flow parameters can be determined.

In determining vibrational relaxation times from shock tube data, certain limitations are apparent: (1) With weak shocks in which the temperature rise is small, the fringe displacements are relatively small, and the transition region may be too long; and (2) at higher temperatures the relaxation region soon becomes very short. In both these cases, the evaluation of the density profile is necessarily quite inaccurate. Within certain limits a long relaxation region can be shortened by increasing the pressure of the gas into which the shock front propagates, and to widen a short transition region the pressure can be decreased. To maintain a desired accuracy of the density determination from the interferograms, it is then necessary either to increase the accuracy of reading fringe displacements or to increase the depth of the shock tube to obtain larger fringe displacements. Fringe displacements, however, cannot be reliably estimated more closely than 1/20 of a fringe width.[3] On the other hand, increasing the depth of the test section produces certain optical effects at the shock front which can only be minimized by using a narrow slit light source oriented parallel to the shock front and an illuminating condenser well aligned so that only light rays parallel to the shock front pass the test section. Where the shock front is followed by a region of varying density, experiments with model disturbances showed that, due to the steep density gradients at the shock front, relaxation regions may be recorded wider than they actually are, and that the fringe displacements cannot be positively correlated to the actual density variation. These effects increase noticeably in magnitude with increasing test section depth. An estimate of the optical distortions cannot be given without a knowledge of the exact density profile. For this reason, a narrow shock tube has been used in this study.

INSTRUMENTATION

The shock tube[4] is made of 3 by $1\frac{3}{4}$ inch extruded aluminum alloy tubing. The wall thickness is $\frac{1}{8}$ inch. The pressure chamber is 4 feet long, the expansion chamber, with the test section, 14 feet long. The test section is constructed of aluminum stock. The inside surfaces of the shock tube are silver-plated to minimize the corrosion by chlorine. The test section windows are of interferometer quality. Wherever possible, O-rings are used as seals between the various sections.

For time-position measurements of the shock front, glow discharge probes are used because they have

* This work was supported by the Office of Naval Research.

[1] H. A. Bethe and E. Teller, Aberdeen Proving Ground Rept. X-117.

[2] Smiley, Winkler, and Slawsky, J. Chem. Phys. **20**, 923 (1952); W. Griffith, Phys. Rev. **87**, 234 (1952).

[3] E. H. Winkler, Rev. Sci. Instr. **24**, 1067 (1953).

[4] For general reference on shock tubes see, e.g., W. Payman and W. C. F. Shepherd, Proc. Roy. Soc. (London) **A186**, 293 (1946); Bleakney, Weimer, and Fletcher, Rev. Sci. Instr. **20**, 807 (1949).

proved more reliable than light screens for operation at low initial pressures in the expansion chamber. The probes have iron electrodes, mounted in ceramic two-hole insulators. They are operated with 300 to 400 volts and a discharge current of about 0.5 ma. Proper performance of the probes requires that the cathode voltage gradient be largely contained within the ceramic insulation. The discharge current change, caused by the pressure increase behind the shock front, creates a signal which is fed through isolating and amplifying circuits into an electronic counter. The response time for this circuit has been measured as 5 microseconds. The probes can be used for initial pressures between 0.5 mm Hg and 50 mm Hg. Their operation has been found to be unaffected by mechanical vibrations carried by the walls of the shock tube. Two probes are located ahead of the test section 4 feet apart. A third probe is mounted past the test section. With the stations 4 feet apart, the shock velocities measured correspond to times of at least 1 millisecond. Errors in the velocity measurements due to the response time of 5 microseconds are therefore smaller than ± 1 percent.

In measuring the density profile of the transition region, a Mach-Zehnder interferometer with 9-inch plates is used. The light source is a short-duration spark[5] with magnesium electrodes and a suitable filter. The effective spark duration has been estimated from photographs of fast shocks to be of the order of 10^{-7} second. The spark is fired by a proportional delay unit when the shock front arrives in the center of the test section. The delay unit, operated by the signals of the glow discharge probes ahead of the test section, selects a delay time depending on the time elapsed between the passing of the shock at the two probe stations and the ratio of the distance between these stations and the second station and the test section center.

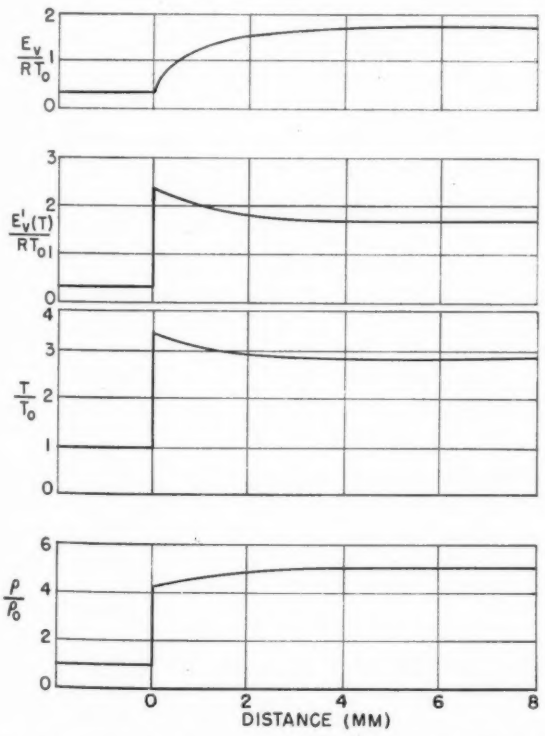

FIG. 1. Computed changes in vibrational energy E_v, equilibrium vibrational energy $E_v'(T)$, temperature T, and density ρ behind a shock wave in Cl_2 traveling at 3.5 times the room temperature speed of sound.

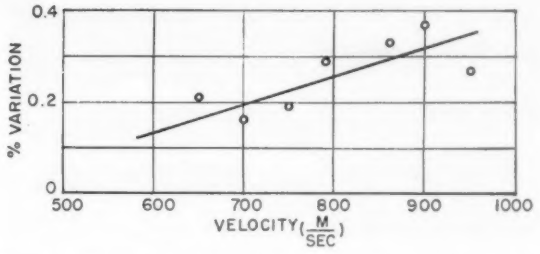

FIG. 2. Scatter in the percentage changes in shock velocity.

The shock tube can be evacuated with a large mechanical pump to 5×10^{-3} mm Hg. The over-all leakage rate is kept to less than 1 mm Hg per hour. Pressure measurements in the expansion chamber are made with a mercury manometer, a McLeod gauge, or an oil manometer, depending on the pressure range and type of gas to be used. The oil manometer, filled with a light oil of the trifluorochloroethylene polymer type, was calibrated for pressure measurements in chlorine and found accurate to ± 2 percent.

In studying the behavior of our particular shock tube, the flow behind the shock front has been observed with the interferometer. Density variations could not be detected until the arrival of the mixing region at the contact surface. Shock speed and shock deceleration data have been evaluated to estimate the accuracy with which the shock velocity can be determined in the test section. Measured shock speeds in air, carbon dioxide, and chlorine have been compared with the values computed from theory. For air at normal pressure in the pressure chamber, the measured data are about 10 percent lower than the theoretical values. The average deviation from the theoretical curve becomes larger as the initial pressure ratio across the diaphragm is decreased. With carbon dioxide or chlorine in the expansion chamber, the mean deviations are comparable to those obtained with air. With helium instead of air in the pressure chamber, the data show a somewhat larger scatter.

Because the velocity in the test section was computed from time measurements at the first two probes, separate shock deceleration measurements across the test section were made. The observed mean scatter which adds to the uncertainty with which the velocity can be determined in the test section is shown in Fig. 2. The points shown represent averages obtained from five to eight measurements. In general it has been assumed

[5] L. S. G. Kovasznay, Rev. Sci. Instr. **20**, 696 (1949).

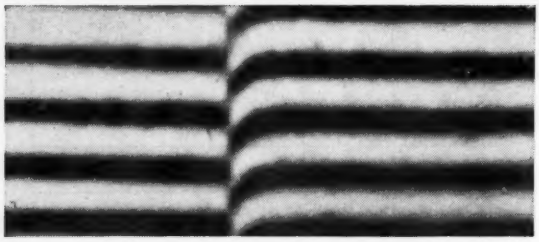

FIG. 3. Fringe shifts showing short relaxation region in CO_2.

that the velocity measurements are accurate to within ± 2 percent.

MEASUREMENTS AND RESULTS

The present investigations were mainly directed towards establishing the possibilities and limitations of the shock tube technique for relaxation time measurements. Qualitatively, the present data compare quite well with those obtained with other methods at lower temperatures and thus illustrate the usefulness of the shock tube method proposed in reference 2. A larger number of individual measurements would be needed, however, to establish an empirical curve of the temperature dependence of the vibrational relaxation times.

The experiments were performed in carbon dioxide at pressure ratios across the shock between 3 and 18, and in chlorine between 6 and 25. The pressure ratios needed to produce particular shock strengths have been calcuated from the ideal shock tube equations. Initial pressure ratios were reset for each series of measurements made at any selected shock strength. The ratios of the density in the equilibrium region to the density ahead of the shock front agree, within the accuracy of the measurements, with the theoretically expected values. The actual flow parameters established under these conditions have been evaluated from the measurements of the shock velocity using the appropriate thermodynamic data.

Figure 3 shows a typical fringe pattern produced in carbon dioxide by a shock strength of 8. The variation of the density with distance from the shock front, as pictured by the fringe pattern, can be fitted closely by an exponential curve.

The interferograms have been evaluated with a small Gaertner comparator. The procedure will be outlined and discussed, since the accuracy with which relaxation times can be evaluated is mainly determined by the accuracy with which the fringe displacements can be measured. The method is illustrated in Fig. 4. The lines X_1 and X_2 correspond to the total displacement of the fringes in the relaxation region; the line Y_1 is placed at the shock front. The positions X_1, X_2, and Y_1 are determined from multiple measurements on the interferograms. After X_1 and X_2 are established, a line parallel to the lines X_1 and X_2 is located where the fringe displacement has reached $(1-1/e)$ of its final value. The vertical line Y_2 is then placed so that it intersects the $(1-1/e)$ line in the middle of the fringe. The difference (Y_2-Y_1) will be referred to as the apparent relaxation distance.

The accuracy of determining the apparent relaxation distance is obtained from the deviations in the determinations of the lines X_1, X_2, Y_1, and Y_2. X_1 and Y_1 can be placed to 1/20 of a fringe width. The asymptotes X_2 are difficult to place, particularly for long relaxation times. In general, the placing of X_2 is affected by the slight curvature in the fringes produced by plate imperfections in the interferometer. Deviations here were as much as $\frac{1}{10}$ of a fringe. The inaccuracies calculated in this manner vary between ± 20 percent and ± 50 percent. The larger error given for the CO_2–water vapor mixture (Fig. 5) was caused by the very small relaxation distances found in this case. Deviations from the average value of the apparent relaxation distance as obtained from individual measurements, including those of different observers, are somewhat smaller than the inaccuracies based on an assumed reading accuracy of the interferogram to 1/20 fringe width.

In view of the inaccuracies inherent in the present measurements, the computation of the relaxation times has been done in an approximate manner. For the transition region we start from the relaxation equation for vibrational excitation of diatomic molecules[6]

$$\frac{dE_v}{dt}=\frac{E_v'(T)-E_v}{\tau}, \tag{1}$$

where E_v is the local value of the vibrational energy, dE_v/dt its variation with time, $E_v'(T)$ the equilibrium value of the vibrational energy at temperature T, and τ the vibrational relaxation time. We assume with Bethe and Teller[1] that

$$dE_v'(T)/dE_v=-\mu, \tag{2}$$

where μ is a constant. With x equal to the distance from the shock front, and u the local velocity of the gas, we obtain

$$\frac{E_v'(T_2)-E_v}{E_v'(T_2)-E_v'(T_0)}=\exp\left\{-\int_0^x\frac{(1+\mu)dx}{\tau u}\right\}. \tag{3}$$

Inserting the values of E_v' at the shock front (T_1), and in the equilibrium region (T_2), and with $E_v(T_1)$ equal

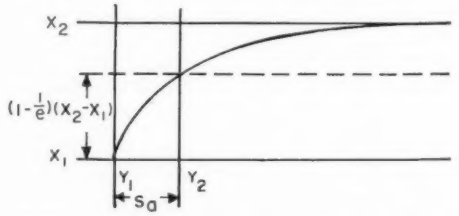

FIG. 4. Method used in measuring the relaxation distance S_a from the fringe shift behind the shock front.

[6] Markham, Beyer, and Lindsay, Revs. Modern Phys. 23, 353 (1951).

to $E_v'(T_0)$, where the primed E always refers to thermal equilibrium, we have

$$1+\mu=\frac{E_v'(T_1)-E_v'(T_0)}{E_v'(T_2)-E_v'(T_0)}. \tag{4}$$

We assume that the final value of τu is exponentially approached from its value at the shock front, and write

$$\tau u=\tau_1 u_1+(\tau_2 u_2-\tau_1 u_1)(1-\exp(-x/\tau_1 u_1)). \tag{5}$$

Equation (3) can then be integrated. Defining the value of the relative variation of the vibrational energy α, calculated for the location behind the shock front where the relative density change equals $1/e$, i.e.,

$$\exp(-\alpha)=\left[\frac{E_v'(T_2)-E_v}{E_v'(T_2)-E_v'(T_0)}\right]_{(\rho_2-\rho/\rho_2-\rho_0)=1/e} \tag{6}$$

and with $(\tau_2 u_2-\tau_1 u_1)/\tau_1 u_1$ assumed small, we finally obtain

$$\tau_1=\frac{S_a}{u_1}\left\{\frac{\alpha}{1+\mu}+\frac{1}{e}\frac{\tau_2 u_2-\tau_1 u_1}{\tau_1 u_1}\right\}^{-1}. \tag{7}$$

Here S_a is the apparent relaxation distance measured from the interferograms (Fig. 4) as the distance in which the density change reaches to $1/e$ of its final value. The density change, related by α to the change in the vibrational energy, is computed from the continuity equations of mass, momentum, and energy for steady flow. The correction term, $(\tau_2 u_2-\tau_1 u_1)/e\tau_1 u_1$, is obtained from the uncorrected experimental data ($\tau(T)$ *vs* T) and from the computed values of u_1 and u_2. The largest value of this term is about 0.05. The relaxation times obtained from Eq. (7) correspond to the temperatures (T_1) and the densities (ρ_1) immediately behind the shock wave.

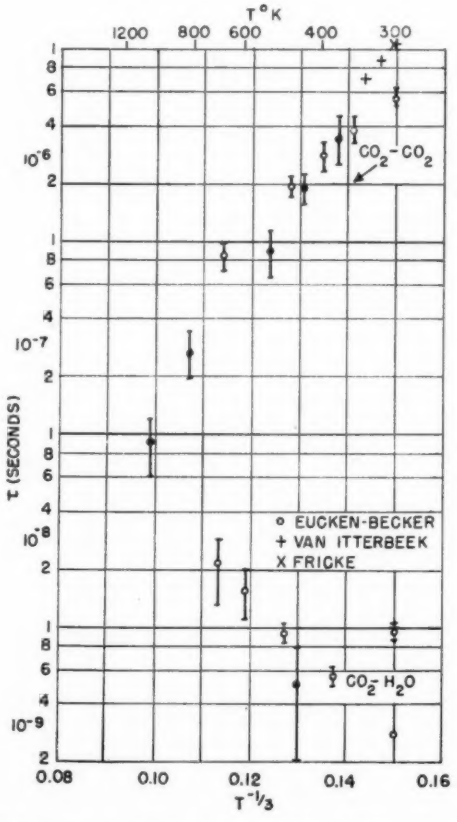

FIG. 5. Relaxation times measured in CO_2 and CO_2-H_2O mixture shown with acoustical data.

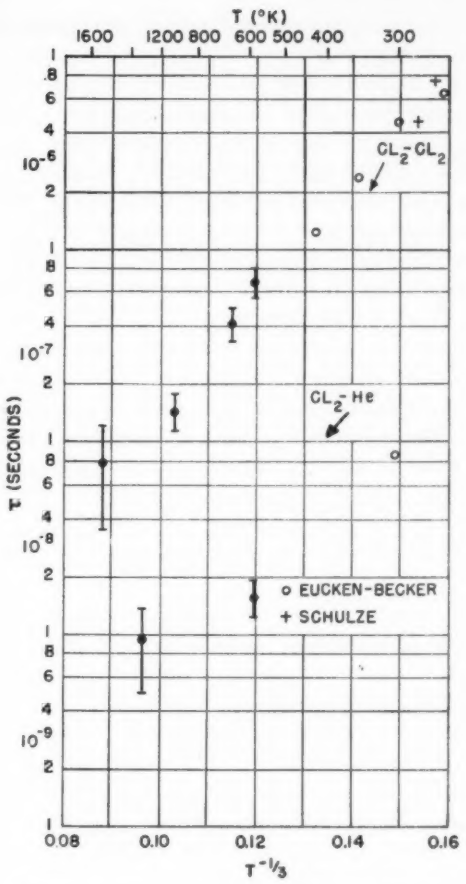

FIG. 6. Relaxation times measured in Cl_2 and Cl_2-He mixture shown with acoustical data.

The numerical results of the present investigations and their accuracies are shown in Figs. 5 and 6, together with results obtained by Eucken and his coworkers,[7] Schulze,[8] van Itterbeck,[9] and Fricke.[10] All data in these figures have been reduced to standard density. The present tests have been made with commercially pure carbon dioxide and chlorine. The water content of the carbon dioxide was specified to be less than 1 part in 20 000. For the shock tube data which

[7] A. Eucken and R. Becker, Z. physik. Chem. **27(B)**, 235 (1934); A. Eucken and E. Nümann, Z. physik. Chem. **36(B)**, 163 (1937); A. Eucken and L. Küchler, Physik. Z. **39**, 831 (1938); and L. Küchler, Z. physik. Chem. **41(B)**, 199 (1938).
[8] R. Schulze, Ann. Physik **34**, 41 (1939).
[9] A. van Itterbeck, Physica **6**, 511 (1939).
[10] E. F. Fricke, J. Acoust. Soc. Am. **12**, 245 (1940).

are evaluated from measured shock velocities and from interferograms of the shock front, the conditions immediately behind the shock and the downstream equilibrium conditions are obtained from the usual continuity equations. The thermodynamic data of carbon dioxide have been taken from Kassel,[11] and for chlorine the harmonic oscillator approximation[12] has been used. The measurements made with admixtures of water vapor and helium have been evaluated with appropriately weighted values of the heat content and molecular weight. Each of the present data represents the mean value of measurements made from 4 to 8 different interferograms. In all cases, with the exception of the carbon dioxide measurements at 430°K and 530°K, the scatter of the measured values is less than the calculated error. The error width indicated in Figs. 5 and 6 represents the mean deviation in eight measurements for the carbon dioxide data at 430°K and 530°K, and for the other data it represents the calculated measuring accuracy.

The measurements in chlorine could not be extended to overlap the acoustical data, since the glow-discharge probes used in determining the shock velocities did not work satisfactorily in chlorine at pressures above 50 mm Hg. The results group reasonably well, however, about a curve extrapolated from the room temperature data. The dispersion of the present data about this curve is approximately of the same order of magnitude as exhibited by the various acoustical measurements. The measurements in carbon dioxide, Fig. 5, show a larger scatter. In this case, however, the effects of water vapor impurities, due to leakage, must be accounted for in comparing the shock tube low-temperature data with the acoustical data.

Figures 5 and 6 also show the observed relaxation times for carbon dioxide and chlorine when impurities were added. Concentrations of 3 to 10 percent water vapor have been used with carbon dioxide, and an admixture of 10 percent helium with chlorine. Some results from acoustical measurements in mixtures are included. To reduce the measurements made in gas mixtures, the following relationship has been used:

$$\frac{1}{\tau}=\frac{C}{\tau_{AB}}+\frac{1-C}{\tau_{AA}}, \tag{8}$$

where τ is the observed relaxation time of the mixture reduced to standard density, τ_{AA} that of the pure gas (A), τ_{AB} that for the type AB collisions, and C the concentration of the impurity.

The accuracy achieved in the present tests is, in general, low. Impurities introduced into the gas due to leakage and wall absorption of the shock tube are more difficult to reduce than with the acoustical technique. For more accurate results, it would be necessary to increase the test section width so that the relaxation region could be lengthened by decreasing the pressure but without sacrificing fringe displacement. The effects of the density gradient and diffraction phenomena on the fringe position and displacement would, however, have to be known.

The authors wish to express their appreciation to Dr. Z. I. Slawsky for his stimulating suggestions and to Mr. B. J. Crapo and Mr. E. L. White, who were responsible for the design and construction of the electronic instrumentation.

[11] L. S. Kassel, J. Am. Chem. Soc. **56**, 1838 (1934).
[12] M. Trautz and H. Ader, Z. Physik 89, 12 (1934).

Nuclear Quadrupole Resonances in Bromobenzene Derivatives

P. J. BRAY,* *Department of Physics, Rensselaer Polytechnic Institute, Troy, New York*

AND

R. G. BARNES,† *Department of Physics, University of Delaware, Newark, Delaware*

(Received May 21, 1954)

The pure nuclear quadrupole resonance frequencies of the Br^{79} isotope are given for a number of previously unreported bromobenzene derivatives. The resonance frequencies of the Br^{81} isotope in these and other previously reported compounds are compared with the electron density in the vicinity of the carbon atom to which the bromine is bonded.

SEVERAL investigations have previously been reported of the dependence of certain effects in the radio-frequency resonance spectra of halogen substituted benzene derivatives upon the electron density in the vicinity of the carbon atom to which the halogen is bonded. The magnetic shielding of F^{19} in benzene derivatives, determined from the nuclear magnetic resonance spectra, has been correlated[1] with the electron density parameter sigma used by Hammett.[2] Similarly, the nuclear quadrupole resonance frequency of Cl^{35} in singly substituted chlorobenzene compounds has been correlated[3] with the sigma parameter. In this article the nuclear quadrupole resonance frequencies of Br^{81} in various bromobenzene derivatives are compared with the sigma values.‡ The correlation found is satisfying, although crystal structure effects give rise to some dispersion in the plot of frequency *versus* sigma.

The resonance frequencies of the Br^{79} isotope in a number of bromobenzene derivatives are listed in Table I. Table II contains the full list of compounds appearing in Fig. 1 which is a plot of Br^{81} resonance frequencies at liquid nitrogen temperature against the corresponding sigma values which are taken from Hammett's book or the review article of Jaffe.[4] Compounds 1 through 11 in Table II appear in the same order in Table I. Conversion from Br^{79} to Br^{81} frequencies in these cases has been made with the ratio number 1.1970. The frequencies for compounds 12 through 19 are taken from previous reports.[5,6]

In the cases of multiple substitution on bromobenzene, the sigma value used in Table II and Fig. 1 is the simple sum of the sigma values for all substituents or is taken in whole or in part from the observed disubstitution sigma values given by Jaffe.[4] For those cases where the addition process yields multiple sigma values,[7] the frequency of each observed bromine resonance in the compound is plotted against that one of the sigma values which gives the best fit of the plotted point to the rest of the data.

It is apparent from Fig. 1 that one can predict the Br^{81} resonance frequency of a bromobenzene derivative within 3 mcps in almost all cases if the sigma values are known. It is also apparent from the frequency of *o*-bromoaniline and Fig. 1 that the sigma value for the *o*-NH_2 substitution should be approximately -0.840. However, the resonances in 2,4,6-tribromoaniline (18 in Table II) require a sigma value for the *o*-NH_2 substitution between -0.060 and -0.480 if the resonances

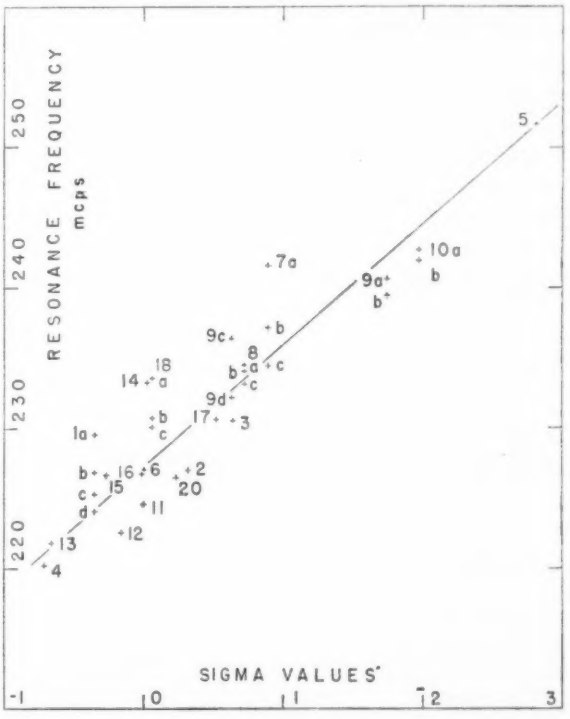

FIG. 1.

* Research supported by a grant-in-aid from the Rensselaer Polytechnic Institute Research Grants Committee.

† Research supported by the Office of Ordnance Research and the Research Corporation.

[1] Gutowsky, McCall, McGarvey, and Meyer, J. Am. Chem. Soc. 74, 4809 (1952).

[2] L. P. Hammett, *Physical Organic Chemistry* (McGraw-Hill Book Company, Inc., New York, 1940).

[3] H. C. Meal, J. Am. Chem. Soc. 74, 6121 (1952).

‡ Since submittal of this article, similar work by Hatton and Rollin has been published in Trans. Faraday Soc. 50, 358 (1954). Their frequency measurements apparently contain a systematic error of several megacycles per second.

[4] H. H. Jaffe, Chem. Revs. 53, 191 (1953).

[5] P. J. Bray, J. Chem. Phys. 22, 950 (1954).

[6] Barnes, Miller, and Wooten, J. Chem. Phys. 22, 946 (1954).

[7] For example in 1,2,4-tribromobenzene the sigma value may arise from *o*-Br+*m*-Br, or *o*-Br+*p*-Br, or *m*-Br+*p*-Br combinations.

arise from a bromine with substituents o-NH_2+m-Br +m-Br on the ring. Further bromobenzene derivatives containing an o-NH_2 substitution should be investigated.

There are at least two possible crystalline phases for p-bromophenol. A polycrystalline sample taken directly from the available supply[8] and cooled to liquid nitrogen temperature yields the resonances shown in Table I as pair B. If this sample is now melted into the vial, solidified, and cooled to liquid nitrogen temperature, only the pair A of frequencies appears while the sample expands markedly and often shatters the containing vial. Both the polycrystalline and melted down states of the compound yield the single room temperature resonance listed in Table I. The resonance frequency for bromobenzene at dry ice temperature, reported by Kojima and co-workers,[9] differs from the frequency at 77°K reported here by about twice the amount expected from temperature dependence. Evidently this compound possesses a phase transition or an unusually large temperature dependence. Further investigation will be of interest.

The three resonances in 2,4,6-tribromoanisole and 1,3,5-tribromobenzene should be considered with the three appearing in 2,4,6-tribromoaniline. One would ordinarily expect two resonances in 2,4,6-tribromoanisole and in 2,4,6-tribromoaniline and one resonance in 1,3,5-tribromobenzene unless there are nonequivalent positions for the halogen atoms in the crystalline unit cell. It is interesting to note that in none of the three cases do the frequencies show a tendency to coalesce to a common value at the melting point as found for Cl

TABLE I. Nuclear quadrupole resonance frequencies of the Br^{79} isotope in some previously unreported bromobenzene derivatives.

Compound	Frequency (megacycles per second)	Temperature	Approximate signal-to-noise ratio
(1) p-bromophenol BrC_6H_4OH	A 274.795±0.035[a,b]	Liquid nitrogen	2–3
	A 271.500±0.010[a]	Liquid nitrogen	6
	B 269.683±0.010	Liquid nitrogen	5
	B 268.222±0.010	Liquid nitrogen	5
	264.733±0.020	24°C	2–4
(2) methyl m-bromobenzoate[a,b] $BrC_6H_4COOCH_3$	271.772±0.020	Liquid nitrogen	5–8
(3) methyl p-bromobenzoate[a] $BrC_6H_4COOCH_3$	275.960±0.020	Liquid nitrogen	12–15
(4) 4-bromo-2-methylaniline[a] $BrC_6H_4(CH_3)NH_2$	263.616±0.010	Liquid nitrogen	20–25
(5) 1-bromo-2,4-dinitrobenzene[a] $BrC_6H_3(NO_2)_2$	301.270±0.020	Liquid nitrogen	5–6
(6) 5-bromosalicyclic acid[a,b] 5-BrC_6H_3-2-OH-COOH	271.820±0.050	Liquid nitrogen	6–7
(7) 2,4,6-tribromoanisole[a] $Br_3C_6H_2OCH_3$	289.194±0.010	Liquid nitrogen	10
	283.888±0.010	Liquid nitrogen	10
	280.632±0.010	Liquid nitrogen	10
	285.800±0.085	26°C	2–3
	279.980±0.100	26°C	2–3
	277.255±0.100	26°C	2–3
(8) 1,3,5-tribromobenzene[a,e] $C_6H_3Br_3$	280.721±0.010	Liquid nitrogen	15–20
	280.228±0.010	Liquid nitrogen	15–20
	279.075±0.010	Liquid nitrogen	15–20
	277.356±0.020	25–26°C	5–6
	277.094±0.020	25–26°C	5–6
	275.744±0.020	25–26°C	5–6
(9) 1,2,4-tribromobenzene[a,d,e] $C_6H_3Br_3$	288.080±0.050	Liquid nitrogen	1–2
	286.650±0.050	Liquid nitrogen	2–3
	282.940±0.100	Liquid nitrogen	3–5
	277.985±0.050	Liquid nitrogen	2–3
(10) 1,2,4,5-tetrabromobenzene[a] $C_6H_2Br_4$	290.572±0.015	Liquid nitrogen	10–12
	289.675±0.015	Liquid nitrogen	10–12
	286.935±0.020	23°C	3–4
(11) bromobenzene C_6H_5Br	268.856±0.075	Liquid nitrogen	5–7
(12) α-bromo-1,4-dimethylbenzene[a] $CH_2BrC_6H_4CH_3$	254.290±0.020	Liquid nitrogen	8–10
(13) 4,4′-dibromobiphenyl[a] $BrC_6H_4C_6H_4Br$	271.835±0.020	Liquid nitrogen	5–8
	271.110±0.020	Liquid nitrogen	5–8
	269.461±0.020	Liquid nitrogen	5–8
	267.439±0.020	Liquid nitrogen	5–8
(14) 9,10-dibromoanthracene[b] $C_6H_4CBrC_6H_4CBr$	275.053±0.020	Liquid nitrogen	3–5
	272.975±0.085	Liquid nitrogen	2–4

A,B See text of article.
[a] Compound melted into vial-solid at room temperature.
[b] Resonance is broad and requires strong frequency modulation to be observed readily (amplitude of modulation is 2 or 3 times that normally used).
[e] The two higher frequency resonances overlap somewhat as observed on the oscilloscope due to sidebands of the superregenerative oscillator. The center of each pattern is clearly located, however.
[d] Amplitude of frequency modulation is 4 to 6 times that normally required.
[e] Samples have so far crystallized from more than one seed or spot in the containing vial. Hence, there may be more than one crystalline phase present. Some weak resononces may be unobserved so far.

[8] Distillation Products Industries, Eastman grade purity.
[9] Kojima, Tsukada, Ogawa, and Shimauchi, J. Chem. Phys. **21**, 1415 (1953).

TABLE II. Correlation of the nuclear quadrupole resonance frequencies of the Br^{81} isotope in bromobenzene derivatives with the electron density parameter sigma.

Compound	Frequency (megacycles per second)	Substituents with respect to the resonant Br^{81}	σ value
(1) *p*-bromophenol	229.57 a	*p*-OH	−0.357
	226.82 b		
	225.30 c		
	224.08 d		
(2) methyl-*m*-bromobenzoate	227.04	*m*-$COOCH_3$	0.315
(3) methyl-*p*-bromobenzoate	230.54	*p*-$COOCH_3$	0.636
(4) 4-bromo-2-methylaniline	220.23	*m*-CH_3+*p*-NH_2 (3,4 disubstitution)	−0.716
(5) 1-bromo-2,4-dinitrobenzene	251.69	*o*-NO_2+*p*-NO_2	2.807
(6) 5-bromosalicylic acid	227.08	*m*-COOH+*p*-OH	0.000
(7) 2,4,6-tribromoanisole	241.60 a	*o*-OCH_3+*m*-Br+*m*-Br	0.981
	237.17 b		
	234.45 c		
(8) 1,3,5-tribromobenzene	234.52 a	*m*-Br+*m*-Br (3,5 disubstitution)	0.720
	234.11 b		
	233.14 c		
(9) 1,2,4-tribromobenzene	240.67 a	*o*-Br+*m*-Br	1.739
	239.47 b	*o*-Br+*m*-Br	1.739
	236.37 c	*m*-Br+*p*-Br	0.623
	232.24 d	*m*-Br+*p*-Br	0.623
(10) 1,2,4,5-tetrabromobenzene	242.75 a	*o*-Br+*m*-Br+*p*-Br	1.971
	242.00 b		
(11) bromobenzene[a]	224.61		0.000
(12) *m*-bromoaniline	222.61	*m*-NH_2	−0.161
(13) *p*-bromoaniline	221.86	*p*-NH_2	−0.660
(14) *o*-bromoanisole	233.25	*o*-OCH_3	0.019
(15) *p*-bromoanisole	226.69	*p*-OCH_3	−0.268
(16) *p*-bromoacetanilide	226.80	*p*-$NHCOCH_3$	−0.015
(17) *p*-bromoacetophenone	230.67	*p*-$COCH_3$	0.516
(18) 2,4,6-tribromoaniline	233.56 a		
	230.75 b	3-Br, 5-Br+*p*-NH_2 (3,5 disubstitution+*p*-NH_2)	0.060
	230.10 c		
(19) *o*-bromoaniline	220.26	*o*-NH_2	
(20) *p*-dibromobenzene[b]	226.49	*p*-Br	0.223

[a] Dry ice temperature frequency of 220.89±0.10 mcps reported in reference 8.
[b] Manring, Brown, and Williams, Phys. Rev. **90**, 348 (1953); (room temperature frequency only).

resonances in $HgCl_2$.[10] In the case of 1,2,4,5-tetrabromobenzene, two resonances appear at liquid nitrogen temperature while only one is resolved at room temperature.

All resonances reported here were observed using self-quenched or externally quenched superregenerative oscillators of the push-pull Lecher-wire tuned type. The uncertainties assigned to each measurement in Table I arise from the difficulty in knowing with certainty that one has correctly superposed on the oscilloscope screen the nuclear quadrupole resonance pip pattern and the pip pattern of the external oscillator (TS-175/U). In the case of the broader and weaker resonances, it would be relatively easy for the measurements to be in error by an amount equal to the quench frequency of the superregenerative oscillator (140 to 150 kilocycles per second).

[10] M. Buyle-Bodin and A. Monfils, Compt. rend. **236**, 1157 (1953).

Chemical Effects of (d,p), $(n,2n)$, and (γ,n) Activation of Iodine*

ROBERT H. SCHULER
Chemistry Department, Brookhaven National Laboratory, Upton, Long Island, New York
(Received May 20, 1954)

The organic retentions for (d,p), $(n,2n)$, and (γ,n) activation of iodine in liquid methyl and ethyl iodide, containing added iodine, have been found to be equal to the retentions observed in radiative neutron capture. This demonstrates that the chemical effects are independent of the recoil energy of the activated nucleus, of the mode of nuclear formation, and of variation of fragmentation effects within the recoil track. In the absence of scavenger iodine, the increase in retention due to radiation damage is less than 10 percent in all cases studied.

SINCE the original discovery by Szilard and Chalmers[1] that radioactive I^{128} could be extracted, as free iodine, from neutron bombarded ethyl iodine, many investigations have been carried out on the chemical effects of the (n,γ) process.[2,3] Very little work has, however, been done on the effects of other types of activation. In particular, no adequate comparison has been made between radiative neutron capture and the other activation processes which produce products isotopic with the initial reactant, namely the (d,p), $(n,2n)$, and the (γ,n) reactions. It was the purpose of this investigation to make such a comparison in the case of iodine activated in methyl and ethyl iodide.

Investigations of the chemical effects of (n,γ) activation of organic halogen systems have by far outnumbered those on other target substances and because of the effort with which these studies have been pursued, the chemistry of the species resulting from the activation appears to be understood in some detail. Iodine, being monoisotopic, is the least complicated of the halogens for purposes of the present study. Also, since the hot atom reactions in the alkyl iodides are known to be somewhat less susceptible to effects of impurities than for the other halides, one expects difficulties from this source to be minimized. Comparative data for activation by neutron capture are available in the work of Levey and Willard.[4]

As mentioned above, previous investigations of the chemical effects of the activation processes other than neutron capture, which do not lead to a change in atomic number, are extremely few. Kamen has shown that active sulfur formed in the reaction $S^{34}(d,p)S^{35}$ carries with the parent species when irradiated as elemental sulfur and as ferrous sulfide.[5] Melander compared the reaction $U^{238}(n,2n)U^{237}$ to the reaction $U^{238}(n,\gamma)U^{239}$, and separated similar yields of activity from the parent uranium salicyldehyde-o-phenylenediimine by adsorption on charcoal.[6] Barkas, *et al.* found that bromine (Br^{78}, Br^{80}, and Br^{80m}) formed in the (γ,n) activation of ethyl bromide could be concentrated in the same manner as in the Szilard-Chalmers process,[7] and Perlman has used a similar separation to prepare high specific activity I^{126} from potassium iodate subjected to fast neutron bombardment.[8] Rowland and Libby have recently investigated the chemical effects on the photonuclear disintegration of carbon as $CO_2(C^{12}(\gamma,n)C^{11})$, and have found that while in the liquid state the product was predominantly CO, in the solid phase equal amounts of CO and CO_2 were formed.[9] Unfortunately, the analogous thermal neutron process is not amenable to experimental study. The work of Holmes and McCallum on the reaction $Cu^{63}(\gamma,n)Cu^{62}$ provides, to date, the most direct comparison between different activation processes.[10] Copper salicylaldehyde-o-phenylenediimine, both as the solid and in pyridine solution, was activated with the x-rays from a 18-Mev betatron and the yield of Cu^{62} retained as the chelate found to be very similar to that observed in neutron capture.

EXPERIMENTAL

$I^{127}(d,p)I^{128}$

Deuterons of 22-Mev energy from the Brookhaven 60-inch cyclotron were used for the activation of the iodine. The alkyl iodide samples (~10 cc) were irradiated in Pyrex tubes having a 0.006-in. window. A defining diaphragm, consisting of a half-inch aluminum plate with a quarter-inch hole, allowed only the thin window portion of the cell to be exposed to the deflected beam. A tungsten lead served to conduct

* Research carried out under the auspices of the U. S. Atomic Energy Commission.

[1] L. Szilard and T. A. Chalmers, Nature **134**, 462 (1934).

[2] See J. E. Willard, Ann. Revs. Nuclear Sci. **3**, 193 (1953), for a recent excellent review of the chemical effects of nuclear transformations.

[3] Barnes, Burgus, and Miskel in *Radioactivity Applied to Chemistry*, edited by Wahl and Bonner (John Wiley and Sons, Inc., New York, 1951), give a tabular summary of studies of the chemical effects of induced nuclear reactions (pp. 466–476), and of spontaneous decay processes (pp. 477–484); see also pp. 244–283.

[4] G. Levey and J. E. Willard, J. Am. Chem. Soc. **74**, 6161 (1952).

[5] M. Kamen, Phys. Rev. **60**, 537 (1941).

[6] L. Melander and H. Slatis, Phys. Rev. **74**, 709 (1948); Arkiv. Mat. Astron. Fys. **36A**, No. 16 (1949).

[7] Barkas, Carlson, Henderson, and Moore, Phys. Rev. **58**, 577 (1940).

[8] M. L. Perlman and G. Friedlander, Phys. Rev. **82**, 449 (1951); M. L. Perlman and J. Welker (to be published).

[9] F. S. Rowland and W. F. Libby, J. Chem. Phys. **21**, 1493 (1953).

[10] O. G. Holmes and K. J. McCallum, J. Am. Chem. Soc. **72**, 5319 (1950).

the beam current from the cell through a monitoring galvanometer to ground.

Preliminary experiments, where a large circulating current (~200 μa) was present in the cyclotron for a period of 10–15 minutes before the exposure, indicated that a considerable (n,γ) activation was being produced by neutrons present in the cyclotron vault. Since the highest fractional current deflection is obtained when the cyclotron is pulsed, the beam was run with a duty cycle of 6 μsec on -400 μsec off. The circulating current was 1–1.5 μa, the deflected current 0.4 μa, and the target current, which was essentially homogeneous over the circular area of $\frac{1}{4}$-in. diameter, was 0.4×10^{-8} ampere. Irradiations lasted about 5 minutes. The cyclotron was preset to approximate operating conditions and the circulating beam was turned on only while the target was being exposed. The activation yield under these conditions was about one I^{128} produced per 2000 deuterons, which appears to be about a normal thick target yield for (d,p) reactions.[11]

In spite of the above precautions, there is still a component of neutron activation. This contribution of neutron activation has been shown to be about 7 percent in a separate experiment where the beam was stopped in a 650 mg/cm^2 aluminum absorber placed in front of the cell. The arrangement here was otherwise identical to that used in the deuteron experiments. The (d,p) activation appears to contribute a major fraction of the activity observed here.

The activation level (~50 μC immediately after the irradiations described above) was sufficient to work with the 25-minute isotope for about five hours. Beginning two hours after the irradiation the activity showed a half-life of 24.8 minutes (over three half-lives). It decayed to within 0.5 c/sec of background 6 hours after the activation. The radiation decomposition of the sample was shown in separate experiments to result in the production of the order of 3 μmoles of free iodine. This is in agreement with the radiation yields observed in fast electron and gamma bombardments.[12]

$I^{127}(n,2n)I^{126}$

Samples of the alkyl iodides were exposed to the fast neutron flux produced by bombarding a thick beryllium target with 22-Mev deuterons from the Brookhaven cyclotron. Neutrons up to 26-Mev energy are present due to the reaction $Be^9(d,n)B^{10}$ which is exoergic by 4.3 Mev. The samples were placed in the neutron beam about 1 foot from the target and given exposures corresponding, in two successive runs, to 10 and 100 μah of deuteron current. After irradiation the samples were allowed to stand to let the short lived activity decay out. For purposes of the present work the activation level is quite high with the 100 μah run producing about 2μC of activity in a 10-cc sample.

$I^{127}(\gamma,n)I^{126}$

Photonuclear disintegration of iodine in the alkyl iodides was induced by exposure to the bremsstrahlung from 22-Mev electrons accelerated in the betatron at Picatinny Arsenal.[13] The samples were irradiated 3 ft from the target for one hour at an intensity of 100 r/min. The activation obtained here (~50 dps/10 ml) was considerably lower than for the other experiments. In the samples to which iodine was not initially added, there was no observable production of free iodine by the radiation decomposition of the sample.

Method

Methyl and ethyl iodide were purified by washing with sodium thiosulfate, treating with elemental bromine, reextracting, thoroughly washing with water, drying, passing the iodide through a silica gel column, followed by a rough distillation and a final fractionation with a three foot helix packed column. The center cuts of constant boiling point and refractive index were taken for irradiation. In the samples to which no iodine was added, there was no visible coloration, indicating that the iodine concentration was less than $10^{-5}M$.

Since it was desirable to minimize any radiation-induced exchange occurring as a result of radiation damage to the system, attention was focused on solutions to which considerable iodine had been added before irradiation. Such exchange might be expected to occur in the absence of iodine, particularly in the case of the deuteron bombardments, where of the order of 10^{10} radicals are produced for each activated nucleus and where the radiation decomposition results in the production of considerable molecular iodine. An iodine concentration of 1 g/10 ml was chosen as being sufficient to eliminate any ambiguity due to radiation chemical effects since the radiation yields would indicate that, for the doses given, these effects would not result in exchange of more than a small fraction of one percent of the total iodine. In order to minimize post irradiation exchange in the (d,p) and (γ,n) activation of the iodine free samples, iodine was added after the irradiation and portions of the samples immediately extracted. In the $(n,2n)$ case, the addition of the iodine was delayed until two days after the irradiation and the samples not extracted until later, as described below.

The activations were carried out, inactive parent material was added to dilute the activity to a level suitable for counting, and a portion of the resulting solution was extracted with sodium thoisulfate. The activities were measured with a liquid cell jacketed

[11] G. Friedlander and J. W. Kennedy, *Introduction to Radiochemistry* (John Wiley and Sons, Inc., New York 1949), p. 393.
[12] R. H. Schuler and W. H. Hamill, J. Am. Chem. Soc. **74**, 6171 (1952); R. C. Petry and R. H. Schuler, J. Am. Chem. Soc. **75**, 3792 (1953).

[13] We are grateful to the U. S. Army Ordnance Corps for placing the Picatinny betatron at our disposal for these experiments.

Geiger tube having a counting volume of about 6 cc. The retentions were determined directly as the ratio of the activity of the organic fraction to that of the total sample. In this manner no correction needs to be made for dilution or counting efficiency.

In the $(n,2n)$ and (d,p) activations, 4096 counts were accumulated at least twice, corrected for background, and in the case of I^{128} for decay. The standard deviation of the retention values, due to counting statistics, corresponds to about ± 0.5 percent. The activation was not nearly as great in the (γ,n) investigations, the activities of the organic fractions being only 2–3 times background. Here 2048 counts were twice taken for each sample and the standard deviations of the retentions are about ± 1.5 percent.

Results

The results of the various activation experiments are given in Table I along with comparative data from the work of Levey and Willard.[4] It is seen that except for the activation of methyl iodide in the absence of scavenger iodine, the retentions for the various forms of activation are in agreement with those observed in radiative neutron capture.

The retentions for the $(n,2n)$ reaction were measured 16 days and 8 days, respectively, after the 100 and 10 μah runs. For the 100 μah run the retentions were again measured after 60 days and found to increase to 51.9 and 34.0 percent, respectively, for the methyl and ethyl iodide samples. If this data can be extrapolated back to the time of irradiation, it would indicate that these particular methyl and ethyl iodide results are, respectively, 2–3 percent and 1–2 percent high as a result of post irradiation exchange.

In order to be sure that there was no interference from Te^{127} or Sb^{124} which might be formed in the fast neutron experiments by the reactions $I^{127}(n,p)Te^{127}$, and $I^{127}(n,\alpha)Sb^{124}$, the samples were first extracted with water. This did not reduce the specific activity of the sample. The individual samples of the organic and aqueous portions were then followed over a period of one month and each was found to decay exponentially with a half life respectively of 13.2 and 13.0 days in the case of methyl iodide and of 13.2 and 13.1 days in the case of ethyl iodide. Contamination from the activities described above appears to be considerably less than 1 percent.

Immediately after the (γ,n) activation, activity decaying with about a 25-minute half-life was observed. This is probably due mainly to 25 min I^{128} formed by the capture of photoneutrons produced at the betatron, although 20-min C^{11} could also be contributing.

It is estimated that the enrichment factors achieved in the separations in the absence of added carrier range from 3×10^4 for the (d,p) case, where there is considerable iodine produced by the decomposition of the sample, to better than 10^6 in the (γ,n) case, where radiation damage is much less.

TABLE I. Organic retentions (percent) in the activation of the alkyl iodides.

I_2 mole %	(d,p)	$(n,2n)$	(γ,n)	(n,γ)[a]
		Methyl Iodide		
0	64.2	63.4[c]	55.7	56
2.5[b]	39.1	43.1[d]	40.0[c]	41
	40.7[e]	42.5[c,e]		
5.9	37.0	...	...	37
12.2	...	34.6[c]	...	32
		Ethyl Iodide		
0	...	41.3[c]	41.5	41
3.2[b]	29.5	29.8[d]	28.4[f]	28
	28.5[f]	29.1[c,f]		
15.0	...	22.2[c]	...	20

[a] See reference 4.
[b] 1g I_2/10 ml.
[c] Irradiated for 10 μah.
[d] Irradiated for 100 μah.
[e,f] Same parent preparation.

DISCUSSION

The recoil energy of the activated nucleus in each of the cases considered here is of the order of 100 000 ev.[14] It is seen though, that in spite of the tremendous increase over the energy available in radiative neutron capture, that the ultimate fate of the labeled atom is not changed.

Since the presently accepted theories of retention are predicated on the re-entry of the activated atom into the organic material after the recoil energy has been reduced to a value not greatly above thermal, the present results are not entirely unexpected. No effect of energy on retention is expected from the billiard ball model[15–17] for an atom losing energy by elastic collisions with species of like mass. Only a slight energy dependence, which does not appear to be of significance for the high energies present here, is expected if collisions with unequal masses are included in the model. Reaction in the epithermal region, as proposed by Friedman and Libby[18] and Miller and Dodson,[19] occurs as the recoil passes through the reactive energy region and one would not expect any influence of initial energy as long as this is above the maximum at which stable bonds may be formed. An important result of the present work is that it demonstrates that the fragments left behind in the wake of the recoiling atom do not influence the organic retention. The random fragmentation model

[14] See W. F. Libby, J. Am. Chem. Soc. **69**, 2523 (1947). The fragments resulting from each of the activation reactions have have a total kinetic energy of some 10 Mev. In the (d,p) case 1/129th of this will go to the I^{128} formed as will 1/127th in the (γ,n) case and somewhat less in the $(n,2n)$ case.
[15] W. F. Libby, J. Am. Chem. Soc. **69**, 2523 (1947).
[16] Miller, Gryder, and Dodson, J. Chem. Phys. **18**, 579 (1950).
[17] P. C. Capron and Y. Oshima, J. Chem. Phys. **20**, 1403 (1952).
[18] L. Friedman and W. F. Libby, J. Chem. Phys. **17**, 647 (1949).
[19] J. M. Miller and R. W. Dodson, J. Chem. Phys. **18**, 965 (1950).

proposed by Willard[4,20] is consistent with this as long as the fate determining reaction is considered as occurring on the edge of the "brush heap" of radicals formed by the recoil, i.e., if the atom comes to rest in a region where it can effectively react with only the last several radicals produced. With the exception of this latter qualification, the present data do not appear to favor any of the three current models for retention over the others.

Several additional points appear to be implicit in the present results. The variation in nuclear processes might be expected to influence the retention. In particular, internal conversion of the γ rays produced in neutron capture has been suspect by most investigators as a possible source of chemical activation. Wexler and Davies[21] have shown that about 50 percent of the I^{128} formed in neutron irradiated ethyl iodide vapor at low pressure can be collected by applying electric fields during the irradiation. Since the various nuclear reactions would not be expected to have identical effects on the charge of the atom, we conclude that any charge resulting from the internal conversion does not play any important role in determining the fate of the species. Presumably the charge is neutralized by electron exchange with the surrounding medium before the atom undergoes the formation of stable products. In this same regard, the retentions of the bromine isotopes have been found to be the same in the liquid and glassy states[22] in spite of the fact that the fractional conversion observed by Wexler and Davies is somewhat different.

The large excess of recoil energy in the cases presently under consideration leaves no room for failure of the bond to rupture. It emphasizes that, as has of course been demonstrated by other methods, in (n,γ) activation the retention is not due to nonrupture of the C–X bond. Similarly, since the initial separation of the atom and radical fragment must be very great in the (d,p), $(n,2n)$, and (γ,n) processes, the retention cannot be influenced by primary Frank-Rabinowitch recombination. The diffusion-controlled recombination model of retention, as recently proposed by Roy, Hamill, and Williams,[23] is consonant with the present work only if the recombination can be regarded as occurring between the activated atom and the final radical produced in the recoil track.

The various investigators in the field seem now well agreed that, short of gross decomposition of the system, radiation damage has little effect on the observed retentions. In the presence of free iodine no radiation effect is expected or observed since the radioactive species are highly diluted by the inactive iodine present. The increase in retention observed in the (d,p) and $(n,2n)$ activation of pure methyl iodide can be ascribed either to the presence of impurities or to radiation-induced exchange such as that observed in the radiolysis of alkyl iodide solutions of radioiodine.[12]

$$R\cdot + I_2^* \longrightarrow RI^* + I\cdot$$

The minimal nature of the increase noted above and of the absence of any such effect in the $(n,2n)$ and (γ,n) activation of ethyl iodide and of methyl iodide in the (γ,n) case are, perhaps, somewhat surprising but illustrate again that radiation effects are not of much concern except where the products are liable to reaction with the fragments produced by the radiation.

Activation of I^{126} by fast neutron bombardment possesses the advantages of producing an isotope of 13 days half-life thus making it possible to employ separation procedures too time consuming for use with I^{128}. The activation levels observed here are sufficiently high to permit studies in dilute solutions ($>10^{-3}M$) and even in gases.

ACKNOWLEDGMENTS

The authors wishes to thank the staffs of the Brookhaven cyclotron and the Picatinny betatron for their aid with the irradiations. He is indebted to Dr. R. W. Dodson and Dr. A. O. Allen for valuable discussions on the subject.

[20] See reference (2), pp. 196–202; J. F. Hornig and J. E. Willard, J. Am. Chem. Soc. **75**, 461 (1953); S. Goldhaber and J. E. Willard, *ibid.* **74**, 318 (1952).

[21] S. Wexler and T. H. Davies, J. Chem. Phys. **20**, 1688 (1952).

[22] M. L. Fox and W. F. Libby, J. Chem. Phys. **20**, 487 (1952); F. S. Rowland and W. F. Libby, J. Chem. Phys. **21**, 1479 (1953).

[23] Roy, Williams, and Hamill, J. Am. Chem. Soc., **76**, 3274 (1954).

Infrared Spectrum and Molecular Constants of C_2D_2*†

ROBERT M. TALLEY‡ AND ALVIN H. NIELSEN
Department of Physics, The University of Tennessee, Knoxville, Tennessee

(Received May 24, 1954)

The infrared spectrum of C_2D_2 has been reinvestigated in the region 500 to 8000 K with a prism-grating spectrometer. Thirty-nine absorption bands were observed, of which twenty-six are new, and ten have been resolved into rotational fine structure. This brings the present total of observed bands to fifty one. Figures of the bands are shown, wave numbers of all observed lines are given in kaysers reduced to vacuum, and the absorption regions are described. All the bands observed have been given vibrational assignments, and a vibrational analysis has been made which yields the wave numbers of the harmonic frequencies and the values of the anharmonic constants. Rotational analyses of all the resolved bands have been made, and from these the rotational constants which agree with those obtained by Saksena have been determined.

I. INTRODUCTION

THE infrared spectrum of C_2H_2 has been thoroughly investigated from 500 K to 18 500 K by a large number of workers.[1] Something over one hundred bands have been observed, many of which have been resolved into rotational fine structure. Up to the present time the deuterated molecules C_2HD and C_2D_2 have not been subjected to nearly so complete a study. Through 1945 twenty-three bands in C_2HD [1] had been observed from 500 K to 13 000 K, and only thirteen bands had been observed for C_2D_2 [1] in the region 500 K to 5000 K. Since then, Talley and Nielsen[2] have published preliminary reports of the results which are given in this paper. Recently, Saksena[3] published a paper reporting twelve vibration-rotation bands of C_2D_2 between 8500 K and 13 000 K photographed with a 21-foot grating and extremely long absorbing paths. From these bands he has calculated accurate values of the rotational constants and some of the vibrational constants. Previous attempts by Bradley and McKellar[4] failed because C_2D_2 is a much weaker absorber than C_2H_2 and C_2HD, and their path lengths were too short. In addition, bands in the lead sulfide region at 4190.46 and 5097.07 K have recently been reported by Plyler.[5]

The investigation reported in this paper was undertaken in 1950 in an attempt to measure with high dispersion, and long absorbing paths, the complete infrared spectrum from 500 K to the photographic region. When this work was begun only the bands σ_3, σ_5, and $\sigma_4{}^1+\sigma_5{}^1$ had been resolved; the vibration frequencies σ_1 and σ_2 had been observed in Raman effect by Glockler and Morrell[1]; and a number of overtone and combination bands had been observed prismatically by Stitt.[1]

In the present work thirty-nine bands have been observed with a prism-grating spectrometer with path lengths ranging from 0.03 to 12.1 meter-atmospheres. Of these bands twenty-six are new, and ten have been resolved into rotational fine structure. This brings the present total of observed bands to fifty-one. The bands observed have been assigned and analyzed according to well-known combination principles. Vibrational and rotational constants have been determined. In addition, three weak Q branches were observed which could not be assigned to C_2D_2 bands.

II. EXPERIMENTAL DETAILS

With the exception of $\sigma_5{}^1$, the measurements reported in this paper were carried out on the prism-grating spectrometer of The University of Tennessee which has previously been described.[6] This instrument is equipped to operate from about 1.0 μ to 25.0 μ utilizing lead sulfide cells, thermocouple, and a Golay pneumatic detector. The spectra are recorded automatically on a Leeds and Northrup type G Speedomax on which fiducial marks are made for frequency determination. For the present work replica echelette gratings of 15 000, 7200, and 3600 lines per inch made by R. W. Wood were used.

At the time this investigation was carried out, it was not possible to work out to 500 K, and the two bands in this region were accordingly measured on the Ohio State University infrared spectrometer described by Bell, Noble, and Nielsen.[7] This instrument was equipped with a 1200 lines-per-inch original grating ruled by Professor E. F. Barker of the University of Michigan.

The C_2D_2 was generated by passing D_2O vapor through a tube containing CaC_2 powder which had been baked for about 48 hours at 480°C to drive off

* This paper is based on a thesis submitted to the Graduate School of The University of Tennessee in partial fulfillment of the requirements for the Ph.D. degree in Physics.

† Supported in part by the Office of Ordnance Research, U. S. Army.

‡ Present address: Naval Ordnance Laboratory, White Oak, Silver Spring, Maryland.

[1] For bibliography through 1945 see G. Herzberg, *Infrared and Raman Spectra of Polyatomic Molecules* (D. Van Nostrand Company, Inc., New York, 1945), pp. 288–293; E. E. Bell and H. H. Nielsen, J. Chem. Phys. **18**, 1382 (1950); R. M. Talley and A. H. Nielsen, J. Chem. Phys. **19**, 805 (1951); H. H. Nordin and R. N. H. Haslam, Can. J. Research **A26**, 279 (1948).

[2] R. M. Talley and A. H. Nielsen, Phys. Rev. **82**, 338 (1951); J. Chem. Phys. **19**, 805 (1951).

[3] B. D. Saksena, J. Chem. Phys. **20**, 95 (1952).

[4] C. A. Bradley and A. McKellar, Phys. Rev. **47**, 914 (1935).

[5] E. K. Plyler and N. Gailor, J. Research Natl. Bur. Standards **47**, 248 (1951).

[6] A. H. Nielsen, J. Tenn. Acad. Sci. **22**, 241 (1947).

[7] Bell, Noble, and Nielsen, Rev. Sci. Instr. **18**, 48 (1947).

any ordinary water vapor. The D_2O was 99.5 percent pure and the only contaminants observed were small amounts of C_2H_2 and C_2HD. These were probably formed because it was impossible to drive off all the water completely, and because the heavy-water sample was not 100 percent D_2O.

Several bands fell in regions where atmospheric absorption rendered the region nearly opaque, or caused serious overlapping. In the region of σ_5^1 at 500 K, the background interference was eliminated because the Ohio State University spectrograph is evacuable. In the other regions of interference the spectrometer box was sealed with Apiezon-Q wax and partially dried of water vapor and CO_2 by means of P_2O_5, Ascarite, and a stream of oil-pumped nitrogen.

Cells of various lengths filled to various pressures of the gas were used throughout the experiment. For the fundamentals and the more intense combination bands a 10-cm glass cell fitted with KBr and NaCl windows was found satisfactory. For several weaker bands a 41-cm glass cell with NaCl windows was used. Because C_2D_2 is a weak absorber compared with C_2H_2 and C_2HD it was necessary to construct a multiple reflection cell of the sort described by White[8] in order to observe higher overtone and combination bands. This cell was made of brass about two feet long, of such size and aperture as enabled it to fit into the grating spectrograph. The maximum number of traversals used in this work was 28 with a gas pressure of 50 cm of mercury. This is equivalent to a path length of about 12.1 meters of gas at atmospheric pressure. In certain regions energy was detectable for as many as 72 traversals, but the slits had to be excessively large. The long path length of gas made it possible to observe and measure a large number of hitherto unknown overtone and combination bands in the lead sulfide region of the near infrared.

Because C_2D_2 has two low-lying vibrational levels $v_4=1$ and $v_5=1$ which are populated with 18 and 14 percent, respectively, of the C_2D_2 molecules many so-called "hot bands" or difference bands occur with these states as lowest levels. These bands are quite useful in making correct assignments and in obtaining the wave numbers of the infrared inactive vibrations σ_1, σ_2, and σ_4. To render assignments of difference bands more certain it was arranged to cool the multiple reflection cell with "dry ice." Records were made at room temperature and at the low temperature in order to study the temperature sensitivity of such bands.

III. EXPERIMENTAL RESULTS

Thirty-nine bands which can be ascribed with good certainty to C_2D_2 and which have been assigned vibrationally were observed in this investigation. In describing the experimental results only the bands which were resolved, and for which rotational analyses were performed, will be discussed in detail. The others are listed as to frequency and assignment in Table I, wherein the complete list of known bands is given. A large number of the unresolved bands occur as Q branches overlapping the resolved bands. References to these will be found in the discussions of the resolved bands.

A superscript following σ_4 or σ_5 will, as is customary, represent the value of the quantum number of internal angular momentum l; for example, σ_5^1 represents the transition from the ground state to $v_5=1$, $l_5=1$, all other vibrational quantum numbers being zero.

The activity of the upper states has been determined from symmetry considerations with the aid of Tables

[8] J. U. White, J. Opt. Soc. Am. 32, 285 (1942).

TABLE I. Complete table of observed vibrational data for C_2D_2. All constants in kaysers.

Band assignment	$\sigma_0-B'l'^2+B''l''^2$ Obs	σ_0 Band center Obs	σ_0 Band center Calc	Δ Obs − Calc	$B'-B''$ Obs
$\sigma_4^1+\sigma_5^1-\sigma_4^1$	530.86	530.02	530.11	−0.09	
$2\sigma_5^2-\sigma_5^1$	532.86	535.31	535.06	+0.25	
σ_5^1	537.81	538.66	538.66	0.00	+0.0003
$\sigma_4^1+\sigma_5^1$	1041.49	1041.49	1041.49	0.00	+0.0038
$\sigma_2-\sigma_5^1$	1226.9	1226.05	1226.05	0.00	
$4\sigma_5^2-\sigma_5^1$	1595.0	1597.55	1595.58	+1.97	
$4\sigma_5^0-\sigma_5^1$	1599.0	1598.15	1595.98	+2.17	
$3\sigma_5^1$	1604.4	1605.25	1605.98	−0.73	
$\sigma_3-\sigma_4^1$	1928.57	1927.72	1927.72	0.00	−0.0044
$\sigma_1+\sigma_5^1-2\sigma_5^0$?	2153.7	2154.55	2160.53	−5.98	
$\sigma_1+\sigma_5^1-2\sigma_5^2$?	2159.1	2156.55	2160.93	−4.38	
$\sigma_1-\sigma_5^1$	2165.75	2164.90	2164.90	0.00	−0.0062
	2279.7				
$\sigma_2+\sigma_4^1+\sigma_5^1-\sigma_4^1$	2286.3	2288.85	2285.87	+2.98	
$\sigma_2+2\sigma_5^2-\sigma_5^1$	2292.5	2291.65	2289.65	+2.00	
$\sigma_2+\sigma_5^1$	2297.2	2298.05	2298.31	−0.26	
σ_3	2439.10	2439.10	2439.10	0.00	−0.0042
$5\sigma_5^1$	2658.5	2659.35	2659.70	−0.35	
$\sigma_3+\sigma_4^1+\sigma_5^1-\sigma_5^1$	2932.6	2931.75	2931.75	0.00	
$\sigma_3+2\sigma_4^2-\sigma_4^1$	2939.8	2942.35	2942.34	+0.01	
$\sigma_3+2\sigma_4^0-\sigma_4^1$	2942.2	2941.35	2941.34	+0.01	
$\sigma_3+\sigma_4^1$	2944.7	2945.55	2945.55	0.00	−0.0046
$\sigma_1+2\sigma_5^0-\sigma_5^1$	3226.6	3225.75	3223.76	+1.99	
$\sigma_1+\sigma_5^1$	3234.9	3235.75	3234.69	+1.06	
$\sigma_2+\sigma_3$	4190.63	4190.63	4190.21	+0.42	−0.0077
	4190.46[a]				
$\sigma_1+3\sigma_5^1$	4283.9	4284.75	4286.95	−2.20	
$2\sigma_3-\sigma_5^1$	4311.0	4310.15	4310.52	−0.37	
$\sigma_2+\sigma_3+2\sigma_4^{0,2}-\sigma_4^1$	4685.5	4684.65	4684.67	−0.02	
		4688.05	4685.67	+2.38	
$\sigma_2+\sigma_3+\sigma_4^1$	4692.34	4693.19	4692.77	+0.42	−0.008
$2\sigma_1-\sigma_5^1$	4848.67	4847.82	4846.72	+1.10	
$\sigma_1+\sigma_3$	5097.12	5097.12	5097.12	0.00	−0.0106
	5097.07[a]				
$\sigma_1+\sigma_3+\sigma_4^1$	5586.8	5587.65	5587.65	0.00	
$3\sigma_2+\sigma_5^1$	5792.8	5793.65	5789.95	−6.30	
$2\sigma_1+\sigma_4^1+\sigma_5^1-\sigma_4^1$	5876.3	5875.45	5868.59	+6.89	
$2\sigma_1+2\sigma_5^2-\sigma_5^1$	5890.1	5892.69	5890.32	+2.37	
$2\sigma_1+\sigma_5^1$	5907.7	5908.55	5908.98	−0.43	−0.01
	5959.5				
	5972.2				
$\sigma_1+\sigma_2+\sigma_3$	6827.5	6827.5	6828.03	−0.53	
$2\sigma_1+\sigma_3-\sigma_4^1$	7212	7211.15	7222.02	−10.87	
$2\sigma_1+\sigma_3$	7734	7734.00	7733.40	+0.60	

Photographic bands (Saksena)[b]

Band assignment	σ_0 Obs	σ_0 Calc from present ω_i and x_{ik}	Δ Obs − Calc	σ_0 Calc by Saksena	δ Obs − Calc
$\sigma_1+2\sigma_2+\sigma_3$	8550.12	8549.72	+0.40	8549.12	+1.00
$\sigma_2+3\sigma_3$	8952.89	8954.15	−1.26	8950.53	+2.36
$2\sigma_1+\sigma_2+\sigma_3$	9444.51	9444.11	+0.40	9439.11	+5.40
$\sigma_1+3\sigma_3$	9794.06	9797.18	−3.12	9794.44	−0.38
$3\sigma_1+\sigma_3$	10 347.92	10 347.94	−0.02	10 350.94	−3.02
$2\sigma_1+2\sigma_2+\sigma_3$	11 146.00	11 145.60	+0.40	11 143.94	+2.06
$\sigma_1+\sigma_2+3\sigma_3+\sigma_4^1-\sigma_4^1$	11 455.79	11 466.29	−10.50		
$\sigma_1+\sigma_2+3\sigma_3$	11 492.66	11 500.89	−8.32	11 492.30	+0.36
$5\sigma_3$	11 905.34	11 905.30	+0.04	11 905.30	+0.04
$3\sigma_1+\sigma_2+\sigma_3$	12 036.87	12 038.45	−1.58	12 036.88	−0.01
$2\sigma_1+3\sigma_3$	12 344.50	12 342.38	+2.12	12 339.16	+5.34
$\sigma_1+2\sigma_2+3\sigma_3$	13 181.90	13 195.38	−13.48	13 187.82	−5.92

[a] See reference 5.
[b] See reference 3.

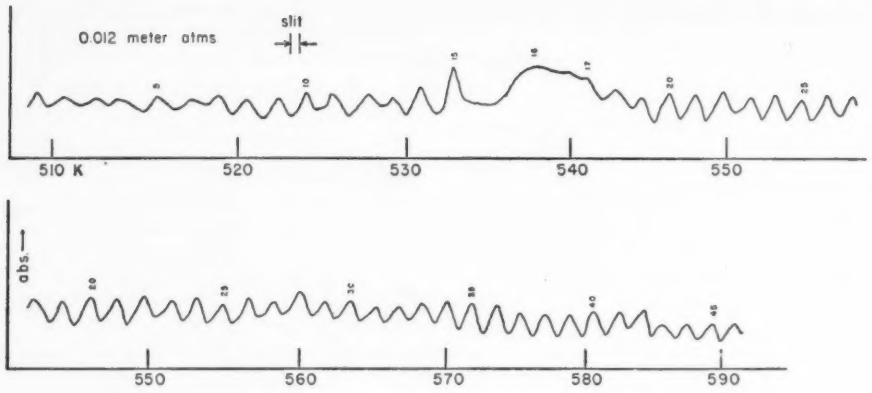

FIG. 1. Trace of a grating record of the absorption by the vibration-rotation band σ_5^1.

32 and 33 as given by Herzberg.[1] The vibration selection rules have been determined for a large number of overtone and combination bands with the aid of Herzberg's[1] Table 55 in order to be able to interpret the many observed bands.

Fundamental Bands

σ_5^1, $(\Pi_u-\Sigma_g^+)$, *Region 510–590 K*

The intense active fundamental σ_5^1 was observed with 0.012 meter atmospheres of C_2D_2 using a 1200 lines-per-inch grating in vacuum, with effective slit widths of 0.6 K. This band is shown in Fig. 1 with absorption as ordinates and wave numbers in kaysers as abscissas. For identification the lines in the figure are numbered from low to high wave numbers. These numbers, as well as the line wave numbers corrected to vacuum and their rotational assignments, are given in Table II.§

TABLE II. σ_5^1 line wave numbers, reduced to vacuum.

No.	Wave numbers Kaysers	Assignment	No.	Wave numbers Kaysers	Assignment
1	509.24	*P*17	24	553.18	*R*8
2	510.67	*P*16	25	554.80	*R*9
3	512.37	*P*15	26	556.61	*R*10
4	513.93	*P*14	27	558.23	*R*11
5	515.65	*P*13	28	560.00	*R*12
6	517.60	*P*12	29	561.67	*R*13
7	519.19	*P*11	30	563.20	*R*14
8	520.80	*P*10	31	565.01	*R*15
9	522.49	*P*9	32	566.59	*R*16
10	524.27	*P*8	33	568.25	*R*17
11	525.71	*P*7	34	570.09	*R*18
12	527.80	*P*6	35	571.74	*R*19
13	529.21	*P*5	36	573.57	*R*20
14	530.86	*P*4	37	575.18	*R*21
15	532.86	*Q*	38	577.14	*R*22
16	536.02	*Q*	39	578.83	*R*23
17	540.91	*R*1	40	580.56	*R*24
18	542.73	*R*2	41	582.27	*R*25
19	544.56	*R*3	42	583.99	*R*26
20	546.31	*R*4	43	585.47	*R*27
21	547.90	*R*5	44	587.37	*R*28
22	549.66	*R*6	45	589.23	*R*29
23	551.45	*R*7	46	590.93	*R*30

§ For the sake of brevity in future paragraphs, it should be noted that all figures showing band structures have the lines numbered thus.

A rotational analysis was performed for this band with the aid of well-known combination relations. The vibration frequency‖ was found to be 537.81 K, and the band center $\sigma_0=538.66$ K. The difference between the ground state and upper state rotational constants $B'-B''=+0.0003$ K. Evidence of the positive character of $B'-B''$ is given by the degrading of the Q branch toward higher frequencies. The present value of the band center is considered more reliable than the value 539.95 K of Randall and Barker[1] because it was determined by means of a band analysis.

The appearance of the band clearly shows that overlapping by at least one band occurs. For example, lines 14 and 15 appear to be more intense than might be expected of the lines $P(4)$ and $P(3)$ which occur there. Reasonable assignments for the Q branches occurring at 530.86 K and 532.86 K are $\sigma_4^1+\sigma_5^1-\sigma_4^1$, $(\Sigma_u^+, \Sigma_u^-, \Delta_u-\Pi_g)$ and $2\sigma_5^2-\sigma_5^1$, $(\Delta_g-\Pi_u)$, respectively. The band $2\sigma_5^0-\sigma_5^1(\Sigma_g^+-\Pi_u)$, which should appear at 536.56 K, probably contributes to line 16.

The expected 2-to-1 intensity alternation of the lines is apparently obscured somewhat by the interference of these overlapping bands. In addition, a longer path than was optimum for best resolution was used to make the weaker lines stand out above noise. Some intensity alternation is, however, observable near the extremities and this was an aid in proper identification of the P and R lines near the center. The intense lines originate from levels for which J is even.

σ_3, $(\Sigma_u^+-\Sigma_g^+)$, *Region 2390–2480 K.*

The only other active fundamental of C_2D_2 is the parallel-type band σ_3 shown in Fig. 2. It was observed

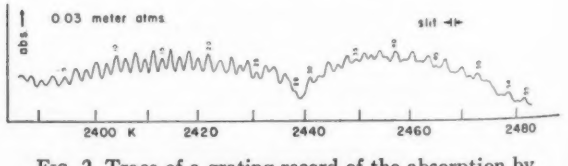

FIG. 2. Trace of a grating record of the absorption by the vibration-rotation band σ_3.

‖ See discussion of vibrational analysis. The vibration wave number and the band center σ_0 are the same only if there is no internal angular momentum change in the transition.

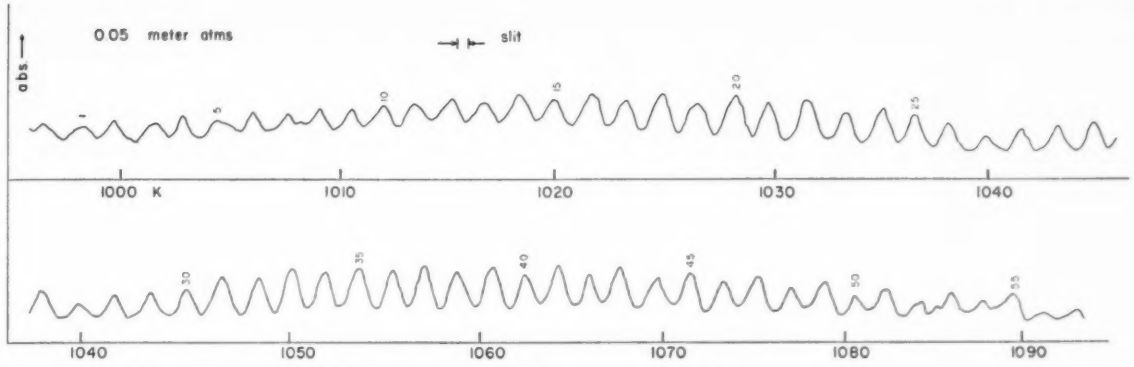

FIG. 3. Trace of a grating record of the absorption by the vibration-rotation band $\sigma_4^1+\sigma_5^1$.

with the 7200 lines-per-inch grating, an equivalent path length of 0.03 meter atmosphere, and slits with spectral width of 0.8 K. Though the intensity alternation is quite clear, the band appears to be overlapped by weak bands which tend to increase the general absorption. A possible band in this region is $\sigma_3+\sigma_4^1-\sigma_4^1$, $(\Pi_u-\Pi_g)$, and it is perhaps the Q branch of it which causes line 27 at 2433.76 K to be more intense than expected. The Q branch for this band is predicted at 2434.17 K, and could easily contribute to the intensity in the neighborhood of lines 26, 27, and 28.

A rotational analysis of this band is quite unambiguous and leads to a vibration wave number and band center which are identical at 2439.10 K. The difference between the upper and lower state rotational constants, $B'-B''$, is -0.0042 K. The earlier value of the band center 2427 K was determined prismatically by Stitt[1] and is not considered as accurate as the present one. The wave numbers, corrected to vacuum, and their J assignments are given in Table III.

Overtone and Combination Bands

$\sigma_4^1+\sigma_5^1$, $(\Sigma_u^+-\Sigma_g^+)$, *Region 1000–1090 K*

This extremely intense parallel-type band, shown in Fig. 3, was observed with the 3600 lines-per-inch grating, an equivalent path of 0.05 meter atmosphere, and slits of about 0.55 K. Despite the excellent resolution of the lines, the intensity alternation is difficult to discern. Also, there appears to be a Q branch at the center of the band. These two effects must be caused by overlapping of bands. The possible difference bands in this region are $2\sigma_4^{0,2}+\sigma_5^1-\sigma_4^1$, $(2\Pi_u-\Pi_g)$ and $\sigma_4^1+2\sigma_5^{0,2}-\sigma_5^1$, $(2\Pi_g-\Pi_u)$. A rotational analysis based on the assumption that line 28 is at the band center, which appears to be reasonable, places the band center at 1041.49 K and $B'-B''=+0.0038$ K. The present band center is somewhat lower than the value given by Randall and Barker,[1] but because an analysis was possible it is believed more reliable.

The observed frequencies, corrected to vacuum, and the line assignments are given in Table IV.

$\sigma_2-\sigma_5^1$, $(\Sigma_g^+-\Pi_u)$, *Region 1226 K*

With the exception of the Raman line of liquid C_2D_2[1] at 1762.4 K, the only source of information about the inactive vibration σ_2 comes from the Q branch of the difference band $\sigma_2-\sigma_5^1$ which emerges from the R lines of the impurity band $\sigma_4^1+\sigma_5^1$ of C_2HD at 1226.9 K. As no lines of this band were observed, its band center 1226.05 K was determined from the Q branch alone. The temperature sensitivity of this band was tested at dry ice temperature, and it is undoubtedly a difference band as the Q branch weakened by a reasonable amount. From the combination $\sigma_2-\sigma_5^1+\sigma_5^1$ the value of σ_2 was found to be 1764.71 K.

$3\sigma_5^1$, $(\Pi_u-\Sigma_g^+)$, *Region 1600 K*

The spectral region from 1560–1620 K was recorded with the 3600 lines-per-inch grating, 2.1 meter atmos-

TABLE III. σ_3 line wave numbers, reduced to vacuum.

No.	Wave numbers Kaysers	Assignment	No.	Wave numbers Kaysers	Assignment
1	2386.29	*P29*	30	2440.79	*R0*
2	2388.32	*P28*	31	2442.29	*R1*
3	2390.49	*P27*	32	2444.11	*R2*
4	2392.26	*P26*	33	2445.88	*R3*
5	2394.28	*P25*	34	2447.59	*R4*
6	2396.04	*P24*	35	2449.10	*R5*
7	2398.01	*P23*	36	2450.73	*R6*
8	2399.91	*P22*	37	2452.37	*R7*
9	2401.77	*P21*	38	2453.99	*R8*
10	2403.63	*P20*	39	2455.49	*R9*
11	2405.52	*P19*	40	2457.22	*R10*
12	2407.30	*P18*	41	2458.73	*R11*
13	2409.24	*P17*	42	2460.49	*R12*
14	2411.00	*P16*	43	2462.07	*R13*
15	2412.76	*P15*	44	2463.52	*R14*
16	2414.55	*P14*	45	2464.96	*R15*
17	2416.35	*P13*	46	2466.60	*R16*
18	2418.22	*P12*	47	2468.26	*R17*
19	2419.93	*P11*	48	2469.67	*R18*
20	2421.70	P10	49	2471.13	*R19*
21	2423.39	P9	50	2472.70	*R20*
22	2425.20	*P8*	51	2474.11	*R21*
23	2427.05	*P7*	52	2475.60	*R22*
24	2428.81	*P6*	53	2477.39	*R23*
25	2430.57	*P5*	54	2478.66	*R24*
26	2432.43	*P4*	55	2481.58	*R26*
27	2433.76	*P3*			
28	2435.74				
29	2437.45				

TABLE IV. $\sigma_4^1+\sigma_5^1$ line wave numbers, reduced to vacuum.

No.	Wave numbers Kaysers	Assignment	No.	Wave numbers Kaysers	Assignment
1	998.40	*P*27	30	1044.90	*R*1
2	999.72	*P*26	31	1046.63	*R*2
3	1001.31	*P*25	32	1048.39	*R*3
4	1002.85	*P*24	33	1050.16	*R*4
5	1004.40	*P*23	34	1051.89	*R*5
6	1005.93	*P*22	35	1053.64	*R*6
7	1007.41	*P*21	36	1055.34	*R*7
8	1009.01	*P*20	37	1057.16	*R*8
9	1010.58	*P*19	38	1058.94	*R*9
10	1012.21	*P*18	39	1060.68	*R*10
11	1013.61	*P*17	40	1062.51	*R*11
12	1015.26	*P*16	41	1064.24	*R*12
13	1016.78	*P*15	42	1066.08	*R*13
14	1018.41	*P*14	43	1067.81	*R*14
15	1020.03	*P*13	44	1069.75	*R*15
16	1021.65	*P*12	45	1071.46	*R*16
17	1023.25	*P*11	46	1073.31	*R*17
18	1024.84	*P*10	47	1075.16	*R*18
19	1026.54	*P*9	48	1077.17	*R*19
20	1028.08	*P*8	49	1078.73	*R*20
21	1029.69	*P*7	50	1080.65	*R*21
22	1031.35	*P*6	51	1082.42	*R*22
23	1033.00	*P*5	52	1084.29	*R*23
24	1034.74	*P*4	53	1086.12	*R*24
25	1036.34	*P*3	54	1087.87	*R*25
26	1038.11	*P*2	55	1089.62	*R*26
27	1039.86	*P*1	56	1091.33	*R*27
28	1041.32		57	1093.21	*R*28
29	1043.22	*R*0			

TABLE V. $\sigma_3-\sigma_4^1$ line wave numbers, reduced to vacuum.

No.	Wave numbers Kaysers	Assignment	No.	Wave numbers Kaysers	Assignment
1	1889.97	*P*22	26	1940.33	*R*6
2	1891.81	*P*21	27	1943.31	*R*8
3	1893.52	*P*20	28	1945.12	*R*9
4	1895.26	*P*19	29	1946.56	*R*10
5	1897.07	*P*18	30	1948.14	*R*11
6	1898.88	*P*17	31	1949.79	*R*12
7	1900.64	*P*16	32	1951.36	*R*13
8	1902.46	*P*15	33	1952.75	*R*14
9	1904.21	*P*14	34	1954.48	*R*15
10	1906.00	*P*13	35	1955.89	*R*16
11	1907.81	*P*12	36	1957.50	*R*17
12	1909.61	*P*11	37	1959.09	*R*18
13	1911.35	*P*10	38	1960.28	*R*19
14	1913.09	*P*9	39	1961.92	*R*20
15	1914.84	*P*8	40	1963.51	*R*21
16	1916.62		41	1964.99	*R*22
17	1920.31	H_2O	42	1966.23	*R*23
18	1923.35	H_2O	43	1967.69	*R*24
19	1928.85		44	1969.37	*R*25
20	1930.08	*R*0	45	1970.76	*R*26
21	1931.97	*R*1	46	1972.09	*R*27
22	1934.84	*R*2	47	1973.38	*R*28
23	1936.02	*R*3	48	1974.83	*R*29
24	1937.05	*R*4	49	1976.51	*R*30
25	1938.61	*R*5	50	1978.80	*R*31

pheres of C_2D_2, and slits including 0.6 K. The spectrometer was dried as thoroughly as possible, but serious interference from strong water vapor lines of the 6.2-μ atmospheric band occurred. Three C_2D_2 bands with Q branches fall in this region: $4\sigma_5^2-\sigma_5^1(\Delta_g-\Pi_u)$, $4\sigma_5^0-\sigma_5^1(\Sigma_g^+-\Pi_u)$, and $3\sigma_5^1$ at 1595.0, 1599.0, and 1604.4 K, respectively. The band centers obtained from these Q branch positions are 1597.55, 1598.15, and 1605.25 K, respectively. All the Q branches degrade toward higher wave numbers. As not enough rotation lines were observed for an analysis of these bands, the Q branches are simply listed in Table I.

$\sigma_3-\sigma_4^1$, $(\Sigma_u^+-\Pi_g)$, *Region 1890–1970 K*

The perpendicular type band shown in Fig. 4, identified as $\sigma_3-\sigma_4^1$, was observed with the 7200 lines-per-inch grating, a path length of 2.1 meter atmospheres, and slits of about 0.7 K. Interference by several intense water vapor lines occurs near lines 17, 18, and 27. The P branch is also overlapped by σ_2 of C_2HD. This is probably the reason that the intensity alternation is clearly discernible only in the R branch.

With regard to the vibrational analysis this is an important band because it permits the calculation of the band center of the inactive vibration σ_4^1 by means of the combination $\sigma_3-(\sigma_3-\sigma_4)$. The value calculated for σ_4^1, 511.38 K, is as reliable as any of the active fundamentals because it depends only upon the accurate determination of the band centers of σ_3 and $\sigma_3-\sigma_4^1$. Band analysis gives the center of the latter as 1927.72 K. Table V gives a list of the observed lines of the band.

$\sigma_1-\sigma_5^1$, $(\Sigma_g^+-\Pi_u)$, *Region 2110–2210 K*

Figure 5 shows the difference band $\sigma_1-\sigma_5^1$ with vibration frequency of 2165.75 K recorded with the 7200 lines-per-inch grating, a path length of 2.4 meter atmospheres, and slits of 0.47 K. This is one of the best resolved bands of the spectrum and exhibits the 2:1 intensity alternation very clearly. Lines 23 and 27 of Fig. 5 appear to be enhanced as if there were Q branches superposed upon them. These Q branches are

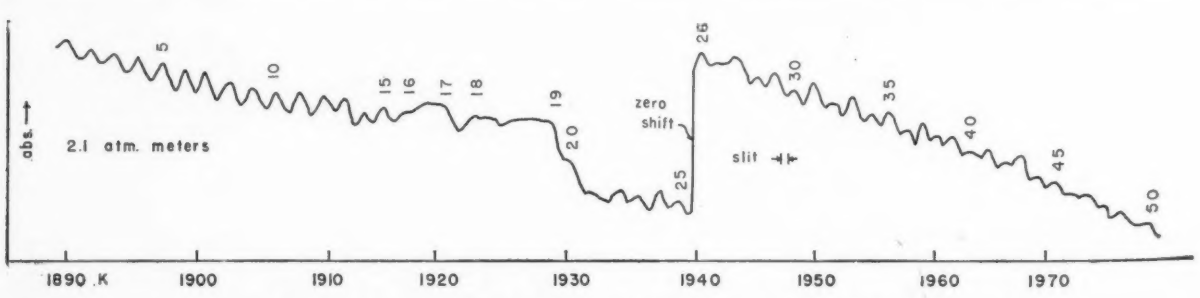

FIG. 4. Trace of a grating record of the absorption by the vibration-rotation band $\sigma_3-\sigma_4^1$.

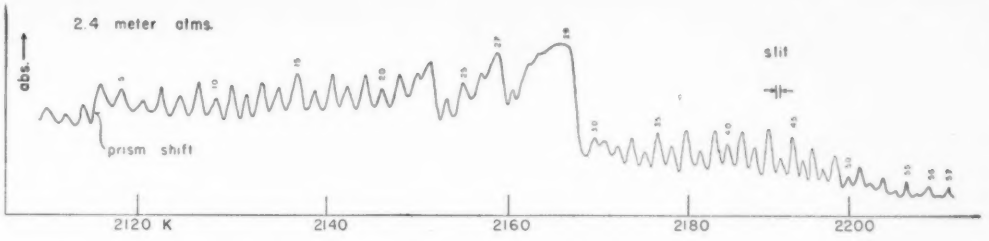

FIG. 5. Trace of a grating record of the absorption by the vibration-rotation band $\sigma_1-\sigma_5^1$.

difficult to explain because the bands most likely to be found in this region are $\sigma_4^1+3\sigma_5^1$ and $3\sigma_4^1+\sigma_5^1$, both of which are parallel-type bands. The only intense C_2H_2 Q branch in this region is that of $3\sigma_5^1$ which should be observed, if present, at 2170.84 K where it would enhance line 30. It is possible that these Q branches at 2153.7 and 2159.1 K can be ascribed to the Q branches of $\sigma_1+\sigma_5^1-2\sigma_5^{0,2}(\Pi_u-\Sigma_g^+, \Sigma_g^-, \Delta_g)$ which may be predicted to occur at 2159.68 K and 2163.48 K, respectively. The observed lines are tabulated in Table VI, with appropriate assignments.

$\sigma_2+\sigma_5^1$, $(\Pi_u-\Sigma_g^+)$ *and* $\sigma_2+2\sigma_5^{0,2}-\sigma_5^1$, $(\Sigma_g^+, \Sigma_g^-, \Delta_g-\Pi_u)$, *Region 2300 K*

Four absorption maxima were observed at 2279.7, 2286.3, 2292.5, and 2297.2 K with the 7200 lines-per-inch grating, 2.1 meter atmospheres path length, and slits of about 1.0 K. These bands fall in the 4.25-μ atmospheric CO_2 band. Though a great deal of the CO_2 was removed by means of Ascarite, the region did not clean up sufficiently to permit any analysis. The bands have been assigned as follows: $\sigma_2+\sigma_4^1+\sigma_5^1-\sigma_4^1$, $\sigma_2+2\sigma_5^2-\sigma_5^1$, and $\sigma_2+\sigma_5^1$ with band centers at 2288.85, 2291.65, and 2298.05 K, respectively. The absorption at 2279.7 K is unaccounted for.

TABLE VI. $\sigma_1-\alpha_5^1$ line wave numbers, reduced to vacuum.

No.	Wave numbers Kaysers	Assignment	No.	Wave numbers Kaysers	Assignment
1	2109.19	*P*30	30	2169.79	*R*1
2	2111.45	*P*29	31	2170.87	*R*2
3	2113.39	*P*28	32	2172.66	*R*3
4	2115.22	*P*27	33	2174.21	*R*4
5	2117.45	*P*26	34	2175.78	*R*5
6	2119.42	*P*25	35	2177.34	*R*6
7	2121.43	*P*24	36	2179.04	*R*7
8	2123.40	*P*23	37	2180.64	*R*8
9	2125.39	*P*22	38	2182.14	*R*9
10	2127.26	*P*21	39	2183.65	*R*10
11	2129.17	*P*20	40	2185.33	*R*11
12	2131.07	*P*19	41	2186.90	*R*12
13	2132.93	*P*18	42	2188.28	*R*13
14	2134.78	*P*17	43	2189.96	*R*14
15	2136.86	*P*16	44	2191.29	*R*15
16	2138.75	*P*15	45	2192.88	*R*16
17	2140.74	*P*14	46	2194.40	*R*17
18	2142.42	*P*13	47	2195.72	*R*18
19	2144.42	*P*12	48	2197.23	*R*19
20	2146.26	*P*11	49	2198.57	*R*20
21	2148.16	*P*10	50	2200.04	*R*21
22	2150.14	*P*9	51	2201.46	*R*22
23	2150.84		52	2202.85	*R*23
24	2153.04	*P*7	53	2204.35	*R*24
25	2155.41	*P*6	54	2205.63	*R*25
26	2157.36	*P*5	55	2207.26	*R*26
27	2159.20		56	2209.76	*R*28
28	2161.15	*P*3	57	2212.28	*R*30
29	2167.87	*Q*			

$5\sigma_5^1$, $(\Pi_u-\Sigma_g^+)$, *Region 2650 K*

The region from 2600 to 2800 K yielded only one band which could be assigned to C_2D_2. This band, with a Q branch, was observed with 2.2 meter atmospheres of gas, and has been assigned to the overtone $5\sigma_5^1$ with band center at 2659.35 K. $\sigma_2+\sigma_4^1+\sigma_5^1(\Sigma_u^+-\Sigma_g^+)$ should lie in the neighborhood of 2800 K, but it was not identified with certainty.

$\sigma_3+\sigma_4^1$, $(\Pi_u-\Sigma_g^+)$, *Region 2890–2990 K*

The spectrum of $\sigma_3+\sigma_4^1$, shown in Fig. 6, was recorded with the 7200 lines-per-inch grating, a path length of 0.9 meter atmosphere, and slits of 0.62 K. Between 2930 and 2950 K may be seen a number of Q branches of overlapping difference bands. This overlapping of bands probably accounts for the poor rendering of the region. The alternation of intensities is clearly visible only on the R side of the band.

From an analysis involving the usual combination relations the band center of $\sigma_3+\sigma_4^1$ was found to be 2945.55 K. The slope of the straight line from which the band center was obtained is $B'-B''$, the difference between the rotational constants in the lower and upper states. This constant, which is also $-(\alpha_3+\alpha_4^{PR})$, is found to be -0.0046 K. Table VII gives a tabulation of the observed line wave numbers, and their assignments in terms of the J value of the ground state.

The band observed at 2932.61 K has been assigned

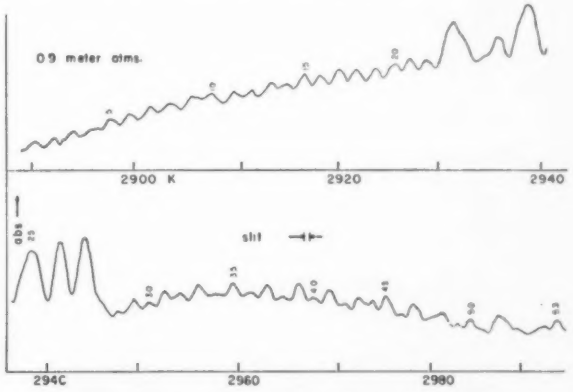

FIG. 6. Trace of a grating record of the absorption by the vibration-rotation band $\sigma_3+\sigma_4^1$.

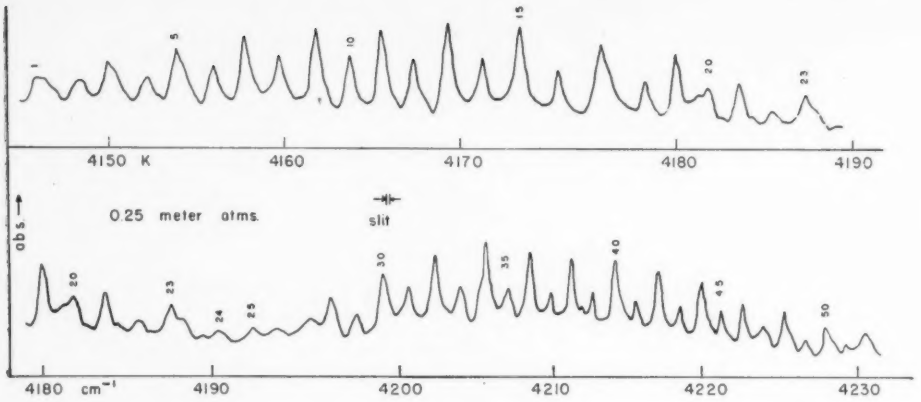

FIG. 7. Trace of a grating record of the absorption by the vibration-rotation band $\sigma_2+\sigma_3$.

as $\sigma_3+\sigma_4^1+\sigma_5^1-\sigma_5^1(\Sigma_g^+, \Sigma_g^-, \Delta_g-\Pi_u)$ with band center at 2931.75 K. The Q branch at 2935.97 K remains unassigned. The two Q branches at 2939.8 and 2942.29 K have been assigned as $\sigma_3+2\sigma_4^2-\sigma_4^1(\Delta_u-\Pi_g)$ and $\sigma_3+2\sigma_4^0-\sigma_4^1$, $(\Sigma_u^+-\Pi_g)$, respectively, with band centers coinciding at 2941.35 K.

$\sigma_1+\sigma_5^1$, $(\Pi_u-\Sigma_g^+)$, *Region 3230 K*

Two Q branches, one of which is quite intense, were observed projecting above the water vapor in this region with the 7200 lines-per-inch grating, 0.16 meter atmospheres path length and 0.5-K slits. These have been assigned as $\sigma_1+2\sigma_5^0-\sigma_5^1$, $(\Sigma_g^+, \Delta_g-\Pi_u)$ with band center at 3225.75 K and $\sigma_1+\sigma_5^1$ at 3235.75 K.

$\sigma_2+\sigma_3$, $(\Sigma_u^+-\Sigma_g^+)$, *Region 4150–4230 K*

This well-resolved parallel-type band, shown in Fig. 7, was recorded with the 15 000 lines-per-inch grating, the lead sulfide detector, 0.25 meter atmosphere of path, and slits of 0.2 K. This region is quite free of interference from difference bands and the 2:1 alternation of intensities is clearer than in any other band observed. The band center and $B'-B''$ were determined from combination relations and are probably more reliable than from other bands. They were found to be 4190.63 K and −0.0077 K, respectively. The observed wave numbers, and assignments with respect to the ground state J values, are given in Table VIII.

In addition, a weak band at 4284.75 K was found in a survey with 12 meter atmospheres of gas. The band has been ascribed to $\sigma_1+3\sigma_5^1$, $(\Pi_u-\Sigma_g^+)$.

$2\sigma_3-\sigma_5^1$, $(\Sigma_g^+-\Pi_u)$, *Region 4310 K*

This band appeared as a weak Q branch at 4311 K in a survey with the 15 000 lines-per-inch grating and a path of 12.1 meter atmospheres. Low temperature studies indicated that this band originated in either

TABLE VII. $\sigma_3+\sigma_4^1$ line wave numbers, reduced to vacuum.

No.	Wave numbers Kaysers	Assignment	No.	Wave numbers Kaysers	Assignment
1	2890.22	*P*30	28	2947.96	*R*1
2	2892.11	*P*29	29	2949.57	*R*2
3	2894.04	*P*28	30	2951.03	*R*3
4	2896.03	*P*27	31	2952.82	*R*4
5	2897.97	*P*26	32	2954.46	*R*5
6	2899.62	*P*25	33	2956.13	*R*6
7	2901.61	*P*24	34	2957.75	*R*7
8	2903.27	*P*23	35	2959.47	*R*8
9	2905.37	*P*22	36	2961.20	*R*9
10	2907.00	*P*21	37	2962.77	*R*10
11	2909.19	*P*20	38	2964.37	*R*11
12	2910.97	*P*19	39	2965.95	*R*12
13	2912.99	*P*18	40	2967.50	*R*13
14	2914.81	*P*17	41	2969.08	*R*14
15	2916.70	*P*16	42	2970.69	*R*15
16	2918.32	*P*15	43	2972.14	*R*16
17	2920.14	*P*14	44	2973.46	*R*17
18	2921.92	*P*13	45	2975.10	*R*18
19	2923.60	*P*12	46	2977.25	*R*19
20	2925.58	*P*11	47	2978.39	*R*20
21	2927.16	*P*10	48	2981.05	*R*22
22	2928.92	*P*9	49	2982.96	*P*23
23	2932.61	*Q*	50	2984.40	*P*24
24	2935.97		51	2987.50	*R*26
25	2939.75	*Q*	52	2992.67	
26	2942.20	*Q*	53	2994.68	
27	2945.09	*Q*			

TABLE VIII. $\sigma_2+\sigma_3$ line wave numbers, reduced to vacuum.

No.	Wave numbers Kaysers	Assignment	No.	Wave numbers Kaysers	Assignment
1	4145.66	*P*24	26	4195.63	*R*2
2	4148.48	*P*23	27	4197.28	*R*3
3	4149.86	*P*22	28	4198.90	*R*4
4	4152.01	*P*21	29	4200.45	*R*5
5	4153.76	*P*20	30	4201.97	*R*6
6	4155.92	*P*19	31	4203.64	*R*7
7	4147.84	*P*18	32	4205.15	*R*8
8	4159.68	*P*17	33	4206.76	*R*9
9	4161.68	*P*16	34	4208.19	*R*10
10	4163.62	*P*15	35	4209.79	*R*11
11	4165.45	*P*14	36	4211.26	*R*12
12	4167.34	*P*13	37	4212.78	*P*13
13	4169.29	*P*12	38	4214.19	*R*14
14	4171.17	*P*11	39	4215.59	*R*15
15	4172.92	*P*10	40	4217.13	*R*16
16	4174.82	*P*9	41	4218.55	*R*17
17	4176.63	*P*8	42	4219.99	*R*18
18	4178.31	*P*7	43	4221.16	*R*19
19	4179.91	*P*6	44	4222.68	*R*20
20	4182.00	*P*5	45	4224.07	*R*21
21	4183.61	*P*4	46	4225.41	*R*22
22	4185.38	*P*3	47	4226.71	*R*23
23	4187.20	*P*2	48	4227.97	*R*24
24	4189.16	*P*1	49	4229.12	*R*25
25	4194.46	*R*1	50	4230.53	*R*26

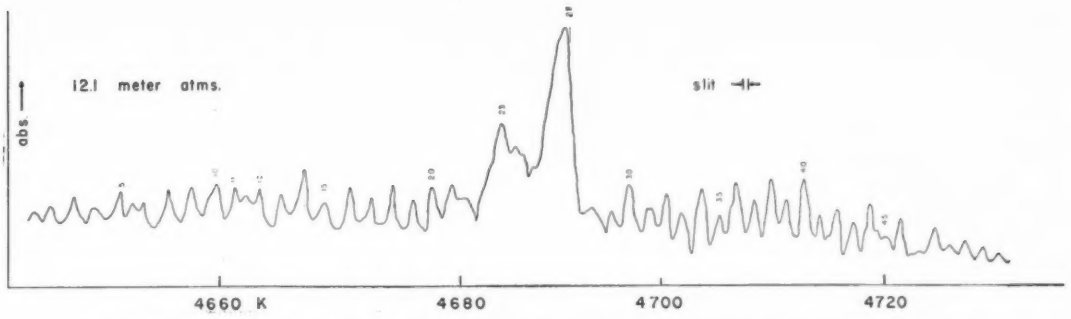

FIG. 8. Trace of a grating record of the absorption by the vibration-rotation band $\sigma_2+\sigma_3+\sigma_4^1$.

the level $v_4=1$ or $v_5=1$. The latter is favored from anharmonic constant considerations.

$\sigma_2+\sigma_3+\sigma_4^1$, $(\Pi_u-\Sigma_g^+)$, Region 4650–4730 K

The 15 000-lines-per-inch grating and a path length of 12.1 meter atmospheres of gas were used to observe the band shown in Fig. 8. The record was made with slit widths of 0.5 K, and the band appears to be well resolved. Several lines appear to be abnormally intense which probably is the consequence of overlapping by other bands. The intensity alternation is somewhat obscured. It was, however, possible to perform a rotational analysis along the conventional lines from which the band center was found to be 4693.19 K and $B'-B''$ was evaluated as -0.008 K. Table IX gives the observed frequencies and the rotational assignments of the lines.

Line 23, at 4685.5 K, appears to be enhanced and has been ascribed to $\sigma_2+\sigma_3+2\sigma_4^0-\sigma_4^1(\Sigma_u^+-\Pi_g)$ with its band center at 4684.65 K.

$2\sigma_1-\sigma_5^1$, $(\Sigma_g^+-\Pi_u)$, Region 4800–4870 K

This perpendicular band was recorded with the 15 000-lines-per-inch grating, 12 meter atmospheres equivalent path length, and slits of 0.6 K. Though there appear to be no overlapping bands in this region, the band is so poorly resolved that no rotational analysis was successful. The band center was, therefore, taken from the leading edge of the Q branch as 4847.82 K. Low temperature studies indicated that the band was temperature sensitive, and it was, therefore, assigned as $2\sigma_1-\sigma_5^1$.

$\sigma_1+\sigma_3$, $(\Sigma_u^+-\Sigma_g^+)$, Region 5030–5140 K

The fairly intense parallel-type band shown in Fig. 9 was recorded with the 15 000-lines-per-inch grating, the lead sulfide detector, 0.25 meter atmosphere of gas, and slits of 0.27 K. The expected intensity alternation is clearly seen, and no difficulty in assigning the J-values and establishing the band center was encountered. A rotational analysis gives the band center as 5097.12 K and $B'-B''$ as -0.0106 K. Observed line wave numbers and assignments are given in Table X.

Some overlapping by other bands is apparent in $\sigma_1+\sigma_3$. It is possible that $2\sigma_3(\Sigma^+-\Sigma^+)$ of C_2HD accounts for some of the absorption on the R side of the band. Lines 29 and 31 on the P side are of about the same intensity and are found to have a spacing of 1.67 K. This spacing is about $2B$ for C_2D_2 and as the lines are of about the same intensity they must originate from a $(\Pi-\Pi)$ transition in which no intensity alternation occurs. Such a band in this vicinity is $\sigma_1+\sigma_3+\sigma_4^1-\sigma_4^1(\Pi_u-\Pi_g)$, which would have a band center at 5076.3 K.

$\sigma_1+\sigma_3+\sigma_4^1$, $(\Pi_u-\Sigma_g^+)$, $3\sigma_2+\sigma_5^1$, $(\Pi_u-\Sigma_g^+)$, Region 5500–5800 K

A survey with the 15 000 lines-per-inch grating and 12.1 meter atmospheres path length revealed Q branches at 5586.8 and 5792.8 K. Low temperature studies suggest that these bands are summation bands originating in the ground state. They have been assigned as $\sigma_1+\sigma_3+\sigma_4^1$ and $3\sigma_2+\sigma_5^1$ with band centers at 5587.7 K and 5793.7 K, respectively.

TABLE IX. $\sigma_2+\sigma_3+\sigma_4^1$ line wave numbers, reduced to vacuum.

No.	Wave numbers Kaysers	Assignment	No.	Wave numbers Kaysers	Assignment
1	4642.72	*P26*	27	4692.49	*Q*
2	4645.58	*P25*	28	4693.84	*R0*
3	4647.65	*P24*	29	4695.73	*R1*
4	4649.62		30	4697.19	*R2*
5	4631.54	*P22*	31	4698.94	*R3*
6	4652.50		32	4700.46	*R4*
7	4653.63	*P21*	33	4701.76	*R5*
8	4655.58	*P20*	34	4703.57	*R6*
9	4657.42	*P19*	35	4705.21	*R7*
10	4659.46	*P18*	36	4706.79	*R8*
11	4661.23	*P17*	37	4708.42	*R9*
12	4663.27	*P16*	38	4709.83	*R10*
13	4665.26	*P15*	39	4711.33	*R11*
14	4667.13	*P14*	40	4712.98	*R12*
15	4668.74	*P13*	41	4714.35	*R13*
16	4670.91	*P12*	42	4715.94	*R14*
17	4672.83	*P11*	43	4717.31	*R15*
18	4674.80	*P10*	44	4718.73	*R16*
19	4676.44	*P9*	45	4720.24	*R17*
20	4678.45	*P8*	46	4721.80	*R18*
21	4680.37	*P7*	47	4722.33	*R19*
22	4681.94	*P6*	48	4724.39	*R20*
23	4685.54	*Q*	49	4725.87	*R21*
24	4687.27	*P3*	50	4727.05	*R22*
25	4687.92		51	4728.45	*R23*
26	4688.98	*P2*	52	4730.03	*R24*

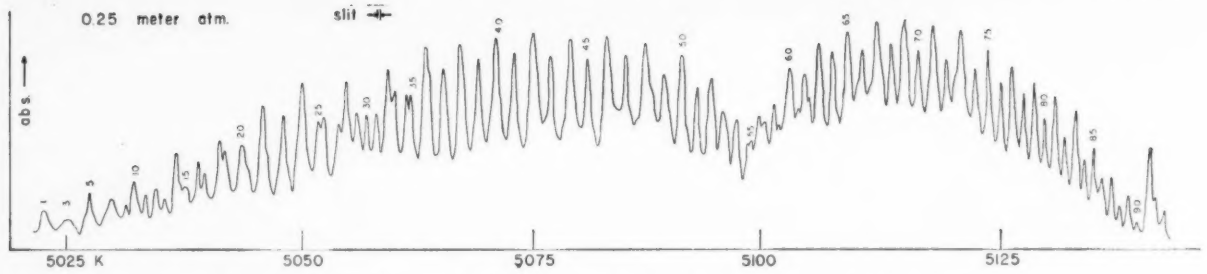

FIG. 9. Trace of a grating record of the absorption by the vibration-rotation band $\sigma_1+\sigma_3$.

$2\sigma_1+\sigma_5^1$, $(\Pi_u-\Sigma_g^+)$, Region 5850–5970 K

Figure 10 shows another perpendicular band recorded with the 15 000 lines-per-inch grating, 12.1 meter atmospheres equivalent path, and slits of 0.6 K. The most intense Q branch belongs to $2\sigma_1+\sigma_5^1$. The band center and $B'-B''$ were found to be 5908.55 K and -0.01 K, respectively, from a rotational analysis.

TABLE X. $\sigma_1+\sigma_3$ line wave numbers, reduced to vacuum.

No.	Wave numbers Kaysers	Assignment	No.	Wave numbers Kaysers	Assignment
1	5022.08	*P36*	46	5082.94	*P8*
2	5023.54		47	5084.84	*P7*
3	5025.08	*P35*	48	5086.70	*P6*
4	5025.95		49	5088.43	*P5*
5	5027.02		50	5090.27	*P4*
6	5027.33	*P34*	51	5091.93	*P3*
7	5029.41		52	5093.60	*P2*
8	5029.78	*P33*	53	5095.06	*P1*
9	5031.56		54	5096.55	
10	5032.47	*P32*	55	5097.94	
11	5033.78		56	5098.74	*R0*
12	5035.03	*P31*	57	5101.39	
13	5035.94		58	5100.31	*R1*
14	5036.96	*P30*	59	5102.05	*R2*
15	5037.77		60	5103.76	*R3*
16	5039.22	*P29*	61	5105.33	*R4*
17	5039.96		62	5106.90	*R5*
18	5041.52	*P28*	63	5108.40	*R6*
19	5042.06		64	5109.77	*R7*
20	5043.95	*P27*	65	5111.38	*R8*
21	5044.26		66	5112.96	*R9*
22	5046.12	*P26*	67	5114.39	*R10*
23	5048.09	*P25*	68	5115.83	*R11*
24	5050.40	*P24*	69	5117.34	*R12*
25	5052.03		70	5118.57	*R13*
26	5052.68	*P23*	71	5119.83	*R14*
27	5054.21		72	5121.42	*R15*
28	5055.02	*P22*	73	5122.54	*R16*
29	5056.11		74	5123.92	*R17*
30	5056.97	*P21*	75	5125.26	*R18*
31	5057.78		76	5126.60	*R19*
32	5059.05	*P20*	77	5127.90	*R20*
33	5059.80		78	5128.96	*R21*
34	5061.23	*P19*	79	5130.16	*R22*
35	5061.78		80	5131.29	*R23*
36	5063.45	*P18*	81	5132.53	*R24*
37	5065.51	*P17*	82	5133.77	*R25*
38	5067.36	*P16*	83	5134.87	*R26*
39	5069.38	*P15*	84	5136.00	*R27*
40	5071.37	*P14*	85	5137.17	*R28*
41	5073.36	*P13*	86	5138.16	*R29*
42	5075.42	*P12*	87	5139.19	*R30*
43	5077.25	*P11*	88	5140.12	*R31*
44	5079.00	*P10*	89	5141.36	*R32*
45	5080.87	*P9*	90	5142.96	*R33*

Some confusion exists in this region because of the overlapping of a number of bands. Low temperature studies suggest that the bands at 5876.3 K (line 16) and 5890.1 K (line 24) originate in an excited state, while the Q branches at 5907.7 (line 31), 5959.5 (line 62), and 5972.3 K (line 63) originate in the ground state. These bands have been assigned as $2\sigma_1+\sigma_4^1+\sigma_5^1-\sigma_4^1(\Sigma_u^+, \Sigma_u^-, \Delta_u-\Pi_g)$, $2\sigma_1+2\sigma_5^2-\sigma_5^1(\Delta_g-\Pi_u)$, $2\sigma_1+\sigma_5^1$, with band centers at 5875.45, 5892.69, and 5908.55 K, respectively. No assignment of the vibrations observed at 5959.5 and 5972.3 K has been made, as no bands of C_2D_2, C_2H_2, or C_2HD appear to fit. The observed wave numbers and rotational assignments are listed in Table XI.

$\sigma_1+\sigma_2+\sigma_3$, $(\Sigma_u^+-\Sigma_g^+)$, Region 6800 K

This band appears as an intense, poorly resolved parallel band in 2.4 meter atmospheres of the gas. The band center was taken to be 6827.5 K, which was the position of minimum absorption at the center of the band.

$2\sigma_1+\sigma_3$, $(\Sigma_u^+-\Sigma_g^+)$, $2\sigma_1+\sigma_3-\sigma_4^1$, $(\Sigma_u^+-\Pi_g)$, Region 7000–7800 K

These two bands appear, respectively, as an unresolved doublet and as a Q branch in a survey with 12 meter atmospheres equivalent path. The wave numbers, 7734 and 7212 K, are not very accurate because of poor resolving power in this region. Furthermore, the difference between these two bands should be the frequency σ_4^1, 511.38 K but actually is 522 K. This discrepancy probably results from poor frequency measurement rather than from misassignment.

Table I gives a collected list of all the known bands for C_2D_2, including those photographed by Saksena.[3]

IV. VIBRATIONAL ANALYSIS

The thirty-nine bands observed in this investigation plus the twelve observed in the photographic infrared by Saksena[3] are more than sufficient for the calculation of the zero-order frequencies ω_i and the anharmonic constants x_{ij} in the expression for the vibrational energy given by Shaffer and Nielsen.[9] This expression is repeated here in the interest of clarity and conven-

[9] W. H. Shaffer and A. H. Nielsen, J. Chem. Phys. 9, 847 (1941).

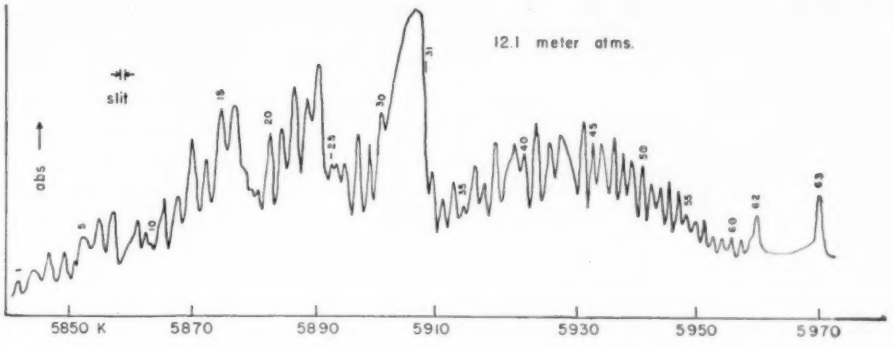

FIG. 10. Trace of a grating record of the absorption by the vibration-rotation band $2\sigma_1+\sigma_5^1$.

ience:

$$G_v(\text{kaysers})=G_0+\sum_{i=1}^{5}\omega_i(v_i+d_i/2)+\sum_{i=1}^{5}x_{ii}(v_i+d_i/2)^2+\sum_{i=1}^{5}\sum_{j>i=1}^{5}x_{ij}(v_i+d_i/2)(v_j+d_j/2)+\sum_{i=4}^{5}g_{ii}(l_i^2-1),$$

where v_i is the vibrational quantum number associated with the normal frequency ω_i, and d_i is the degeneracy of the mode ω_i. The degeneracy is 1 for all frequencies except ω_4 and ω_5, for which it is 2. l_i is the quantum number of internal angular momentum associated with the twofold degenerate vibrations ω_4 and ω_5, and may assume values $\pm v_i$, $\pm v_i-2$, $\cdots\pm 1$, 0. The values of G_0, x_{ii}, x_{ij}, and g_{ii} are given in terms of the generalized force constants in the paper by Shaffer and Nielsen.

The rotational energy F_R containing the vibration-rotation interactions was also obtained by Shaffer and Nielsen and has the form

$$F_R=B_v[J(J+1)-(l_4+l_5)^2]-D_v[J(J+1)-(l_4+l_5)^2]^2.$$

J is the quantum number of total angular momentum and may assume values $J\geqslant|l_4+l_5|$. The rotational constant

$$B_v=B_e-\sum_{i=1}^{5}\alpha_i(v_i+d_i/2),$$

where B_e is the equilibrium value and α_i is the vibration-rotation interaction constant associated with ω_i. D_v is the centrifugal stretching constant.

Expressions for the vibration-rotation lines in the bands may be obtained by taking the difference between the energies of the upper and lower state, i.e., $\sigma=\Delta G_v+\Delta F_R$, where ΔG_v is the frequency of the band center σ_0. Wave numbers of the lines in the R branch are given by

$$R(J+1)=[\sigma_0-B'l'^2+B''l''^2]+(B'+B'')(J+1)+(B'-B'')(J+1)^2,\quad J=0,\,1,\,2,\,\cdots$$

and lines in the P branch by

$$P(J)=[\sigma_0-B'l'^2+B''l''^2]-(B'+B'')J+(B'-B'')J^2,\quad J=1,\,2,\,3,\,\cdots.$$

Bands in which Q branches occur have the following relation for the component lines of the Q branch:

$$Q(J)=[\sigma_0-B'l'^2+B''l''^2]+(B'-B'')J(J+1),\quad J=1,\,2,\,\cdots,$$

where J is the value in the lower state. It may be seen that for $J=0$ or $Q(0)$ the frequency differs from the band center σ_0 by the amount $-(B'l'^2-B''l''^2)$, which may be zero if l' and l'' are zero. It should be noted that in Table I columns 3 and 4 differ by just this amount, which must be evaluated in each case.

It is possible to write the expression G_v in a somewhat more convenient form referred to the lowest level following Herzberg[1]:

$$G_0(v_1,v_2,\cdots)=\sum_{i=1}^{5}\omega_i^0(v_i)+\sum_{i=1}^{5}\sum_{k\geq i}x_{ik}^0v_iv_k+\sum_{i=4}^{5}\sum_{k\geq i}g_{ik}l_il_k,$$

TABLE XI. $2\sigma_1+\sigma_5^1$ line wave numbers, reduced to vacuum.

No.	Wave numbers Kaysers	Assignment	No.	Wave numbers Kaysers	Assignment
1	5842.89		33	5911.13	*R*1
2	5844.16		34	5912.97	*R*2
3	5847.15		35	5914.56	*R*3
4	5849.52		36	5916.06	*R*4
5	5852.43		37	5917.60	*R*5
6	5854.86		38	5919.14	*R*6
7	5857.09		39	5921.94	*R*8
8	5859.77		40	5923.13	*R*9
9	5860.94		41	5924.78	*R*10
10	5862.55	*P*23	42	5926.53	*R*11
11	5865.23		43	5927.93	*R*12
12	5866.30	*P*21	44	5930.58	*R*14
13	5869.87	*P*20	45	5932.29	*R*15
14	5872.17	*P*19	46	5933.69	*R*16
15	5874.52	*P*18	47	5935.59	*R*18
16	5876.34	*Q*	48	5937.05	*R*19
17	5877.76	*P*16	49	5938.57	*R*20
18	5878.99		50	5940.46	*R*21
19	5879.97	*P*15	51	5942.22	*R*22
20	5881.88	*P*14	52	5943.78	*R*23
21	5884.90	*P*13	53	5945.44	*R*24
22	5886.01	*P*12	54	5947.01	*R*25
23	5888.27	*P*11	55	5948.27	*R*26
24	5890.14	*Q*	56	5949.83	*R*27
25	5892.61		57	5951.24	*R*28
26	5893.74	*P*8	58	5952.61	*R*29
27	5894.93	*P*7	59	5954.04	*R*30
28	5897.25	*P*6	60	5955.58	*R*31
29	5899.18	*P*5	61	5957.10	*R*32
30	5901.40	*P*4	62	5959.54	*Q*
31	5908.40	*Q*	63	5972.28	*Q*
32	5909.58	*R*0			

TABLE XII. Wave numbers of the harmonic frequencies and the anharmonic constants.

Constant	Numerical value (K)		Source	Saksena[a]
ω_1^0	2714.43		σ_1, σ_3, $2\sigma_1+3\sigma_3$	2710.98
ω_2^0	1769.32		σ_1, σ_2, σ_3, $\sigma_1+2\sigma_2+\sigma_3$, $2\sigma_1+\sigma_2+\sigma_3$	1766.07
ω_3^0	2453.61		σ_3, $5\sigma_3$	2453.11
ω_4^0	510.52		$\sigma_3+\sigma_4^1$, $\sigma_3+2\sigma_4^1-\sigma_4^1$	
ω_5^0	540.46		σ_5^1, $3\sigma_5^1$, $5\sigma_5^1$, $2\sigma_5^2-\sigma_5^1$, $4\sigma_5^{0,2}-\sigma_5^1$	
ω_1	2778.65		Same as above and including the appropriate x_{ik}	
ω_2	1805.47		Same as above	
ω_3	2508.87		Same as above	
ω_4	534.10		Same as above	
ω_5	560.38		Same as above	
x_{11}	−10.87		σ_1, σ_3, $3\sigma_1+\sigma_3$	− 9.14
x_{22}	− 4.61		σ_2, $\sigma_1+2\sigma_2+\sigma_3$, $2\sigma_1+2\sigma_2+\sigma_3$	− 1.17
x_{33}	−14.51		σ_3, $5\sigma_3$	−13.91
x_{44}	0.61		$\sigma_3+\sigma_4^1$, $\sigma_3+2\sigma_4^0-\sigma_4^1$, $\sigma_3+2\sigma_4^2-\sigma_4^1$	
x_{55}	− 1.70		σ_5^1, $3\sigma_5^1$, $5\sigma_5^1$, $2\sigma_5^2-\sigma_5^1$, $4\sigma_5^{0,2}-\sigma_5^1$	
g_{44}	0.25		$\sigma_3+2\sigma_4^0-\sigma_4^1$, $\sigma_3+2\sigma_4^2-\sigma_4^1$	
g_{55}	− 0.10		σ_5^1, $3\sigma_5^1$, $5\sigma_5^1$, $2\sigma_5^2-\sigma_5^1$, $4\sigma_5^{0,2}-\sigma_5^1$	
x_{12}	−20.20		σ_1, $\sigma_1+2\sigma_2+\sigma_3$, $2\sigma_1+2\sigma_2+\sigma_3$	−21.23
x_{13}	−45.54		σ_1, σ_3, $\sigma_1+\sigma_3$	−46.28
x_{14}	−15.92		σ_1, σ_4^1, $\sigma_1+\sigma_3+\sigma_4^1$	
x_{15}	− 8.81		σ_1, σ_5^1, $2\sigma_1+\sigma_5^1$	
x_{15}	− 7.47		σ_1, σ_5^1, $2\sigma_1+2\sigma_5^2-\sigma_5^1$	
x_{15}	− 6.64	− 7.53	σ_1, σ_5^1, $\sigma_1+2\sigma_5^0-\sigma_5^1$	
x_{15}	− 6.47	(Av)	σ_1, σ_5^1, $\sigma_1+\sigma_5^1$	
x_{15}	− 8.26		σ_1, σ_5^1, $\sigma_1+3\sigma_5^1$	
x_{23}	−14.02	−13.60	σ_2, σ_3, $\sigma_2+3\sigma_3$	
x_{23}	−13.18	(Av)	σ_2, σ_3, $\sigma_2+\sigma_3$	−15.27
x_{24}	− 3.89		σ_3, $\sigma_2+\sigma_3$, $\sigma_3+\sigma_4$, $\sigma_2+\sigma_3+\sigma_4$	
x_{25}	− 5.61		σ_2, σ_5^1, $\sigma_2+2\sigma_5^2-\sigma_5^1$	
x_{25}	− 4.26	− 5.06	σ_2, σ_5^1, $\sigma_2+2\sigma_5^0-\sigma_5^1$	
x_{25}	− 5.32	(Av)	σ_2, σ_5^1, $\sigma_2+\sigma_5^1$	
x_{34}	− 4.93		σ_3, σ_4, $\sigma_3+\sigma_4^1$	
x_{35}	− 5.25		σ_3, σ_4^1, $\sigma_3+\sigma_4^1+\sigma_5^1-\sigma_5^1$	
x_{45}	− 8.55		σ_4^1, σ_5^1, $\sigma_4^1+\sigma_5^1$	

[a] See reference 3.

where $G_0(v_1,v_2,\cdots)$ is the band center σ_0 of a particular band, and where

$$\omega_i^0=\omega_i+x_{ii}d_i+\tfrac{1}{2}\sum_{k\neq i}x_{ik}d_k.$$

The $x_{ik}^0=x_{ik}$ if higher powers are neglected. With this expression and appropriate values of v_i and l_i, the band centers of all the bands listed in Table I may be written in terms of the ω_i^0 and the x_{ik}. In all, this gives fifty-one relations with which to calculate the constants. It is possible to calculate several of the x_{ik} from several different bands. Where this was possible an average x_{ik} was calculated for the best present value. Some of the present constants differ from those calculated by Saksena. His values are listed in Table XII along with the present ones. Information concerning the fundamental vibrations has been gathered into Table XIII.

These constants may now be used to calculate the band centers of the remaining bands which were not used in their determination, as a check on their accuracy and on the assignments. Column 4 of Table I gives the calculated band centers for all the known bands of C_2D_2. The agreement between observed and calculated band centers is seen to be excellent, the largest discrepancy being about 0.1 percent. Though the band centers computed for the photographic bands are somewhat different from those computed by Saksena, the differences are, on the average, little greater than his, and it is believed that the present fit is more consistent, as it fits all the presently known bands.

TABLE XIII. Table of the fundamental frequencies.

Fundamental vibration	Band center relation	Numerical value (K)	Source	Infrared activity
σ_1	$\omega_1^0+x_{11}$	2703.56	Calc $(\sigma_1-\sigma_5^1)+\sigma_5^1$	Inactive
σ_2	$\omega_2^0+x_{22}$	1764.71	Calc $(\sigma_2-\sigma_5^1)+\sigma_5^1$	Inactive
σ_3	$\omega_3^0+x_{33}$	2439.10	Obs	Active
σ_4	$\omega_4^0+x_{44}+g_{44}$	511.38	Calc $\sigma_3-(\sigma_3-\sigma_4^1)$	Inactive
σ_5	$\omega_5^0+x_{55}+g_{55}$	538.66	Obs	Active

V. ROTATIONAL ANALYSIS

Eight bands, namely σ_5^1, $\sigma_4^1+\sigma_5^1$, σ_3, $\sigma_3+\sigma_4^1$, $\sigma_2+\sigma_3$, $\sigma_2+\sigma_3+\sigma_4^1$, $\sigma_1+\sigma_3$, and $2\sigma_1+\sigma_5^1$, were sufficiently well resolved, and not too badly overlapped with other bands, so that rotational analyses could be performed by means of combination relations. All of these bands, which originate in the ground vibrational state, may be used to evaluate B_0, the rotational constant in the ground state. This has been done by computing $\Delta_2F''(J)=R(J-1)-P(J+1)$ for all of these bands, finding the average for a given J and plotting $\Delta_2F''(J)/(J+\frac{1}{2})$ *versus* $(J+\frac{1}{2})^2$. The intercept of the resulting straight line is $4B_0$, and the slope of this line is $8D_0$. The values determined from a graph of these data are $B_0=0.8478_8$ K and $D_0=8.4\times10^{-7}$ K. The value of B_0, found here, is a little smaller than the preliminary value 0.8482_7 K given by Talley and Nielsen,[2] and somewhat larger than the 0.8471 ± 0.0003 K given by Plyler and Gailor, but is in perfect agreement with $B_0=0.8478_7$ K given by Saksena.[3] The present value of D_0 is in perfect agreement with Saksena's value $D_0=8.0\times10^{-7}\pm0.7\times10^{-7}$ K. The percentage error in the present case is probably larger than in Saksena's measurements because the scatter of the points is greater than for the photographic bands. Thus, the rotational constants may be said to be in perfect agreement.

In their preliminary reports on C_2D_2, Talley and Nielsen[2] pointed out that there appeared to be a discrepancy between α_4 determined from the band analysis of $\sigma_4^1+\sigma_5^1$ and that determined from $\sigma_3-\sigma_4^1$. This discrepancy was cleared up by Saksena,[3] who pointed out that the difficulty arose from l-type doubling. He observed the band $\sigma_1+\sigma_2+3\sigma_3+\sigma_4^1-\sigma_4^1$, a $\Pi_u-\Pi_g$ transition in which there is no intensity alternation. This is because in a transition involving l-type doubling the transitions are from the lower level of the pair in the original state to the lower level of the pair in the final state. The effect of this on the spectrum is that each rotation line consists of an unresolved pair, one line resulting from transitions between levels of ordinary statistical weights, and the other resulting from transitions between levels of enhanced weights. As the two lines are unresolved no intensity alternation is observed. In his band analysis, Saksena, therefore, measured the B in the vibrational state $v_4=1$ as this is the original state for that band. With this B and B_0 he obtained $\alpha_4=-0.0012$ K. The band $\sigma_4^1+\sigma_5^1$ is a $\Sigma_u^+-\Sigma_g^+$ band in which no l-type doubling occurs, and,

therefore, the $\alpha_4+\alpha_5$ determined therefrom might be said to be the true value, whereas the value of α_4 from $\sigma_3-\sigma_4^1$, a $\Sigma_u^+-\Pi_g$ band, is α_4^{PR} because the transitions in the P and R branches are to the lower levels of the state and the Q-branch transitions are to the upper levels of the Π state. The B value associated with the lower levels would not be expected to be the same as that associated with the upper levels, and, therefore, the α's would be expected to be different. When this explanation is applied to the $B'-B''$ values determined from bands measured in this investigation, excellent agreement is found between the present α_i and those given by Saksena. His values are, however, perhaps somewhat more accurate because his line wave numbers are more accurately measured than in the infrared bands. The α_i have been collected and are listed in Table XIV.

Several cross checks are possible from $\sigma_3-\sigma_4^1$, $\sigma_2+\sigma_3+\sigma_4^1$, $\sigma_1+\sigma_3$, and $2\sigma_1+\sigma_5^1$. From $\sigma_3-\sigma_4^1$, $\alpha_3-\alpha_4^{PR}=0.0044$ K, and α_3 is, therefore, 0.0040 K, in reasonable agreement with the directly observed value. From $\sigma_2+\sigma_3+\sigma_4^1$, $\alpha_2+\alpha_3+\alpha_4^{PR}=0.0080$ K, and upon adding $\alpha_2+\alpha_3$ and α_4^{PR} from the table above, the value 0.0081 K is obtained in excellent agreement. From $\sigma_1+\sigma_3$, $\alpha_1+\alpha_3=0.0106$ K, while upon adding α_1 and α_3 from the table, the value 0.0101 K results. Finally, from $2\sigma_1+\sigma_5^1$, $2\alpha_1+\alpha_5^{PR}=0.01$ K, and upon adding $2\alpha_1$ and α_5^{PR} from the table above the value 0.0105 is obtained.

TABLE XIV. Table of vibration-rotation constants α_i (K) from the observed bands.

α_i	Present work Source (Table XI)	Observed value	Numerical value by Saksena[a]
α_1	from $\sigma_1-\sigma_5^1$; $\alpha_1-\alpha_5^{PR}=0.0062$	0.0059	0.0057_8
α_2	from $\sigma_2+\sigma_3$; $\alpha_2+\alpha_3=0.0077$	0.0035	0.0030_2
α_3	from σ_3; $\alpha_3=0.0042$	0.0042	0.0045_5
α_4^{PR}	from $\sigma_3+\sigma_4^1$; $\alpha_3+\alpha_4^{PR}=0.0046$	0.0004	...
α_4		...	−0.0012
α_5^{PR}	from σ_5^1; $\alpha_5^{PR}=-0.0003$	−0.0003	...
α_5	from $\sigma_4^1+\sigma_5^1$; $\alpha_4+\alpha_5=-0.0038$ and Saksena's α_4	−0.0026	−0.0026

[a] See reference 3.

Saksena[3] has calculated the B_e, the moments of inertia, and the internuclear distances. The reader is referred to his paper for their values as the rotational constants from the present investigation are in perfect agreement with his values.

ACKNOWLEDGMENT

One of the authors (Robert M. Talley) wishes to acknowledge with gratitude a Frederick Gardner Cottrell Fellowship set up at The University of Tennessee under a grant from the Research Corporation of New York.

Microwave Spectrum of 1,1-Difluoroethane*

N. Solimene and B. P. Dailey
Department of Chemistry, Columbia University, New York 27, New York
(Received May 24, 1954)

The spectrum of 1,1-difluoroethane has been investigated over the region 18 000 Mc to 38 000 Mc with a conventional Stark-modulation spectrometer. This molecule is a moderately asymmetric rotor of the oblate type with components of its dipole moment along the A and C axes. About 30 lines have been identified with the aid of the Stark effect and an approximate model for the molecule. The analysis yields the following rotational constants: $A=9491.95$ Mc; $B=8962.65$ Mc; $C=5170.43$ Mc; $\varkappa=0.75504$. The barrier hindering internal rotation has been determined as $(1.25\pm0.20)\times10^3$ cm^{-1} from intensity ratio measurements of the torsional frequency.

INTRODUCTION

THE microwave spectrum of 1,1-difluoroethane has been studied as part of a general survey of hindered rotation phenomena in ethane and its fluorinated derivatives. As yet no completely satisfactory solution to the problem of predicting the height and shape of the potential barriers to molecular internal rotation has been presented. In order to obtain a fundamental understanding of hindered rotation phenomena, reliable experimental data on series of related molecules are necessary. In the series of four molecules of which 1,1-difluoroethane forms a part with ethane, ethyl fluoride, and 1,1,1-trifluoroethane, all four molecules have similar symmetry, but it would be expected that the difference in the electrical properties of the C—F and C—H bonds would be sufficient to lead to marked differences in hindered rotational effects in their spectra.

Since data for the other three members of this series were already available the determination of the structure and barrier to hindered rotation in 1,1-difluoroethane was carried out to complete the series.

SPECTRUM AND ITS INTERPRETATION

The observations here reported were made with a conventional Stark modulation microwave spectrometer. The measurements of frequency were made to ±0.1 Mc using a communications receiver for interpolation between frequency markers supplied by a frequency standard periodically compared with the standard 5-Mc signal broadcast by station WWV.

The sample used in this work was kindly supplied by Dr. R. C. McHarness of the Jackson Laboratory of E. I. du Pont de Nemours Company, Inc.

Approximate rotational constants of 1,1-difluoroethane, computed using rough bond distances and angles, indicate that it is an asymmetric rotor of the oblate type with components of its dipole moment along the A and C axes. These constants were used to predict approximate transition frequencies using rigid rotor theory and neglecting as a first approximation any effects due to internal rotation.

The extremely rich spectrum of this molecule was studied over the frequency range 18 000 Mc to 38 000 Mc. The lines listed in Tables I, II, and III were identified with the aid of the Stark effect, the line strengths, and the approximate frequencies obtain from a rough model.

Precise values of the rotational constants A and B, given in Table I, were computed from the observed frequencies listed in Table I. Since the rotational constant C enters only in the $1_{10}-2_{20}$ transition in terms, which are of second and higher order in the asymmetry parameter $b=(A-B)/(2C-A-B)$, contributing 50.2 Mc to the observed frequency, it can only be determined to three significant figures from this transition.

The $J=1$ to $J=2$ and $J=2$ to $J=3$ asymmetric type doublets listed in Table II were identified by their Stark effects which for the $M=0$ components approach first order and are of opposite sign for the members of a doublet. It is possible from these transitions to obtain a precise value for C which is given in Table II. It is to be noted that this value of C differs by about one hundred megacycles from the less precise one given in Table I. This changes the predicted frequency of the $1_{10}-2_{20}$ transition from 36 959.4 Mc to 36 961.0 Mc. This dis-

Table I.

$J_{K_1,K_{+1}}-J+1_{K_1,K_{+1}}$	$A=9491.95$ Mc; $B=8962.65$ Mc; Observed (Mc)	$C=5.04\times10^3$ Mc Calculated (Mc)
$0_{00}-1_{10}$	18 454.7	18 454.6
$1_{10}-2_{20}$	36 959.4	36 959.4
$1_{11}-2_{21}$	37 438.4	37 438.5
$1_{01}-2_{11}$	36 379.9	36 379.9

Table II.

	$A=9491.95$ Mc; $B=8962.65$ Mc; Observed (Mc)	$C=5170.43$ Mc Calculated (Mc)
$1_{01}-2_{02}$	24 951.6	24 951.5
$1_{11}-2_{12}$	24 473.8	24 473.9
$2_{01}-3_{02}$	35 097.0	35 097.3
$2_{12}-3_{13}$	35 049.0	35 048.7
$(1_{10}-2_{20}$	36 959.4	36 961.0)
$1_{10}-2_{11}$	32 049.0	32 048.7

* Work supported in part by a Signal Corps contract and a grant from the Research Corporation.

crepancy in the value of C might be due to the neglect of effects due to torsional vibration.

In addition to the foregoing, several of the lower J lines have been observed in each of three $\Delta J=0$ bands. These are listed in Table III. The calculated frequencies were computed to fifth order in the asymmetry parameter b. The coefficients for this expansion in terms of b were calculated from general expressions given by E. E. Witmer.[1] The discrepancies between the measured and calculated frequencies are due to a considerable extent to the termination at fifth order of a poorly converging series. Since the molecule is rather asymmetric ($\varkappa=0.755040$; $b=-0.065229$), the convergence becomes worse with increasing J. Also centrifugal distortion contributions become larger with increasing J.

TABLE III.

$A=9491.95$ Mc $B=8962.65$ $C=5170.43$		$b=-0.065229$ $\varkappa=0.755040$
	Observed (Mc)	Calculated (Mc)
$K_1=3\rightarrow2$		
$6_{43}-6_{42}$	18 061.2	18 272.1
$5_{33}-5_{32}$	19 055.8	19 089.7
$4_{23}-4_{22}$	19 705.1	19 709.0
$3_{13}-3_{12}$	20 059.7	20 060.4
$3_{03}-3_{22}$	20 317.9	20 318.3
$4_{13}-4_{32}$	20 470.9	20 471.9
$5_{23}-5_{42}$	20 796.2	20 798.4
$6_{33}-6_{52}$	21 399.2	21 402.0
$K_1=4\rightarrow3$		
$8_{44}-8_{63}$	28 364.6	28 336.1
$7_{34}-7_{53}$	28 265.6	28 262.5
$6_{24}-6_{43}$	28 254.8	28 258.7
$5_{14}-5_{33}$	28 280.6	28 282.4
$4_{04}-4_{23}$	28 312.4	28 313.2
$4_{14}-4_{13}$	28 290.1	28 291.0
$5_{24}-5_{23}$	28 192.1	28 193.6
$6_{34}-6_{33}$	27 991.3	27 994.5
$7_{44}-7_{43}$	27 618.3	27 612.7
$8_{54}-8_{53}$	26 985.8	26 947.4
$K_1=5\rightarrow4$		
$5_{05}-5_{24}$	36 403.3	36 405.6
$5_{15}-5_{14}$		36 404.1
$6_{15}-6_{34}$	36 358.5	36 361.6
$6_{25}-6_{24}$	36 351.2	36 354.2
$7_{25}-7_{44}$	36 291.4	36 296.2
$7_{35}-7_{34}$	36 263.9	36 269.2

The lines in Table III were identified by means of their characteristic $\Delta J=0$ Stark patterns. The Stark effect of these lines approaches first order because of the K type near degeneracy of the levels involved and is of opposite sign for the lines in the $\Delta K_{-1}=0$ and $\Delta K_{-1}=2$ branches of each of the $\Delta J=0$ bands. As expected, zero field forbidden lines are observed due to the mixing of the nearly degenerate levels by the matrix elements of the dipole moment along the C axis.

[1] E. E. Witmer, *Tabulation of a Function for Calculating Rotational Energy Levels of a Rigid Polyatomic Molecule* (University of Pennsylvania Thermodynamics Research Laboratory Technical Report, Navy Contract N6 ONR-24907, 1950).

TABLE IV. Structural parameters.

$(d_{CH}=1.100)$[a]	
$(d_{CH'}=1.100)$[b]	
$(d_{CC}=1.540)$	
$d_{CF}=1.345\pm0.001$	
$(\angle HCH=110°\ 13')$	
$\angle FCF=109°\ 8'\pm5'$	
$\angle CCF=109°\ 26'\pm5'$[c]	
$\angle CCH=109°\ 49'\pm10'$	

[a] Values in parentheses are assumed.
[b] H′ refers to hydrogen of difluoromethyl group.
[c] These angles are related by $s-p$ hybridization formulas, i.e., $\cos\theta_{ij}=-[\alpha_i\alpha_j/(1-\alpha_i)(1-\alpha_j)]^{\frac{1}{2}}$, where θ_{ij} is angle between ith and jth bond and α_k is fraction of s character in kth bond.

In addition to the lines reported, there are many others. The stronger of these are presumed to be higher J members of the $\Delta J=0$ bands reported above. Some other lines are undoubtedly vibrational satellites.

PARTIAL STRUCTURAL DETERMINATION

Since only the three rotational constants of the normal species have been experimentally observed it is not possible to determine completely the structure of the molecule which involves eight parameters. However a partial structural determination is possible if some assumptions are made. The methyl halide parameters are assumed for the methyl group.[2] The CH distance in the difluoromethyl group is assumed to be equal to that in the methyl group. The CC distance is taken to be 1.540 A. Finally, the three angles specifying the structure of the difluoromethyl group are assumed to be related by the bond angle formulas for $s-p$ hybridization. The structure found with these assumptions is given in Table IV. The rotational constants computed from this structure are compared with the experimentally observed values in Table V.

SINUSOIDAL BARRIER HEIGHT DETERMINATION

Since the rotational constants of a molecule depend somewhat on the vibrational state of the molecule, it is possible to observe rotational transitions at slightly different frequencies for molecules which are in vibrational states other than the ground state. The relative intensities of these transitions are to a very good approximation directly proportional to the ratio of the populations of the vibrational states. Therefore, using the Boltzmann distribution equation and measuring the

TABLE V. Rotational constants.

	Observed (Mc)	Calculated (Mc)[a]
A	9491.95	9494
B	8962.65	8962
C	5170.43	5172

[a] Computed for structure given in Table IV.

[2] Miller, Aamodt, Dousmanis, Townes, and Kraitchman, J. Chem. Phys. **20**, 1112 (1952).

relative intensities of spectral lines corresponding to the same rotational transition of molecules in different vibrational states, it is possible to determine the difference in energy of the vibrational states.

The energies of the two lowest excited vibrational states above the ground state were measured by determining the relative intensities at room temperature of the two most prominent satellites of two conveniently located rotational transitions (see Table VI). Because of the characteristic Stark effects of these transitions there is no doubt as to the identification of the satellite lines. The satellites were not observed to have any fine structure. Also, none of the lines believed to be satellites of other identified transitions exhibited any observable fine structure. However, some unidentified transitions did have in their vicinity doublets or triplets, with qualitatively similar Stark effects, which may have been satellites. The intensities of satellites I and II of the transitions given in Table VI correspond, respectively, to vibrational states having frequencies of 235 $cm^{-1}\pm 20$ percent and 395 $cm^{-1}\pm 20$ percent above the ground state. The higher of these frequencies is in good agreement with the value 392 cm^{-1} which is the lowest frequency fundamental determined from the infrared and Raman spectra.[3] The lower frequency is presumed to be the torsional vibration frequency.

The structural data given in Table IV yield a value for the "reduced moment"[4] of normal 1,1-difluoroethane of 5.122×10^{-40} gcm^2. This value was used to determine from the tabulated energies given by Wilson[4] how large a sinusoidal barrier would be required to give a torsional frequency equal to the experimentally determined value, 235 cm^{-1}. It was found that the sinusoidal barrier height required is $(1.25\pm 0.20)\times 10^3$ cm^{-1} or $(3.57\pm 0.58)\times 10^3$ cal/mole. The large uncertainty in this value is due for the most part to the uncertainties in the intensity ratio data used to determine the torsional frequency and only partially due to the uncertainty in the structure of the molecule.

TABLE VI. Frequencies of satellites used for intensity measurements.

Transition	Frequency (Mc)
$1_{01}-2_{02}$, ground state	24 951.6
satellite I	24 926.3
satellite II	24 894.3
$1_{11}-2_{12}$, ground state	24 473.8
satellite I	24 425.7
satellite II	24 382.5

[3] Smith, Saunders, Nielsen, and Ferguson, J. Chem. Phys. **20**, 847 (1952).
[4] E. B. Wilson, Jr., Chem. Revs. **27**, 17 (1940).

DISCUSSION

The analysis of the observed spectrum of CH_3CHF_2 has been successfully accomplished using the "bound" case approximation for the internal motion. The use of the "bound" case approximation is justified by the rather high barrier height determined from the experimentally observed torsional frequency.

For low barrier heights one may expect the rotational energy levels of an asymmetric rotor to be appreciably perturbed.[5] The effects of such perturbations will be particularly apparent for transitions which involve changes in the quantum number K_1 or K_{-1} for almost oblate or almost prolate rotors, respectively. Also such transitions will necessarily involve changes in the state of torsion unless the rotor is sufficiently asymmetric to cause a breakdown of the selection rules.[5] Even if such changes were to occur they would contribute no more than a few tenths of a megacycle to the frequencies of rotational transitions of molecules in the ground vibrational state.[6]

The approximate value of the rotational constant C determined from the $1_{10}-2_{20}$ transition is in definite disagreement with the precise value determined from the $\Delta K_1=1$ transitions. However, these two values of C predict frequencies for the $1_{10}-2_{20}$ transition which are only 1.6 Mc apart. Since the manner in which the calculations were performed would throw all of the experimental errors and all of the effects of centrifugal distortion from the transitions used to obtain the values of A, B, and C onto the $1_{10}-2_{21}$ frequency, it does not appear possible to definitely assign this discrepancy to the effects of the torsional motion.

While the structural determination of this molecule is incomplete, it is felt that the assigned structural parameters are reasonably correct. It is to be noted that the CF distance is appreciably shorter than the value 1.38 A for ethyl fluoride. This is consistent with the known trend of CF distances to be shortened by the presence of additional fluorine atoms bonded to a carbon atom. For the molecule CH_2F_2, the shortened CF distance is accompanied by an increase in the HCH angle and a decrease in the FCF angle from the tetrahedral values.[7] Although the CF distance in CH_3CHF_2 is shorter than that in CH_2F_2 by about 0.01 A, the bond angles of the difluoromethyl group are not appreciably different from the tetrahedral configuration.

For a comparison of the barrier height of this molecule with the other members of the series mentioned in the introduction, refer to the paper by Kraitchman and Dailey.[6]

[5] D. H. Burkhard and D. M. Dennison, Phys. Rev. **84**, 408 (1951); E. V. Ivash and D. M. Dennison, J. Chem. Phys. **21**, 1804 (1953).
[6] J. Kraitchman and B. P. Dailey, J. Chem. Phys. **22**, 1477 (1954).
[7] D. R. Lide, Jr., J. Am. Chem. Soc. (to be published).

Emission Bands of NO in the Vacuum Ultraviolet Region Excited in the NO Afterglow

YOSHIO TANAKA
Geophysics Research Directorate, Air Force Cambridge Research Center, Air Research and Development Command, Cambridge, Massachusetts

(Received May 28, 1954)

The emission bands of the NO molecule excited in an impure afterglow were studied in the vacuum ultraviolet region. The abrupt cutoff at a certain v' value was observed in the β, γ, and δ bands and also the nonappearance of the ϵ, and β' bands was confirmed. An explanation for these observations was attempted in connection with the dissociation energy of the NO molecule and with the mechanism of the afterglow.

INTRODUCTION

IN 1927, Jenkins, Barton, and Mulliken[1] observed that when NO gas was introduced into a flow of active nitrogen, the color of the afterglow was changed to blue from its original yellow. In their studies on the production of the pure nitrogen afterglow, Cario[2] and Kaplan[3] found several stages of excitation, one of which (early stage) showed strong emission bands of NO. The same excitation stage of the glow was also found by Tanaka and Shimazu[4] in their study of the air afterglow. They showed that the spectrum of this stage was composed only of NO bands.

The emission spectrum of the NO molecule excited in active nitrogen was studied by Knauss[5] in the vacuum region. During this work he discovered the δ bands. Later on, Anand and his co-worker[6] repeated the Knauss experiment using a narrower slit and obtained more accurate wavelength data for the δ bands as well as the β, and γ bands. At almost the same time, Gaydon[7] discovered the ϵ bands in emission in the ordinary discharge, and also tried an excitation of NO by active nitrogen. In his latter work, Gaydon mentioned that all the systems are readily excited up to about the same energy, 52 000 cm^{-1}. (β, $v'=6$; γ, $v'=3$; δ, $v'=0$), and this might be interpreted either as predissociation in all three electronic states at about this energy or as the limiting energy available for the excitation of NO by active nitrogen. However, since Gaydon used quartz optics, it is desirable to repeat his experiment using a vacuum spectrograph, particularly in view of the fact that most of the strong bands of ϵ, and β' systems which Gaydon did not observe in the active nitrogen excitation appear below about 2000 A.

The main purpose of the present experiment was to confirm the abnormal features of the NO spectrum in the nitrogen afterglow using a vacuum spectrograph and to try to explain the evidence in connection with the dissociation energy of the NO molecule and with the mechanism of the afterglow.

EXPERIMENTAL

A Hilger, 2-meter, normal-incidence, vacuum spectrograph which has a grating of 15 000 lines per inch and a dispersion of about 8 A/mm was used. The glow tube made of Pyrex was about 1 meter long and 2 cm in diameter and was provided with a thin LiF window a few mm from the slit. The discharge tube which produces active substances was attached at a right angle to the glow tube about 6 cm from the slit. To avoid a stray discharge and an internal reflection of the light of the main discharge, a zig-zag tube about 25 cm in length was used between the two tubes and both the spectrograph and one electrode near the glow tube were carefully grounded.

The power supply was a 15 kv transformer (0.9 kva) connected to a small Leyden jar in parallel and a spark gap in series with the main discharge tube. Commercial tank nitrogen was introduced into the discharge tube without purification and it was continuously pumped through the glow tube maintaining the pressure at the value desired. It was found that the tank nitrogen had enough impurity of oxygen to produce fairly strong NO bands in the glow; however, to obtain much stronger NO bands, tank oxygen was introduced into the nitrogen flow in an amount less than about 2 percent of the total pressure. The total pressure was changed from time to time in the range of 3–6 mm Hg and was measured by a McLeod gauge at the rear end of the glow tube. By adding such a small amount of oxygen, the color of the afterglow was changed to blue. At the same time, NO bands were strongly intensified, but the characteristics of the glow spectrum did not show any change in the whole region ($\lambda \leq 3000$ A). However, in the visible region under this condition, the first positive bands of N_2 almost disappeared and, instead, the β bands of NO were strengthened.

We also tried a mixture of a small amount of tank nitrogen with an excess of helium or argon. In both cases, the total pressure was varied from about 3 to 15 mm Hg and tank nitrogen did not exceed about 5 percent of the total pressure. As was mentioned by

[1] Jenkins, Barton, and Mulliken, Phys. Rev. **30**, 150 (1927).
[2] G. Cario and U. Stille, Z. Physik **107**, 396 (1937).
[3] J. Kaplan, Phys. Rev. **54**, 176 (1938).
[4] Y. Tanaka and M. Shimazu, J. of Sci. Research Inst. (Tokyo) **43**, 241 (1949).
[5] H. P. Knauss, Phys. Rev. **32**, 417 (1928).
[6] Anand, Kalia, and Mela Ram, Indian J. Phys. **17**, 69 (1943); B. M. Anand, Indian J. Phys. **17**, 246 (1943).
[7] A. G. Gaydon, Proc. Phys. Soc. (London) **56**, 95, 160 (1944).

Rayleigh and McLennan, in such a case, the color of the afterglow was observed as a deep brown. Particularly, with high pressures of a rare gas and relatively small amounts of nitrogen it was seen as a reddish brown. In the case of a mixture, the intensity of all NO bands was either greatly reduced or the bands disappeared and, at the same time, the first positive bands of N_2 showed a distinct red shift in their intensity distribution.

Most of the plates were taken with a 15μ slit width and exposure times from 15 minutes to 2 hours. With the purpose of looking for any faint NO bands below 1915 A, several plates were taken using a 0.1 mm slit width and exposures up to 7 hours. Eastman SWR film and plates were used throughout.

RESULTS AND DISCUSSION

All the bands observed in the present region ($\lambda \leq 3000$ A) were caused by the NO molecule, except the L-B-H bands of the N_2 molecule which were extremely weak but observed near 1800 A. One of the spectra of the afterglow obtained in the present experiment is reproduced in Fig. 1(a) and, for comparison, there is also reproduced an ordinary NO spectrum in Fig. 1(b) which was taken with the same instrument using a transformer discharge of nitric oxide as a light source. In Fig. 1, one can see three striking differences between (a) and (b). The first is that, in (a), the spectrum was cut off abruptly at about 1915 A (6.47 ev) and nothing appeared below this wavelength. This evidence was confirmed even in the plates which were taken with a wide slit (0.1 mm) and a long exposure (7 hours). However, in (b), no such evidence of abrupt cutoff was observed and the spectrum extended below 1915 A with fairly strong NO bands. The second difference is that in (b), above 1915 A the ϵ and β' bands appeared fairly strongly, but in (a), these were completely absent as noted also by Gaydon[7] in the case of ϵ bands.

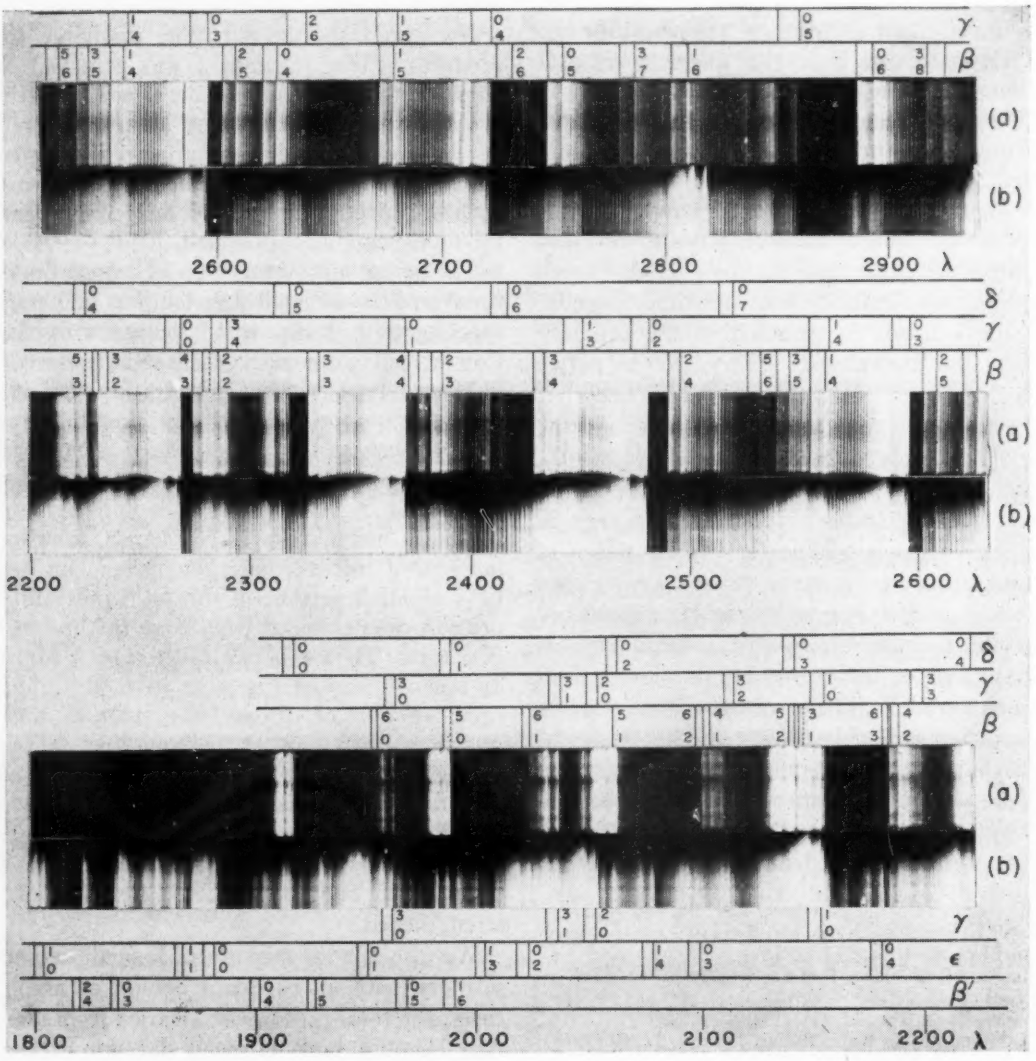

FIG. 1. NO emission bands: (a) in the NO afterglow, (b) in an ordinary discharge of NO.

The last remarkable difference is that in (a), all three systems (β, γ, and δ bands) appeared with nearly the same intensity; however, in (b) both β and δ bands were weak compared to γ bands.

Although it is not as conspicuous as the differences mentioned above, one can also see by close inspection that in (b) the intensity distribution in the sequence $\Delta v=+2$ of γ bands is normal, but in (a) the relation is changed; that is, (3,1) band is stronger than (2,0). A similar intensity anomaly seems to exist in the sequence $\Delta v=+1$ of the γ bands, but since in this case strong δ bands appear close by, it is not as clear as in the $\Delta v=+2$ sequence.

As shown in Fig. 1(a), and as observed by Gaydon, the highest upper vibrational levels of the β, γ, and δ bands were $v'=6$, 3, and 0, respectively, and the ϵ, and β' bands were not observed at all.

For the β system, all the bands observed by Gaydon[7] were identified in the present work and, in addition, a few new bands were observed: (6,0), (5,0), and (5,1), the last two of which are superposed on strong (0,1) and (0,2) δ bands, respectively. In absorption, the v' of this system has been observed up to 16,[8] and above $v'=8$ several anomalies both in intensity and in spacing also have been reported by several authors, but no such anomalies were ever reported below $v'=7$.

Recently, Sutcliffe and Walsh[8] proposed that all these irregularities are caused by perturbations of the $B^2\Pi$ state by the $A^2\Sigma^+$ and $D^2\Sigma^+$ states while, according to Glockler's theory[9] (see Fig. 2) one can expect perturbations at about $v=7$ and 9 of the $B^2\Pi$ state because this state would be crossed by the $A^2\Sigma^+$ and $C^2\Sigma$ states at these points, respectively. Furthermore, in his theory, the $B^2\Pi$ state should also be crossed by the flat $^2\Sigma^+$ state at about $v=7$ in its attractive branch because Glockler has assumed $D_0(\mathrm{NO})=6.48$ ev. As mentioned above, since no conspicuous anomaly was reported between $v=6$ and 7 of $B^2\Pi$ state in absorption, it will be safe to assume that the expected perturbation at $v=7$ should be very weak even if it does exist. On the other hand, in the glow spectrum the nonappearance of the β bands higher than $v'=6$ is rather abrupt, and also in the afterglow spectrum, no one has observed the bands higher than $v'=6$ even in the visible region. Therefore, it is likely that the reason for this may be found in the excitation mechanism in the afterglow rather than a perturbation or a predissociation.

For $A^2\Sigma^+$ (upper state of γ bands), the existence of the $v=4$ level seems to be still in question. In absorption, Tanaka[10] has made an extension up to $v'=8$ without using the ϵ bands which come close to the γ bands, but Sutcliffe and Walsh[8] have extended the same progression up to $v'=3$ and attributed the one classified as (4,0) by Tanaka to $\epsilon(0,0)$. In emission,

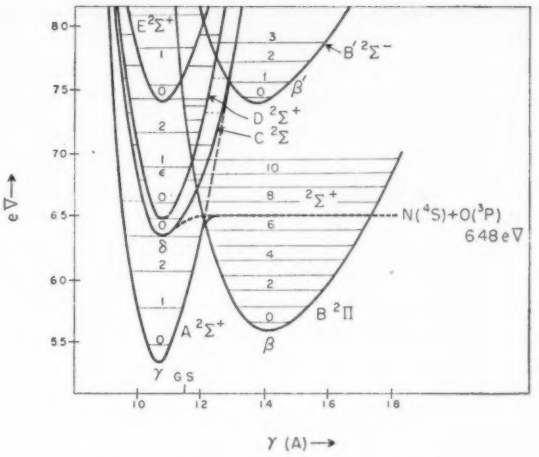

FIG. 2. Potential curves of NO molecule.

Guillery[11] classified some of the bands observed by Bair[12] as γ bands with $v'\geq 4$, but these seem to be better explained at present as belonging to the ϵ bands instead of the γ bands.

If we follow Glocker's[9] theory, the $A^2\Sigma^+$ state is perturbed by a flat $^2\Sigma^+$ state between $v=3$ and 4, and the actual potential curve of the state will dissociate to $\mathrm{N}(^4S)+\mathrm{O}(^3P)$; while from Sutcliffe and Walsh's[8] proposal, the perturbation between $v=3$ and 4 should be caused by the $B^2\Pi$ state. From the two theories mentioned above, it seems natural to ascribe the abrupt nonappearance of bands at $v'=4$ to perturbation either by a flat curve of $^2\Sigma^+$ or $B^2\Pi$ state. However, in the glow spectrum, the relative intensity distribution in some of the γ bands was different from that in ordinary excitation; that is, the higher vibration bands were relatively strong. This evidence would suggest that the nonappearance of bands is caused by an excitation peculiar to the glow.

In the present experiment, the clearest evidence of abrupt cutoff at a certain v' value was seen in the δ bands; that is, the $(0,v'')$ progression appeared very strong but $v'\geq 1$ were never observed. Previously, δ bands with $v'=0,1,2$, were observed[10] in absorption, and their intensities were found to be greater than those of the γ, and β bands. Furthermore, it was found that the $\Delta G:v$ curve of $C^2\Sigma$ state was reversed from the usual form and it was suggested that there might be a predissociation at $v=1$ or possibly $v=0$. As in the case of the γ bands, Sutcliffe and Walsh[8] ascribed the observed irregularities to perturbation caused by the $B^2\Pi$ state. Apart from the existence of the predissociation or perturbation, the abrupt cutoff at $v'=1$ of the δ system in the glow spectrum could be explained by assuming again a special mechanism of the glow in which the excitation energy available is limited to an energy almost equal to ν_{00} of the bands.

Strong support of the possibility of another mecha-

[8] L. H. Sutcliffe and A. D. Walsh, Proc. Phys. Soc. (London) A66, 209 (1953).
[9] G. Glockler, J. Chem. Phys. **16**, 604 (1948).
[10] Y. Tanaka, J. Sci. Research Inst. (Tokyo) **43**, 28 (1949).
[11] M. Guillery, Z. Physik **42**, 121 (1927).
[12] W. H. Bair, Astrophys. J. **52**, 301 (1920).

nism instead of perturbation and predissociation acting in all the β, γ, and δ bands lies in the fact that in the glow spectrum no other NO bands were observed in the entire region studied in the present work. Of particular interest is the complete nonappearance of ϵ bands, even $v'=0$ level. One can see in Fig. 2 that the $B^2\Pi(v=6)$ and $A^2\Sigma^+(v=3)$ come close together and if we take 6.48 ev as the dissociation energy of NO, they come close to this value but do not exceed it. The energy of $C^2\Sigma(v=0)$ level is greater than $D_0(\mathrm{NO})$ but the difference is only about 0.01 ev. The $D^2\Sigma(v=0)$ also comes close to $D_0(\mathrm{NO})$ but about 0.12 ev above it. Since Gaydon[7] did not observe any predissociation or perturbation in the $D^2\Sigma$ state, the complete absence of the ϵ bands in the glow is most probably caused by characteristics of the glow itself. The $^2\Sigma^-(v=0)$[13] (upper state of β' bands) is much higher ($\sim$0.96 ev) than $D_0(\mathrm{NO})$, and the same explanation can be applied to the nonappearance of this system in the glow spectrum.

As was mentioned previously, when a small amount of oxygen was introduced into the flow of tank nitrogen, the color changed to blue and the NO bands were much intensified at the same time, but did not change their characteristic appearance. This seems to suggest that the energy necessary to excite the NO molecule does not come from the active nitrogen and that we may need to assume other mechanisms for the blue glow.

It is suggested that in the blue glow, the following reactions occur to produce strong NO bands:

$$\mathrm{NO}(X^2\Pi)+\mathrm{N}(^4S)+\mathrm{O}(^3P)\rightarrow\mathrm{NO}^*+\mathrm{NO}(X^2\Pi)\cdots \quad (1)$$

$$\mathrm{NO}^*\rightarrow\mathrm{NO}(X^2\Pi)+h\nu(\beta,\ \gamma,\ \text{and}\ \delta\ \text{bands})\cdots. \quad (2)$$

If we take $D_0(\mathrm{NO})=6.48$ ev, all the observations can be explained simply by the above reactions without any serious difficulty, but if we assume $D_0(\mathrm{NO})=5.29$ ev, the evidence cannot be explained in such a simple way, as stated above. As mentioned above, the $C^2\Sigma(v=0)$ level is above $D_0(\mathrm{NO})$ but their energy difference is so small that the kinetic energy of the colliding particles will cover this difference. Likewise, one can also expect β bands which originate from $v'=7$ because the energy of this level is greater than $D_0(\mathrm{NO})$ by only about 0.01 ev. However, we could not identify them mainly because the expected bands come close to or coincide closely with strong δ, and γ bands. According to Oldenberg's theory,[14] there should not be expected a sharp resonance phenomena in a collision process such as reaction (1), and our observation agrees with this theory.

In addition to reactions (1) and (2), we can expect another reaction:

$$\mathrm{N}_2(X^1\Sigma_g^+)+\mathrm{N}(^4S)+\mathrm{O}(^3P)\rightarrow\mathrm{N}_2^*+\mathrm{NO}(X^2\Pi)\cdots \quad (3)$$

which should occur more frequently than (1) because the main constituent in the glow tube should be the N_2 molecule in its ground state. If $D_0(\mathrm{NO})$ is 6.48 ev, the only possible levels of N_2^* in (3) are $A^3\Sigma_u^+(v=0,1)$ which are the upper states of the Vegard-Kaplan bands; however, we could not observe any bands belonging to this system.

The weak appearance of NO bands in the mixture of an excess of rare gas and small amounts of tank nitrogen seems to be caused by a lack of enough atomic oxygen to promote reaction (1). In the case of the active nitrogen afterglow, the presence of a rare gas plays an important role in the intensity distribution in the first positive bands of N_2.[15] In the present work, we could not observe a similar effect on the NO bands; except in the case of the mixture, the β bands were relatively stronger than the γ bands.

On the mechanism of the Lewis-Rayleigh afterglow of active nitrogen, Cario and Reinecke[16] have recently proposed a new theory introducing an inverse predissociation of nitrogen atoms along the $^5\Sigma_g$ potential curve which arises from dissociation products $\mathrm{N}(^4S)+\mathrm{N}(^4S)$, and this theory was confirmed by Brook and Kaplan.[15] However, in the present case of NO afterglow, it is not certain whether inverse predissociation has an important role because the existence of predissociation in the NO molecule is not experimentally well established.

As a summary of the present experiment, it is suggested that there should exist a particular afterglow in a mixture of nitrogen and a trace of oxygen which is composed of three systems of NO bands (β, γ, and δ) in its spectrum. It is also suggested that the excitation energy available in the afterglow originates from the dissociation energy of the NO molecule. The interpretation of the observed abrupt cutoff at certain v' values in β, γ, and δ bands and of the complete nonappearance of ϵ, and β' bands seems to favor the value $D_0(\mathrm{NO})=6.48$ ev.

[13] P. Baer and E. Miescher, Helv. Phys. Acta **26**, 91 (1953).
[14] O. Oldenberg, Phys. Rev. **90**, 727 (1953).
[15] M. Brook, Scientific Report No. 2, Institute of Geophysics, University of California (March, 1953); J. Kaplan and M. Brook (private communication).
[16] G. Cario and L. Reinecke, Abhandl. braunschweig. wiss. ges. **1**, 8 (1949); L. Reinecke, Z. Physik **135**, 361 (1953).

Redetermination of the Crystal Structure of Lithium Sulfate Monohydrate $Li_2SO_4 \cdot H_2O$*

ALLEN C. LARSON AND LINDSAY HELMHOLZ
Department of Chemistry, Washington University, St. Louis, Missouri

(Received June 2, 1954)

The crystal structure of lithium sulfate monohydrate has been reinvestigated in order to determine the position of the hydrogen bonds and to check on the asymmetry of the sulfate group in this substance suggested by the earlier work of Zeigler.

A disposition of the hydrogen bonds in agreement with the proton magnetic resonance results has been found and the sulfate group has the configuration of a regular tetrahedron within the limits of error of our measurements. Our results are in agreement with Zeigler in most essentials.

INTRODUCTION

BECAUSE of recent interest in the crystal structure of the compound lithium sulfate monohydrate, arising out of proton magnetic resonance studies[1,2] and Raman investigations[3] it seemed worthwhile to us to carry out a redetermination of the structure with presently existing techniques which were not available at the time of the original work by Ziegler[4] in 1934.

Ziegler arrived at a structure by essentially qualitative arguments concerning the intensities which were given values strong (S), strong plus ($S+$), etc. On the basis of parameters obtained in this way he postulated positions of the hydrogen bonds between the water molecules and the oxygen atoms of the sulfate groups and thus placed the hydrogen atoms. The vector between the hydrogen atoms of a water molecule, according to this structure, is parallel to the b axis of the monoclinic crystal. This is in disagreement with the magnetic resonance results. In addition, Ziegler's parameters give for the configuration of the sulfate ion a decidedly distorted tetrahedron with S—O distances ranging from 1.60 A to 1.35 A. A resolution of these difficulties is offered by the following determination.

PROCEDURE

A straightforward structure determination was undertaken without reference to Ziegler's previous work. The unit cell was found to have the dimensions given in Table I (with Ziegler's values for comparison).

TABLE I.

	L and H	Z
$a°$	5.430±0.010A	5.43A
$b°$	4.836±0.010A	4.84A
$c°$	8.140±0.015A	8.14A
β	107°14′±5′	107°35′

Laue photographs showed no reflection requiring a larger unit, and the absence of reflections *oko* with k odd, together with the crystallographic observations[5] indicate that the space group is $C_2^2-P2_1$ for the substance.

A Patterson projection on (010) was made using 90 ($h0l$) reflections obtained using CuK_α radiation and a crystal of dimensions 0.02×0.05×0.07 cm. The intensities were obtained visually by the multiple film technique, and we estimate that they are reliable to 50 percent, a considerable part of the uncertainty being due to absorption in the irregularly shaped crystal.

The approximate parameters obtained from the Patterson projection indicated that in all qualitative essentials Ziegler's structure is correct. A Fourier projection was then made, improved parameters obtained from it, and finally the x and z, parameters varied by small amounts in order to obtain the best fit between observed and calculated F values. The trial parameter changes were suggested by structural arguments and by discrepancies existing between observed and calculated intensities, limitations being placed on the changes by the projections. Since the distribution of the hydrogen bonds was of principal interest, numerous trials were made in accordance with what might be expected if the hydrogen bonds were in different positions, for example, in the positions suggested by Ziegler. It was found necessary to include an extinction correction and a temperature factor

TABLE II.[a]

	L and H			Zeigler		
	x	y	z	x^*	y^*	z^*
S	0.300	0.000	0.206	0.292	0.000	0.211
OI	0.020	0.080	0.170	0.000	0.028	0.192
OII	0.440	0.115	0.385	0.422	0.078	0.397
OIII	0.415	0.110	0.075	0.347	0.139	0.083
OIV	0.310	−0.310	0.210	0.339	−0.306	0.197
OV	0.815	0.480	0.385	0.831	0.531	0.386
LiI	0.32	0.505	−0.02	0.333	0.522	−0.003
LiII	0.58	0.480	0.39	0.569	0.458	0.386

[a] x^*, y^*, and z^* are related to x, y, and z of Ziegler's paper by $x^* = \frac{1}{2} - x$, $y^* = -y$, and $z^* = -z$.

* Abstracted from a thesis submitted by Allen C. Larson in partial fulfillment of the requirements for the degree of Master of Arts at Washington University.

[1] Soutif, Dreyfus, and Ayant, Compt. rend. **233**, 395 (1951).
[2] G. E. Pake, thesis, Harvard (1948).
[3] C. Vassas-Dubuisson, J. chim. phys. **50**, C98 (1953).
[4] Ziegler, Z. Krist. **89**, 456 (1934).
[5] P. Groth, Chem. Krist. **II** (1908).

TABLE III.

hkl	F(obs) L and H	F(Calc) L and H	F(Calc) Z	hkl	F(obs) L and H	F(Calc) L and H	F(Calc) Z
006	1.8	1.9	3.0	$20\bar{5}$	8.7	6.5	0.5
040	4.6	5.6	9.2	$20\bar{6}$	10.0	9.9	7.6
044	3.9	4.1	1.9	$30\bar{4}$	12.8	13.9	6.9
045	5.8	6.8	10.1	$30\bar{6}$	1.6	0.8	4.9
051	1.1	1.2	2.7	$30\bar{7}$	5.0	4.4	7.0
056	1.1	1.6	3.5	400	1.0	1.3	0.4
061	1.6	1.3	2.5	$40\bar{1}$	9.1	8.2	6.7
$10\bar{3}$	16.4	14.6	7.1	$40\bar{6}$	9.4	7.7	5.4
$10\bar{4}$	10.7	10.6	7.5	$40\bar{7}$	4.1	4.3	1.0
$10\bar{5}$	1.7	1.4	2.9	500	4.8	5.1	3.7
$10\bar{8}$	6.3	7.2	4.1	$50\bar{1}$	1.0	0.9	4.3
200	2.1	2.0	0.9	$50\bar{2}$	6.1	6.9	2.9
$20\bar{2}$	7.7	8.2	2.4	$50\bar{5}$	11.3	8.7	2.2
$20\bar{3}$	2.4	3.1	1.3	$60\bar{1}$	2.5	2.3	0.8
$20\bar{4}$	10.2	7.9	2.3	$60\bar{2}$	5.3	4.1	2.3

$\exp[-\beta(\sin/\lambda)^2]$ with $\beta=1.0$ to obtain agreement for the very intense reflections and for the over-all variation in intensity with $\sin/\lambda$.

The determination of the y parameters was undertaken in much the same manner. Approximate values were obtained from a Patterson projection on (100). Then the values varied to obtain the best fit between observed and calculated intensities.

The final parameter values, with those of Ziegler for comparison, are given in Table II. Table III gives the comparison of some observed F values and the values calculated on the basis of our parameters and on the basis of Ziegler's. These are chosen with the purpose of illustrating discrepancies; the agreement between Ziegler's values and the observed is in general much better than in the cases given here. The F values of approximately 200 reflections were calculated. The fractional discrepancies, $\Sigma||F|_{obs}-|F|_{calc}|/\Sigma F_{obs}$, for these was 0.165.

DISCUSSION

The parameters given in Table II give for the sulfate ion the configuration of a regular tetrahedron within the limits of error of our determination. The sulfur-oxygen distance is 1.50A±0.02A the O−O distance (within the ion) 2.45A±0.03A.

TABLE IV.

x	O_V-O_X Distances in A
I	2.87A, 3.48A
II	3.06[a]A, 3.14[a]A, 3.35A, 3.48A
III	3.65A
IV	3.12A, 3.32[a]A
V	2.94A

[a] Indicates edge of Li coordination tetrahedron.

The position of hydrogen bonds has been fixed by making the assumption that the shortest oxygen-oxygen distances (with the exception of those in a sulfate group) correspond to hydrogen-bonded contacts. The various oxygen-oxygen distances (those below 3.50A in length) are given in Table IV.

The choice of hydrogen bonded contacts, as indicated above, places one O−H−O bond between O_V and O_I and the other between the two equivalent O_V's in the unit cell giving a disposition of the bonds illustrated in Fig. 1. Assuming that the water molecule is not appreciably distorted (see below) and that the hydrogen atoms lie in the $O_V-O_V-O_I$ plane the H−H vector is very nearly in a plane parallel to (100) and makes an angle of 38.4 degrees with the b axis. The proton resonance results place the H−H vector very nearly in the (100) plane and making an angle of 40 degrees with the b axis. The hydrogen bond distances are longer than expected, but this finding is in agreement with the Raman experiments which show only very slight shifts from the frequencies observed for the gaseous molecules. Long hydrogen bonds have also been observed in other crystals in which water molecules are coordinated with lithium ions. For example, in $Li\cdot ClO_4\cdot 3H_2O$ the hydrogen bonded distance is found to be 2.94A.[6]

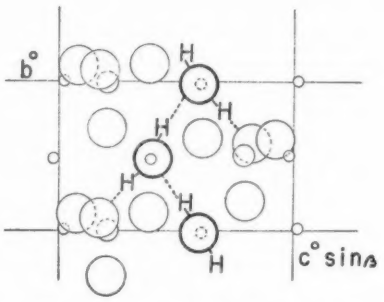

FIG. 1. Projection of atoms on plane perpendicular to the c axis, with the hydrogen bonds indicated by dotted lines.

The structure we have found is in agreement with the magnetic data, and the agreement between observed and calculated intensities we believe is good. We have no explanation for the "long" hydrogen bonds. The disposition of the bonds may be more satisfactory than that proposed by Ziegler since it gives the O_V (water molecule oxygen) a coordination of four positive particles, 3 hydrogen atoms and one lithium ion, rather than three. It would be interesting to have these findings checked by neutron diffraction.

[6] C. D. West, Z. Krist. 88, 198 (1934).

High-Speed Machine Computation of Ideal Gas Thermodynamic Functions. I. Isotopic Water Molecules*

ABRAHAM S. FRIEDMAN AND LESTER HAAR
National Bureau of Standards, Washington 25, D. C.

(Received June 4, 1954)

A procedure is developed for the machine computation of the partition functions for non-rigid rotating anharmonic oscillators. Vibrational-rotational coupling terms and low temperature rotational corrections are included. A general code has been designed to permit the calculation of the ideal gas thermodynamic functions for a large variety of molecular structures on the National Bureau of Standards Eastern Automatic Computer—SEAC. The method is illustrated by evaluating the thermodynamic functions for an asymmetric top molecule. Tables of C_p^0/R, $(H^0-E_0^0)/RT$, $(E_0^0-F^0)/RT$, and S^0/R have been evaluated for H_2O, HDO, D_2O, HTO, DTO, and T_2O at close intervals from 50° to 5000°K. The time required for these computations is of the order of several minutes per molecule. The results for H_2O are in good agreement with those obtained by direct summation.

INTRODUCTION

As part of a general program on the correlation of the properties of the hydrogen isotopes, a procedure has been developed for utilizing the National Bureau of Standards Eastern Automatic Computer—SEAC, to calculate the thermodynamic functions of substances in their ideal gas states. The partition functions are expanded with the inclusion of first-order correction terms for anharmonicity, rotation-vibration interaction, and centrifugal stretching. Low-temperature correction terms are also included. The procedure is adaptable to all diatomic and triatomic molecules; larger polyatomic molecules can also be treated with slight modification. The SEAC had previously been programmed for the calculation of thermodynamic functions for harmonic oscillators.[1]

THE PARTITION FUNCTION

The partition function can be represented as the product of factors representing translational, vibrational, rotational, coupling, etc., contributions to the total partition function.

The rotational partition function for an asymmetric top has been derived by Stripp and Kirkwood[2] and by Woolley:[3]

$$Q_R=\left[\frac{\pi}{\sigma_A\sigma_B\sigma_C}\right]^{\frac{1}{2}}\left[1+\frac{1}{12}\left(2\sigma_A+2\sigma_B+2\sigma_C-\frac{\sigma_A\sigma_B}{\sigma_C}-\frac{\sigma_B\sigma_C}{\sigma_A}-\frac{\sigma_C\sigma_A}{\sigma_B}\right)+\frac{1}{480}\left\{10(\sigma_A^2+\sigma_B^2+\sigma_C^2)+12(\sigma_A\sigma_B+\sigma_B\sigma_C+\sigma_C\sigma_A)-12\left(\frac{\sigma_A^2\sigma_B+\sigma_A\sigma_B^2}{\sigma_C}+\frac{\sigma_B^2\sigma_C+\sigma_B\sigma_C^2}{\sigma_A}+\frac{\sigma_C^2\sigma_A+\sigma_C\sigma_A^2}{\sigma_B}\right)+7\left(\frac{\sigma_A^2\sigma_B^2}{\sigma_C^2}+\frac{\sigma_B^2\sigma_C^2}{\sigma_A^2}+\frac{\sigma_C^2\sigma_A^2}{\sigma_B^2}\right)\right\}+\cdots\right].$$

TABLE I. Ground state molecular constants used in the calculation of ideal gas thermal properties.

	Units	H_2O	HDO	D_2O	HTO	DTO	T_2O
ν_1	cm^{-1}	3657.05	2723.66	2671.69	2295	2290	2233
ν_2	cm^{-1}	1594.59	1402.80	1178.33	1343	1097	998
ν_3	cm^{-1}	3755.79	3707.47	2788.02	3703	2733	2365
X_{11}	cm^{-1}	42.566	43.39	21.88	30.4	30.2	15.3
X_{22}	cm^{-1}	16.813	10.12	9.42	9.22	6.09	6.41
X_{33}	cm^{-1}	47.566	82.58	26.30	82.4	43.8	18.2
X_{12}	cm^{-1}	15.933	8.50	8.77	6.76	5.48	5.88
X_{13}	cm^{-1}	165.824	12.99	85.73	11.1	8.09	61.6
X_{23}	cm^{-1}	20.332	20.68	10.17	19.6	11.6	7.75
δ_1	dimensionless	0.063	0.047	0.041	0.039	0.039	0.038
δ_2	dimensionless	−0.1016	−0.082	−0.070	−0.077	−0.063	−0.062
δ_3	dimensionless	+0.0648	+0.062	+0.051	+0.062	+0.045	+0.040
I_e^A	g $cm^2\times10^{40}$	1.0224	1.211	1.833	1.250	2.068	2.502
I_e^B	g $cm^2\times10^{40}$	1.9180	3.060	3.841	4.225	4.861	5.742
I_e^C	g $cm^2\times10^{40}$	2.9404	4.271	5.674	5.475	6.928	8.244
θ_1	°K	4.448	3.076	2.326	2.406	1.823	1.606
θ_2	°K	19.39	9.13	5.13	5.57	3.16	2.43
ρ	$(°K)^{-1}\times10^5$	2.13	2.13	2.13	2.13	2.13	2.13

* This work was supported in part by the U. S. Atomic Energy Commission Division of Research.

[1] Mann, Acquisita, and Plyler, J. Chem. Phys. **21**, 1949 (1953).

[2] K. F. Stripp and J. G. Kirkwood, J. Chem. Phys. **19**, 1131 (1951).

[3] H. W. Woolley (private communication). Woolley's treatment also takes cognizance of the different symmetry classes for rotational levels of the asymmetric rotor.

TABLE II. Ideal gas thermodynamic functions for H_2O.

°K	$\frac{C_p^0}{R}$	$\frac{(H^0-E_0^0)}{RT}$	$\frac{-(F^0-E_0^0)}{RT}$	$\frac{S^0}{R}$
50	4.00719	3.90579	11.63213	15.53793
60	4.00634	3.92262	12.34582	16.26844
70	4.00590	3.93454	12.95144	16.88599
80	4.00573	3.94345	13.47744	17.42089
90	4.00571	3.95037	13.94232	17.89269
100	4.00581	3.95591	14.35883	18.31474
110	4.00599	3.96045	14.73609	18.69655
120	4.00622	3.96425	15.08086	19.04512
130	4.00649	3.96749	15.39830	19.36580
140	4.00680	3.97029	15.69243	19.66273
150	4.00715	3.97273	15.96644	19.93918
160	4.00755	3.97490	16.22290	20.19781
170	4.00803	3.97683	16.46394	20.44078
180	4.00860	3.97858	16.69130	20.66989
190	4.00931	3.98018	16.90646	20.88664
200	4.01020	3.98166	17.11065	21.09231
210	4.01132	3.98304	17.30495	21.28800
220	4.01272	3.98436	17.49027	21.47463
230	4.01446	3.98563	17.66741	21.65304
240	4.01658	3.98687	17.83706	21.82394
250	4.01912	3.98811	17.99984	21.98796
260	4.02214	3.98936	18.15628	22.14565
270	4.02565	3.99063	18.30687	22.29751
280	4.02970	3.99196	18.45202	22.44398
290	4.03428	3.99334	18.59213	22.58547
300	4.03942	3.99478	18.72753	22.72232
310	4.04511	3.99631	18.85855	22.85486
320	4.05136	3.99794	18.98545	22.98339
330	4.05815	3.99966	19.10850	23.10816
340	4.06547	4.00148	19.22793	23.22941
350	4.07329	4.00342	19.34395	23.34737
360	4.08160	4.00548	19.45676	23.46224
370	4.09038	4.00765	19.56653	23.57419
380	4.09958	4.00995	19.67344	23.68339
390	4.10920	4.01237	19.77763	23.79000
400	4.11919	4.01491	19.87925	23.89417
450	4.17394	4.02948	20.35295	24.38243
500	4.23453	4.04691	20.77837	24.82529
550	4.29891	4.06687	21.16500	25.23188
600	4.36590	4.08898	21.51980	25.60879
650	4.43498	4.11293	21.84803	25.96097
700	4.50589	4.13846	22.15376	26.29222
750	4.57847	4.16536	22.44019	26.60556
800	4.65252	4.19349	22.70991	26.90340
850	4.72776	4.22270	22.96501	27.18771
900	4.80384	4.25287	23.20722	27.46010
950	4.88035	4.28388	23.43799	27.72188
1000	4.95688	4.31562	23.65853	27.97415
1050	5.03302	4.34797	23.86987	28.21784
1100	5.10838	4.38082	24.07289	28.45372
1150	5.18263	4.41407	24.26836	28.68244
1200	5.25547	4.44762	24.45693	28.90456
1300	5.39600	4.51521	24.81560	29.33082
1400	5.52862	4.58291	25.15269	29.73561
1500	5.65262	4.65014	25.47118	30.12132
1600	5.76780	4.71644	25.77341	30.48986
1700	5.87429	4.78146	26.06130	30.84277
1800	5.97247	4.84494	26.33641	31.18135
1900	6.06284	4.90669	26.60002	31.50672
2000	6.14596	4.96661	26.85324	31.81985
2100	6.22241	5.02461	27.09697	32.12159
2200	6.29278	5.08068	27.33202	32.41270
2300	6.35761	5.13481	27.55906	32.69388
2400	6.41741	5.18702	27.77871	32.96573
2500	6.47267	5.23736	27.99148	33.22884
2600	6.52381	5.28586	28.19784	33.48371
2700	6.57122	5.33260	28.39822	33.73082
2800	6.61527	5.37764	28.59297	33.97061
2900	6.65625	5.42103	28.78244	34.20347
3000	6.69447	5.46285	28.96693	34.42978
3200	6.76361	5.54203	29.32205	34.86409
3400	6.82440	5.61571	29.66027	35.27599
3600	6.87824	5.68439	29.98323	35.66762
3800	6.92626	5.74851	30.29230	36.04082
4000	6.96936	5.80849	30.58871	36.39720
4200	7.00826	5.86471	30.87348	36.73820
4400	7.04358	5.91751	31.14754	37.06505
4600	7.07580	5.96718	31.41169	37.37887
4800	7.10532	6.01400	31.66665	37.68065
5000	7.13248	6.05820	31.91306	37.97126

Since $\sigma=h^2/8\pi^2kTI$, this takes the form

$$[\pi/\sigma_A\sigma_B\sigma_C]^{\frac{1}{2}}(1+\theta_1/T+\theta_2/T^2+\theta_3/T^3+\cdots)$$

and, at high temperatures, approaches the classical value of $[\pi/\sigma_A\sigma_B\sigma_C]^{\frac{1}{2}}$. The dependence of σ_A, σ_B, σ_C on the vibrational coordinates is accounted for by using the expression

$$\sigma_A=\sigma_{A_0}(1-\sum_{i=1}^{n}\delta_i^A V_i),$$

where σ_0 is the value of σ in the lowest vibration and rotation state and δ_i^A represents the interaction of the rotational state with the ith fundamental. A binomial expansion of the high temperature rotational term then gives

$$\left[\frac{\pi}{\sigma_{A_0}\sigma_{B_0}\sigma_{C_0}}\right]^{\frac{1}{2}}(1+\tfrac{1}{2}\sum_{i=1}^{n}\delta_i V_i+\cdots),$$

where $\delta_i=\delta_i^A+\delta_i^B+\delta_i^C$. The sum over the vibrational coordinates is

$$\prod_i(1-e^{-u_i})^{-1}\left(1+\sum_{i\leq j}f_{ij}+\tfrac{1}{2}\sum_i\frac{\delta_i}{e^{u_i}-1}\right),$$

where $u_i=\nu_i hc/kT$; ν_i is the observed fundamental and $\sum_{i\leq j}f_{ij}$ accounts for the anharmonicity of the vibrations (see, for example, Stockmayer[4] and Wagman).[5]

$$f_{ij}=\frac{X_{ij}(hc/kT)}{(e^{u_i}-1)(e^{u_j}-1)},\quad (i\neq j);$$

$$f_{ii}=\frac{2X_{ii}(hc/kT)}{(e^{u_i}-1)^2}.$$

[4] Stockmayer, Kavanagh, and Mickley, J. Chem. Phys. **12**, 408 (1944).

[5] Wagman, Kilpatrick, Pitzer, and Rossini, J. Research Natl. Bur. Standards **35**, 467 (1945); RP 1682.

TABLE III. Ideal gas thermodynamic functions for HDO.

°K	$\frac{C_p^0}{R}$	$\frac{(H^0-E_0^0)}{RT}$	$\frac{-(F^0-E_0^0)}{RT}$	$\frac{S^0}{R}$
50	4.00480	3.93645	12.88338	16.81984
60	4.00450	3.94781	13.60215	17.54997
70	4.00446	3.95591	14.21135	18.16726
80	4.00456	3.96198	14.74000	18.70199
90	4.00476	3.96672	15.20694	19.17367
100	4.00501	3.97054	15.62508	19.59562
110	4.00531	3.97368	16.00367	19.97736
120	4.00565	3.97633	16.34954	20.32588
130	4.00602	3.97860	16.66791	20.64652
140	4.00645	3.98058	16.96283	20.94341
150	4.00696	3.98232	17.23752	21.21985
160	4.00760	3.98388	17.49459	21.47847
170	4.00843	3.98530	17.73615	21.72145
180	4.00951	3.98661	17.96398	21.95060
190	4.01091	3.98785	18.17956	22.16742
200	4.01273	3.98905	18.38414	22.37319
210	4.01502	3.99023	18.57880	22.56903
220	4.01786	3.99142	18.76445	22.75587
230	4.02132	3.99264	18.94190	22.93455
240	4.02544	3.99392	19.11185	23.10578
250	4.03026	3.99527	19.27492	23.27020
260	4.03580	3.99672	19.43165	23.42837
270	4.04208	3.99828	19.58251	23.58080
280	4.04909	3.99997	19.72795	23.72793
290	4.05683	4.00180	19.86835	23.87015
300	4.06529	4.00377	20.00405	24.00782
310	4.07443	4.00590	20.13536	24.14127
320	4.08423	4.00819	20.26258	24.27078
330	4.09465	4.01065	20.38596	24.39662
340	4.10566	4.01328	20.50573	24.51902
350	4.11723	4.01609	20.62210	24.63820
360	4.12932	4.01906	20 73528	24.75435
370	4.14188	4.02221	20.84544	24.86766
380	4.15489	4.02553	20 95275	24.97829
390	4.16831	4.02902	21.05736	25.08639
400	4.18211	4.03267	21.15941	25.19209
450	4.25578	4.05331	21.63555	25.68886
500	4.33522	4.07749	22.06383	26.14132
550	4.41850	4.10468	22.45371	26.55839
600	4.50444	4.13440	22.81212	26.94652
650	4.59218	4.16623	23.14429	27.31052
700	4.68108	4.19982	23.45426	27.65409
750	4.77049	4.23488	23.74521	27.98010
800	4.85983	4.27115	24.01968	28.29083
850	4.94855	4.30840	24.27973	28.58813
900	5.03613	4.34640	24.52706	28.87346
950	5.12212	4.38497	24.76309	29.14807
1000	5.20613	4.42394	24.98900	29.41294
1050	5.28787	4.46314	25.20579	29.66894
1100	5.36709	4.50244	25.41432	29.91677
1150	5.44362	4.54171	25.61533	30.15704
1200	5.51735	4.58083	25.80945	30.39029
1300	5.65619	4.65829	26.17918	30.83747
1400	5.78355	4.73418	26.52719	31.26137
1500	5.89986	4.80808	26.85634	31.66443
1600	6.00576	4.87967	27.16895	32.04863
1700	6.10208	4.94879	27.46687	32.41566
1800	6.18967	5.01534	27.75163	32.76697
1900	6.26937	5.07927	28.02452	33.10379
2000	6.34197	5.14062	28.28662	33.42725
2100	6.40823	5.19943	28.53887	33.73830
2200	6.46881	5.25577	28.78205	34.03783
2300	6.52433	5.30974	29.01688	34.32662
2400	6.57532	5.36142	29.24396	34.60539
2500	6.62228	5.41093	29.46384	34.87477
2600	6.66562	5.45836	29.67699	35.13536
2700	6.70573	5.50383	29.88385	35.38768
2800	6.74294	5.54743	30.08480	35.63223
2900	6.77754	5.58926	30.28020	35.86946
3000	6.80980	5.62941	30.47037	36.09978
3200	6.86817	5.70505	30.83613	36.54118
3400	6.91958	5.77501	31.18412	36.95914
3600	6.96525	5.83989	31.51607	37.35597
3800	7.00614	5.90021	31.83346	37.73367
4000	7.04300	5.95645	32.13754	38.09400
4200	7.07646	6.00900	32.42945	38.43845
4400	7.10701	6.05822	32.71013	38.76836
4600	7.13505	6.10444	32.98046	39.08491
4800	7.16091	6.14793	33.24119	39.38913
5000	7.18486	6.18893	33.49300	39.68194

X_{ij} is the first anharmonicity coefficient in cm^{-1}.

To a first approximation, the effect on the partition function of the centrifugal stretching is a linear function of the temperature. The stretching constant ρ has been evaluated for several molecules from their force constants by E. B. Wilson.[6]

We can now write as an approximate factored form of the partition function

$$Q=Q_T\left[\prod_i (1-e^{u_i})^{-1}\right]\frac{1}{S}\left[\frac{\pi}{\sigma_{A_0}\sigma_{B_0}\sigma_{C_0}}\right]^{\frac{1}{2}}\left[1+\frac{\theta_1}{T}+\frac{\theta_2}{T^2}\right]$$

$$\times[1+\rho T]\left[\prod_{i\leq j}(1+f_{ij})\right]\left[\prod_i\left(1+\frac{1}{2}\frac{\delta_i}{(e^{u_i}-1)}\right)\right]. \quad (1)$$

Q_T is the translational partition function and is obtained in the usual manner: S is the symmetry number. The nuclear spin contribution to the partition function is omitted.

The thermodynamic functions can be expressed in terms of $\ln Q$ or its derivatives:

$$(F^0-E_0^0)/RT=-\ln Q,$$

$$(H^0-E_0^0)/RT=-(Q'/QT),$$

$$S^0/R=-(Q'/QT)+\ln Q,$$

and

$$C^0/R=(Q''/QT^2)-(Q'/QT)^2,$$

where

$$Q'/Q=d\ln Q/d(1/T).$$

Each algebraic expression, after differentiation, had to be coded into the SEAC for each of the thermal functions. For this to be feasible some of the terms of Eq. (1) and their derivatives were expressed in terms of the harmonic oscillator functions as follows.

[6] E. B. Wilson, J. Chem. Phys. 4, 526 (1936).

TABLE IV. Ideal gas thermodynamic functions for D_2O.

°K	C_p^0/R	$(H^0-E_0^0)/RT$	$-(F^0-E_0^0)/RT$	S^0/R
50	4.00371	3.95278	12.71364	16.66642
60	4.00369	3.96126	13.43511	17.39638
70	4.00383	3.96733	14.04622	18.01356
80	4.00406	3.97191	14.57630	18.54821
90	4.00436	3.97550	15.04434	19.01984
100	4.00469	3.97840	15.46336	19.44176
110	4.00508	3.98081	15.84265	19.82347
120	4.00554	3.98285	16.18912	20.17197
130	4.00613	3.98462	16.50799	20.49261
140	4.00695	3.98618	16.80334	20.78953
150	4.00808	3.98760	17.07841	21.06601
160	4.00968	3.98893	17.33581	21.32474
170	4.01184	3.99021	17.57767	21.56788
180	4.01472	3.99149	17.80578	21.79727
190	4.01843	3.99280	18.02163	22.01443
200	4.02305	3.99420	18.22646	22.22067
210	4.02864	3.99570	18.42138	22.41708
220	4.03526	3.99734	18.60730	22.60464
230	4.04291	3.99915	18.78502	22.78418
240	4.05158	4.00115	18.95527	22.95643
250	4.06125	4.00336	19.11865	23.12201
260	4.07187	4.00579	19.27571	23.28150
270	4.08339	4.00845	19.42694	23.43539
280	4.09574	4.01134	19.57277	23.58412
290	4.10886	4.01448	19.71359	23.72807
300	4.12267	4.01785	19.84974	23.86760
310	4.13710	4.02146	19.98154	24.00301
320	4.15210	4.02531	20.10928	24.13459
330	4.16759	4.02939	20.23321	24.26260
340	4.18353	4.03368	20.35356	24.38725
350	4.19986	4.03820	20.47055	24.50875
360	4.21653	4.04292	20.58438	24.62730
370	4.23351	4.04784	20.69521	24.74306
380	4.25076	4.05295	20.80323	24.85619
390	4.26827	4.05825	20.90858	24.96683
400	4.28598	4.06372	21.01139	25.07512
450	4.37728	4.09345	21.49171	25.58516
500	4.47224	4.12655	21.92468	26.05124
550	4.57026	4.16241	22.31965	26.48207
600	4.67083	4.20058	22.68345	26.88403
650	4.77323	4.24068	23.02124	27.26193
700	4.87652	4.28241	23.33703	27.61944
750	4.97967	4.32545	23.63395	27.95941
800	5.08169	4.36954	23.91451	28.28405
850	5.18170	4.41438	24.18075	28.59514
900	5.27897	4.45973	24.43436	28.89409
950	5.37295	4.50534	24.67670	29.18204
1000	5.46324	4.55099	24.90896	29.45995
1050	5.54958	4.59650	25.13210	29.72861
1100	5.63185	4.64171	25.34698	29.98869
1150	5.71001	4.68647	25.55430	30.24078
1200	5.78409	4.73068	25.75469	30.48537
1300	5.92044	4.81705	26.13678	30.95383
1400	6.04203	4.90029	26.49683	31.39712
1500	6.15030	4.98009	26.83765	31.81774
1600	6.24672	5.05630	27.16151	32.21781
1700	6.33273	5.12890	27.47025	32.59915
1800	6.40963	5.19795	27.76538	32.96334
1900	6.47860	5.26357	28.04819	33.31177
2000	6.54065	5.32590	28.31977	33.64568
2100	6.59669	5.38511	28.58107	33.96618
2200	6.64747	5.44135	28.83290	34.27425
2300	6.69366	5.49481	29.07596	34.57078
2400	6.73583	5.54565	29.31090	34.85656
2500	6.77447	5.59404	29.53828	35.13233
2600	6.80999	5.64014	29.75858	35.39873
2700	6.84277	5.68408	29.97228	35.65636
2800	6.87312	5.72601	30.17976	35.90577
2900	6.90129	5.76606	30.38139	36.14746
3000	6.92754	5.80434	30.57752	36.38187
3200	6.97503	5.87606	30.95445	36.83051
3400	7.01693	5.94196	31.31269	37.25465
3600	7.05426	6.00274	31.65406	37.65681
3800	7.08781	6.05898	31.98014	38.03913
4000	7.11821	6.11119	32.29227	38.40347
4200	7.14596	6.15982	32.59163	38.75145
4400	7.17143	6.20523	32.87924	39.08448
4600	7.19496	6.24775	33.15602	39.40378
4800	7.21679	6.28768	33.42278	39.71047
5000	7.23713	6.32526	33.68022	40.00549

Anharmonicity:

$$f_{ii}\equiv\frac{2X_{ii}}{\nu_i u_i}\left(\frac{H^0-E_0^0}{RT}\right)^2_{\text{h.o.}},$$

$$-\frac{df_{ii}}{d(1/T)}\Big/T\equiv\frac{2X_{ii}}{\nu_i u_i}\left(\frac{H^0-E_0^0}{RT}\right)_{\text{h.o.}}\times\left(2\left(\frac{C^0}{R}\right)_{\text{h.o.}}-\left(\frac{H^0-E_0^0}{RT}\right)_{\text{h.o.}}\right),$$

$$\frac{d^2f_{ii}}{d(1/T)^2}\Big/T^2\equiv\frac{4X_{ii}}{\nu_i u_i}\left[3\left(\frac{C^0}{R}\right)^2_{\text{h.o.}}-(u_i+2)\left(\frac{C^0}{R}\right)_{\text{h.o.}}\left(\frac{H^0-E_0^0}{RT}\right)_{\text{h.o.}}\right].$$

Coupling:

$$\frac{\delta_i}{(e^{ui}-1)}\equiv\frac{\delta_i}{u_i}\left(\frac{H^0-E_0^0}{RT}\right)_{\text{h.o.}},$$

$$-\frac{d}{d(1/T)}\left(\frac{\delta_i}{(e^{ui}-1)}\right)\Big/T\equiv\frac{\delta_i}{u_i}\left(\frac{C^0}{R}\right)_{\text{h.o.}},$$

$$\frac{1}{T^2}\frac{d^2}{d(1/T)^2}\left(\frac{\delta_i}{(e^{ui}-1)}\right)\equiv\frac{\delta_i}{u_i}\left[\left(\frac{C^0}{R}\right)_{\text{h.o.}}\left(\frac{2(C^0/R)_{\text{h.o.}}}{(H^0-E_0^0/RT)_{\text{h.o.}}}-u_i\right)\right].$$

In the foregoing expressions $(H^0-E_0^0/RT)_{\text{h.o.}}$ and $(C^0/R)_{\text{h.o.}}$ are the contributions of harmonic oscillation

TABLE V. Ideal gas thermodynamic functions for HTO.

°K	C_p^0/R	$(H^0-E_0^0)/RT$	$-(F^0-E_0^0)/RT$	S^0/R
50	4.00386	3.95100	13.24697	17.19798
60	4.00380	3.95980	13.96815	17.92796
70	4.00391	3.96610	14.57906	18.54516
80	4.00413	3.97084	15.10898	19.07982
90	4.00441	3.97455	15.57690	19.55145
100	4.00473	3.97755	15.99582	19.97338
110	4.00508	3.98004	16.37504	20.35509
120	4.00545	3.98214	16.72144	20.70359
130	4.00588	3.98395	17.04026	21.02421
140	4.00637	3.98553	17.33556	21.32110
150	4.00698	3.98694	17.61058	21.59753
160	4.00777	3.98822	17.86794	21.85616
170	4.00882	3.98940	18.10976	22.09916
180	4.01020	3.99051	18.33782	22.32833
190	4.01201	3.99159	18.55360	22.54520
200	4.01433	3.99267	18.75837	22.75105
210	4.01726	3.99377	18.95320	22.94698
220	4.02087	3.99492	19.13902	23.13394
230	4.02521	3.99614	19.31663	23.31277
240	4.03034	3.99745	19.48673	23.48418
250	4.03629	3.99888	19.64994	23.64883
260	4.04308	4.00045	19.80681	23.80727
270	4.05072	4.00217	19.95782	23.95999
280	4.05921	4.00405	20.10340	24.10746
290	4.06854	4.00611	20.24395	24.25006
300	4.07867	4.00836	20.37980	24.38816
310	4.08960	4.01080	20.51127	24.52208
320	4.10128	4.01345	20.63865	24.65210
330	4.11369	4.01629	20.76219	24.77849
340	4.12679	4.01935	20.88214	24.90149
350	4.14053	4.02261	20.99869	25.02131
360	4.15488	4.02609	21.11206	25.13815
370	4.16979	4.02977	21.22242	25.25220
380	4.18523	4.03366	21.32994	25.36360
390	4.20116	4.03774	21.43477	25.47252
400	4.21754	4.04203	21.53705	25.57909
450	4.30507	4.06632	22.01449	26.08082
500	4.39927	4.09486	22.44436	26.53923
550	4.49731	4.12697	22.83613	26.96310
600	4.59710	4.16199	23.19670	27.35869
650	4.69720	4.19931	23.53130	27.73061
700	4.79656	4.23843	23.84393	28.08236
750	4.89441	4.27891	24.13772	28.41663
800	4.99019	4.32038	24.41519	28.73558
850	5.08348	4.36254	24.67838	29.04092
900	5.17398	4.40512	24.92894	29.33406
950	5.26146	4.44790	25.16826	29.61616
1000	5.34577	4.49070	25.39749	29.88820
1050	5.42682	4.53336	25.61763	30.15099
1100	5.50456	4.57575	25.82950	30.40526
1150	5.57899	4.61776	26.03383	30.65160
1200	5.65014	4.65931	26.23124	30.89055
1300	5.78286	4.74071	26.60741	31.34813
1400	5.90340	4.81953	26.96164	31.78117
1500	6.01267	4.89549	27.29676	32.19225
1600	6.11162	4.96845	27.61505	32.58351
1700	6.20126	5.03838	27.91838	32.95676
1800	6.28252	5.10528	28.20827	33.31355
1900	6.35632	5.16921	28.48603	33.65524
2000	6.42345	5.23027	28.75274	33.98301
2100	6.48466	5.28857	29.00934	34.29792
2200	6.54060	5.34423	29.25666	34.60089
2300	6.59186	5.39737	29.49541	34.89278
2400	6.63896	5.44814	29.72620	35.17434
2500	6.68234	5.49665	29.94959	35.44625
2600	6.72241	5.54303	30.16608	35.70912
2700	6.75953	5.58741	30.37612	35.96353
2800	6.79400	5.62989	30.58009	36.20999
2900	6.82608	5.67060	30.77837	36.44897
3000	6.85603	5.70962	30.97127	36.68090
3200	6.91034	5.78300	31.34214	37.12514
3400	6.95832	5.85075	31.69479	37.54555
3600	7.00108	5.91350	32.03101	37.94451
3800	7.03950	5.97177	32.35232	38.32409
4000	7.07426	6.02604	32.66002	38.68606
4200	7.10593	6.07672	32.95528	39.03200
4400	7.13496	6.12417	33.23907	39.36324
4600	7.16170	6.16870	33.51230	39.68100
4800	7.18645	6.21060	33.77573	39.98633
5000	7.20947	6.25010	34.03006	40.28017

for frequency u_i to the enthalpy and the heat capacity, respectively. The contributions of the f_{ij} terms were approximated by setting

$$f_{\substack{ij\\ i\neq j}}=\frac{X_{ij}(hc/kT)}{(e^{u_k}-1)^2},$$

where u_k is the geometric mean of u_i and u_j, $u_k^2=u_iu_j$. Thus, the f_{ij} can be put into the same form as the f_{ii}. This combination rule for u_iu_j yields the contribution of f_{ij} to C_p^0 to better than 2 percent for even the extreme case of $u_i/u_j=3$, in the range of anticipated u_i values.

The contributions of the factors for translation, rigid rotation, rotational stretching, and nonclassical rotation are each polynomials in powers of T. These are easily treated by the SEAC. The contributions of the term involving f_{ij} and $(\delta_i)/(e^{u_i}-1)$ are given above as simple functions of the contributions of thermal properties of harmonic oscillators.

MOLECULAR CONSTANTS

Benedict, Gailar, and Plyler[7] have recently studied the infrared spectra of H_2O, HDO, and D_2O. Their analysis yielded the molecular constants used in the calculations for these molecules. Rotational stretching for H_2O, HDO, and D_2O were calculated by Woolley.[8] As was to be expected, the three stretching coefficients were nearly equal, $\rho_{H_2O}=2.13$, $\rho_{HDO}=2.10$, and

[7] Benedict, Gailar, and Plyler, J. Chem. Phys. **21**, 1301 (1953); *ibid.*, 1302; Benedict, Claassen, and Shaw, J. Research Natl. Bur. Standards **49**, 91 (1952), RP 2347. A more detailed treatment of these data is in preparation.

[8] H. W. Woolley (private communication).

TABLE VI. Ideal gas thermodynamic functions for DTO.

°K	C_p^0/R	$(H^0-E_0^0)/RT$	$-(F^0-E_0^0)/RT$	S^0/R
50	4.00315	3.96348	13.74166	17.70514
60	4.00328	3.97010	14.46491	18.43501
70	4.00352	3.97486	15.07728	19.05214
80	4.00382	3.97846	15.60829	19.58675
90	4.00417	3.98130	16.07706	20.05836
100	4.00455	3.98360	16.49665	20.48026
110	4.00501	3.98553	16.87642	20.86195
120	4.00561	3.98717	17.22328	21.21046
130	4.00644	3.98862	17.54248	21.53111
140	4.00764	3.98994	17.83812	21.82806
150	4.00938	3.99117	18.11344	22.10462
160	4.01180	3.99238	18.37106	22.36345
170	4.01507	3.99361	18.61314	22.60676
180	4.01932	3.99492	18.84144	22.83637
190	4.02465	3.99634	19.05748	23.05382
200	4.03115	3.99791	19.26250	23.26042
210	4.03884	3.99967	19.45760	23.45728
220	4.04773	4.00165	19.64371	23.64537
230	4.05780	4.00387	19.82164	23.82551
240	4.06900	4.00635	19.99209	23.99844
250	4.08127	4.00909	20.15570	24.16479
260	4.09453	4.01212	20.31299	24.32512
270	4.10871	4.01543	20.46447	24.47991
280	4.12371	4.01903	20.61057	24.62961
290	4.13947	4.02291	20.75167	24.77459
300	4.15590	4.02707	20.88812	24.91520
310	4.17293	4.03150	21.02024	25.05174
320	4.19049	4.03619	21.14831	25.18450
330	4.20853	4.04114	21.27259	25.31373
340	4.22698	4.04633	21.39330	25.43964
350	4.24580	4.05176	21.51067	25.56244
360	4.26496	4.05742	21.62489	25.68231
370	4.28441	4.06329	21.73614	25.79943
380	4.30413	4.06937	21.84458	25.91395
390	4.32410	4.07564	21.95037	26.02601
400	4.34429	4.08210	22.05364	26.13574
450	4.44813	4.11696	22.53641	26.65338
500	4.55581	4.15544	22.97214	27.12758
550	4.66632	4.19684	23.37012	27.56696
600	4.77855	4.24063	23.73715	27.97779
650	4.89126	4.28635	24.07838	28.36473
700	5.00318	4.33356	24.39775	28.73131
750	5.11314	4.38188	24.69838	29.08026
800	5.22017	4.43095	24.98274	29.41369
850	5.32348	4.48043	25.25285	29.73328
900	5.42253	4.53004	25.51035	30.04039
950	5.51697	4.57952	25.75660	30.33612
1000	5.60662	4.62865	25.99275	30.62141
1050	5.69142	4.67726	26.21976	30.89703
1100	5.77143	4.72519	26.43846	31.16366
1150	5.84676	4.77234	26.64955	31.42189
1200	5.91758	4.81859	26.85363	31.67223
1300	6.04659	4.90820	27.24289	32.15110
1400	6.16028	4.99366	27.60978	32.60345
1500	6.26052	5.07484	27.95710	33.03195
1600	6.34910	5.15177	28.28711	33.43888
1700	6.42761	5.22456	28.60164	33.82620
1800	6.49744	5.29337	28.90223	34.19561
1900	6.55979	5.35841	29.19019	34.54861
2000	6.61571	5.41991	29.46662	34.88653
2100	6.66606	5.47807	29.73247	35.21055
2200	6.71160	5.53312	29.98860	35.52172
2300	6.75296	5.58527	30.23571	35.82099
2400	6.79068	5.63472	30.47448	36.10920
2500	6.82521	5.68166	30.70546	36.38712
2600	6.85695	5.72626	30.92917	36.65544
2700	6.88623	5.76869	31.14609	36.91478
2800	6.91334	5.80909	31.35662	37.16571
2900	6.93852	5.84761	31.56114	37.40876
3000	6.96199	5.88437	31.76001	37.64438
3200	7.00451	5.95308	32.14200	38.09509
3400	7.04208	6.01605	32.50482	38.52088
3600	7.07563	6.07400	32.85036	38.92436
3800	7.10587	6.12753	33.18021	39.30775
4000	7.13334	6.17714	33.49579	39.67294
4200	7.15847	6.22328	33.79831	40.02159
4400	7.18162	6.26633	34.08882	40.35515
4600	7.20305	6.30659	34.36826	40.67486
4800	7.22299	6.34436	34.63748	40.98185
5000	7.24162	6.37989	34.89719	41.27709

$\rho_{D_2O}=2.11\times10^{-5}$ deg^{-1}. The value $\rho=2.13\times10^{-5}$ deg^{-1} was used for all six isotopes.

The necessary molecular data for the HTO, DTO, and T_2O isotopes were obtained from the data for the H_2O, D_2O, and HDO species. A normal coordinate analysis, corroborating an earlier analysis by Libby,[9] yielded zero-order vibrational frequencies. The zero-order moments of inertia were calculated using the bond length and angle given by Benedict, Gailar, and Plyler.[7] Anharmonic constants were obtained from the relation $x_{ij}'=x_{ij}(\omega_i'\omega_j'/\omega_i\omega_j)$, where the prime quantities refer to the molecule whose x_{ij} is to be calculated; the unprimed constants refer to the reference molecule. For the calculation of the T_2O anharmonicity coefficient, H_2O was used as the reference molecule; for DTO and HTO, HDO was the reference molecule. The rotation-vibration interaction constants were obtained by the relation $\delta_i'=\delta_i(\omega_i'/\omega_i)$, analogous to the Morse relation for diatomic molecules. In the cases of H_2O, HDO, and D_2O this relation is experimentally verified. As in the case of the anharmonicity coefficients, the unknown δ_i' was calculated from the known δ_i of the isotope having the same symmetry. Thus the δ_i values for H_2O were used for T_2O and the δ_i for HDO were used for HTO and DTO.

The chemical atomic weights used in the calculations of the translational partition functions were obtained from the values listed by Wichers.[10] The isotopic masses used in the zero-point frequency and zero-point mo-

[9] W. F. Libby, J. Chem. Phys. **11**, 101 (1943).

[10] E. Wichers, J. Am. Chem. Soc. **74**, 2447 (1952).

TABLE VII. Ideal gas thermodynamic functions for T_2O.

°K	$\frac{C_p^0}{R}$	$\frac{(H^0-E_0^0)}{RT}$	$\frac{-(F^0-E_0^0)}{RT}$	$\frac{S^0}{R}$
50	4.00292	3.96809	13.38370	17.35180
60	4.00311	3.97391	14.10771	18.08163
70	4.00339	3.97810	14.72063	18.69874
80	4.00373	3.98129	15.25205	19.23334
90	4.00411	3.98380	15.72112	19.70493
100	4.00457	3.98585	16.14097	20.12683
110	4.00520	3.98758	16.52095	20.50853
120	4.00612	3.98908	16.86798	20.85707
130	4.00753	3.99045	17.18733	21.17778
140	4.00964	3.99174	17.48310	21.47484
150	4.01264	3.99302	17.75855	21.75158
160	4.01676	3.99437	18.01629	22.01067
170	4.02214	3.99584	18.25849	22.25434
180	4.02890	3.99748	18.48694	22.48442
190	4.03709	3.99935	18.70312	22.70247
200	4.04673	4.00147	18.90831	22.90978
210	4.05777	4.00388	19.10360	23.10749
220	4.07017	4.00661	19.28992	23.29654
230	4.08382	4.00966	19.46809	23.47776
240	4.09862	4.01306	19.63881	23.65187
250	4.11447	4.01679	19.80271	23.81951
260	4.13124	4.02087	19.96033	23.98120
270	4.14883	4.02528	20.11216	24.13744
280	4.16714	4.03002	20.25863	24.28866
290	4.18606	4.03507	20.40014	24.43522
300	4.20552	4.04043	20.53702	24.57746
310	4.22545	4.04607	20.66960	24.71568
320	4.24579	4.05200	20.79815	24.85015
330	4.26649	4.05818	20.92293	24.98112
340	4.28750	4.06462	21.04417	25.10880
350	4.30880	4.07129	21.16209	25.23339
360	4.33036	4.07819	21.27688	25.35507
370	4.35215	4.08530	21.38872	25.47402
380	4.37416	4.09261	21.49776	25.59037
390	4.39637	4.10011	21.60417	25.70428
400	4.41879	4.10780	21.70807	25.81587
450	4.53356	4.14869	22.19422	26.34291
500	4.65215	4.19308	22.63360	26.82668
550	4.77338	4.24031	23.03544	27.27575
600	4.89567	4.28982	23.40650	27.69633
650	5.01732	4.34112	23.75188	28.09300
700	5.13671	4.39370	24.07551	28.46922
750	5.25253	4.44712	24.38047	28.82759
800	5.36377	4.50096	24.66919	29.17015
850	5.46976	4.55485	24.94368	29.49854
900	5.57010	4.60850	25.20555	29.81405
950	5.66463	4.66162	25.45614	30.11777
1000	5.75336	4.71401	25.69659	30.41061
1050	5.83641	4.76550	25.92784	30.69335
1100	5.91401	4.81597	26.15070	30.96667
1150	5.98642	4.86530	26.36587	31.23117
1200	6.05396	4.91344	26.57396	31.48740
1300	6.17563	5.00596	26.97093	31.97689
1400	6.28151	5.09337	27.34514	32.43852
1500	6.37390	5.17573	27.69938	32.87512
1600	6.45484	5.25320	28.03592	33.28912
1700	6.52606	5.32602	28.35660	33.68263
1800	6.58904	5.39448	28.66298	34.05747
1900	6.64501	5.45885	28.95639	34.41525
2000	6.69502	5.51943	29.23795	34.75739
2100	6.73992	5.57650	29.50864	35.08514
2200	6.78044	5.63032	29.76931	35.39964
2300	6.81718	5.68114	30.02072	35.70186
2400	6.85065	5.72918	30.26353	35.99272
2500	6.88127	5.77066	30.49834	36.27300
2600	6.90940	5.81777	30.72567	36.54345
2700	6.93535	5.85869	30.94601	36.80470
2800	6.95939	5.89757	31.15979	37.05737
2900	6.98173	5.93458	31.36739	37.30198
3000	7.00256	5.96983	31.56918	37.53902
3200	7.04034	6.03558	31.95660	37.99219
3400	7.07379	6.09569	32.32433	38.42003
3600	7.10373	6.15088	32.67434	38.82522
3800	7.13077	6.20175	33.00828	39.21004
4000	7.15537	6.24883	33.32760	39.57643
4200	7.17793	6.29254	33.63355	39.92610
4400	7.19873	6.33326	33.92723	40.26050
4600	7.21801	6.37132	34.20961	40.58093
4800	7.23596	6.40697	34.48153	40.88851
5000	7.25273	6.44047	34.74376	41.18424

ment of inertia calculations are the values listed by Mattauch and Fluegge.[11]

The molecular constants are listed in Table I.

THERMAL PROPERTIES

The heat capacity, enthalpy, free energy, and entropy for H_2O, HDO, D_2O, HTO, DTO, and T_2O are tabulated in Tables II–VII. The entries are listed in dimensionless units. The very small changes in the constants of Table I obtained by using the other isotopes of oxygen in the compound formulas, together with the very large relative abundance of O^{16}, result in a completely negligible difference between the properties of XYO^{16} tabulated here and the naturally occurring mixture of XYO^{16}, XYO^{17}, and XYO^{18}. The entropy contribution of nuclear spin and the entropy of isotopic mixing have been omitted. The contributions of the excited electronic states, only significant near the highest temperatures tabulated, have also been omitted. The *ortho-para* effect, only significant for the H_2O molecule at low temperatures (below 80°K) has been neglected.

The uncertainty in the calculated anharmonicity and rotation-vibration constants of HTO, DTO, and T_2O are probably well below 20 percent, particularly for T_2O. The resulting uncertainty in the vibrational and rotational fundamentals is less than 1 percent, assuming negligible uncertainty for the calculated zero point

[11] J. Mattauch and S. Fluegge, *Nuclear Physics Tables and an Introduction to Nuclear Physics* (Interscience Publishers, Inc., New York, 1946).

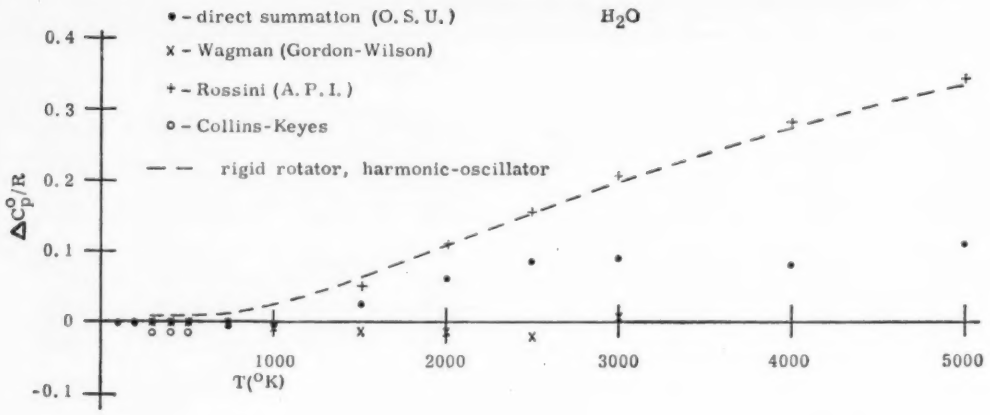

FIG. 1. Comparison of ideal gas heat capacity functions. The results of the earlier calculations are subtracted from the values computed on the SEAC.

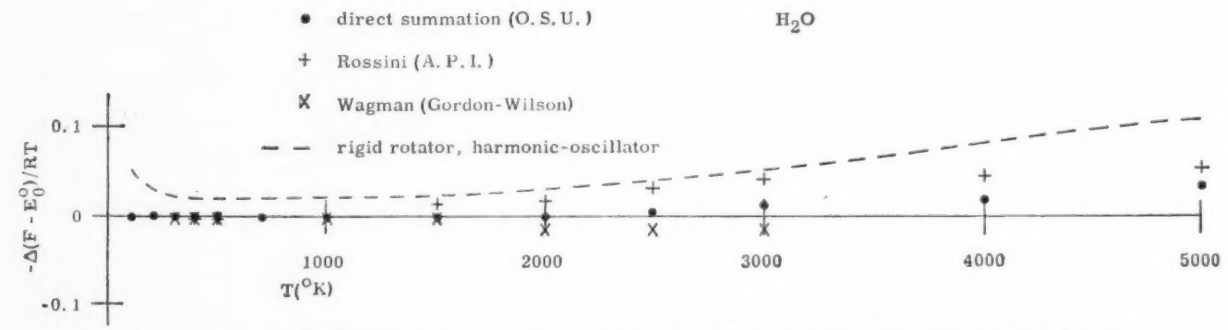

FIG. 2. Comparison of ideal gas free energy functions. The results of the earlier calculations are subtracted from the values computed on the SEAC.

vibrational and rotational frequencies. At temperatures below 1000°K this will result in an uncertainty in the third place to the right of the decimal for the tabulated properties for these substances. At higher temperatures the uncertainty due to neglected higher order terms in the energy-level expressions and the omission of the effect of rotational cutoff is considerably larger. The uncertainty at the higher temperatures for these is thus about the same as for H_2O, HDO, and D_2O at these temperatures.

The SEAC calculations for H_2O are compared with calculations obtained at The Ohio State University Cryogenic Laboratory by a term by term summation of the unexpanded partition function in which all the available spectroscopic energy-level data was utilized and rotational cutoff was included.[12] The very small differences are probably less than the uncertainty in the direct summation values. The SEAC calculations for HDO and D_2O are considered as reliable as the H_2O calculations.

Calculations of ideal gas properties for H_2O have also been reported by Gordon[13] using an expansion of the partition function similar to the one employed by the SEAC. The Gordon data were later revised at the National Bureau of Standards to include a stretching correction.[14] More recently Rossini *et al.*[15] have recalculated the thermal properties.

The SEAC calculations are compared in Fig. 1 and 2 with those of the National Bureau of Standards (1945),[14] Rossini *et al.*,[15] the term-by-term values of The Ohio State University,[12] and the rigid rotator-harmonic oscillator approximation. Figure 1 also includes a few low temperature values of C_p^0 obtained empirically by Collins and Keyes.[16]

The SEAC performs the calculations in less than ten minutes per molecule for the water molecules. The SEAC has also been used to calculate ideal gas thermal properties of CO_2 and a large number of diatomic hydrides, deuterides, and tritium compounds. These will be reported later together with equilibrium data for several isotopic exchange reactions.

ACKNOWLEDGMENTS

The authors are greatly indebted to Lilla Fano of the National Bureau of Standards Thermodynamics Section and Ethel C. Marden of the National Bureau of Standards Mathematics Division coding staff for their assistance.

[12] Glatt, Adams, and Johnston, O.S.U. Res. Foundation Tech. Report No. 316-8 (1953).
[13] A. R. Gordon, J. Chem. Phys. **2**, 65 (1934); *ibid.*, 549.
[14] Wagman, Kilpatrick, Pitzer, and Rossini, J. Res. NBS **34**, 143 (1945); RP 1634.
[15] F. D. Rossini, *et al.*, *Selected Values of Physical and Thermodynamic Properties of Hydrocarbons and Related Compounds* (Carnegie Press, Pittsburgh, Pennsylvania, 1953), A. P. I. Project 44.
[16] S. C. Collins and F. G. Keyes, Proc. Am. Acad. Arts Sci. **72**, 283 (1938).

THE JOURNAL OF CHEMICAL PHYSICS VOLUME 22, NUMBER 12 DECEMBER, 1954

Study of Carbon Monoxide, Nitrogen, Propylene, and Benzene Ionization Probability Curves near Threshold

R. E. Fox and W. M. Hickam
Westinghouse Research Laboratories, East Pittsburgh, Pennsylvania

(Received May 26, 1954)

Ionization probability curves for the formation of CO^+, N_2^+, $C_3H_6^+$, and $C_6H_6^+$ have been obtained for some six volts above threshold. The technique employed provided both ionization by essentially monoenergetic electrons and a m/e separation of the ions. In the case of the diatomic ions, the structure in the curves can be interpreted in terms of spectroscopically identified energy levels. The curves for propylene and benzene exhibit considerable structure which, when analyzed in a similar manner to that used for the diatomic molecules, results in the location of a number of unidentified energy levels. The presence of these levels explains the discrepancies in ionization potential measurements obtained by various electron impact methods.

I. INTRODUCTION

ELECTRON impact studies have yielded important data concerning appearance potentials. However, the lack of monoenergetic electrons has made it difficult to determine energy levels of excited states of the atoms or ions. Recent studies in this laboratory with a mass spectrometer[1] have shown that when ionization by monoenergetic electrons can be achieved, the ionization probability curves begin to exhibit structure. In the studies of the rare gas ions,[2] it was demonstrated that this structure could be correlated with energy levels of the ions. Two main conclusions resulted from this investigation. First, where ionization resulted from excitation of a single energy level, the ionization proceeded linearly with the energy of the incident electron for a considerable distance above the level. Second, where ionization could proceed from two or more levels the resulting curve was a superposition of the curves for the various ionization processes.

In the present work the study of ionization probability curves has been extended to include the diatomic molecules CO and N_2, as well as the more complicated molecules of propylene (C_3H_6) and benzene (C_6H_6). The study of the diatomic ions lends itself to a comparison with spectroscopic data and thus affords a firmer basis for discussion of the propylene and benzene ions where spectroscopic data is very meager.

II. EXPERIMENTAL PROCEDURE

The apparatus consisted of a 90-degree deflection type mass spectrometer. The ions were formed using the pulsing techniques and retarding potential difference method previously described.[1,2] The maximum energy spread of the electrons was 0.2 ev and for most of the work this spread was about 0.1 ev. The ion detection system consisted of a 12 stage electron multiplier, the output of which was measured by an FP-54 electrometer and galvanometer.*

The nitrogen sample was reagent grade from Air Reduction Sales Company; the CO was commercial grade. The propylene sample was reagent grade from Phillips Petroleum Company, and the benzene sample was spectroscopic grade from the National Bureau of Standards. In all cases a careful check was made with the mass spectrometer to determine whether any conflicting impurities were present. A mass spectrum of the background taken prior to and during the runs indicated that no background gases were present in magnitudes large enough to contribute significantly to the observed ion currents. The operating pressure in the ion source was 10^{-5} mm of mercury or less as estimated using an ionization gauge, thus virtually eliminating the possibility that any observable phenomena could be attributed to processes other than single electron-molecule interactions. The correction to the voltage scale was determined by using the appearance potential of Xe^+ as a standard. The difference between that value and the spectroscopically determined ionization potential was used to correct the measured electron energy scale. This correction was usually of the order of 0.2 ev. It is to be understood that for all the curves shown here, the ion current is actually the difference ion current arising from the retarding potential difference method.[1]

III. RESULTS AND DISCUSSION

(a) CO and N_2

Since CO and N_2 have the same number of electrons and the same electronic configuration, one would expect them to have similar term level diagrams. For both of these ions, the ground state is $X\,^2\Sigma$, while the first two excited states are $A\,^2\Pi$ and $B\,^2\Sigma$. In CO^+, the $A\,^2\Pi$ and $B\,^2\Sigma$ states occur at 2.52 and 5.66 ev, respectively, above the ground state.[3] These energies are reasonably well established from band spectra corresponding to the transitions $B\,^2\Sigma \rightarrow A\,^2\Pi$, $B\,^2\Sigma \rightarrow X\,^2\Sigma$, and $A\,^2\Pi \rightarrow X\,^2\Sigma$ giving a self consistent group. For N_2^+ the $B\,^2\Sigma$ state

[1] Fox, Hickam, Kjeldaas, and Grove, Phys. Rev. **84**, 859 (1951).
[2] Fox, Hickam, and Kjeldaas, Phys. Rev. **89**, 555 (1953).
* A detailed description of the instrument is being prepared in a separate paper.

[3] G. Herzberg, *Spectra of Diatomic Molecules* (D. van Nostrand and Company, Inc., New York, 1950), pp. 522 and 554. Based on the conversion factor of 8066.83 cm^{-1} per electron volt.

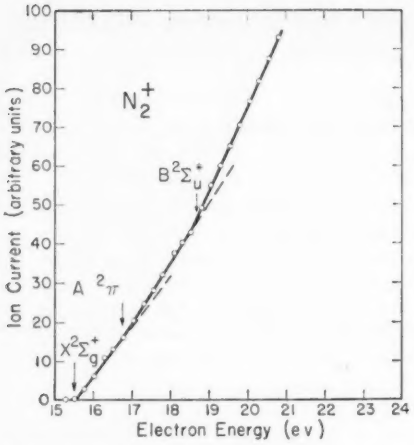

FIG. 1. Relative ionization probability curve for the formation of N_2^+ from N_2. The energy scale has been corrected to make the onset agree with the spectroscopic ionization potential.

has been established at 3.17 ev above the ground state of the ion[4–8] from a study of band spectra. Although the presence of the $A\ ^2\Pi$ state had been predicted, it is only recently that transitions from this state have been observed. Meinel, in 1951,[9] observed band spectra from the aurora which he attributed to the $A\ ^2\Pi \rightarrow X\ ^2\Sigma$ transition in N_2^+. Shortly after, Dalby and Douglas[10] photographed this series using a laboratory source. More recently, Worley[11] has discovered a third Rydberg series arising from the o state of N_2 and converging to a limit at 16.93 ev. This would place the $A\ ^2\Pi$ level at 1.36 ev above the N_2^+ ground state. However, Worley points out that this limit agrees with the $v=1$ vibrational level of the $A\ ^2\Pi$ state found by Dalby and Douglas. If this is true then the $v=0$ level for the $A\ ^2\Pi$ state would be placed at about 1.1 ev above the $X\ ^2\Sigma$ ground state. A search of the literature has failed to disclose any information concerning a $B\ ^2\Sigma \rightarrow A\ ^2\Pi$ transition as a check on the position of this level.

The ionization probability curve for N_2 is shown in Fig. 1. The method for drawing the curve is similar to that used in previous work. With a previous knowledge of the position of the energy levels from spectroscopic data, we draw straight line segments to give the best fit to the experimental points and simultaneously to yield reasonable agreement with the energy levels. The first linear portion of the curve is then attributed to ionization arising from excitation to the $X\ ^2\Sigma$ ground state of the ion. The first break represents the ionization threshold for the $A\ ^2\Pi$ state. The sum of ionization to these two states then proceeds linearly until the ionization threshold of the $B\ ^2\Sigma$ state is reached. The curve then exhibits a sharp break upward and the curve representing the sum of ionization to the three states again proceeds linearly for several volts. Eleven runs, using Xe^+ as a standard, yielded a value of 15.60±0.01†

TABLE I.

Energy levels	Energy separation: This work CO^+ [a]	This work N_2^+ [b]	Spectroscopic value CO^+	Spectroscopic value N_2^+
$A\ ^2\Pi \rightarrow X\ ^2\Sigma$	2.4±0.1	1.33±0.04	2.52[c]	1.36[d]
$B\ ^2\Sigma \rightarrow X\ ^2\Sigma$	5.0±0.1	3.24±0.04	5.66[c]	3.17[e]

[a] Based on ten runs.
[b] Based on eleven runs.
[c] See reference 3.
[d] Worley's Rydberg series limit (see reference 11).

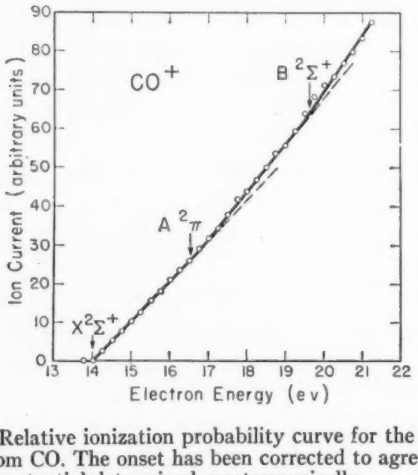

FIG. 2. Relative ionization probability curve for the formation of CO^+ from CO. The onset has been corrected to agree with the ionization potential determined spectroscopically.

ev for the ionization potential of N_2 as compared to the spectroscopic value of 15.58 ev.

The ionization probability curve for CO is shown in Fig. 2. This curve exhibits the same general features as Fig. 1 and the same analysis is applied. The results of several runs for these two gases are shown in Table I. Four runs on CO^+ yielded an ionization potential of 13.98±0.02 ev as compared with the spectroscopic value of 14.01 ev.

The results as shown by Table I indicate good agreement for the two levels in nitrogen and for the $A\ ^2\Pi$ level in CO with spectroscopic data. However, there is considerable disagreement between the $B\ ^2\Sigma$ value in CO^+ obtained in this work and the spectroscopic value. Referring to Fig. 2, it will be noticed that in the region around the $B\ ^2\Sigma$ onset the experimental points exhibit considerably greater deviation from linearity than in the lower portion of the curve. This deviation is not observed in the N_2 curve. Since

† This error as well as all errors quoted here refer to statistical probable errors arising from a small number of determinations. It is not implied that the absolute location of the lines is known to this accuracy.

[4] R. E. Worley and F. A. Jenkins, Phys. Rev. **54**, 305 (1938).
[5] R. E. Worley, Phys. Rev. **64**, 207 (1943).
[6] J. J. Hopfield, Phys. Rev. **36**, 789 (1930).
[7] Tanaka and Takamine, Sci. Pap. Inst. Phys. Chem. Res. (Tokyo) **39**, 427 (1942).
[8] R. S. Milliken, Phys. Rev. **46**, 144 (1934).
[9] A. B. Meinel, Astrophys. J. **113**, 583 (1951).
[10] F. W. Dalby and A. E. Douglas, Phys. Rev. **84**, 843 (1951).
[11] R. E. Worley, Phys. Rev. **89**, 863 (1953).

the data from a number of runs on CO^+ indicates that the departure from linearity is not instrumental, it is proposed that this deviation is indicative of an additional ionization process. A possible explanation would be the process of autoionization. Since the $A\ ^2\Pi$ and $B\ ^2\Sigma$ states of both CO^+ and N_2^+ are limits of Rydberg series lying above the $X\ ^2\Sigma$ ground state, there are a large number of excited energy levels of the molecule in this region which may undergo autoionization. Such contributions would certainly change the shape of the curve in a direction as to make the break appear too low.

A comparison of ionization to these excited levels of the ion relative to that of the ground state is shown in Table II. It is seen that the ratio of the slope of the curve representing ionization of the $A\ ^2\Pi$ state to the slope of the curve for the $X\ ^2\Sigma$ state is the same for both gases. For the $B\ ^2\Sigma$ state, however, the ionization ratio is found to be different by about a factor of two for the two gases. This difference may be influenced by autoionization contributions to the CO^+ curve near the $B\ ^2\Sigma$ onset.

TABLE II.

	Relative ionization probabilities	
	CO^+	N_2^+
$\frac{I(A\ ^2\Pi)}{I(X\ ^2\Sigma)}$	0.20	0.20
$\frac{I(B\ ^2\Sigma)}{I(X\ ^2\Sigma)}$	0.25 (?)	0.55

(b) Propylene

The ionization probability curve for C_3H_6 is shown in Fig. 3. It is seen that the curve exhibits considerable "tailing" near the onset, followed by a linear portion for about 3 volts after which a rather sharp break occurs at D followed by a second linear portion. The tailing near threshold is too large to be explained by the energy distribution and is attributed largely to the structure of the curve itself. This lower portion, reexamined with greater sensitivity, is shown in Fig. 4. The breaks marked C are at the same energy for the two curves. A curve for xenon is shown in Fig. 4 to indicate how much of the tailing can be attributed to the electron energy spread. The xenon curve, taken just prior to the propylene curve, shows that the electron energy spread is only 0.2 ev. It is now seen that below the point C there are two linear portions with breaks at A and B, and below A there is the tailing comparable to the xenon curve. The point A yields an ionization potential of 9.78. This value would also be obtained by the vanishing current or initial break method, and indeed is in agreement with the value of 9.77 ev obtained by Stevenson and Hipple.[12] This does

[12] D. P. Stevenson and J. A. Hipple, J. Am. Chem. Soc. **64**, 2769 (1942).

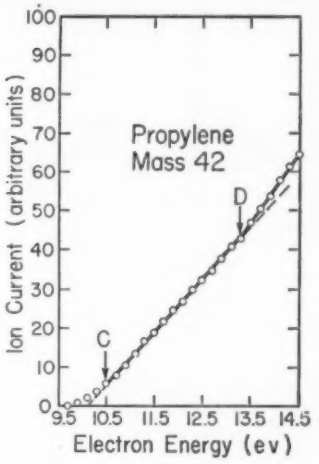

FIG. 3. Relative ionization probability curve for the formation of the parent ion of propylene. The ionization potential was determined by using xenon as a reference for the energy scale.

not agree, however, with a value of 10.05 ev obtained by Mitchell and Coleman.[13] They used a modified vanishing current method based on a linear extrapolation over about a 0.5-ev energy range near the ionization onset. This method would very likely be subject to influence by energy levels lying very near the ionization potential. The more conventional linear extrapolation method would probably yield a value of 10.13 ev obtained by the intercept of $C\,D$. The value obtained by the critical slope method would certainly be influenced by other close lying energy levels, such as to give a value which would be slightly too large. Honig,[14] using this method obtained a value of 9.84 ev. Price and Tuttle[15] obtained a value of 9.7 ev from absorption spectra in the far ultraviolet. This value, however, is based on very diffuse band spectra and is not considered to be very accurate.

One must then conclude from the evidence that the ground state of the propylene ion is located at 9.78 $\pm$0.04 ev, and that there are two other close lying

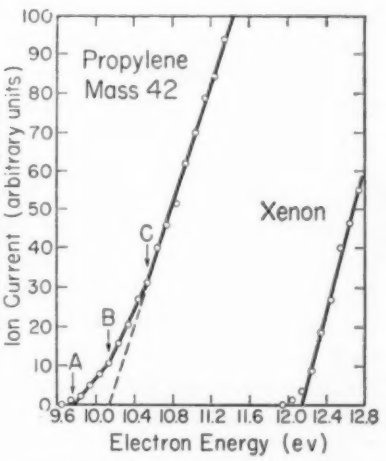

FIG. 4. The initial portions of the ionization probability curves for $C_3H_6^+$ and Xe^+ taken with increased sensitivity. The energy scale has been adjusted to make the onset of Xe^+ curve agree with the spectroscopically determined ionization potential.

[13] J. J. Mitchell and F. F. Coleman, J. Chem. Phys. **17**, 44 (1949).

[14] R. E. Honig, J. Chem. Phys. **16**, 105 (1948).

[15] W. C. Price and W. T. Tuttle, Proc. Roy. Soc. (London) **A174**, 207 (1940).

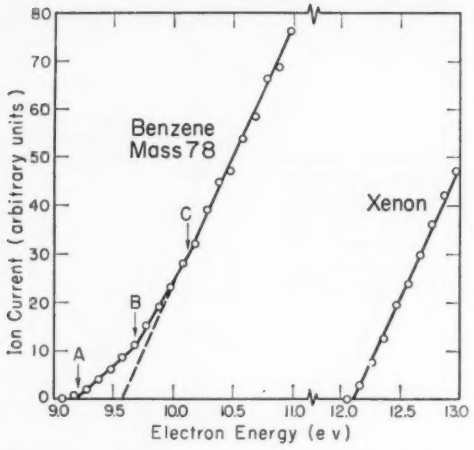

FIG. 5. The initial portion of the ionization probability curves for $C_6H_6^+$ and Xe^+. The energy scale has been adjusted to make the onset of the Xe^+ curve agree with the spectroscopically determined ionization potential.

levels, one at 10.13±0.04 ev and the other at 10.54 ±0.04 ev. In addition, there is another level at 13.23 ±0.04 ev.

(c) Benzene

The initial portion of the $C_6H_6^+$ curve is shown in Fig. 5 along with the reference xenon curve to demonstrate the small tailing due to energy spread. The *A B* portion of the $C_6H_6^+$ curve yields an ionization potential of 9.21 ev, which is in excellent agreement with the spectroscopic value of 9.24 ev obtained by Price and Wood.[16] The extrapolated value of the upper portion of the curve yields an appearance potential of 9.59 which is in good agreement with the linear extrapolation value of 9.60 obtained by Morrison.[17] Using the critical slope method, he obtained a value of 9.53 for the ionization potential. On the other hand, Honig[14] and Nief[18] obtained values of 9.43 and 9.3 ev, respectively, using this same method. Here, as in the case of propylene, the presence of levels near the ionization threshold will strongly influence the value obtained by using either the critical slope or linear extrapolation methods.

The ionization probability curve for C_6H_6 taken over a considerably larger energy range is shown in Fig. 6. Of considerable interest is the peculiar structure exhibited by the curve in the regions *D* and *E*. The propylene curve (Fig. 3) is quite linear in the energy range 10.5–13.2 ev, while the xenon curve is linear in the region 13.5–17.0 ev and exhibits the expected break at *B* which is due to the onset of the $^2P_{\frac{1}{2}}$ state.[2] It is therefore concluded that the unusual structure observed in the benzene curve is not instrumental in origin.

[16] Price and Wood, J. Chem. Phys. **3**, 439 (1935); see also Price and Walsh, Proc. Roy. Soc. (London) **A191**, 22 (1947). Hammond, Price, Teegan and Walsh, Discussions Faraday Soc., No. 9, 53 (1950).
[17] J. D. Morrison, J. Chem. Phys. **19**, 1305 (1951).
[18] G. Nief, J. chim. Phys. **48**, 333 (1951).

It can be seen from Fig. 6 that the curve exhibits a number of pronounced changes in the slope. From previous work it has been demonstrated that a sudden increase in the slope can be associated with an energy level. Using this as a criterion, the locations of the levels have been indicated by the arrows and are listed in Table III. These values are actually the average of three separate runs. The two spectroscopic valuse listed in Table III are the only levels that have been spectroscopically identified.

This lack of information concerning known energy levels makes a straightforward interpretation of the curve somewhat difficult. The dashed lines are drawn (Fig. 6) to indicate the ionization one would expect from a linear excitation function of states located at *A*, *B*, and *E*. If one uses the same arguments as were applied to the diatomic molecules, then the departure from linearity over the region *C E* requires additional processes such as autoionization from excited molecular states in this region. If autoionization is responsible for the contributions in this region, then there must be, in addition to the Rydberg series limit at about 11.8 volts observed by Price and Wood,[16] at least one more series converging to a limit considerably above *D*.

Another possibility for explaining a decrease in slope in certain portions of the curve is that one or more of the lower lying states of the ion has an excitation function which reaches a maximum and then begins to fall off rapidly. For example, the level marked *C* would possess an excitation function which rises for a small energy range and then begins to decrease, but a new level can now be excited and the curve again begins to rise (point near *D*). This time, however, the excitation function rises for a considerably longer energy range before the maximum is reached and the excitation begins to fall off. Possibly another level (at *E*) would be required to explain the linear rise between *E* and *F*.

A study has been made by Hustrulid *et al.*[19] of the appearance potentials of the ionic fragments of benzene under electron impact. The lowest appearance potential

TABLE III.

Pronounced breaks (energy level ?)	Spec. value[a]	Remarks
(*A*) 9.21±0.01[b]	9.24	First π potential
(*B*) 9.7		
(*C*) 10.4		This break is doubtful
(*D*) 11.5	11.8±0.3	First σ potential (?).
(*E*) 14.3		These values may be in
(*F*) 15.5		considerable error due to unusual shape of curve in this region.

[a] See reference 16.
[b] This ionization potential is based on 8 determinations using Xe^+ as a standard.

[19] Hustrulid, Kusch, and Tate, Phys. Rev. **54**, 1037 (1938).

of any fragment was for the $C_6H_5^+$ ion at 4.7 ev above the ionization potential of C_6H_6. Energywise, this places the formation of this ion at 14.0 volts which is at a point where the curve (Fig. 6) is undergoing a decrease in slope. There is, however, no dissociation process which can be identified with the decrease in the region of 11.5 ev. Furthermore, there is no evidence that the formation of the $C_4H_4^+$ ion[19] at 15.0 ev is influencing the shape of the curve in this region.

From the above discussion of the benzene ionization probability curve and the associated breaks, it is apparent that any interpretation must be highly speculative until more information can be obtained concerning energy levels and processes resulting from electron impact.

IV. SUMMARY

The ionization probability curves of CO and N_2 taken with essentially monoenergetic electrons has demonstrated that when the ionization probability curves are analyzed as the sum of a number of linear ionization processes with different thresholds, reasonable agreement is obtained with known spectroscopic data. When a similar analysis is made for the more complicated molecules C_3H_6 and C_6H_6 there is strong evidence for a number of energy levels of the molecular ions lying near the ground state. This structure in the ionization probability curves has been contributing to the lack of agreement in the determination of ionization potentials by electron impact methods. It is quite evident from the data presented that mass spectrometric studies using a monoenergetic electron beam will make it possible to obtain considerably more information concerning molecular ionization processes and opens up an entirely new field of study in molecular physics.

The authors wish to thank their colleagues of the physics department for their helpful discussions and suggestions both in the analysis of the data and in the preparation of the manuscript.

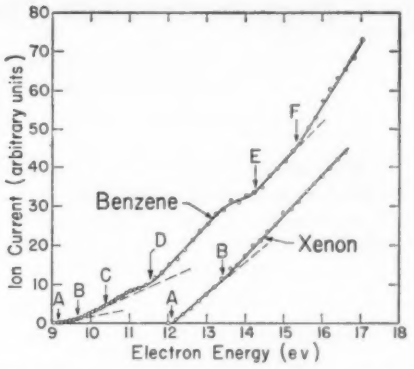

FIG. 6. The ionization probability curves for $C_6H_6^+$ and Xe^+ taken over a considerably larger energy range. The arrows and letters mark pronounced changes in the slopes. The energy scale has been adjusted to make the onset of the Xe^+ curve agree with the spectroscopically determined ionization potential.

Magnetic Moments of Some Octahedral Complexes of Iridium*

ERIC N. SLOTH† AND CLIFFORD S. GARNER
Department of Chemistry, University of California, Los Angeles 24, California
(Received April 30, 1954)

Magnetic susceptibilities of Na_2IrCl_6, $Na_3IrCl_6 \cdot 2H_2O$, and $(NH_4)_2Ir(H_2O)Cl_5$ were determined for these solids and for aqueous solutions 0.6*f* in the complex compound and 1*f* in HCl by the Gouy method. Na_2IrCl_6 is paramagnetic in the solid state and in solution, with a magnetic moment corresponding to one unpaired 5*d* electron and to d^2sp^3 covalent Ir-Cl bonds. The two iridium (III) complexes are diamagnetic, corresponding likewise to d^2sp^3 bond formation.

INTRODUCTION

IN the course of a study of isotopic exchange reactions of iridium (III) and iridium (IV) complexes we have investigated the magnetic susceptibilities of Na_2IrCl_6, $Na_3IrCl_6 \cdot 2H_2O$, and $(NH_4)_2Ir(H_2O)Cl_5$ in the solid state, as well as in O_2-free solutions 0.6*f* in the iridium compound and 1*f* in HCl (to repress hydrolysis). The magnetic criterion[1,2] for chemical bond type may be applied to these iridium complexes, provided adequate quenching of the orbital moment is achieved in these compounds and solutions.

Previous magnetic studies of iridium compounds were made by Bose and Bhar[3,4] on $IrCl_3 \cdot 1.5H_2O$, $IrCl_4$, and four octahedral nitro complexes of iridium (III), by Cabrera and Duperier[5] on $IrCl_3$, and by Guthrie and Bourland[6] on $IrCl_3$ and $IrCl_4$. All compounds were investigated as solids. With the exception of the four nitro complexes of iridium (III), the magnetic data on these compounds are difficult to interpret.[7] Griffiths, Owen, and Ward[8] have determined at 20°K the paramagnetic resonance spectra of magnetically highly diluted mixed crystals of K_2IrCl_6, $Na_2IrCl_6 \cdot 6H_2O$, and $(NH_4)_2IrCl_6$, each diluted with the corresponding isomorphous diamagnetic platinum (IV) compound; they also report a value for the moment of pure solid K_2IrCl_6. Apparently no magnetic studies of iridium compounds in solution have been reported.

PREPARATION AND ANALYSIS OF COMPOUNDS

Sodium Hexachloroiridate (IV)

Cp $(NH_4)_2IrCl_6$ was dissolved in aqua regia and taken to dryness on a steam bath in order to remove ammonium ion. The solid was dissolved in 12*f* HCl and taken to dryness on a steam bath, and this step was repeated to remove nitrate ion. The solid was next dissolved in 2*f* HCl, a slight excess of NaCl added, then purified Cl_2 was bubbled through the solution for several hours to ensure the oxidation of any iridium (III) to iridium (IV). The resulting solution was evaporated to dryness and the solid treated with purified acetone at 0°C to extract the Na_2IrCl_6. The mixture was filtered (the residue insoluble in $(CH_3)_2CO$ was recycled into the next batch) and the filtrate concentrated by evaporation. Purified $CHCl_3$ was added to the filtrate until precipitation began, the solution was heated to the boiling temperature and filtered, then more $CHCl_3$ was added. Cooling produced a crop of crystals of Na_2IrCl_6 which was washed with a cold $CHCl_3-(CH_3)_2CO$ mixture. The fractional crystallization of the Na_2IrCl_6 was repeated, and the final crop of washed crystals dried in an oven at 100°C, ground in an agate mortar, then dried at 100°C in an Abderhalden drier with P_2O_5 present, first in a Cl_2 atmosphere, then in vacuum. The dry product, deep black-red in color, was subsequently always stored and handled under a dry inert atmosphere because of the hygroscopic nature of this substance.

Weighed portions of the dried substance were analyzed by reduction to metallic iridium in a stream of H_2 at 750°C, the hydrogen chloride formed being absorbed in an excess of standard $AgNO_3$ solution which was later back-titrated with standardized KSCN solution by the Volhard method. The residue, consisting of metallic iridium and an equivalent amount of sodium chloride was weighed, then the sodium chloride leached out with water and the remaining iridium metal dried and weighed. Analysis (42.6 percent Ir, 47.2 percent Cl, 10.2 percent Na) demonstrated that the substance was Na_2IrCl_6 (42.63 percent Ir, 47.17 percent Cl, 10.20 percent Na).[9]

Sodium Hexachloroiridate (III) Dihydrate

$Na_3IrCl_6 \cdot 2H_2O$ was prepared by an adaptation of the methods of Delepine[10] and Ogawa.[11] The over-all

* These investigations were carried out under contract AT-(11-1)-34, Project 12, between the University of California and the U. S. Atomic Energy Commission.
† Present address: Chemistry Division, Argonne National Laboratory, Lemont, Illinois.
[1] L. Pauling, J. Am. Chem. Soc. **53**, 1367 (1931).
[2] L. Pauling, *The Nature of the Chemical Bond* (Cornell University Press, Ithaca, New York, 1940), second edition, Chapter III.
[3] D. M. Bose and H. G. Bhar, Z. Physik **48**, 716 (1928).
[4] D. M. Bose, Z. Physik **65**, 677 (1930).
[5] B. Cabrera and A. Duperier, Proc. Phys. Soc. (London) **51**, 845 (1939).
[6] A. N. Guthrie and L. T. Bourland, Phys. Rev. **37**, 303 (1931).
[7] See J. H. Van Vleck, *Electric and Magnetic Susceptibilities* (Oxford University Press, London, 1932), pp. 311 ff.
[8] Griffiths, Owen, and Ward, Proc. Roy. Soc. (London) **A219**, 526 (1953).
[9] The atomic weight of Ir was taken throughout this research as 192.2, the new 1953 international value. See report of the Committee on Atomic Weights of the American Chemical Society, E. Wichers, J. Am. Chem. Soc. **76**, 2033 (1954).
[10] M. Delepine, Bull. soc. chim. **[4]3**, 901 (1908); *ibid.* **[4]9**, 771 (1911).
[11] E. Ogawa, J. Chem. Soc. Japan **50**, 248 (1929).

reaction may be represented as

$$2Na^{+}{}_2IrCl_6^{=}+Na^{+}{}_2C_2O_4^{=}=2Na^{+}{}_3IrCl_6^{=}+2CO_2.$$

Na_2IrCl_6, prepared as above, and an equivalent amount of cp $Na_2C_2O_4$ were weighed out, dissolved in distilled water, and the resulting solution concentrated nearly to dryness by evaporation on a steam bath. Cooling produced a crop of crystals which was washed repeatedly with absolute ethanol, sucked dry on a filter disk, then dried in an oven. The dry solid was ground in an agate mortar, then dried for several hours at 100°C in an Abderhalden drier with P_2O_5 present in a vacuum. The product was olive green in color. Analysis by the method described above for Na_2IrCl_6 gave 37.9 percent Ir, 41.7 percent Cl, 13.5 percent Na, and 6.9 percent H_2O (H_2O was determined from the loss in weight on treatment with H_2 at 750°C, taking into account the removal of half of the Cl as HCl). These analytical results correspond to the formula $Na_3IrCl_6 \cdot 2H_2O$ (37.69 percent Ir, 41.71 percent Cl, 13.54 percent Na, 7.06 percent H_2O).

Ammonium Aquopentachloroiridate (III)

This compound was prepared essentially by the method of Delepine[10,12,13] and Ogawa.[14] Cp $(NH_4)_2IrCl_6$ and an equivalent amount of cp $H_2C_2O_4 \cdot 2H_2O$ were weighed out, dissolved separately in hot distilled water, and the hot solutions combined and evaporated to dryness to expel the HCl and CO_2 formed, and presumably to give time for the aquation to proceed. The resulting solid was twice recrystallized from hot distilled water, then dried in an oven at 100°C. The product had a pale olive-green color. Analysis (45.3 percent Ir, 41.2 percent Cl) indicated the formula $(NH_4)_2Ir(H_2O)Cl_5$ (45.4 percent Ir, 41.9 percent Cl).

MAGNETIC MEASUREMENTS

Magnetic susceptibilities were determined at 298°K by the Gouy method.[15] The electromagnet employed was water cooled and had a thermostated air chamber around the pole pieces between which Pyrex susceptibility tubes were suspended from one arm of an analytical balance. The field between the pole pieces could be held constant by manual regulation of the current to within 0.2 percent. Weighings were made at three field strengths generated at 8, 10, and 15 amperes. The weight changes at 8 and 15 amperes were reduced by experimentally determined factors to changes at 10 amperes, and the resulting changes averaged with the closely agreeing change at 10 amperes to give the reported Δw_{s-a} values. All measurements were made relative to air in the lower half of the susceptibility tubes, and with O_2-free N_2 over the solids or solutions in the upper half. In addition, the susceptibilities of dried cp $K_3Fe(CN)_6$ as solid and in 1f HCl were determined as a check. All solutions were measured immediately after synthesis.

RESULTS

The gram susceptibility of each solid or solution was calculated at 298°K from the relation

$$\bar{\chi}=(1/\rho)\left[(\kappa_w-\kappa_a)\frac{\Delta w_{s-a}}{\Delta w_{w-a}}+\kappa_a\right],$$

where ρ is the density of the solution or bulk density of the solid, Δw_{s-a} and Δw_{w-a} are the weight changes for sample *vs* air and water *vs* air, respectively, and κ_w and κ_a are the volume (cm³) susceptibilities of water and air (25°C, 750 mm), taken respectively as -0.719×10^{-6} from the results of Auer[16] and 0.027×10^{-6} from the data of Klemm.[17] Under our conditions, Δw_{w-a} was -11.0 mg for the solids and -34.2 mg for the solutions; Δw_{s-a} ranged from -1.6 mg for the Na_2IrCl_6 solution to 139.7 mg for solid $K_3Fe(CN)_6$, and was usually in the neighborhood of 30 mg. The susceptibility per mole of complex compound χ_M was calculated for the solids from the equation $\chi_M=M\bar{\chi}$, where M is the gram molecular weight of the compound. For the solutions $\chi_M=M\bar{\chi}_c$, where $\bar{\chi}_c$ was obtained assuming the Wiedemann additivity relation, $\chi_{soln}=\bar{\chi}_c f_c+\bar{\chi}_{solv}(1-f_c)$, in which f_c is the weight fraction of the complex compound in the solution, and $\bar{\chi}_c$ and $\bar{\chi}_{solv}$ are the gram susceptibilities of the complex compound and solvent (1f HCl), respectively. The latter was determined experimentally from Δw for O_2-free 1f HCl *vs* air. As a check, the molar susceptibility of pure HCl was calculated from this experimental $\bar{\chi}_{solv}$ by the Wiedemann law, giving a value of -21.2×10^{-6} in good agreement with the value -21.8×10^{-6} reported by Myers.[18] Molar paramagnetic susceptibilities $\chi_{M,p}$, were computed from χ_M values by subtraction of the diamagnetic contributions of all atoms including the iridium. Molar diamagnetic susceptibilities were taken from Angus,[19] except for Ir^{+3} (assumed $5d^6$) and Ir^{+4} (assumed $5d^5$) for which the values -45.4×10^{-6} and -37.6×10^{-6}, respectively, were calculated by the method of Angus. The effective magnetic moments μ_{eff} (molar Bohr magnetons) were then computed by the equation $\mu_{eff}=2.84(\chi_{M,p}T)^{\frac{1}{2}}$, with $T=298$°K. Inasmuch as the complex compounds studied are not expected to follow Curie's law behavior accurately, the calculated moments are of interest primarily as a measure of the number of unpaired electrons in each complex ion. Tables I and II present the susceptibilities and moments for the solids and solutions, respectively.

[12] M. Delepine, Compt. rend. **146**, 1269 (1908).
[13] M. Delepine, Ann. chim. **[9] 7**, 328 (1917).
[14] E. Ogawa, J. Chem. Soc. Japan **51**, 1 (1930).
[15] L. G. Gouy, Compt. rend. **109**, 935 (1889).
[16] H. Auer, Ann. Physik **18**, 593 (1933).
[17] W. Klemm, *Magnetochemie* (Akademische Verlagsgesellschaft, Leipzig, 1936), p. 45.
[18] W. R. Myers, Revs. Modern Phys. **24**, 15 (1952).
[19] W. R. Angus, Proc. Roy. Soc. (London) **A136**, 569 (1932).

TABLE I. Susceptibilities and moments of solid complex compounds (298°K).

Compound	Gram suscept. $\chi \times 10^6$	Molar suscept. $\chi_M \times 10^6$	Molar paramag. susc., $\chi_{M,p} \times 10^6$	μ_{eff}
$K_3Fe(CN)_6$	7.14	2350	2481	2.43
Na_2IrCl_6	1.94	875	1054	1.58
$Na_3IrCl_6 \cdot 2H_2O$	−0.316	−150	65	0.39
$(NH_4)_2Ir(H_2O)Cl_5$	−0.349	−148	48	0.34

TABLE II. Susceptibilities and moments of complex compounds in 1*f* HCl (298°K).

Compound	Gram suscept. $\chi_{soln} \times 10^6$	Molar suscept. $\chi_M \times 10^6$	Molar paramag. susc., $\chi_{M,p} \times 10^6$	μ_{eff}
$K_3Fe(CN)_6$, 0.723*f*	1.10	2669	2800	2.58
Na_2IrCl_6, 0.609*f*	−0.0064	1108	1286	1.75
Na_3IrCl_6, 0.627*f*	−0.532	25	215	0.72
$(NH_4)_2Ir(H_2O)Cl_5$, 0.551*f*	−0.669	−213	−17	0.0

DISCUSSION

Assuming essentially complete quenching of the orbital moments, one may use the "spin only" equation $\mu=[n(n+2)]^{\frac{1}{2}}$ to ascertain the number of unpaired electrons n for each complex ion.

Solid Na_2IrCl_6 and the $IrCl_6^{=}$ ion in 1*f* HCl are seen to be paramagnetic, with μ_{eff} corresponding favorably with μ_{eff} for one unpaired electron, namely, 1.73. This result suggests that six equivalent d^2sp^3 Ir−Cl bonds are formed in $IrCl_6^{=}$, the remaining three 5*d* orbitals not used in bond formation then being available for the five unshared 5*d* electrons, thus giving rise to a single unpaired electron. (An ionic bond would correspond presumably to five unpaired electrons, or $\mu_{eff}=5.92$, with an unshared electron in each of the five 5*d* orbitals, in marked disagreement with the data.) Our value for the moment of solid Na_2IrCl_6 is in satisfactory agreement with the value 1.65 reported by Griffiths, Owen, and Ward[8] for solid K_2IrCl_6. These investigators have interpreted their paramagnetic resonance measurements on magnetically dilute crystals of octahedral iridium (IV) compounds as indicating covalent Ir−Cl σ bonds in the $IrCl_6^{=}$ ion with a small π bond contribution.

The moments for solid $Na_3IrCl_6 \cdot 2H_2O$, solid $(NH_4)_2Ir(H_2O)Cl_5$, and the $IrCl_6^{=}$ and $Ir(H_2O)Cl_5^{=}$ ions in 1*f* HCl indicate diamagnetism and no unpaired electrons. The apparent slight paramagnetism could arise from the failure to use the Curie-Weiss law in computing μ_{eff}. Octahedral covalent complexes of Ir(III) are expected to be diamagnetic because of the three 5*d* orbitals unused in d^2sp^3 bond formation being available for the six unshared 5*d* electrons. The octahedral nitro complexes of Ir(III) studied by Bose[4] were all found to be diamagnetic. (Ionic bonds would correspond to four unpaired electrons, or $\mu_{eff}=4.90$, in disagreement with the results.)

The effective moment found for solid $K_3Fe(CN)_6$, 2.43, is in satisfactory agreement with the value reported by Pauling,[2] namely, 2.33.

As pointed out by Hocart[20] and by Flordal and Frivold,[21] molar susceptibilities of compounds obtained from measurements in aqueous solution are always greater than the values obtained from measurements of the solids. With the possible exception of $(NH_4)_2Ir(H_2O)Cl_5$, for which our data are not sufficiently accurate, comparison of the moments from Table I with those from Table II shows that such behavior is encountered with the compounds investigated by us. Moreover, this comparison indicates that there is no shift in bond type occurring in the dissolution of these complex compounds in 1*f* HCl. Aquation reactions which might conceivably give rise to such changes in bond type are generally slow for Ir(III) and Ir(IV) complexes, as evidenced by hydrolysis and isotopic exchange studies.

[20] R. Hocart, Compt. rend. **188**, 1151 (1929).
[21] M. Flordal and O. E. Frivold, Ann. Physik **23**, 425 (1935).

Ionization of Strong Electrolytes. III. Proton Magnetic Resonance in Nitric, Perchloric, and Hydrochloric Acids

G. C. Hood, O. Redlich, and C. A. Reilly
Shell Development Company, Emeryville, California

(Received June 7, 1954)

Since the proton magnetic resonance shift in an acid is a colligative property, the derivation of degrees of dissociation requires assumptions which cannot be tested directly. Results derived from measurements of this resonance shift in nitric acid and in perchloric acids are in sufficient agreement with earlier results obtained from a specific property (intensity of Raman lines) to confirm the interpretation of the shift. The value 22 has been found for the thermodynamic dissociation constant of nitric acid, the value 38 for perchloric acid.

The association of nitric acid in aqueous solutions containing more than 50 mole percent of acid is reflected in the shift. Differences in the limiting slopes of the resonance shift of the proton in various acids at high dilution are interpreted as due to different influences of the anions on the association of water.

THE comparison of the intensities of Raman lines of acids and their salts[1] has furnished quite reliable information of the molecular state of some strong acids. But the accuracy of the published results for nitric[2] and for perchloric[3] acids is by no means satisfactory. Although the method has been greatly improved,[4] new data by an independent method are highly desirable. The results of Gutowsky and Saika[5] on the proton magnetic resonance shifts of several acids and the work of Masuda and Kanda[6] on the nitrogen magnetic resonance shift of nitric acid have shown clearly that nuclear magnetic resonance can furnish significant information concerning incomplete dissociation.

In order to obtain a sufficient basis for conclusive quantitative results regarding the dissociation of nitric and perchloric acids, we have extended the measurement of the proton magnetic resonance over the whole concentration range. Some influence of the association of nitric acid[7] on the resonance was to be expected, especially in view of Chédin's careful studies[8] of the molecular state of aqueous nitric acid.

Any conclusions regarding dissociation are extremely sensitive to the value of the limiting slope of the resonance shift at low concentration. Particular attention has been given, therefore, to relatively low concentrations of the two acids and, for comparison, also of hydrochloric acid.

1. EXPERIMENTAL DETAILS

Measurements of nuclear magnetic resonance shifts were made with a high-resolution NMR spectrometer[9] operated at a fixed frequency of 40 Mc/sec. The applied magnetic field of about 9400 oersteds was provided by a Varian electromagnet and power supply. Additional stabilization of the magnetic field against slow drift was obtained by means of a Varian nuclear magnetic resonance field control unit.[10]

The NMR spectrometer utilizes Bloch's detection scheme.[11] It contains a sweep generator which provides a sawtooth voltage for feeding a pair of Helmholtz coils in the probe. These coils produce a magnetic field sweep at the sample which is superimposed on that of the electromagnet and is of such a magnitude that the total applied field includes the resonance value for the nucleus under study. In the present study a sweep field of about 150 millioersteds was used. The resonances were recorded with a Sanborn recording system. The scale of abscissas on the records (dispersion) was determined by superimposing an audio-frequency of 40 cps on the sweep field to produce side band peaks to the water resonance[12] spaced 40 cps (9.4 millioersteds) apart.

The shift of the resonance in each solution was measured with respect to that of water used as a reference. The accuracy is limited by the stability of the applied field. Fluctuations of a few millioersteds occur sometimes. In general, the error of an average of five or more readings is believed to be smaller than 1 millioersted.

The volume magnetic susceptibility of each solution was measured by a new method[13] which uses the same NMR equipment.

Anhydrous nitric and perchloric[3] acids were prepared by vacuum distillation of mixtures with sulfuric acid.

[1] O. Redlich and P. Rosenfeld, Sitz. ber. Akad. Wiss. Wien. Math. Naturw. Kl. Abt. IIb **145**, 87; or Monatsh. Chem. **67**, 223 (1936).
[2] N. R. Rao, Indian J. Phys. **15**, 185 (1941); O. Redlich and J. Bigeleisen, J. Am. Chem. Soc. **65**, 1883 (1943); see also O. Redlich, Chem. Revs. **39**, 333 (1946).
[3] Redlich, Holt, and Bigeleisen, J. Am. Chem. Soc. **66**, 13 (1944).
[4] T. F. Young, Record Chem. Progr. Kresge-Hooker Sci. Lib. **12**, 81 (1951).
[5] H. S. Gutowsky and A. Saika, J. Chem. Phys. **21**, 1688 (1953).
[6] Y. Masuda and T. Kanda, J. Phys. Soc. Japan **8**, 432 (1953).
[7] R. Dalmon and R. Freymann, Compt. rend. **211**, 472 (1940).
[8] J. Chédin, J. chim. phys. **49**, 109 (1952); J. Chédin and S. Fénéant, Compt. rend. **224**, 930 (1947), **228**, 1120 (1949); Mém. services chim. état Paris **32**, 92 (1946). Chédin, Fénéant, and Vandoni, Compt. rend. **226**, 1722 (1948).
[9] Varian Associates, Palo Alto, California.
[10] W. E. Packard, Rev. Sci. Instr. **19**, 435 (1948).
[11] Bloch, Hansen, and Packard, Phys. Rev. **70**, 474 (1946).
[12] J. T. Arnold and M. E. Packard, J. Chem. Phys. **19**, 1608 (1951).
[13] McConnell, Meisenheimer, and Reilly (to be published).

The samples were sealed into the upper compartments of Pyrex capillary tubes (3 mm i.d.), each liquid sample being several centimeters in length. The lower compartments of all tubes contained water. For every solution, several records of the resonance curve of water were taken first. Then the tube was pushed down so that the solution was in the probe region, and several records of the resonance curve of the solution were taken immediately. The change from water to solution could be made in about one second, which is less than the period of one sweep through resonance (about 5 seconds).

2. ASSUMPTIONS

In nuclear magnetic resonance experiments small differences of the energy of a nucleus in various states are observed. The order of magnitude of these differences, expressed on a frequency scale, amounts to several hundred cycles per second for the proton in the molecular species (water, hydrogen ion, undissociated acid) involved in the present work. The lifetime of each of these states is undoubtedly much smaller than one millisecond. The observed energy is, therefore, as has been recognized by previous authors, an average of the energies of the proton in the various molecular (or ionic) species present, weighted by their concentrations. Accordingly, the observed energy is a colligative property.

In the present work, nuclear magnetic resonance is used for the determination of the concentration of a specific molecular or ionic species. Compared with the use of a specific property such as the intensity of a Raman line or an optical absorption band, magnetic resonance presents the considerable advantage that the experimental difficulties of intensity measurements are avoided. On the other hand, the use of a colligative property involves assumptions which cannot be tested directly.

The quantity observed is the applied magnetic field. The macroscopic field in the substance being investigated is obtained from the applied field and the volume magnetic susceptibility. The internal field acting on the nucleus is the sum of the macroscopic field and a small term which is *assumed* to depend only on the *intra*molecular environment of the nucleus, i.e., on the nature of the molecule (or ion) and the position of the nucleus in the molecule. In other words, the difference of the internal and macroscopic fields is assumed to be a property of the molecular species. It is implied that the influence of the *extra*molecular environment on the field is sufficiently taken into account by means of the magnetic susceptibility, i.e., as the average influence at a fixed place in the solution. Any order in the environment of the molecule or ion under consideration (such as an ionic atmosphere) could conceivably cause a deviation from the influence expressed by the susceptibility. Such deviations are assumed to be negligible.

On the basis of this assumption definite values, independent of the composition of the solution examined, are ascribed to the energies of a nucleus in various molecular species at a given macroscopic field.

Another assumption is necessary for the special case of the proton magnetic resonance in aqueous solutions

TABLE I. Nitric acid.

Moles per liter c	p	Susceptibility correction g	Resonance shift s	Degree of dissociation α	a/c
4.00	0.119	0.15	1.36	0.954	4.6
5.57	0.172	0.16	1.82	0.845	12
7.96	0.265	0.19	2.59	0.736	32
15.98	0.789	0.32	3.85	0.091	560
17.93	1.023	0.40	4.30	...	...
19.96	1.376	0.48	4.82	...	...
21.95	1.971	0.52	5.44	...	...
23.98	3.025	0.52	7.11	...	...
4.00	0.119	0.15	1.24	0.831	4.6
5.99	0.187	0.17	1.89	0.752	15
7.99	0.265	0.19	2.41	0.646	32
9.97	0.355	0.23	2.98	0.545	67
11.99	0.466	0.25	3.20	0.354	140
14.06	0.612	0.27	3.65	0.234	290

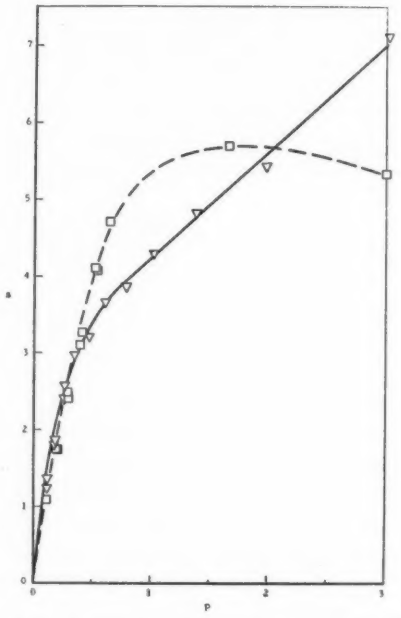

FIG. 1. Observed resonance shift of nitric (▽) and perchloric (□) acids.

or in the presence of other substances which are associated by hydrogen bonds. The proton resonance values in a free and a hydrogen-bonded hydroxyl are noticeably different.[12] Since the presence of any solute shifts the association equilibrium, the proton resonance value is indirectly influenced by the solutes.[14]

It is not necessary to assume that a given amount of any solute changes the association of water to the

[14] We are obliged to Dr. B. J. Alder for informing us that he found different resonance shifts in aqueous solutions of various salts.

same extent. We need only the assumption that the contribution of water to the proton resonance value is a linear function of the mole fractions of the dissolved molecular species, i.e., that the influence of the addition of a certain species is independent of the composition of the solution. Even this assumption can hardly be more than a crude approximation. It could probably be examined by the investigation of such binary systems as water-dioxane and water-acetone.

The best test of these assumptions is believed to be the comparison of the results based on them with the results derived from a specific property, namely, the intensity of Raman lines.

The (corrected) resonance shift s, reported in the following, has been obtained from the applied magnetic

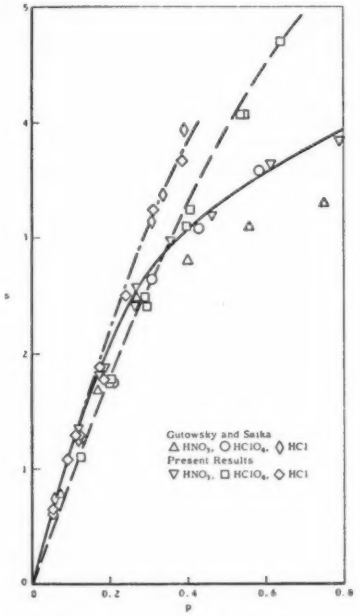

FIG. 2. Resonance shift at moderate concentrations.

resonance field H for the solution and H_0 for pure water according to

$$s=(H_0/H-1)\cdot 10^6+g \tag{1}$$

with

$$g=(2\pi/3)(\varkappa-\varkappa_0)\cdot 10^6, \tag{2}$$

where $\varkappa$ is the volume magnetic susceptibility of the solution and $\varkappa_0$ that of water. It is this resonance shift s which is assumed to be a linear function of the mole fractions of the molecular species present in the solution (see Eqs. (4) and (6)).

3. NITRIC ACID

The observed resonance shift s (Table I) is shown in Fig. 1 as a function of the quantity p of Gutowsky and Saika

$$p=3x/(2-x), \tag{3}$$

where x is the stoichiometric mole fraction of the acid.

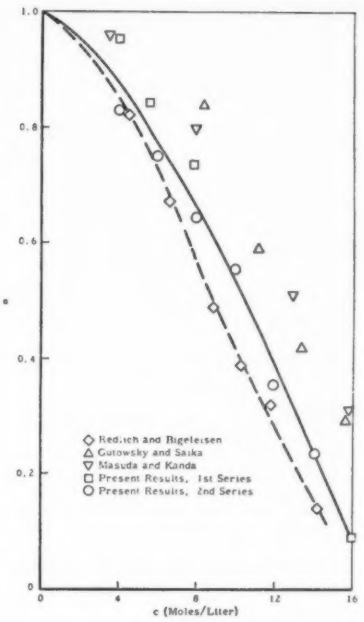
◇ Redlich and Bigeleisen
△ Gutowsky and Saika
▽ Masuda and Kanda
□ Present Results, 1st Series
○ Present Results, 2nd Series
c (Moles/Liter)

FIG. 3. Degree of dissociation of nitric acid.

The quantity p is the stoichiometric or apparent mole fraction of the hydrogen in H_3O^+ on a total hydrogen basis.

Within the experimental errors, the resonance shift of nitric acid is a linear function of p,

$$s=0.5(s_3-s_2)p+1.5s_2-0.5s_3, \tag{4}$$

in the range from $p=1$ (monohydrate H_3NO_4, $s=s_2=4.25$) to $p=3$ (anhydrous acid HNO_3, $s=s_3=7.00$).

Within this range nitric acid contains, therefore, as far as can be concluded from proton magnetic resonance, only two molecular species, the monohydrate or undissociated acid H_3NO_4 and the anhydrous acid HNO_3, which is known to be associated to dimers or perhaps higher polymers.[7] The deviations of the curve in Fig. 1 from linearity above $p=1$ may be due to the presence of nitrate and hydrogen ions at the lower end of the range and of nitrate and nitronium ions at the upper end. In view of the experimental uncertainty it appears to be advisable to neglect such minor effects at present.

The limiting slope (Fig. 2)

$$s_1=\lim_{p\to 0} s/p$$

has been calculated according to the least squares method. The eight results for s/p in the range from $p=0$ to $p=0.466$ have been represented by a second-order function with two different assumptions regarding the weights (weight proportional to p^2 or to p). The second of the two results

$$s_1=11.75 \text{ and } s_1=11.82 \tag{5}$$

has been adopted.

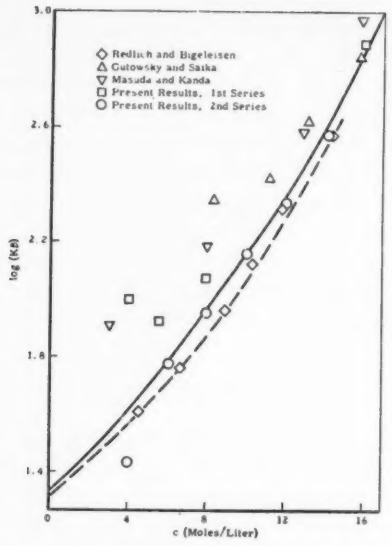

FIG. 4. Dissociation constant of nitric acid.

The degree of dissociation α is given by the relation

$$s/p=s_1\alpha+s_2(1-\alpha) \quad (p<1). \tag{6}$$

The results (Table I and Fig. 3) are higher[15] than the values previously derived from Raman line intensities.[2] The differences are well within the limits of experimental errors of both methods.

The result of Gutowsky and Saika[5] for their lowest concentration deviates from their smooth curve and is undoubtedly a little too high. The other results of these authors agree quite well with the present data if the susceptibility correction g is applied to their observations and if their value $s_3/3=5.6/3$ is replaced by $s_2=4.25$. Since Masuda and Kanda[6] used the nitrogen magnetic resonance shift observed for the anhydrous acid as s_2 in Eq. (6), a revision of their calculations would be required for a conclusive comparison with the present results.

For the determination of the thermodynamic dissociation constant K, the logarithm of

$$K\beta=a/c(1-\alpha) \tag{7}$$

(a=activity of nitric acid,[16] c=concentration in moles per liter, β=activity coefficient of the undissociated molecule) has been extrapolated to zero concentration (Fig. 4). The second series has been given more weight in the extrapolation. The close agreement of the result

$$\log K=1.34; \quad K=22 \tag{8}$$

with the earlier[2] value $K=21$ is, of course, fortuitous.

TABLE II. Perchloric acid.

Moles per liter c	m	p	Susceptibility correction g	Resonance shift s	Degree of dissociation α	log a
5.97	8.06	0.203	0.00	1.77	0.920	3.98
7.95	12.1	0.294	0.00	2.41	0.868	6.01
9.95	17.25	0.404	0.00	3.26	0.851	8.39
11.94	···	0.542	0.00	4.08	0.777	···
13.07	···	0.640	0.02	4.71	0.756	···
16.82	···	1.660	0.18	5.70	0.224	···
17.60	···	3.000	0.26	5.32	0.000	···
3.94	4.79	0.124	0.00	1.10	0.960	2.25
5.92	7.97	0.201	0.00	1.75	0.936	3.93
7.90	12.0	0.292	0.00	2.50	0.918	5.97
9.86	16.95	0.397	0.00	3.10	0.816	8.23
11.84	···	0.535	0.00	4.09	0.794	···

[15] This is in accord with unpublished measurements of Raman intensities by T. F. Young and L. F. Maranville.

4. PERCHLORIC ACID

The curve for perchloric acid (s *vs* p, Fig. 1, Table II) does not contain a straight line portion as does that for nitric acid. For this reason, and in accord with our previous knowledge, the result for the anhydrous acid is interpreted as the shift of the undissociated acid

$$s_2=5.32. \tag{9}$$

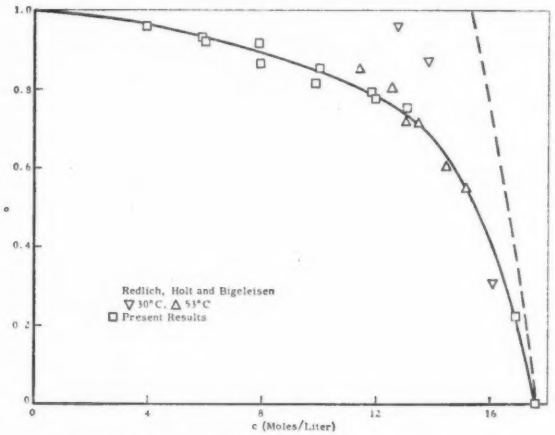

FIG. 5. Degree of dissociation of perchloric acid.

The limiting slope (Fig. 2)

$$s_1=9.17 \tag{10}$$

has been determined as before.

The degrees of dissociation (Fig. 5) obtained from these data support the interpretation that only ions and undissociated molecules $HClO_4$ exist in aqueous solutions. The curve approaches the limiting slope, indicated in Fig. 5 by a broken line, for the complete dissociation of water in anhydrous perchloric acid according to

$$HClO_4+H_2O=H_3O^++ClO_4^-. \tag{11}$$

The same conclusion was drawn earlier.[3]

The fact that the present results agree with the Raman data for 53°C rather than those for 30°C is not too satisfactory but the error may well be in the Raman measurements, which at 30°C are restricted to an unfavorable concentration range.

[16] See reference 2.

The range of the present results overlaps sufficiently with the range of the activity coefficients of Robinson and Baker[17] to permit an estimate of the thermodynamic dissociation constant. Table II contains the logarithms of the activities a obtained from their data. The values of $K\beta$ and the least squares curve are shown in Fig. 6. The result

$$\log K = 1.58; \quad K = 38 \tag{12}$$

is surprising. It appears that perchloric acid at moderate concentrations is not much more strongly dissociated than nitric acid. It is an extremely strong acid rather because the degree of dissociation is high even in highly concentrated solutions.

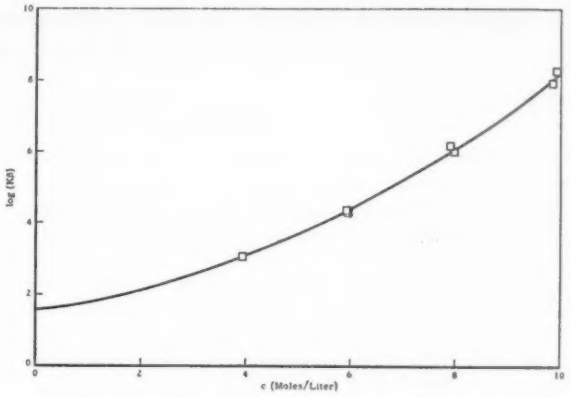

FIG. 6. Dissociation constant of perchloric acid.

5. HYDROCHLORIC ACID

The measurements (Table III, Fig. 2) give the limiting slope

$$s_1 = 11.43. \tag{13}$$

The difference between this value and the value 11.82 for nitric acid is hardly significant. But the difference between the slope for perchloric acid (9.17) and those of the other acids is believed to be outside the experimental errors. It is to be concluded that the perchlorate ion breaks up the association of water to a larger extent than do the nitrate or chloride ions.

TABLE III. Hydrochloric acid.

Moles per liter c	p	Susceptibility correction g	Resonance shift s
2.00	0.055	−0.02	0.61
3.24	0.092	−0.03	1.07
4.25	0.121	−0.04	1.28
6.07	0.176	−0.06	1.88
2.02	0.056	0.00	0.65
4.03	0.114	−0.02	1.28
6.05	0.175	−0.04	1.82
8.06	0.240	−0.06	2.51
10.09	0.310	−0.10	3.25
12.10	0.384	−0.15	3.68

The differences between the present results for perchloric and hydrochloric acids and those of Gutowsky and Saika are small (Fig. 2).

6. CONCLUSIONS

The comparison of the Raman data with the proton magnetic resonance shifts of nitric and perchloric acids confirms the interpretation of the concentration dependence of this shift. The previously known association of nitric acid in solutions above 50 mole percent is clearly reflected in the resonance shift. The agreement of the degrees of dissociation is quite satisfactory.

It may be concluded that the two assumptions discussed in Sec. 2 are reasonable approximations. Moreover, the differences in the influence of ions on the association of water appear to be minor effects, though not negligible in the calculation of degrees of dissociation.

The authors wish to express their appreciation of Dr. D. P. Stevenson's interest in this work.

[17] R. A. Robinson and O. J. Baker, Trans. Roy. Soc. New Zealand **76**, 250 (1946).

THE JOURNAL OF CHEMICAL PHYSICS VOLUME 22, NUMBER 12 DECEMBER, 1954

Approximate Integral Evaluations Used in the Molecular Quantum Mechanics of Nonlinear Molecules*

ROLAND S. BARKER AND HENRY EYRING
Department of Chemistry University of Utah, Salt Lake City, Utah
(Received June 7, 1954)

Molecular energy calculations employing actual and approximate multicenter angular dependent integral evaluations are compared. Individual integral values for three-center integrals used in calculations for the triangular H_3^+ ion as computed by exact methods and by the approximate formulas of Mulliken and of Rudenberg are given. The results indicate that angular and distance relations of the nuclear skeleton of this polyatomic ion are determinable at almost the identical "best" value found using the much more laborious exact integral calculations. The energies of the approximate evaluations, however, indicate that once these "best" parametric values are determined the more exact calculations must be used. The approximate evaluations of second angular derivatives of integrals that are dependent on the angular and distance relations of component molecular nuclei are also computed and compared. Use of such derivatives in determination of approximate zero point energies, vibrational frequencies, and force constants is indicated.

1. INTRODUCTION

RECENT work[1–4] with approximate integral evaluations of multicenter integrals used in molecular quantum mechanics renders a study of the deviation of such computations from exact evaluations desirable. That such deviations will not be invariant with the angular and distance arrangements of the nuclei is obvious. The extent of dependence of these integral values on the angular arrangement of the nuclei and the comparative energy calculations for the simplest nonlinear polynuclear system, the H_3^+ ion, are here presented.

Most of the integral approximations of the recent literature are developed for "un certain nombre d'integrals, et en particulier celles du type,

$$L_{ab,\,cd}=\int a(1)b(1)\frac{1}{r_{12}}c(2)d(2)d\tau, \qquad (1.1)$$

qui sont, en général, pratiquement impossible à calculer exactement."[3] The notation of this integral type is the same as that more fully described in section 2. The difficulty of obtaining exact values of the multi-center integrals (1.1) is not exaggerated in the quoted statement of Vroelant[3] as may be observed on examination of work dealing with "exact" evaluations of special forms of these general integrals.[5–8] It is thus understandable that such approximations as those here examined have not been extensively compared with "exact" evaluations. In previous communications[9,10] we have tabulated a few comparative values for the linear H_3 molecule. Since such values show no angular dependence, the true magnitude of simplification introduced by use of the Mulliken and of the Rudenberg approximations were not fully illustrated. The difficult three- and four-center integrals of molecular quantum mechanics are approximated in terms of two-center overlap, coulombic, and exchange integrals. Thus, in the triangular configuration of the H_3^+ ion (which may be considered as represented by three nonlinear atomic hydrogen nuclei "A," "B," and "C"), the three-center integral dependence on the $\angle ABC$ enters the approximate integration formulas only by variation of the distance parameters, R_{AC}, R_{AB}, and R_{BC}. Elimination of difficult angular dependent integrations is thus achieved. Investigation of the accuracy of this procedure is made in section 2.

2. APPROXIMATIONS OBTAINED BY USING THE FIRST TERM OF THE SERIES OF SIMULTANEOUS EXPANSION OF TWO ATOMIC ORBITALS

Rudenberg[2] mathematically derived a general approximation for electron repulsion integrals earlier obtained intuitively by Mulliken. This approximation may be written,

$$L_{AB,\,CD}=\int \chi_A(1)\chi_B(1)\frac{1}{r_{12}}\chi_C(2)\chi_D(2)d\tau \qquad (2.1)$$

$$\approx\tfrac{1}{4}I_{AB}\cdot I_{CD}\{L_{AA,\,CC}+L_{AA,\,DD}+L_{BB,\,CC}+L_{BB,\,DD}\}\quad\text{(M. approx.)},$$

where $\chi_A(1)$, $\chi_B(1)$, $\chi_C(2)$, and $\chi_D(2)$ are functions representing the general AO's (atomic orbitals) of electron 1 and 2 on nuclei "A," "B," "C," and "D;" I_{AB} and I_{CD} are overlap integrals of the type

* Sponsored by the Office of Ordnance Research, U. S. Army.
[1] R. S. Mulliken, J. chim. phys. **46**, 500, 521 (1949).
[2] K. Rudenberg, J. Chem. Phys. **19**, 1433 (1951).
[3] C. Vroelant, J. chim. phys. **49**, 141 (1952).
[4] C. W. Scherr, J. Chem. Phys. **22**, 149 (1954).
[5] Hirschfelder, Eyring, and Rosen, J. Chem. Phys. **4**, 121 (1936).
[6] M. P. Barnett and C. A. Coulson, Trans. Roy. Soc. (London) **243**, 221 (1951).
[7] S. O. Lundquist and P. O. Lowdin, Arkiv Fysik (Stockholm) **3**, 147 (1951).
[8] R. S. Barker and H. Eyring, J. Chem. Phys. **21**, 912 (1953); **22**, 114 (1954).
[9] Barker, Eyring, Thorne, and Baker, J. Chem. Phys. **22**, 699 (1954).
[10] R. S. Barker and H. Eyring, J. Chem. Phys. **22**, 1182 (1954).

$I_{AB}=\int \chi_A\chi_B d\tau$; r_{12} is the distance between the electrons, $d\tau$ the volume elements of the electrons; and $L_{AA,CC}$, $L_{AA,DD}$, $L_{BB,CC}$, and $L_{BB,DD}$ are the two-center Coulombic integrals of the type $L_{AA,CC}=\int \chi_A(1)\chi_A(1)(1/r_{12})\chi_C(2)\chi_C(2)d\tau$.

Expression (2.1) was obtained by Rudenberg by expanding the orbitals of electron one and of electron two in series. After neglect of all but the initial terms, these series may be written as the Coulombic-like orbital expansions (2.2) and (2.3):

$$\chi_A(1)\chi_B(1)\approx\tfrac{1}{2}I_{AB}\{\chi_A(1)\chi_A(1)+\chi_B(1)\chi_B(1)\}, \quad (2.2)$$

$$\chi_C(2)\chi_D(2)\approx\tfrac{1}{2}I_{CD}\{\chi_C(2)\chi_C(2)+\chi_D(2)\chi_D(2)\}. \quad (2.3)$$

The substitution of (2.2) and (2.3) in the general electron repulsion integral definition (2.1) leads at once to the general Mulliken approximation. Similar substitution of (2.3) into the general three-center nuclear attraction integral definition (2.4) leads to the so-called R.-M. nuclear attraction integral approximation. Thus,

$$K_{A,BC}=\int \chi_A(1)\chi_B(1)d\tau \quad (2.4)$$

$$\approx\tfrac{1}{2}I_{BC}\{G_{A,B^2}+G_{A,C^2}\} \quad \text{(R.-M. approx.)},$$

where $G_{A,B}$ and $G_{A,C}$ are the well-known two-center single electron Coulombic attraction integrals. For example

$$G_{A,B^2}=\int (1/r_{a1})\chi_B(1)\chi_B(1)d\tau_1.$$

It has further been suggested by Rudenberg[2] that somewhat analogous approximations might be obtained by expanding the composite orbitals of the integrals in a slightly different manner. After similar neglect of all but the initial terms, these alternative forms may be written as the exchange-like orbital expansions (2.5), (2.6), (2.7), and (2.8) below.

$$\chi_A(1)\chi_C(2)\approx\tfrac{1}{2}I_{AC}\{\chi_A(1)\chi_A(2)+\chi_C(1)\chi_C(2)\} \quad (2.5)$$

$$\chi_B(1)\chi_D(2)\approx\tfrac{1}{2}I_{BD}\{\chi_B(1)\chi_B(2)+\chi_D(1)\chi_D(2)\} \quad (2.6)$$

$$\chi_A(1)\chi_D(2)\approx\tfrac{1}{2}I_{AD}\{\chi_A(1)\chi_A(2)+\chi_D(1)\chi_D(2)\} \quad (2.7)$$

$$\chi_B(1)\chi_C(2)\approx\tfrac{1}{2}I_{BC}\{\chi_B(1)\chi_B(2)+\chi_C(1)\chi_C(2)\}. \quad (2.8)$$

Substitution of the above expressions into the general electron repulsion integral definition (2.1) leads to two general approximations. These approximations may be written as (2.9) and (2.10) below. They will be disignated as Rudenberg's approximation I, when using the "*AC*" and "*BD*" expansions, and Rudenberg's approximation II, when using the "*AD*" and "*BC*" expansions. One thus obtains

General formula (I) "*AC*" and "*BD*" expansions

$$L_{AB,CD}\approx\tfrac{1}{4}I_{AC}\cdot I_{BD}$$

$$\times\{L_{AB,AB}+L_{CD,CD}+L_{AD,AD}+L_{BC,BC}\}. \quad (2.9)$$

General formula (II) "*AD*" and "*BC*" expansions

$$L_{AB,CD}\approx\tfrac{1}{4}I_{AD}\cdot I_{BC}$$

$$\times\{L_{AB,AB}+L_{CD,CD}+L_{AC,AC}+L_{BD,BD}\}. \quad (2.10)$$

In general the exchange integrals are more difficult than the Coulombic integrals to evaluate and thus these alternative approximations are not as easily applied as the earlier Mulliken approximation. Further the exchange-like orbital expansions cannot be adapted for used in the three-center nuclear attraction integral (2.4). The results of our investigation also indicate that these alternative approximations are not generally as accurate as the more easily applied Mulliken formulas, even when the distance between the centers of the orbitals in the two approximations are the same. Thus for example the integral $L_{AB,BC}$ employed in calculations of the equilateral triangular H_3^+ ion configuration disclosed that both alternative approximations were less accurate at the nuclear distances tried than the original Mulliken approximation. The alternative approximations are, however, occasionally useful in obtaining integral derivatives as described in section 5 and may be more accurate at some internuclear distances.

3. APPROXIMATE AND ACTUAL VALUES OF ANGULAR DEPENDENT MULTI-CENTER INTEGRALS

Previous work[9,10] has compared nonangular dependent approximate and "actual" integral evaluations. "Actual" integral computations being defined as those obtained from closed form integrated formulas or from evaluations by other means which yield values believed accurate to a stated number of places (here taken to be four or five). Some of the "actual" values cited for comparative purposes in the tables of this and other sections of this paper were obtained by rather elaborate methods. Others were taken from the work of Hirschfelder and Weygandt[11] who made use of the differential analyzer. All labeled "actual" values are believed to be accurate to four or five significant figures.

The cited integral values of the tables included in this paper involve only 1*s* *AO*'s and are for an ad-

TABLE I. Angular dependence of $L_{ab,bc}(R=R_{ab}=R_{bc})$.

R	R_{ac}	$\angle ABC$	Actual value	Value M. approx.[a]	Value R. (I)[b]	Value R. (II)[c]
2.0	0	0° ($L_{ab,ba}$)	0.184156	0.1807	···	0.184156
2.0	2	60° (Eq. Δ)	0.169845	0.1636	0.1012	0.1080
2.0	4	180° (Linear)	0.141207	0.1483	0.0868	0.0349
2.5	0	0° ($L_{ab,ba}$)	0.106622	0.1043	···	0.106622
2.5	2.5	60° (Eq. Δ)	0.095383	0.0909	0.0496	0.1043
2.5	5	180° (Linear)	0.075091	0.0820	0.0442	0.0103
3.0	0	0° ($L_{ab,ba}$)	0.058508	0.0574	···	0.058508
3.0	3	60° (Eq. Δ)	0.050862	0.0481	0.0243	0.0204
3.0	6	180° (Linear)	0.039101	0.0435	0.0226	0.0028

[a] $L_{ab,bc}\approx\tfrac{1}{4}I_{ab}^2\{3L_{aa,bb}+L_{bb,bb}\}$ (M. approx.).
[b] $L_{ab,bc}\approx\tfrac{1}{4}I_{ab}^2\{L_{bb,bb}+L_{ac,ac}+2L_{ab,ab}\}$ (R. approx. I).
[c] $L_{ab,bc}\approx I_{ac}\cdot L_{ab,ab}$ (R. approx. II).

[11] J. O. Hirschfelder and C. N. Weygandt, J. Chem. Phys. **6**, 806 (1938).

TABLE II. Angular dependence of $L_{aa,\,bc}(R=R_{ab}=R_{bc})$.

R	R_{ac}	$\angle ABC$	Actual value	Value M. approx.[a]	Value R. (I)[b]	Value R. (II)[c]
2.0	0	0° ($L_{aa,\,ab}$)	0.308036	0.3082	0.2373	0.2373
2.0	2.0	60° (Eq. Δ)	0.258356	0.2498	0.1012	0.1012
2.0	4.0	180° (Linear)	0.188392	0.1975	0.0280	0.0182
2.5	0	0° ($L_{aa,\,ab}$)	0.225595	0.2276	0.1677	0.1677
2.5	2.5	60° (Eq. Δ)	0.177685	0.1688	0.0496	0.0496
2.5	5	180° (Linear)	0.121967	0.1301	0.0093	0.0082
3.0	0	0° ($L_{aa,\,ab}$)	0.160742	0.1646	0.1191	0.1191
3.0	3	60° (Eq. Δ)	0.119193	0.1115	0.0243	0.0243
3.0	6	180° (Linear)	0.078436	0.0848	0.0031	0.0028

[a] $L_{aa,bc}\approx\frac{1}{2}I_{bc}\{L_{aa,bb}+L_{aa,cc}\}$ (M. approx.).
[b] $L_{aa,bc}\approx\frac{1}{2}I_{ab}\cdot I_{ac}\{L_{aa,aa}+2L_{ab,ab}+L_{ac,ac}\}$ (R. approx. I).
[c] $L_{aa,bc}\approx\frac{1}{4}I_{ab}\cdot I_{ac}\{L_{aa,aa}+2L_{ac,ac}+L_{bc,bc}\}$ (R. approx. II).

mittedly limited number of angular configurations. However the small number of readily available "actual" evaluations of three- or four-center integrals and the computational difficulties of securing further values make extension of the table unprofitable. Values obtained from the Mulliken and from the so-called Rudenberg approximate integral methods as well as the "actual" values of the three-center integrals of the isosceles triangular H_3^+ ion are given in Tables I and II.

The special case when the $\angle ABC=0$ (that is when nucleus "A" coincides with nucleus "C") changes these three-center into two-center integrals. It will be noted that while values for the Rudenberg approximations are given for $L_{ab,\,bc}$ for the above special case no simplification is achieved. The integral $L_{ab,\,bc}$ is transformed in this instance into the two-center exchange integral $L_{ab,\,ab}$. The Rudenberg approximate formulas reduce general multicenter integrals to integrals of this form. The formal application of the approximations in the special case cited above leads to expressions in terms of the very integral being approximated. The second Rudenberg approximation of $L_{ab,\,ab}$ reduces directly to this same integral. The first results in an erroneous alteration of the correct value, which must be already known for application of the approximation. Tables III and IV give the "actual" and the Mulliken approximate values for the single electron three-center nuclear attraction integrals of the illustrative H_3^+ ion calculations.

The Rudenberg approximations are inapplicable to the one electron integrals of Table III. The numerical values of the integrals of these and the other tables are given in atomic units, i.e., distances are in units of the first Bohr radius $a_0=0.5292$ A, energies in units of e^2/a_0.

The special case when $\angle ABC=0$ reduces the integral $K_{a,\,bc}$ to the two-center integral $J_{a,\,ab}$. While the closed form integrated expression for this integral is simple, the integral has been calculated from the approximate formula only for comparative purposes.

The special case when $\angle ABC=0$ reduces the integral $K_{b,\,ac}$ to the two-center integral $G_{a,\,b}{}^2$. The approximation also reduces directly to this two-center integral which must be known to apply the approximation.

Illustrative calculations for the isosceles triangular H_3^+ ion made desirable a more extensive examination of the evaluations of certain three-center integrals. Approximate values of the three-center ones needed for these calculations are given in Tables V, VI, and VII. The values of Table V given in parentheses were obtained from Hirschfelder and Weygandt's angular interpolation formula:[11] $L=L_0+L_1\cos\phi+L_2\cos^2\phi+L_3\cos^3\phi$. The four constants L_0, L_1, L_2, and L_3 are evaluated from "actual" values of the integrals for configurations with a bending angle $\phi=0$, π, $2/3\pi$; and from the "actual" value for the second angular derivative of the integrals. Values of $K_{a,\,bc}$ and $K_{b,\,ac}$ for other angles are given in Table III and Table IV.

TABLE III. Angular dependence of $K_{a,\,bc}(R=R_{ab}=R_{ac})$.

R	R_{ac}	$\angle ABC$	Actual value	R.-M. approx.[a]
2	0	0° ($J_{a,\,ab}$)	0.406006	0.4318
2	2	60° (Eq. Δ)	0.294562	0.2771
2	4	180° (Linear)	0.196678	0.2117
2.5	0	0° ($J_{a,\,ab}$)	0.287298	0.3187
2.5	2.5	60° (Eq. Δ)	0.193575	0.1790
2.5	5	180° (Linear)	0.124356	0.1353
3	0	0° ($J_{a,\,ab}$)	0.199148	0.2318
3	3	60° (Eq. Δ)	0.125954	0.1150
3	6	180° (Linear)	0.079102	0.0866

[a] $K_{a,bc}\approx\frac{1}{2}I_{bc}\{G_{a,b}{}^2+G_{a,c}{}^2\}$.

TABLE IV. Angular dependence of $K_{b,\,ac}(R=R_{ab}=R_{bc})$.

R	R_{ac}	$\angle ABC$	Actual value	R.-M. approx.[a]
2	0	0° ($G_{b,\,a}{}^2$)	0.472526	0.472526
2	2	60° (Eq. Δ)	0.294562	0.2771
2	4	180° (Linear)	0.117088	0.0894
2.5	0	0° ($G_{b,\,a}{}^2$)	0.3905669	0.3905669
2.5	2.5	60° (Eq. Δ)	0.193575	0.1790
2.5	5	180° (Linear)	0.0539182	0.0378
3.0	0	0° ($G_{b,\,a}{}^2$)	0.3300283	0.3300283
3.0	3	60° (Eq. Δ)	0.125954	0.1150
3.0	6	180° (Linear)	0.0239953	0.0156

[a] $K_{b,ac}\approx I_{ac}\cdot G_{a,b}{}^2$.

4. CALCULATIONS FOR THE COVALENT ISOSCELES TRIANGULAR TRIATOMIC HYDROGEN ION

The values of individual multicenter integrals obtained by approximate and "exact" methods were given in section 3. While these evaluations are an indication of the accuracy that may be expected for the specific integrals, such individual integral computations do not show the over-all comparative results nor the full utility of these approximate methods. The energy calculations for the isosceles-triangular H_3^+ ion using a simple covalent bond treatment is briefly outlined. The results obtained demonstrate the over-all viewpoint.

The isosceles triangular configurations of H_3^+ include the symmetrical linear form and the equilateral triangular forms as special cases. The restriction to covalent structures does not neglect general principles used in

the covalent bond plus ionic terms treatment and so was selected for illustrative comparison of the "actual" and approximate integral energy calculations.

If the three nuclei "a," "b," and "c" of the H_3^+ ion are arranged in an isosceles triangle, the complete covalent bond treatment yields

$$\psi_{\text{cov}}=K_1\psi_1+K_2\psi_2. \tag{4.1}$$

ψ_1 corresponds to a bond betweeen "a" and "b" alternating with a bond between "b" and "c," and ψ_2 corresponds to a bond between "a" and "c." Thus, using functions formed from atomic orbitals symbolized as $a(1)=(Z^3/\pi)e^{-Zr_{a1}}$, etc., as given in our earlier papers, the complete eigenfunction (4.1) for the covalent H_3^+ ion may be written more explicitly using

$$\psi_1=\psi_{ab,c}=\begin{pmatrix}a & b\\ \alpha & \beta\end{pmatrix}-\begin{pmatrix}a & b\\ \beta & \alpha\end{pmatrix}+\begin{pmatrix}b & c\\ \alpha & \beta\end{pmatrix}-\begin{pmatrix}b & c\\ \beta & \alpha\end{pmatrix}$$

TABLE V. Angular dependence of $L_{ab,ac}(R=R_{ab}=R_{bc}=2.0)$ and of $L_{bb,ac}(R=R_{ab}=R_{bc}=2.0)$.

Integral	$\angle ABC$	ϕ	R_{ac}	Actual value[a]	Value M. approx.[b]	Value R. (I)[c]	Value R. (II)[d]
$L_{ab,ac}$	0° ($L_{ab,aa}$)	π	0	0.308036	0.3082	0.2373	0.2373
$L_{ab,ac}$	28°57′	151°3′	1	(0.268252)	0.2557	0.1820	0.1800
$L_{ab,ac}$	60° (Eq. Δ)	$2/3\pi$	2	0.169844	0.1636	0.1080	0.1012
$L_{ab,ac}$	90° (Rt. Δ)	$\pi/2$	$8^{\frac{1}{2}}$	(0.098042)	0.0958	...	...
$L_{ab,ac}$	180° (Linear)	0°	4	0.051214	0.0479	0.0586	0.0280
$L_{bb,ac}$	0° ($L_{bb,aa}$)	π	0	0.425974	...	0.1391	0.1391
$L_{bb,ac}$	28°57′	151°3′	1	(0.378358)	0.3657	0.1230	0.1230
$L_{bb,ac}$	60° (Eq. Δ)	$2/3\pi$	2	0.258356	0.2498	0.1012	0.1012
$L_{bb,ac}$	90° (Rt. Δ)	$\pi/2$	$8^{\frac{1}{2}}$	(0.165902)	0.1633	...	...
$L_{bb,ac}$	180° (Linear)	0°	4	0.094214	0.0806	0.0158	0.0158

[a] Values in parentheses are interpolated by the formulas:
$L_{ab,ac}(R=2)=0.098042-0.094281\cos\phi+0.081583\cos^2\phi-0.03413\cos^3\phi.$
$L_{bb,ac}(R=2)=0.165902-0.128456\cos\phi+0.094192\cos^2\phi-0.037424\cos^3\phi.$
[b] $L_{ab,ac}\approx\frac{1}{2}I_{ab}\{L_{aa,aa}+L_{bb,ac}\}$
$L_{bb,ac}\approx I_{ac}\cdot L_{bb,aa}$ (M. approx.).
[c] $L_{ab,ac}\approx\frac{1}{2}I_{bc}\{L_{ab,ab}+L_{ac,ac}\}$
$L_{bb,ac}\approx\frac{1}{2}I_{ab}^2\{L_{bb,bb}+L_{ac,ac}+2L_{ab,ab}\}$ (R. approx. I).
[d] $L_{ab,ac}\approx\frac{1}{2}I_{ab}\cdot I_{ac}\{L_{aa,aa}+L_{ac,ac}+2L_{ab,ab}\}$ (R. approx. II).
$L_{bb,ac}\approx\frac{1}{2}I_{ab}^2\{L_{bb,bb}+L_{ac,ac}+2L_{ab,ab}\}$

and

$$\psi_2=\psi_{b,ac}=\begin{pmatrix}a & c\\ \alpha & \beta\end{pmatrix}-\begin{pmatrix}a & c\\ \beta & \alpha\end{pmatrix}.$$

The notation is that used in our earlier papers.[8,9] The structural composition parameters K_1 and K_2 are determined so as to minimize the energy of the H_3^+ system. The equilateral triangular solution is especially simple. The proper linear combination can be written at once[12] as,

$$\psi_{\text{cov}}=\psi_1+\psi_2. \tag{4.2}$$

The energy of the equilateral triangular configuration is then

$$E\leq\frac{\int\psi H\psi^*d\tau}{\int\psi\psi^*d\tau}=\frac{2(a^2b^2+ab\ ab+2a^2bc+2ab\ bc)}{2(1+3I_{ab}^2+2I_{ab})}. \tag{4.3}$$

[12] J. O. Hirschfelder, J. Chem. Phys. **6**, 795 (1938).

TABLE VI. Approximate integral values for isosceles triangular configurations.

Integral	R	R_{ac}	$\angle ABC$	Interpolated values[a]	M. approx.[b]
$L_{ab,bc}$	2	2.4	73°44′	(0.163686)	0.1596
$L_{ab,bc}$	2	$8^{\frac{1}{2}}$	90°	(0.155966)	0.1558
$L_{ab,bc}$	2.5	3	73°44′	(0.093643)	0.0883
$L_{ab,bc}$	2.5	$12.5^{\frac{1}{2}}$	90°	(0.086382)	0.0861
$L_{ab,bc}$	3	3.6	73°44′	(0.048005)	0.0467
$L_{ab,bc}$	3	$18^{\frac{1}{2}}$	90	(0.045079)	0.0455
$L_{aa,bc}$	2	2.4	73°44′	(0.242221)	0.2361
$L_{aa,bc}$	2	$8^{\frac{1}{2}}$	90°	(0.225658)	0.2233
$L_{aa,bc}$	2.5	3	73°44′	(0.159187)	0.1577
$L_{aa,bc}$	2.5	$12.5^{\frac{1}{2}}$	90°	(0.144443)	0.1480
$L_{aa,bc}$	3	3.6	73°44′	(0.107644)	0.1033
$L_{aa,bc}$	3	$18^{\frac{1}{2}}$	90°	(0.098886)	0.0965

[a] These values were obtained from formulas of the type used for Table V. Values for $R=2$, and $R=3$ were taken as those calculated using three term formulas.
[b] The approximate M. formulas are those given with Tables I and II. Values for other angles of the above integrals of Table V may also be found in Tables I and II.

The orbital integrals a^2b^2, etc. are defined and reduced to elemental integrals in a later part of this paper.

The linear symmetrical and general isosceles-triangular configurations lead to the usual secular equations. These energies are obtained as the lowest root of the secular equation

$$\begin{vmatrix}(H_{11}-ES_{11}) & (H_{12}-ES_{12})\\ (H_{21}-ES_{21}) & (H_{22}-ES_{22})\end{vmatrix}=0, \tag{4.4}$$

where $H_{ij}=\int\psi_iH\psi_jd\tau$; $S_{ij}=\int\psi_i\psi_jd\tau$. The matrix components H_{ij} and S_{ij} reduce to elemental integrals. Thus,

$$\begin{aligned}H_{11}&=4(a^2b^2+ab\ ab+b^2ac+ab\ bc),\\ H_{12}&=H_{21}=4(a^2bc+ac\ ab).\\ H_{22}&=2(a^2c^2+ac\ ac),\\ S_{11}&=4(1+2I_{ab}^2+I_{ac}),\\ S_{12}&=S_{21}=4(I_{bc}+I_{ab}\cdot I_{ac}),\\ S_{22}&=2(1+I_{ac}^2).\end{aligned} \tag{4.5}$$

TABLE VII. Approximate integral values for isosceles triangular configurations.

Integral	R	R_{ac}	$\angle ABC$	R.-M. approx.[a]
$K_{a,bc}$	2	2.4	73°44′	0.2573
$K_{a,bc}$	2	$8^{\frac{1}{2}}$	90°	0.2408
$K_{a,bc}$	2.5	3	73°44′	0.1651
$K_{a,bc}$	2.5	$12.5^{\frac{1}{2}}$	90°	0.1541
$K_{a,bc}$	3	3.6	73°44′	0.1057
$K_{a,bc}$	3	$18^{\frac{1}{2}}$	90°	0.0985
$K_{b,ac}$	2	2.4	73°44′	0.2281
$K_{b,ac}$	2	$8^{\frac{1}{2}}$	90°	0.1811
$K_{b,ac}$	2.5	3	73°44′	0.1361
$K_{b,ac}$	2.5	$12.5^{\frac{1}{2}}$	90°	0.0986
$K_{b,ac}$	3	3.6	73°44′	0.0804
$K_{b,ac}$	3	$18^{\frac{1}{2}}$	90°	0.0535

[a] $K_{a,bc}\approx\frac{1}{2}I_{ab}\{G_{a,b^2}+G_{a,c^2}\}$; $K_{b,ac}\approx I_{ac}\cdot G_{a,b^2}$.

TABLE VIII. Energy of the covalent equilateral triangular H_3^+ ion ($\rho = ZR_{ab} = ZR_{bc} = ZR_{ac}$).

	Actual integral energy calc.				M. approx. integral energy calc.	
ρ	Z	k_1	k_2	Binding energy	Z	Binding energy
2.0	1.00	0.4327	0.2352	116.4 kcal/mole	1.00	83.4 kcal/mole
2.0	1.36	0.4327	0.2352	172.5 kcal/mole	1.32	127.9 kcal/mole
2.5	1.00	0.4791	0.2719	120.1 kcal/mole	1.00	109.4 kcal/mole
2.5	1.37	0.4791	0.2719	180.2 kcal/mole	1.36	164.9 kcal/mole
3.0	1.00	0.5282	0.3135	101.0 kcal/mole	1.00	71.2 kcal/mole
3.0	1.38	0.5282	0.3135	147.9 kcal/mole	1.29	108.6 kcal/mole

The orbital integrals, for example

$$ab\ ac = \int a(1)a(2)Hb(1)c(2)d\tau,$$

may be further reduced to expressions in terms of elemental integrals. Thus,

$$a^2\ b^2 = \left(\frac{2}{R} + \frac{1}{R_{ac}} - 1\right) - (3G_{a,b^2} + G_{a,c^2}) + L_{aa,bb},$$

$$ab\ ab = \left(\frac{2}{R} + \frac{1}{R_{ac}} - 1\right) I_{ab}^2 - 2I_{ab}(J_{a,ab} + K_{a,bc}) + L_{ab,ab},$$

$$b^2\ ac = \left(\frac{2}{R} + \frac{1}{R_{ac}} - 1\right) I_{ac} - 2G_{a,b^2} \cdot I_{ac} - J_{a,ac} - K_{b,ac} + L_{bb,ac},$$

$$ab\ bc = \left(\frac{2}{R} + \frac{1}{R_{ac}} - 1\right) I_{ab}^2 - 2I_{ab}(J_{a,ab} + K_{a,bc}) + L_{ab,bc}, \quad (4.6)$$

$$a^2\ bc = \left(\frac{2}{R} + \frac{1}{R_{ac}} - 1\right) I_{ab} - I_{ab}(G_{a,b^2} + G_{a,c^2}) - J_{a,ab} - K_{a,bc} + L_{aa,bc},$$

$$ac\ ab = \left(\frac{2}{R} + \frac{1}{R_{ac}} - 1\right) I_{ab} I_{ac} - I_{ac}(J_{a,ab} + K_{a,bc}) - I_{ab}(J_{a,ac} + K_{b,ac}) + L_{ab,ac},$$

$$a^2\ c^2 = \left(\frac{2}{R} + \frac{1}{R_{ac}} - 1\right) - 2(G_{a,b^2} + G_{a,c^2}) + L_{aa,cc},$$

$$ac\ ac = \left(\frac{2}{R} + \frac{1}{R_{ac}} - 1\right) I_{ac}^2 - 2I_{ac}(J_{a,ac} + K_{b,ac}) + L_{ac,ac}.$$

The elemental integrals used above and not defined before in this paper are described in previous work.[9,13,14]

From the second order secular equation (4.4) one may easily obtain the convenient form,

$$E \leq \frac{-B - (B^2 - 4AC)^{\frac{1}{2}}}{2A}, \quad (4.7)$$

where

$$A = (S_{11}S_{22} - S_{12}^2),$$

$$B = (2H_{12}S_{12} - H_{22}S_{11} - H_{11}S_{22}),$$

and

$$C = (H_{11}H_{22} - H_{12}^2).$$

Once the energy is determined from (4.7) the constants K_1 and K_2 may be found in the usual way from the normalization condition,

$$\int \psi\psi^* d\tau = 1 = K_1^2 S_{11} + 2K_1K_2S_{12} + K_2^2 S_{22}, \quad (4.8)$$

and minimizing the energy with respect to the K's. The convenient Eqs. (4.9) and (4.10) are then readily found. Letting

$$Q = \left\{\frac{(S_{11}E - H_{11})}{(H_{12} - S_{12}E)}\right\},$$

$$K_1 = (S_{11} + 2QS_{12} + Q^2S_{22})^{-\frac{1}{2}} \quad (4.9)$$

and

$$K_2 = QK_1.$$

ψ_1 and ψ_2 were not normalized. However, $\psi_1/(S_{11})^{\frac{1}{2}}$ and $\psi_2/(S_{22})^{\frac{1}{2}}$ obviously are. Thus we can equally well write:

$$\psi_{cov} = K_1\psi_1 + K_2\psi_2 = \frac{k_1}{(S_{11})^{\frac{1}{2}}}\psi_1 + \frac{k_2}{(S_{22})^{\frac{1}{2}}}\psi_2. \quad (4.11)$$

Simple refinements in the outlined energy calculations are possible. Thus a Wang-like procedure, such as previously described[15] may be applied without further integral evaluations. This treatment requires minimization with respect to the k's, and Z. No new integrals are involved. Results from "actual" and approximate integral calculations for equilateral H_3^+ are given in Table VIII. In Table VIII the k's for the actual and approximate integral treatments by symmetry come out exactly the same. In general they will involve approximate values that are slightly different for the latter treatment. For comparative purposes some values of

[13] N. Rosen, Phys. Rev. **38**, 255 (1931); **38**, 2099 (1931).

[14] J. O. Hirschfelder and J. W. Linnett, J. Chem. Phys. **18**, 130 (1950).

[15] J. C. Giddings, R. S. Barker, and H. Eyring (to be published).

TABLE IX. Actual integral energy calculations for the covalent linear symmetrical H_3^+ ion ($\rho = ZR_{ab} = ZR_{bc} = \frac{1}{2}ZR_{ac}$).

ρ	Z	k_1	k_2	Binding energy
2.0	1.00	0.3650	0	92.4 kcal/mole
2.0	1.29	0.3650	0	131.6 kcal/mole
2.0	1.00	0.0457	0.3512	98.3 kcal/mole
2.5	1.00	0.4060	0	76.3 kcal/mole
2.5	1.24	0.4060	0	104.96 kcal/mole
3.0	1.00	0.4517	0	50.65 kcal/mole
3.0	1.16	0.4517	0	64.17 kcal/mole

the linear symmetrical H_3^+ ion configuration are given in Table IX.

The energies in Tables VIII and IX are given with reference to two hydrogen atoms and a proton infinitely far away. The numerical values were obtained using $e^2/a_0 = 27.206$ ev $= 627.23$ kcal/mole. The best value so far obtained for the linear symmetrical H_3^+ion[15] showed a binding energy of 158.09 kcal/mole which is less than that obtained for the triangular configuration. In examining differences in the Z's determined by the approximate and "actual" integral calculations it should be kept in mind that the approximate calculations of Tables VIII and IX were made without the integral "normalization" improvements[10] which would diminish further the already small differences.

5. USE OF APPROXIMATE INTEGRAL CALCULATIONS IN MOLECULAR QUANTUM MECHANICS

The realization that simple approximate integrals may be used in obtaining "best" values for various eigenfunction parameters is perhaps the most encouraging and significant advance in exact value calculations to be made recently. Use of such approximations in obtaining the "best" internuclear distances of the neutral linear symmetrical H_3^+ metastable molecule has been previously examined.[9] The use of such integral approximations in the determination of effective orbital charges has also been suggested.[10] The calculations of sections 3 and 4 show that such calculations may be used in determining the angular relations of the most stable H_3^+ configuration. The value of approximate methods for determining the k's, Z's, interatomic distances and angles are thus substantiated. For best results the basic integral approximations examined may be refined by employing distance, effective charge, and angle "normalization" factors[9,10] as determined from any known "actual" values and/or from interpolations of such known values. Use of these normalization methods, in conjunction with basic approximate integral formulas, should lead to substantially correct parametric values. With such values determined "exact" integral energy calculations using eigenfunctions of a complexity not formerly believed practical may be completed.

TABLE X. Actual and approximate values of the second derivatives of some integrals with respect to ϕ at $\phi = 0$.

Integral derivative	Actual value[a]	M. approx. or R.-M. approx.	R. approx. (I)	R. approx. (II)
$K''_{b,ac}$	0.058053	0.0577		
$K''_{a,bc}$	0.035949	0.0181		
$L''_{bb,ac}$	0.052345	0.0520	0.0019	0.0019
$L''_{aa,bc}$	0.029921	0.0171	...	...
$L''_{ab,ac}$	0.033504	...	0.0063	...
$L''_{ab,bc}$	0.000248	0.0050	0.0019	0.0225

[a] See reference 16.

Use of the approximate integral equations cited to reach conclusions as to the sign of force constants, approximate bending frequencies, etc., can be made easily. Many such applications without "actual" integral comparative results are to be found in the literature. In recognition of this unfortunate lack of comparative values Table X includes "actual" and approximate evaluations for H_3^+ for the second angular derivative (at $\phi = 0$) used in calculations of the normal vibrational frequency, the zero point energy, the force constant and so forth.

The scarcity of "actual" integral data may be understood upon examination of how the cited "actual" values in Table IX were obtained. The values were calculated by Stevenson and Hirschfelder[16] using numerical methods requiring functional evaluations at over a hundred points. The integrations were carried out graphically in limited accuracy regions and analytically in regions of greater sensitivity.

Extension of the approximate calculations are comparatively simple. Evaluation of the first derivatives of I_{ac}, $L_{aa,cc}$, and $L_{ac,ac}$ from well-known integrated expressions would allow evaluation of omitted values of Table VIII. Approximate values could also be obtained for $L''_{aa,ac}$, $L''_{ac,ac}$, and $L''_{aa,cc}$. These and other approximate computations require no further specific comment.

[16] D. Stevenson and J. O. Hirschfelder, J. Chem. Phys. **5**, 933 (1937).

THE JOURNAL OF CHEMICAL PHYSICS VOLUME 22, NUMBER 12 DECEMBER, 1954

Double-Bond Character of Conjugated Carbon-Chlorine Bonds

R. BERSOHN
Department of Chemistry, Cornell University, Ithaca, New York
(Received June 7, 1954)

The π electron loss of a chlorine atom conjugated with a resonating system can be obtained at least approximately from experimental measurements of the asymmetry of the chlorine nuclear electric quadrupole interaction. Using molecular orbital theory the π electron loss ρ can be simply expressed in terms of the chlorine Coulomb integral, the carbon-chlorine resonance integral, and the energies and wave functions of the system with which the chlorine atom is conjugated. Comparison of theoretical and experimental values of ρ show that the carbon-chlorine resonance integral is about one-third of the carbon-carbon resonance integral. The basic conclusion is that chlorine atoms in general resonate only weakly with attached aromatic systems. Most of the effects previously ascribed to double bond character can alternatively be explained by an increased electronegativity of the carbon sp^2 orbital.

1. INTRODUCTION

WHEN a chlorine atom is bonded to an atom which forms a double bond with another atom the chlorine π electrons become partially delocalized in character and "resonate" with the π electrons of the double bond system. The resulting partial double-bond character has been used by Pauling, Brockway, and Beach[1] to explain the shorter bond length and lower reactivity of aryl and vinyl chlorides as compared to alkyl chlorides. The basic assumptions of this theory, discussed by Sherman and Ketelaar[2] were that

(1) the ratio of the single-bond length to the double-bond length is the same for different atoms,
(2) the bond order is the same function of bond distance for C−Cl bonds as for C−C bonds.

With these assumptions and the electron diffraction values of the C−Cl distances in CH_3Cl and $CH_2=CHCl$ of 1.76 A and 1.69 A, respectively, the figure of 15 percent double-bond character can be deduced for the C−Cl bond in vinyl chloride.

The microwave data obtained since the war changed several aspects of this problem. First some of the older bond distances have proved unreliable within the stated limits of error. Moreover, an alternative measure of double bond character, the quadrupole coupling asymmetry parameter has been discovered. In this paper the molecular orbital theory is used to correlate the available data on the asymmetry of C−Cl bonds in various aryl and acyl chlorides.

2. DOUBLE BOND CHARACTER IN THE WEAK INTERACTION APPROXIMATION

Following the simplest version of molecular orbital theory we assume that the delocalized electrons are those in the carbon $2p\pi$ and chlorine $3p\pi$ states. Because (1) electrons in other states are not explicitly taken into account, and (2) the effect of $3d\pi$ functions is neglected, the number of states is equal to the number of atoms with π electrons. Each electron is regarded as moving in the field of all resonating atoms so that we represent a one-electron molecular π orbital Ψ_i as a linear combination of atomic π orbitals:

$$\Psi_i=\sum_r c_{ri}\phi_r. \tag{1}$$

The number of electrons q_r on any atom r is defined by

$$q_r=\sum_i |c_{ri}|^2 n_i, \tag{2}$$

where n_i is the number of electrons 0, 1, or 2 which occupy the state i. In particular a chlorine atom has, neglecting the effect of resonance, two π electrons.

The effect of resonance in a molecule R−Cl is in general to introduce structures of the form $R^-=Cl^+$, in which a fraction of the π electron charge has left the Cl atom. The resulting electron loss of the chlorine atom is given by the parameter

$$\rho=2-q_{Cl}=2-\sum_i |c_{Cl\,i}|^2 n_i. \tag{3}$$

This expression can be rewritten as

$$\rho=\sum_i |C_{Cl\,i}|^2(2-n_i) = 2\sum_{\substack{\text{unoccupied}\\ \text{levels}}} |c_{Cl\,i}|^2+\sum_{\substack{\text{levels with}\\ \text{only one electron}}} |c_{Cl\,i}|^2. \tag{4}$$

The second term in (5) exists only in free radicals and is dropped forthwith.

In order to determine the coefficients C_{ij} we need to specify the values of the Coulomb integrals, $\alpha_r=\int\phi_r H\phi_r d\tau$ and the resonance integrals $\beta_{rs}=\int\phi_r H\phi_s d\tau$. In the numerical work of later sections Coulson's[3] prescription for the Coulomb integrals was used:

$$\alpha_r-\alpha_C=(x_r-x_C)\beta, \tag{5}$$

where x_C, x_r are the electronegativities of the C atom and r atom, respectively, and β is the (negative) C−C resonance integral. Now our basic assumption is that chlorine π electrons interact weakly with carbon π electrons. This means that if $\beta_{CCl}\equiv\lambda\beta$, then λ is assumed to be small, perhaps of the order of $\frac{1}{3}$. In the strong

[1] Pauling, Brockway, and Beach, J. Am. Chem. Soc. **57**, 2693 (1935); *ibid.*, **59**, 2181 (1937).
[2] J. Sherman and J. A. A. Ketelaar, Physica **6**, 572 (1939).
[3] C. A. Coulson, *Valence* (Oxford University Press, London, 1952), p. 242.

interaction theory of Sherman and Ketelaar λ is taken equal to one. Actually, because so many of our conclusions are independent of the precise value of λ provided it is small, the parameter λ will usually be left unspecified.

The perturbation procedure used is as follows. First one determines the energy levels and wave functions for the unsaturated system, with neglect of interaction between the Cl and C π electrons. Next the interaction energy between the Cl atom and adjacent C atom "r" is calculated to the second order, and the first order change in the wave functions are computed. In this way one finds

$$|c_{\mathrm{Cl}\,i}|^2=\left|\frac{\beta_{\mathrm{Cl}\,r}c_{ri}}{\alpha_{\mathrm{Cl}}-\alpha_{\mathrm{C}}+\epsilon_i}\right|^2=\frac{\lambda^2\beta^2|c_{ri}|^2}{(\alpha_{\mathrm{Cl}}-\alpha_{\mathrm{C}}+\epsilon_i)^2}. \quad (6)$$

c_{ri} is the coefficient of the atomic carbon orbital ϕ_r in the ith molecular orbital.

The final form for the π electron loss ρ is

$$\rho=2\lambda^2\sum_i\frac{|c_{ri}|^2\beta^2}{(\alpha_{\mathrm{Cl}}-\alpha_{\mathrm{C}}+\epsilon_i)^2}, \quad (7)$$

where the sum is taken over all the unoccupied states.

One can also show by perturbation theory that the resonance energy caused by the conjugation of the Cl π electrons with the aromatic system is given by

$$-2\lambda^2\sum_i\frac{|c_{ri}|^2\beta^2}{(\alpha_{\mathrm{Cl}}-\alpha_{\mathrm{C}}+\epsilon_i)};\quad i=\text{unoccupied states}. \quad (8)$$

The loss of π electrons of the Cl atoms is therefore strongly correlated with the resonance energy produced by this transfer of charge which certainly agrees with intuition.

3. CONNECTION BETWEEN THE π ELECTRON LOSS AND THE ELECTRIC FIELD GRADIENT SYMMETRY PARAMETER

The resonance of the π electrons of the Cl atom disturbs the cylindrical symmetry of the C−Cl bond. To describe this deviation we set up a coordinate system with origin at the center of the Cl nucleus and mutually perpendicular x, y, z axes such that z lies along the C−Cl bond and x is perpendicular to the plane of the resonating system. The parameter

$$\eta=\frac{\left(\frac{\partial^2V}{\partial x^2}\right)_0-\left(\frac{\partial^2V}{\partial y^2}\right)_0}{\left(\frac{\partial^2V}{\partial z^2}\right)_0} \quad (9)$$

will be a measure of the deviation of the bond from a single bond and therefore is still another measure of the resonance effect. The derivatives are understood to be averaged over all vibrations and evaluated at the nucleus.

TABLE I. Computation of η for a π bond.

State in which hole occurs	No. of holes	Contributions to $\partial^2V/\partial x^2$	Contributions to $\partial^2V/\partial y^2$	Contributions to $\partial^2V/\partial z^2$
p_z	1	$-\frac{1}{2}q_{p\sigma}$	$-\frac{1}{2}q_{p\sigma}$	$q_{p\sigma}$
p_x	ρ	$\rho q_{p\pi}$	$-\frac{1}{2}\rho q_{p\pi}$	$-\frac{1}{2}\rho q_{p\pi}$

The effective electron configuration which the chlorine nucleus sees is $3s^2p_y^2p_x^{2-\rho}p_z$. Inasmuch as a closed p shell contributes nothing to the derivatives, we can consider the field gradients arising from a hole in the p_z state and a partial hole in the p_x state. The total field gradient is the sum of two axially symmetric tensors whose unique axes are perpendicular. Table I outlines the contributions to the field gradients in a π bond. From this table we see that

$$\eta=\frac{\frac{3}{2}\rho eq_{p\pi}Q_{35}}{e(q_{p\sigma}-\frac{1}{2}\rho q_{p\pi})Q_{35}}. \quad (10)$$

For $(e/h)q_{p\pi}Q_{35}$ we assume the value 109.6 Mc/sec which is the frequency observed for the free Cl^{35} atom. The π electrons are necessarily pure p electrons and this assumption is equivalent to the assumption that the radial distribution of the $p\pi$ electron is the same as the radial distribution of the unpaired p electron in the free Cl atom. For $(e/h)(q_{p\sigma}-\frac{1}{2}\rho q_{p\pi})Q_{35}$ we take 2ν where ν is the observed quadrupole resonance frequency in the molecule under discussion.* Finally we have

$$\eta=-\frac{3}{4}\frac{(109.6)}{\nu}\rho. \quad (11)$$

The parameter ρ has been directly connected with the energy levels and wave functions of the molecule. Measurements of η therefore give rise to many new prospects for the comparison of molecular orbital theory with experiment. At present there is no theory for the values of the coupling constants observed in many recent measurements primarily because these are effects of σ bonds. The asymmetry parameter η, on the other hand, although more difficult to obtain experimentally, is strictly a property of π electrons for which simple theories already exist.

Our basic assumption of weak interaction between the electrons of chlorine and carbon atoms is demonstrated by considering Dean's[4] data on paradichlorbenzene. He obtained the results $\eta=0.08\pm0.02$, $\nu\cong34.8$ Mc/sec, which gives a value of $\rho=0.04\pm0.01$. Computation using Eq. (7) gives $\rho=0.350\lambda^2$, from which we deduce that $\lambda=(\beta_{\mathrm{ClC}}/\beta_{\mathrm{CC}})\sim\frac{1}{3}$. The "double bond character," to use Sherman and Ketelaar's definition, is 4 ± 1 percent

* In so doing we omit small corrections higher order in η whose inclusion would be inconsistent.

[4] C. Dean, Phys. Rev. 86, 607A (1952).

and not 15 percent as formerly surmised.[1] In *p*-chlorobenzyl chloride Meal[4a] found the value of η for the ring chlorine to be 0.07 ± 0.02, which further supports the idea of weak interaction. (The effect of hyperconjugation of the CH_2Cl group should be negligible.)

4. POLYCHLORINATED MOLECULES

Although the effects are exceedingly small, it is useful to have—if only for purposes of discussion—expressions for the change of double bond character on introduction of additional chlorine atoms into the molecule.

Suppose we have a molecule with n resonating chlorine atoms. Its excited molecular orbitals must be corrected to fourth order in λ, i.e.,

$$\Psi_i=\Psi_i^{(0)}(1-a_i^{(2)}-a_i^{(3)}-a_i^{(4)}) +\sum_k \Psi_k^{(0)}(a_k^{(1)}+a_k^{(3)}), \quad (12)$$

where $a_k^{(n)}$ is the coefficient of state k which is of order n in the supposedly small parameter $\lambda=\beta_{CCl}/\beta_{CC}$. To calculate ρ_r we require the coefficients of only those states Ψ_k^0 which are chlorine atom states. In order to carry out the perturbation theory correctly, we must use as zero order chlorine states not the $\phi_{Cl\ j}$, but linear combinations

$$\Psi_k^0=\sum_j d_{jk}\phi_{Cl\ j}, \quad (13)$$

so chosen that their degeneracy is not removed in second order.[5]

We are looking for the coefficient of $|\phi_{Cl\ j}|^2$ in $|\Psi_i|^2$ which is just

$$[\sum_k d_{jk}(a_k^{(1)}+a_k^{(3)})]^2 =\sum_k\sum_{k'} d_{jk}d_{jk'}(a_k^{(1)}a_{k'}^{(1)} +a_k^{(3)}a_{k'}^{(1)}+a_{k'}^{(3)}a_k^{(1)}). \quad (14)$$

Now

$$a_k^{(1)}=\frac{H_{ik}'}{\epsilon_i-\epsilon_{Cl}}=\sum_{s=1}^{n}\frac{c_{is}d_{sk}\lambda_s}{\epsilon_i-\epsilon_{Cl}}, \quad (15)$$

where λ_s is the relative resonance integral of the sth carbon chlorine π bond and C_{is} is the coefficient of the carbon atom orbital adjacent to the sth chlorine atom in the ith unfilled orbital of the molecule.

By standard methods one can show that

$$a_k^{(3)}=-\tfrac{3}{2}\sum_p\frac{|H_{ip}'|^2H_{ki}'}{(\epsilon_i-\epsilon_{Cl})^3}. \quad (16)$$

When (16) and (15) are substituted into (14), by extensive use of the orthogonality of the matrix d_{rk} one can show that

$$\rho_r=2\left[\sum_i\frac{c_{ir}^2\lambda_r^2}{(\epsilon_i-\epsilon_{Cl})^2}-3\sum_i\frac{c_{ir}^2\lambda_r^2}{(\epsilon_i-\epsilon_{Cl})^2}\sum_{t=1}^{n}\frac{c_{it}^2\lambda_t^2}{(\epsilon_i-\epsilon_{Cl})^2}\right], \quad (17)$$

where ρ_r is now defined as the π electron loss of the Cl atom bonded to the C atom r.

If we introduce the notation $\rho_r^{(n)}$, the value of ρ_r correct to nth order in the interaction constants λ_t, we can write down a simplified equation

$$\rho_r^{(4)}=\rho_r^{(2)}-6\sum_i\sum_{t=1}^{n}\frac{c_{ir}^2c_{it}^2}{(\epsilon_i-\epsilon_{Cl})^4}\lambda_r^2\lambda_t^2. \quad (18)$$

Our basic conclusion follows from the fundamental assumption of weak interaction. The decrease of double-bond character and consequent increase in quadrupole coupling constant of a carbon-chlorine bond upon introduction of another chlorine atom in the resonating system is a small higher-order effect.

5. ALKENYL HALIDES

The available quadrupole coupling data for chlorinated ethylenes and benzenes is given in Table II. Vinyl chloride provides a simple illustration of the calculation of ρ. The two π electrons of normal ethylene are in the ground state with wave function. $(1/\sqrt{2})(\phi_1+\phi_2)$ and energy (relative to the Coulomb energy) β. There also exists an empty antibonding state with energy $-\beta$. Now in 1-chloroethylene—neglecting interactions—the two $3p\pi$ electrons occupy a state with energy $\beta/2$ because chlorine is presumed to have this much more electronegativity than carbon. On considering the effects of resonance all the states become intermixed to an extent depending on the strength of interaction. For example, the wave function of the vacant state correct to first order in the carbon-chlorine resonance integral is

$$\frac{1}{\sqrt{2}}(\phi_1-\phi_2)+\frac{\lambda/\sqrt{2}}{-1-\frac{1}{2}}\phi_{Cl}.$$

Because the unoccupied state now contains some of the chlorine state, we can conclude that the chlorine

TABLE II. Chlorine quadrupole coupling data in chlorinated hydrocarbons.

Compound	T	ν	η	ρ (calc.)
CH_2CHCl[a]	20°	33.61	0.07 ±0.03	$0.444\lambda^2$
cis $CHClCHCl$[a]	20°	34.98–35.03		$0.444\lambda^2$
trans $CHClCHCl$[a]	20°	35.58		$0.444\lambda^2$
$CFCl\cdot CH_2$[b]	gas	36.65	0.085±0.015	$0.428\lambda^2$
C_6H_5Cl[a]	77°	34.62		$0.350\lambda^2$
o-$C_6H_4Cl_2$[c]	77°	35.58–35.82		$0.350\lambda^2$
m-$C_6H_4Cl_2$[c]	77°	34.81–35.03		$0.350\lambda^2$
p-$C_6H_4Cl_2$[c]	77°	34.78	0.08 ±0.02	$0.350\lambda^2$
C_6Cl_6[d]	77°	38.38–38.49		$0.350\lambda^2$
p-$C_6H_4ClCH_2Cl$[c]	77°	34.57	0.07 ±0.02	$0.350\lambda^2$
p-$C_6H_4ClNH_2$[c]	77°	34.15	0.06 ±0.03	$0.264\lambda^2$
$COCl_2$[a,e]	77°	35.58–36.23	0.25 ±0.03	$1.158\lambda^2$

[a] R. Livingston, J. Phys. Chem. **57**, 496 (1952); J. Chem. Phys. **19**, 1613 (1951).
[b] Bragg, Madison, and Sharbaugh, Phys. Rev. **77**, 148 (1950).
[c] H. C. Meal, J. Am. Chem. Soc. **74**, 6121 (1952); (private communication).
[d] Weatherly, Davidson, and Williams, J. Chem. Phys. **21**, 761 (1953).
[e] See reference 12.

[4a] H. C. Meal (private communication).
[5] L. Schiff, *Quantum Mechanics* (McGraw-Hill Book Company, Inc., New York, 1949), p. 154.

atom no longer has exactly two electrons. The electron loss ρ is $\lambda^2/(\frac{3}{2})^2=0.444\lambda^2$. A similar calculation for 1-fluoro-1-chloroethylene using the values, $\beta_{CF}=\beta/2$ and $\alpha_F=\frac{3}{2}\beta$ results in $\rho=0.428\lambda^2$. The data in Table II shows only that within experimental error η for vinyl chloride, 1-fluoro-1-chloroethylene, and even paradichlorobenzene are all about the same, which is at least consistent with the weak interaction theory.

To see how ρ can vary it is interesting to make computations on the polyenes for which the eigenfunctions and eigenvalues are very well known.[6] The results in Table III illustrate one striking feature, namely, the high positive charge on the chlorine atom at the end of a polyene chain.

While a measurement of η is the most rigorous way to measure the effects of double-bond character, one might expect to find similar results from the quadrupole resonance frequency itself. In practice effects on the frequency will be very hard to demonstrate, as they must be effects due only to *differences* of double-bond character. Consider the case of 1-chlorobutylene-1 and 1-chlorobutadiene, molecules in which the carbon-chlorine σ bonds must be very similar. The difference in

TABLE III. Chlorine π electron loss in chloro-$CH_2(CH)_{2n}CH_2$.

	Position of Cl atom[a]				
n	1	2	3	4	5
0	0.444				
1	0.581	0.360			
2	0.743	0.365	0.528		
3	0.805	0.365	0.619	0.512	
4	0.840	0.354	0.648	0.478	0.556

[a] Each entry should be multiplied by λ^2.

double bond character will produce—by using Tables I and III, and the value $\lambda=\frac{1}{3}$—a difference of coupling constant of only 0.8 Mc/sec. Such an effect is only slightly larger than the so far unpredictable effects due to differences in crystallographic site.

6. ARYL CHLORIDES

(a) Correlation between Double Bond Character and Reactive Positions in Polynuclear Hydrocarbons

The formula for ρ_r (Eq. (7)) can be applied to the aryl halides with some confidence because of the semiquantitative agreement of the molecular orbital theory of hydrocarbons with experiment. The results in Table IV exhibit a correlation between the magnitude of ρ_r and the reactivity of the position r of the hydrocarbon. This connection can be understood qualitatively. We expect the chlorine π electrons to resonate best with the hydrocarbon states which have close to the same energy. ρ will be larger then if there exists a low-lying excited state in which there is a large probability of the

[6] E. Huckel, Z. Physik **76**, 628 (1932).

TABLE IV. Chlorine π electron loss in aryl chlorides.

Position of Cl atom[a]	1	2	3	4	5	9
Benzene	0.350					
Naphthalene	0.442	0.371				
Anthracene	0.397	0.373				0.605
Phenanthrene	0.432	0.365	0.382	0.411		0.443
Naphthacene	0.506	0.426			0.542	

[a] Each entry should be multiplied by λ^2.

electron being at the given carbon atom. However, this is also a condition for ease of electron promotion (triplet state formation) or for maximum stability of an added electron.†

A reasonable correlation has been suggested[7] between the reactivity and self-polarizability of an atom in an aromatic hydrocarbon. The self-polarizability of a carbon atom in an aromatic hydrocarbon is mathematically similar to the π electron loss of a chlorine atom attached to that atom in the corresponding chloroderivative.

(b) The Chlorobenzenes

The data on chlorobenzene, the dichlorobenzenes, and hexachlorobenzene show that the quadrupole coupling constants increase on the addition of chlorine atoms to the benzene nucleus. Duchesne and Monfils[8] have suggested that the increase is due solely to a decrease in double bond character. If all the chlorine atoms are at equivalent positions, then by using Eq. (18)

$$\rho^{(4)}=\rho^{(2)}-6n\lambda^4\sum_i \frac{c_{ir}^4}{(\epsilon_i-\epsilon_{Cl})^4},$$

which is the equation implicit in the Duchesne-Monfils suggestion. The difficulty is that the fourth order effects are tiny and the effect of decreasing ionic character also produces an increase in coupling constant.

Interpretation of the data is complicated by the twisting effect discovered by Bastiansen and Hassel.[9] Namely, in orthochlorobenzene the carbon-chlorine bonds presumably due to chlorine-chlorine, repulsions are above and below the plane of the ring at 18° angles. Duchesne and Monfils concluded that the increase in coupling constant of 1.0–2.0 Mc‡ in going from meta-dichlorobenzene to orthodichlorobenzene was due to a decrease in double bond character of the latter. However, if one accepts the weak $\pi-\pi$ interaction point of view, the entire contribution of the double bond character to the coupling constant is only of the order of 2 Mc so that a twist of 18° out of the plane must produce a much smaller effect. Moreover, the coupling constant of

† See reference 6, p. 640, for an interesting example.

[7] C. A. Coulson and H. C. Longuet-Higgins, Proc. Roy. Soc. (London) **192**, 16 (1947).

[8] J. Duchesne and A. Monfils, J. Chem. Phys. **22**, 562 (1954).

[9] O. Bastiansen and O. Hassel, Acta Chem. Scand. **1**, 489 (1947).

‡ The range of couplings is given because in each of these solids there are four different resonance frequencies.

cis-dichloroethylene whose C—Cl bonds are likely to be similarly twisted is about 1.2 Mc *less* than the trans isomer.

The most reasonable explanation of the rise in coupling constant is the inductive effect, that is, a decrease in ionic character caused by increase in the number of electron seeking chlorine atoms. Inductive effects decrease with distance which is consistent with the trend in coupling constants in the chlorobenzenes.

7. HETEROSUBSTITUTED MOLECULES

(a) Chloroderivatives of Substituted Benzenes

A molecular orbital treatment of heterosubstituted benzenes is beset by a multiplicity of parameters and by a doubtful validity of the underlying theory. Nevertheless, to make a rough guess as to what might be observed computations were made for typical benzene derivatives. All resonance integrals (except β_{CCl}) were taken equal to the carbon-carbon resonance integral and the Coulomb integrals were assigned according to Eq. (5). The ρ values calculated are shown in Table V.

The results can be understood in terms of valence bond structures. π electron sources such as OH or NH_2 supply electrons to the *ortho-* and *para*-positions, which diminishes the flow of π electrons from the chlorine atom into the ring at these points. π electron sinks, such as CHO, NO_2, withdraw electrons primarily from the *ortho-* and *para*-positions, which increases the flow of electrons from chlorine atoms attached at these positions.

The double-bond character in chloranil is so large that perturbation theory fails and ρ had to be computed via Eq. (3) rather than Eq. (7). ($\lambda=\frac{1}{3}$ was used.) The easily hydrolyzed chlorine atoms in picryl chloride and chloranil appear to form bonds with considerable double bond character (~8 and 18 percent, respectively). We conclude that either double-bond character of a carbon chlorine bond is not linked with reactivity toward hydrolysis or that the mechanism of reaction of chlorobenzene differs from that of picryl chloride.

An extension of these computations might include the π electron inductive effects as treated, for example, by Jaffe.[10] The discovery by Meal (reference c, Table II) and Bray and Esteva[11] of a correlation between chlorine resonance frequencies and Hammett's substituent parameter σ could not however be explained by such an extension. Basically the resonance frequencies vary from molecule to molecule because of the inductive effects on the σ electron distribution and not in general on changes in the π electron distribution.

TABLE V. π electron loss in benzene derivatives.

Compound	Position of Cl atom *ortho*	*meta*	*para*
Nitrochlorobenzene	$0.507\lambda^2$	$0.346\lambda^2$	$0.491\lambda^2$
Metadinitrochlorobenzene	$0.667\lambda^2$	$0.342\lambda^2$	$0.644\lambda^2$
Picryl chloride	$0.803\lambda^2$		
Chlorobenzaldehyde	$0.573\lambda^2$	$0.345\lambda^2$	$0.554\lambda^2$
Chloranil	0.179		
Chloroaniline	$0.291\lambda^2$	$0.344\lambda^2$	$0.264\lambda^2$
Chlorophenol	$0.300\lambda^2$	$0.346\lambda^2$	$0.283\lambda^2$
Chlororesorcinol	$0.240\lambda^2$	$0.342\lambda^2$	0.243λ

[10] H. H. Jaffe, J. Chem. Phys. **20**, 279 (1952).
[11] P. J. Bray and D. Esteva, J. Chem. Phys. **21**, 570 (1954).

(b) Acyl Chlorides

By using the parameters $\beta_{CO}=\beta$ and $\alpha_O=-\beta$, the π electron loss for the Cl atom of the group $-\overset{\|}{\underset{O}{C}}-Cl$ is $1.158\lambda^2$, which corresponds, if $\lambda^2\sim0.1$, to 10–15 percent double-bond character. The gas[12] and solid phase (reference a Table II) data on phosgene indicates that $\eta=0.25\pm0.03$ which checks the magnitude of λ. The double-bond character is much greater than in the vinyl halides because of the electron affinity of oxygen. In an acyl halide $R-\overset{\|}{\underset{O}{C}}-Cl$, where R is unsaturated, a diminished double bond character is expected because of the additional source of π electrons in the system. For benzoyl chloride we find $\rho=1.110\lambda^2$.

8. ADDITIONAL EVIDENCE AND CONCLUSIONS

The foregoing description of the conjugated carbon chlorine bond can be rephrased using the valence bond structures for chlorobenzene, i.e., normal covalent, ionic, and doubly bonded structures. The inference from nuclear quadrupole coupling asymmetries is that double-bond structures are a much smaller component of the ground state than was previously believed.[1,2] The effects attributed to these structures—decreased dipole moments and bond lengths as compared to alkyl halides—can be ascribed to a decrease in the importance of the ionic structure because of the increased electronegativity of an sp^2 carbon atom orbital.§

The increase in the electronegativity of a carbon orbital with increase in *s* character results in (1) a smaller effective atomic radius and therefore decreased bond length with respect to any attached atom, (2) a loss of charge of the hydrogen atom of the C—H bond and therefore an increase in acidity, and (3) a decreased ionic character of the C—Cl bond and therefore an increase in quadrupole coupling constant. Table VI illustrates these points.

That the conjugation of a chlorine atom with an adjacent aromatic system is small is also shown by (1) the inferior *ortho-para*-directive power of a halogen atom as compared with an NH_2 or OH group, (2) the equality, within experimental error, of the heats of hydrogenation of ethylene, and vinyl chloride, and (3) the relatively poor overlap of the carbon $2p\pi$ with the chlorine $3p\pi$, bromine $4p\pi$, or iodine $5p\pi$ functions.

[12] G. W. Robinson, J. Chem. Phys. **21**, 1741 (1953).
§ Reference 3, p. 206.

TABLE VI. Variation of molecular properties with hybridization.

Hybridization	Compound	X=H		X=Cl		X=Br		X=I	
		r_{C-H}	pK_A	r_{C-Cl}	$-eqQ^{35}$	r_{C-Br}	eqQ^{81}	r_{C-I}	$-eqQ^{127}$
sp	XCN	1.06	8.7	1.63	83.2	1.79	573.5	2.00	2420
sp	XCCH	1.06	22	1.63	79.7	1.79[a]	539[a]	1.99[a]	2230[a]
sp^2	$XCHCH_2$	1.08		1.69	67.2	1.88[b]	442[b]		1877
sp^3	XCH_2CH_3	1.09	(43)	1.76	66.0	1.94	415.6	2.13	1647

[a] These data are for the methylhaloacetylenes.
[b] These data are for the halobenzenes. Bond lengths are in A and coupling constants in Mc/sec.

Interpolating in the published tables,[13] one finds the overlap integrals are 0.272 (C−C), 0.128 (C−Cl), and 0.134 (C−I).

What has been said for the carbon-chlorine bond applies *a fortiori* to the carbon-bromine and carbon-iodine bonds. Some miscellaneous evidence points to this fact. For example, η is 0.023 in CHICHI[14] *versus* 0.07±0.03 for CH_2CHCl. In paradibromobenzene (DBB) the Br^{79} frequency at 77°K is 270.97 Mc/sec[15] but in 9,10-dibromoanthracene (DBA) there are two transitions at 272.98 and 275.05 Mc/sec. If there were 4 percent double-bond character in DBB as there is in paradichlorobenzene, we would expect to find in DBA 7 percent double-bond character and a frequency 2.9 Mc/sec *lower*. The data are consistent with a very small double bond character.

APPENDIX. AN INTEGRAL REPRESENTATION FOR ρ

Coulson and Longuet-Higgins[16] derived the following expression for the π electron charge on any atom s:

$$q_s=1-\frac{1}{\pi}\int_{-\infty}^{\infty}\frac{\Delta_{s,s}(iy)}{\Delta(iy)}dy. \qquad \text{(A1)}$$

Δ is the secular determinant for the entire molecule and $\Delta_{st\cdots,pq\cdots}$ is the determinant minus rows s, t, $\cdots$ and columns p, q, $\cdots$. The energy in the secular equation is replaced by iy.

For an aromatic molecule with a chlorine atom attached to atom r,

$$\Delta(iy)=(\alpha_{Cl}-iy)\Delta_{Cl,Cl}(iy)-\lambda^2\beta^2\Delta_{Cl\,r,Cl\,r}(iy). \qquad \text{(A2)}$$

After this expression is substituted in (A1), the integral can be expanded in powers of λ^2, with the result

$$q_{Cl}=1-\frac{1}{\pi}\int_{-\infty}^{\infty}\frac{dy}{\alpha_{Cl}-iy}-\lambda^2\beta^2 \times\int_{-\infty}^{\infty}\frac{dy}{(\alpha_{Cl}-iy)^2}\frac{\Delta_{Cl\,r,Cl\,r}(iy)}{\Delta_{Cl,Cl}(iy)}+\cdots. \qquad \text{(A3)}$$

The value of the first integral is $-\pi$, so that

$$\rho_{Cl}=2-q_{Cl}\cong\frac{\lambda^2\beta^2}{\pi}\int_{-\infty}^{\infty}\frac{dy}{(\alpha_{Cl}-iy)^2}\frac{\Delta_{Cl\,r,Cl\,r}(iy)}{\Delta_{Cl,Cl}(iy)}. \qquad \text{(A4)}$$

In the present work solution of the secular equations was performed on a punched card calculator. However, for molecules with complex secular determinants, evaluation of (A4) would be easier than solution of a secular equation; moreover, the variation of ρ with α_{Cl} could be investigated more directly through the use of (A4) and its derivatives.

[13] Mulliken, Rieke, Orloff, and Orloff, J. Chem. Phys. **17**, 1248 (1949).
[14] H. G. Dehmelt, Naturwissenschaften **37**, 398 (1950).
[15] P. J. Bray and R. G. Barnes, **22**, 2023 (1954).
[16] C. A. Coulson and H. C. Longuet-Higgins, Proc. Roy. Soc. (London) **A191**, 39 (1947).

Letters to the Editor

THIS section will accept reports of new work, provided these are terse and contain few figures, and especially few half-tone cuts. The Editorial Board will not hold itself responsible for opinions expressed by the correspondents. Contributions to this section should not exceed 600 words in length and must reach the office of the Editor not later than the 15th of the second month preceding that of the issue in which the Letter is to appear. No proof will be sent to the authors. A publication charge of $10.00 per Letter is made which, when honored, will entitle the Institution to 100 free reprints.

Note on Solutions of Linear Polyelectrolyte Molecules

FUMIO OOSAWA AND NOBUHISA IMAI
Department of Physics, Faculty of Science, Nagoya University, Nagoya, Japan
(Received September 30, 1954)

MOST theories of solutions of linear polyelectrolyte molecules have dealt only with their intrinsic porperties.[1-5] The purpose of this note is to present a simple method of treating these solutions of finite concentrations and to analyze the origin of the extensive force of molecules.

Let us write the number of polyelectrolyte molecules in the solution of volume V as N and that of added low-molecular uni-univalent salts as J. Each polyelectrolyte molecule with n ionized groups of charge $-e_0$ occupies an apparent volume v. Supposing that n_+ counter-ions are retained in this volume by the strong Coulomb attraction with ionized groups, their average concentration is written as (n_+/v). The average concentration of counter-ions outside v's is $[J+(n-n_+)N]/(V-Nv)$. The potential difference between the inside and the outside of v may be approximated by $(n^*e_0/DkTa)$; D is the dielectric constant of the solvent, a the apparent radius of $v[v=(4\pi/3)a^3]$, and $n^*=n-n_++n_-$; n_- is the number of by-ions in v. Then to the distribution equilibrium of counter-ions the relation

$$n_+/v=[J+(n-n_+)N]/(V-Nv)\exp(n^*e_0^2/DkTa) \quad (1)$$

may be applied. Similarly

$$n_-/v=(J-n_-N)/(V-Nv)\exp(-n^*e_0^2/DkTa). \quad (2)$$

From these, for example, at low concentrations of salts

$$(p-p^*)/(p_0+p^*)=c/(1-c)\exp p^*; \quad (3)$$

at low concentrations of polyelectrolytes

$$(p-p^*)+[(p-p^*)^2+4c^2p_0^2]^{\frac{1}{2}}/2p_0=c\exp p^*; \quad (4)$$

where $p=ne_0^2/DkTa$, $p_0=(J/nN)p$, and $c=Nv/V$ (the apparent volume concentration). Thus $p^*[=(n^*/n)p]$ or n^*, which determines various properties of the solution,[6] is known as the function of these quantities (Fig. 1). These results, derived from the idea of chemical equilibria, include those which were obtained by analyzing the Poisson-Boltzmann equation without using the Debye-Huckel approximation and supported by experimental results.[7]

In the same order of approximations the extensive force of the polyelectrolyte molecule is found to be composed of two parts.[7,8] The one P_1 is due to the Coulomb repulsion of its net charge $-n^*e_0$:

$$P_1/kT=\tfrac{1}{2}n^{*2}e_0^2/DkTa^2(da/dv)=(\tfrac{1}{6})n^*p^*/v. \quad (5)^9$$

The other P_2 is the result of the osmotic pressure, being approximately proportional to the concentration difference of ions

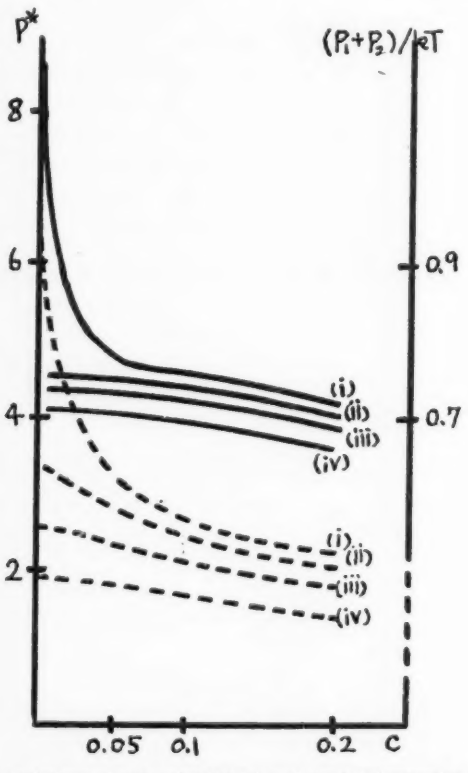

FIG. 1. Relations of $p^*(=n^*e_0^2/DkTa)$ and the total extensive force to the apparent volume concentration in dilute salt solutions of various concentrations. ——: $(P_1+P_2)/kTv/n$; – – –: p^*; (i): $J/nN=0$; (ii): $J/nN=1/50$; (iii): $J/nN=1/20$; (iv): $J/nN=1/10$.

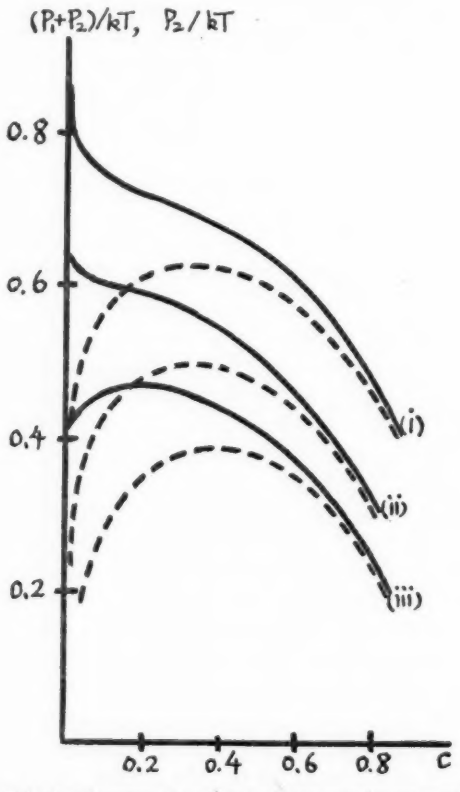

FIG. 2. Relations between the extensive forces and the apparent volume concentration at various values of $p(=ne_0^2/DkTa)$ in solutions without added salts. ——: $(P_1+P_2)/kTv/n$; – – –: $P_2/kTv/n$; (i): $p=7$; (ii): $p=4$; (iii): $p=2.5$.

inside and outside v:

$$P_2/kT=(n_++n_-)/v-[2J+(n-n_+-n_-)N]/(V-Nv). \quad (6)^9$$

(P_1+P_2) is balanced with the contractive force P_3. The entropy force P_2 contributes to (P_1+P_2) much more than the energy force P_1 except at small values of both c and J/nN (Figs. 1 and 2). In salt-free or dilute salt solutions, at constant p and p_0, P_2 takes maxima at $c=0.2$ to 0.5. Such values of c perhaps correspond to quite small net concentrations. (When $J=0$, $P_2/kT=(n/v)\times[1-(n^*/n)(1/1-c)]$ and maxima of P_2 mean minima of the activity coefficient of counter-ions $(n^*/n)(1/1-c)$.[7]) Generally, (P_1+P_2) decreases with increasing c throughout, suggesting the decreasing extension of the molecule. These behaviors of forces meet our expectations based upon experimental results,[10] although quantitatively, owing to rough approximations, Eqs. (5) and (6) gives too much extended forms of the molecule. It is notable that, under suitable values of p and p_0, even (P_1+P_2) sometimes takes maxima, suggesting the maximum extension, at intermediate values of c (Fig. 2).

For small c and large J, expanding (P_1+P_2) in the power series of $nV/Jv(=\beta)$ and employing Flory's expression of P_3,[5]

$$\alpha^5-\alpha^3=n[(1/4)\alpha^3\beta-(5/24p)\beta^2-(1/64-7/48p^2)\beta^2+\cdots], \quad (7)$$

where $v=\alpha v_0$. The first term, coming from P_2, is equivalent to results by the Debye-Huckel and Donnan approximations.[1,5] The higher order terms, containing contributions of P_1, deviate from those results. At high concentrations of salts, P_1/P_2 becomes $n^*/6n$.[8]

The authors wish to express their sincere thanks to Professor P. J. Flory and Professor I. Kagawa for their valuable discussions.

[1] J. J. Hermans and J. T. Overbeek, Rec. trav. chim. **67**, 761 (1948).
[2] Katchalsky, Kunzle, and Kuhn, J. Polymer Sci. **5**, 283 (1950).
[3] A. Katchalsky and S. Lifson, J. Polymer Sci. **11**, 409 (1953).
[4] Kimball, Cutler, and Samelson, J. Phys. Chem. **56**, 57 (1952).
[5] P. J. Flory, J. Chem. Phys. **21**, 162 (1953).
[6] A. Katchalsky, J. Polymer Sci. **12**, 159 (1954).
[7] Oosawa, Imai, and Kagawa, J. Polymer Sci. **13**, 93 (1954). See reference 9.
[8] Asakura, Imai, and Oosawa, J. Polymer Sci. **13**, 499 (1954).
[9] Results similar to Eqs. (5) and (6) can be derived from the free energy given in reference (7).
[10] P. J. Flory, *Principles of Polymer Chemistry* (Cornell University Press, Ithaca, 1953), p. 630.

Spectroscopic Evidence for Stabilized HO_2 Radicals*

PAUL A. GIGUÈRE
Department of Chemistry, Laval University, Québec, Canada
(Received September 13, 1954)

THE existence of HO_2 radicals as intermediate in oxidation reactions has been postulated repeatedly in the past, mostly on the basis of indirect chemical evidence.[1] Recently they have been detected in two independent mass spectrometric investigations of the reaction between atomic hydrogen and oxygen.[2,3] The results of Robertson are particularly convincing as they indicate a 3 to 4 percent conversion of oxygen into HO_2 radicals.

Some time ago we obtained in this laboratory physical evidence of a different nature, which points strongly to stabilization of HO_2 radicals in the dissociation products of water vapor quickly chilled in liquid air. While preparing some D_2O_2 from D_2O vapor dissociated in an electrodeless discharge[4] we noticed that the glassy deposit formed in a liquid air trap always exhibited a distinct color, varying from light yellow to dark brown, depending on the thickness. This faded away upon warming up to around -120°C while at the same time much hydrogen was evolved.

In order to learn more about this glassy deposit its infrared spectrum was examined with a special absorption cell.[5] Besides the well-known bands of ice and solid hydrogen peroxide, a few others were observed, particularly a stong, sharp one at 1305 cm^{-1}. As it appeared unchanged in the deposit from dissociated D_2O, it could not involve vibration of hydrogen atoms nor a lattice mode. On the other hand its frequency is too high for an O—O single bond so that it cannot arise from isomeric molecules H_2O-O[6] as was first believed.[5]

Assuming, as seems logical, that the maximum at 1305 cm^{-1} belongs to oxygen atoms we get by Badger's rule an O—O bond length of 1.30A. Now, the only known instance of such a bond is in the superoxide ion O_2^- for which values of 1.28 to 1.31A have been found by x-ray diffraction of the alkali superoxide MO_2.[7,8] The electronic structure of that ion involves a three-electron bond[9] $[:\dot{O}\cdots\dot{O}:]^-$ and such would be expected normally in the HO_2 radical.

Minkoff[1] has calculated potential energy surfaces[10] for the system H···O···O assuming Coulombic energy contributions of 15, 20, and 25 percent. He has also estimated the force constants and vibrational frequencies of HO_2, and for the O—O stretching he found a value, 1300 cm^{-1}, in perfect agreement with that in the glassy deposit. His calculated O—H frequencies are admittedly less accurate because he assumed the radical to be linear (as required by the method). A bent configuration is much more likely by analogy with the hydrogen peroxide molecule.[11] The same conclusion is borne out by electronic orbital correlations[12] for a 13-electron HAA molecule in the ground state. Incidentally it also agrees with the observation that the frequency of the band at 1305 cm^{-1} is not noticeably altered by substitution of deuterium for hydrogen.

There is, as yet, no sure indication of distinct O—H frequencies belonging to the HO_2 radical in the spectrum of the deposit but this is not surprising as they would be overlapped by those of water and hydrogen peroxide always present in much larger quantities. Finally it may be noted here that the color of the glassy deposit finds a ready, if not unique, explanation in the eventuality of free radicals. All the above constitute particularly strong evidence for stabilization of HO_2 in a glass lattice at low temperature. The original objection[5] based on unfavorable stoichiometric ratio in the reacting mixture may be overruled on account of the reaction

$$2\,OH+M=H_2+O_2+M$$

which always occurs to some extent on the walls. This could also explain why essentially the same results are obtained with dissociated water vapor as with atomic hydrogen and oxygen. Work is continuing with the same technique, on both of these systems.

* Presented at the Annual Conference of the Chemical Institute of Canada, Toronto, June, 1954. The experimental work on which this paper is based has been reported elsewhere (see reference 5).
[1] G. J. Minkoff, Discussions Faraday Soc. **2**, 151 (1947).
[2] S. N. Foner and R. L. Hudson, J. Chem. Phys. **21**, 1608 (1953).
[3] A. J. B. Robertson, Conference on Mass Spectrometry, Institute of Petroleum, London 1953; Paper No. 11.
[4] Giguère, Secco, and Eaton, Discussions Faraday Soc. **14**, 104 (1953).
[5] P. A. Giguère and E. A. Secco, J. phys. radium **15**, 508 (1954).
[6] K. H. Geib and P. Harteck, Berichte **65**, 1551 (1932).
[7] W. Kassatochkin and W. Kotow, J. Chem. Phys. **4**, 458 (1936).
[8] G. S. Zhdanov and Z. V. Zvonkova, Doklady Akad. Nauk. S.S.S.R. **82**, 743 (1952).
[9] L. Pauling, *The Nature of the Chemical Bond* (Cornell University Press, Ithaca, 1939).
[10] Glasstone, Laidler, and Eyring, *The Theory of Rate Processes* (McGraw-Hill Book Company, Inc., New York, 1941).
[11] W. G. Penney and G. B. B. M. Sutherland, J. Chem. Phys. **2**, 492 (1934).
[12] A. D. Walsh, J. Chem. Soc. **1953**, 2288.

Resonance Energy of Graphite

G. S. COLLADAY
Michelson Laboratory, U. S. Naval Ordnance Test Station,
Inyokern, China Lake, California
(Received September 13, 1954)

IN a recent Letter to the Editor, Barrow[1] obtained the value of 10 kcal per g atom for the empirical resonance energy per carbon atom, W_R(emp), of graphite. In obtaining this value for W_R(emp), use was made of an empirical equation for the heats of formation of hydrocarbons at 25°C. Barrow then compared

the 25°C W_R(emp) with a theoretical expression for the resonance energy of graphite, W_R(theory), calculated by Wheland.[2] We concur with Barrow in the empirical determination of the resonance energy, except that we choose to replace his empirical equation for the heats of formation of hydrocarbons at 25°C by a similar expression due to Mulliken and Parr[3] which gives good agreement for nonresonating hydrocarbons at 0°K.[4] Using 2 kcal per gm atom for the interlayer binding energy of graphite,[1] and using Mulliken and Parr's relation

$$H_F°(O°K) = -3.55N_{C-H} + 5.00N_{C-C} + 28.72N_{C=C} - 0.78n - W_R(\text{emp}), \quad (1)$$

with the appropriate values of 1, ½, 8 for N_{C-C}, $N_{C=C}$, n, respectively, one obtains 11 kcal per g atom for W_R(emp).

The resonance energy of a molecule is defined as the difference in its energy when described on one hand by a Kekule structure and on the other by the actual conjugated structure, i.e., W_R(theory) $= W_K - W_A$. In the quantum-mechanical calculation of W_K for graphite one uses a reference state with noninteracting single and double bonds, with both the C−C and C=C bond lengths equal to the observed conjugated bond length in graphite. This Kekule reference is certainly higher in energy than the corresponding empirical reference state which contains single and double bonds whose lengths are equal to those in ethane and ethylene, respectively. This difference in reference states has been termed the compression energy C_K[3,5] and is the energy required to shorten C−C bonds and lengthen C=C bonds to the observed conjugated length against their normal restoring forces. Using for ethane and ethylene equilibrium separations of 1.543A and 1.34A, bond dissociation energies of 84.8 kcal/mole and 148 kcal/mole, and force constants (corrected approximately for zero point vibration) of 4.73×10^5 dynes/cm and 10.36×10^5 dynes/cm, Morse potential curves were constructed. Assuming the single and double bonds in Kekule graphite to behave under compression and extension as do single bonds in ethane and double bonds in ethylene, one obtains $C_K = 8.5$ kcal/g atom.

Before making a comparison between W_R(theory) and W_R(emp), W_R(theory) must be corrected by the amount C_K, i.e.,

$$W_R(\text{theory}) - C_K = W_R(\text{emp}). \quad (2)$$

In his calculation of W_R(theory) Wheland included the resonance integral β_1 between nearest neighbor carbon atoms in the plane, but neglected all overlap integrals. In this approximation

$$W_R(\text{theory}) = 0.574\beta_1. \quad (3)$$

If one includes the overlap integral S_1 between nearest neighbor carbon atoms in the plane, the result is

$$W_R(\text{theory}) = 0.069\alpha + 0.289\beta_1 \quad (4)$$

$$\alpha = \int X_i H X_i d\tau,$$

$$\beta_1 = -\int X_i H X_{i\pm1} d\tau,$$

$$S_1 = \int X_i X_{i\pm1} d\tau = 0.239.$$

The wave function describing a π electron has been taken to be a linear combination of the atomic orbitals X_i. H is the one-electron Hamiltonian for the π electrons and the Coulomb integral α is the energy a π electron would have were it to remain in the vicinity of carbon atom i. If one further includes the overlap S_2 and the resonance integral β_2 between second nearest neighbors in the plane, the result is

$$W_R(\text{theory}) = 0.0663\alpha + 0.2789\beta_1 - 0.0112\beta_2, \quad (5)$$

$$\beta_2 = -\int X_i H X_{i\pm2} d\tau,$$

$$S_2 = \int X_i X_{i\pm2} d\tau = 0.032.$$

The overlap integrals S_1 and S_2 were evaluated from tables in reference 6. Combining Eqs. (2) and (5), one has an equation relating the three energy parameters α, β_1, and β_2:

$$0.0663\alpha + 0.2789\beta_1 - 0.0112\beta_2 = 0.846, \quad (6)$$

where the unit of energy is an electron volt. Details of the above calculations will be published elsewhere.

[1] G. M. Barrow, J. Chem. Phys. **22**, 953 (1954).
[2] G. W. Wheland, J. Chem. Phys. **2**, 474 (1934).
[3] R. S. Mulliken and R. G. Parr, J. Chem. Phys. **19**, 1271 (1951).
[4] "Selected Values of Properties of Hydrocarbons," API Research Project 44, National Bureau of Standards, Washington, D. C. (1949).
[5] Mulliken, Rieke, and Brown, J. Am. Chem. Soc. **63**, 41 (1941).
[6] Mulliken, Rieke, Orloff, and Orloff, J. Chem. Phys. **17**, 1248 (1949).

Multilayer Adsorption of Water near Saturation Pressure on Plane Glass Surfaces

U. GARBATSKI AND M. FOLMAN
Laboratory of Physical Chemistry, Technion, Israel Institute of Technology, Haifa, Israel
(Received October 8, 1954)

THERE is considerable interest in measuring adsorption of vapors on plane surfaces at relative pressures near unity. As the amounts adsorbed are necessarily small, comparatively little work has been done on it, chiefly indirectly by optical methods using the reflection of polarized light,[1,2] and by the method of McHaffie and Lenher[3] using the change of pressure with temperature of known amounts of vapor enclosed in a vessel.

We measured the adsorption of water vapor on glass by changes in capacity. Two microscope cover glasses (Corning Glass) were cemented to metal holders that constituted the two plates of a condenser. This condenser was introduced into a glass vessel connected to a bulb containing aqueous solutions of known capacity. By using different concentrations relative pressures up to 0.9976 were obtained.

The difference in the capacities of the condenser *in vacuo* and in equilibrium with the water vapor was measured with an accuracy better than 0.001 $\mu\mu$f. The frequency used was 5.3 Mc. Thermostating was better than 0.001°C. The cementing was done with baked Araldite and was bubble free. The glass surfaces were cleaned with detergent (Teepol solution) and dilute HNO_3 and rinsed several hours with twice distilled water.

The thicknesses of the absorbed layers were calculated under the assumption that dielectric constant[4] and density are those of water in bulk and the surface identical with the geometric surface.

At 30°C we found values varying from 620 A at $P/P_0 = 0.9976$ to 37 A at $P/P_0 = 0.505$. We don't ascribe too much significance to the smaller thicknesses measurable at still lower relative pressures, as here our assumptions seem questionable.

The dielectric constant of water adsorbed under the conditions of our experiment, if different at all from the value in bulk, should be lower, so that the thicknesses calculated here represent minimum values.

Equilibrium of adsorption was reached in 30–50 sec in thin layers and in a few minutes for the thickest layers. This time lag is ascribed by us to the need of getting rid of the heat of adsorption, as the smallest rise in temperature of the plates will already change significantly the relative pressure, especially one near unity.

Our results show in our opinion, once more, multilayer adsorption as an incontravertible physical fact. It seems to us that a continuous transition from adsorption at high relative pressures to condensation may be established.

Further work with the same method using different vapors and different adsorbent surfaces is under way. A full description of our method and discussion of the results will appear shortly.

[1] M. N. Fraser, Phys. Rev. **33**, 97 (1929); **34**, 644 (1929).
[2] B. V. Deryagin *et al.*, Chem. Abs. **46**, 4881 (1952).
[3] I. R. McHaffie and S. Lenher, J. Chem. Soc. **127**, 1559 (1925).
[4] Waldman, Snelgrove, and McIntosh, Can. J. Chem. **31**, 998 (1953).

Paramagnetic Resonance Absorption of Violanthrone and Violanthrene

Y. YOKOZAWA AND I. TATSUZAKI
The Research Institute of Applied Electricity, Hokkaido University, Japan
(Received September 20, 1954)

THE diamagnetic susceptibilities and anisotropies of condensed polynuclear aromatic hydrocarbons have been measured by Akamatu and Matsunaga,[1] their results for the violanthrone and the violanthrene being shown in Table I in which the small diamagnetic anisotropy of the violanthrone compared with that of the violanthrene is noteworthy.

Present investigation was undertaken to examine a view that this small diamagnetic anisotropy was due to the cancellation by the hidden paramagnetism involved in the violanthrone. This hidden paramagnetism was detected by the method of microwave paramagnetic resonance absorption using a 3.2-cm wave at room temperature. The magnetic absorption was measured using a rectangular reflecting cavity operating in TE_{012} mode. To eliminate the crystal detector noise at audio-frequencies, the reflected power was balanced using a magic tee to a level at which superheterodyne receiver and a local oscillator, followed by a intermediate-frequency amplifier at 30 Mc/sec, could be used.

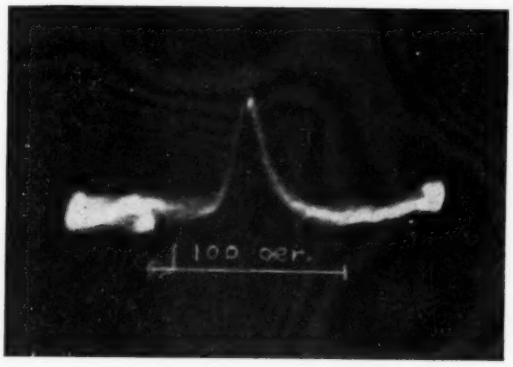

FIG. 1. Oscilloscope trace: absorption spectrum of violanthrone.

The absorption of the violanthrene is also observed (see Fig. 1). The g values, half-widths $\Delta H_{\frac{1}{2}}$, and magnetic susceptibilities are shown in Table II.

The paramagnetic part of the susceptibility involved in the violanthrone was obtained from a comparison of the integrated intensity of the absorption curve with that of a single crystal of $CuSO_4 \cdot 5H_2O$. The absorption intensity of the violanthrene was very small, and the paramagnetic contribution to the total magnetic susceptibility could be neglected. By adding these contributions, the results are obtained: diamagnetic part of the susceptibility $-\chi_M = 264 \times 10^{-6}$, diamagnetic anisotropy $-\Delta K = 330 \times 10^{-6}$ and averaged π orbital radius $(\bar{r}^{-2})^{\frac{1}{2}} = 1.5$, 1A in the violanthrone. These magnitudes are the same orders with those of the violanthrene. Assuming this paramagnetism is originated

TABLE I. Diamagnetic susceptibilities and anisotropies of violanthrone and violanthrene.

	Mole suscept. $-\chi_M \cdot 10^6$	Anisotropy per mole $-\Delta K \cdot 10^6$	Average orbital radius $(\bar{r}^2)^{\frac{1}{2}}$ (A)
Violanthrone	204.8	141	1.05
Violanthrene	273.5	320	1.49

TABLE II. Paramagnetic resonance data.

	g	$\Delta H_{\frac{1}{2}}$ (Oer)	Paramag. suscep. per mole $\chi \cdot 10^6$
Violanthrone	2.00	15	63
Violanthrene	2.00	13	

in unpaired π electrons, the fractional magnetic population of these π electrons x is obtained from the relation,

$$\chi = \frac{Nxg^2\beta^2 S(S+1)}{3kT},$$

where N is Avogadro's number. From this equation, it is found $x \simeq 1/100$.

The authors are greatly indebted to Professor Akamatu for providing them with these organic compounds.

[1] H. Akamatu and Y. Matsunaga, Bull. Chem. Soc. Japan **26**, 364 (1953).

Exchange Potential in the Statistical Model of Atoms*

C. J. NISTERUK AND H. J. JURETSCHKE
Polytechnic Institute of Brooklyn, Brooklyn, New York
(Received October 7, 1954)

THE statistical model of the atom which includes the free-electron exchange potential of Dirac[1] has the shortcoming that it leads to electron distributions decreasing to zero discontinuously at a finite radius R_0 from the nucleus.[2] We want to report some results obtained with a model based on a modification of Dirac's potential in the atomic surface region.[3]

The exchange potential can be interpreted as the potential arising from a distribution of unit positive charge, the exchange hole. Slater[4] has given a simplified expression for such a distribution representing an averaged exchange hole common to electrons of all energies. For electrons described by plane waves this exchange hole has spherical symmetry and is always centered at the position of the electron in question. Wave functions proper to atomic boundary conditions yield an exchange hole of considerably more complex shape. In the interior of the atom the hole is concentrated around the electron position. As the electron distance from the nucleus increases the hole tends to remain in the outermost shell, at first concentrated around the nucleus-electron axis but later distributed more uniformly throughout the shell.

This behavior of the hole suggests that in the atomic interior a density dependent free-electron exchange potential is adequate, while in the far outer region of the atom the exchange potential is more nearly that due to a concentrated unit charge located at first near the outermost shell. but approaching the nucleus as the electron moves far away.

We have extended the variational approach of statistical theory to include a simplified exchange potential with the above general properties. If r is the distance of the electron from the nucleus, then for $r \leq R_i$ the exchange potential is given by the usual electron density-dependent expression of Dirac $+e(3n/\pi)^{\frac{1}{3}}$. For $r \geq R_i$ it is represented by a density-independent function continuous with the inner expression at R_i and approaching e/r at large r. R_i is an additional parameter in the variational problem. Its equilibrium value indicates the extent to which the exchange hole follows its electron in an atom.

The differential equation for the density obtained in the variation is identical with that set up by Jensen[5] on physical grounds. The outer boundary condition, derived formally, differs from that assumed by Jensen. It requires that the density vanish continuously at R_0. Thus, the substitution of a density independ-

ent exchange potential near the surface removes in a natural manner the anomaly of the usual Thomas-Fermi-Dirac boundary condition.

The resulting value of R_i depends on the particular function chosen for the density-independent potential. Actually, there is little choice, since, as Jensen has pointed out, the potential is practically completely determined by its boundary values. We have found that, for all reasonable potentials, R_i lies very close to the nucleus. Thus, for Kr, $R_i \gtrsim 0.6a_0$. This results because a potential asymptotic to $1/r$ is stronger than Dirac's potential over most of the atom. In the interior of the atom the same relationship is maintained because the density there is independent of the exact form of the exchange potential.

The small value of R_i indicates that the exchange hole remains stationary near the nucleus for all positions of its electron. Therefore the electron distributions to be expected in this model are not very different from those obtained in the Fermi-Amaldi[6] modification of Thomas-Fermi's theory. Instead of using a reduced effective number of electrons we substitute an increased effective nuclear charge.

The statistical approach does not lead to an asymptotic exchange hole stationary somewhere in the surface region of the atom. This property of the exchange hole in the more exact theory is intimately connected with atomic shell structure, and one may expect that a statistical model will describe atomic surface properties accurately only when it also exhibits shell structure.

* This work has been supported in part by the Office of Naval Research.
[1] P. A. M. Dirac, Proc. Cambridge Phil. Soc. **26**, 376 (1930).
[2] P. Gombàs, *Die statistische Theorie des Atoms* (Springer Verlag, Vienna, 1949) p. 80.
[3] C. J. Nisteruk, M. S. thesis, Polytechnic Institute of Brooklyn (1954).
[4] J. C. Slater, Phys. Rev. **81**, 385 (1951).
[5] H. Jensen, Z. Physik **101**, 141 (1936).
[6] E. Fermi and E. Amaldi, Mem. Accad. Italia **6**, 117 (1934).

Different Ice Forms under Ordinary Conditions*

R. M. VANDERBERG† AND J. W. ELLIS
Department of Physics, University of California, Los Angeles, California
(Received October 1, 1954)

WHILE determining infrared birefringences of single crystals of ice by means of channeled *interference* spectra, it was observed that a group of interference maxima and minima near 2.0μ replaced a similar group recorded a half year earlier at approximately 0.1μ shorter wavelengths. The earlier results were obtained with several crystals grown at that time, the later with a crystal prepared approximately two months before recording the results. A comparison of the *absorption* spectrum of the new crystal with the spectrum which had been recorded of the earlier material also showed a pronounced difference. Fortunately, some of the earlier crystals had been preserved in a refrigerator. When the absorption and birefringence spectra of the older material were now reinvestigated it was found that both had changed so that they conformed with the spectra of the later crystal. Thus it seems that we have had at least two crystal types. We shall designate these earlier and later grown types by A and B, respectively. Although it is certain that the earlier ice changed from type A to type B during, or at some time during, the half year it was in the refrigerator, unfortunately there is no way of knowing whether the later ice had been grown as type B, because no study had been made of it during the first two months of its existence. The original type A material which had changed to type B showed no further spectral changes during the ensuing four months.

All of the crystals used were grown in the following manner. A small seed crystal was cut from a large ice block and was placed on the lower end of an aluminum rod whose upper end projected into a refrigerating unit kept at approximately -10°C. The seed was dipped into a container of distilled water kept at 0°C by an ice jacket. Crystals grown by this method assume a roughly hemispherical shape, exhibiting no plane faces associated with the usual hexagonal nature of the crystal. The orientation of the optic axis is always the same as that of the seed crystal. Working plates of ice were cut from these larger crystals as desired.

Near the end of our experimental program, after the existence of types A and B had been clearly revealed, another crystal was grown and *immediately* studied. Its absorption spectrum, although more nearly like type A than type B, shows distinct differences. Hence we designate it type C. Its absorption spectrum was occasionally recorded over a four months' period but no observable change occurred. It is possible that this type C crystal was grown more slowly than the others. These results indicate that a more detailed investigation of crystal forms of ice could profitably be made, with careful attention to conditions of growth.

The absorption differences among ice types A, B, and C consist of changes in the structure of absorption bands near 2.0μ, presumably associated with hydrogen bridging between water molecules. In general the shift from A to B involves a displacement of certain absorption maxima to longer wavelengths. Whether the change is from greater order to disorder or vice versa in the crystal structure seems impossible to say.

The changes involved are not associated with strain in the crystals. We have subjected ice plates to stress and have shown that the uniaxial form changes to biaxial without any appreciable change in the absorption spectrum or in the dichroism which, contrary to the findings of Plyler,[1] is small or lacking for all wavelengths in the very near infrared, and with only a slight general shift in the channeled spectrum.

Independently of the several well-known forms of ice produced by Bridgman under extreme conditions, references to two forms of ice found under ordinary conditions occur. Thus in the *Handbook of Chemistry and Physics*[2] α and β forms are tabulated, with hexagonal and rhombohedral symmetry, respectively. Seljakov[3] believed he had shown the existence of two forms by means of x-ray diffraction. However, Berger and Saffer[4] think they have demonstrated an error in Seljakov's technique and hence seriously question his interpretations.

* The material of this letter was taken from the Ph.D. thesis of R. M Vanderberg.
† Now at Sacramento State College, Sacramento, California.
[1] E. K. Plyler, J. Opt. Soc. Am. **9**, 545 (1924).
[2] *Handbook of Chemistry and Physics* (Chemical Rubber Publishing Company, New York, 1950–51), 32nd edition, p. 2225.
[3] N. Seljakov, Compt. rend. acad. sci. U.S.R.R. **10**, 293 (1936); **11**, 92 (1936); **14**, 181 (1937).
[4] C. Berger and C. M. Saffer, Science **118**, 521 (1953).

Formation of Negative Ions in Hydrocarbon Gases*

T. L. BAILEY, J. M. MCGUIRE, AND E. E. MUSCHLITZ, JR.
College of Engineering, University of Florida, Gainesville, Florida
(Received August 23, 1954)

IN connection with studies of collisions of gaseous negative ions with neutral molecules,[1] negative ions produced by electron bombardment of methane, ethane, and acetylene gases have been investigated in a mass spectrometer. The ions observed and their relative intensities under similar source conditions are shown in Table I.

TABLE I. Relative negative ion intensities.

Gas	H^-	Mass 25	Mass 12–15	Electron energy
CH_4	120	12	1.5	35 ev
C_2H_6	73	27	0.5	70 ev
C_2H_2	8.5	55	0.0	70 ev
		($100 \cong 10^{-12}$ amp)		

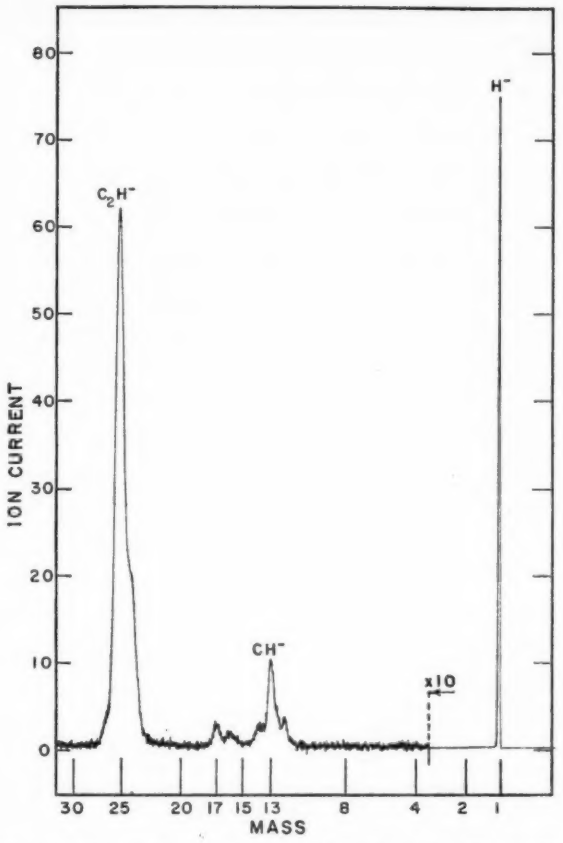

FIG. 1. Negative ion mass spectrum for methane. Amplifier sensitivity has been increased by 10× beyond mass 4. Peaks at mass 16 and 17 are probably O^- and OH^- arising from a small amount of oxygen present in the methane as an impurity.

The ion source, which will be described in detail elsewhere, consisted of two parallel plates maintained at different potentials. Electrons admitted angularly through a slot in the more positive plate (anode) described a parabolic trajectory between the plates. Gas was admitted through a nozzle in the negative plate (repeller) and negative ions formed in the bombardment region were drawn into the focusing electrodes through a hole in the anode opposite the nozzle. The gas pressure behind the nozzle for the data given in the table was 1.85 mm Hg, which was not high enough to produce a discharge between the plates. Electron current to the anode was 3.0 ma and the estimated values given for the electron energy in the source ionization region are probably correct within ±5 ev. The spectrometer employed was a 90°, 6.50 cm radius of curvature instrument similar to an instrument used earlier in the production of positive ion beams.[2] Ionic masses and initial energies above cathode were determined using a rotating coil gaussmeter, whose output emf was linear with the analyzing magnetic field.

In view of the purification to which all three gases were subjected, it appears unlikely that the mass 25 ion originated from impurities in the sample gas. To check this in methane, a purified methane sample was redistilled and mass spectra of both high- and low-boiling cuts were taken. Spectra for both cuts were identical within experimental error and intensities of all ions observed were reduced to zero by cutting off the gas supply. It is doubtful that the mass 25 ion from methane originated from decomposition of a metastable ion, since no higher mass ions were observed and the relative intensities of mass 25, H^-, and masses 12–15 were not changed appreciably as the total ion accelerating potential was varied from about 180 to 385 volts. A typical mass spectrum for methane is shown in Fig. 1.

TABLE II. Mass determinations of C_2H^-.

Gas	1	2	Av.
CH_4	25.1	25.3	25.2
C_2H_6	25.1	25.3	25.2
C_2H_2	25.2	24.8	25.0

We believe the mass 25 ion observed in all three gases to be C_2H^- (see Table II). It must be formed in methane by a multiple collision process. The high intensity of C_2H^- in acetylene indicates strongly that in this case these ions are formed by simple electron collisions. The stability of gaseous C_2H^- is not surprising in view of the known acidic nature of acetylene.

The ions observed in methane in the mass range 12–15 are probably C^-, CH^-, and CH_2^-. They could not be resolved completely and their intensities were too low for accurate mass determinations. There is the suggestion of a shoulder on the mass 25 peak which may be caused by C_2^- (see Fig. 1). Further work is indicated with a spectrometer of higher resolution.

* This research is supported by the Office of Naval Research under Contract No. Nonr 580(01).

[1] E. E. Muschlitz, Jr., Phys. Rev. **95**, 635 (1954).

[2] Simons, Francis, Fontana, and Jackson, Rev. Sci. Instr. **13**, 419 (1942).

Heats of Combustion and Formation of Some Alcohols, Phenols, and Ketones

GEORGE S. PARKS, KENNETH E. MANCHESTER, AND LELAND M. VAUGHAN
Department of Chemistry, Stanford University, Stanford, California
(Received October 8, 1954)

AS one step in the development of a comprehensive table of free energy data for organic compounds containing oxygen, we have recently had occasion to measure the heats of combustion of three aromatic alcohols, two phenols and five ketonic compounds, for which combustion data have hitherto been either uncertain or nonexistent.

Our new measurements were made upon highly purified materials in accordance with the calorimetric bomb procedures which have been described in earlier papers[1,2] from this laboratory. They are based upon Jessup's value of 26 429.9 international joules per gram mass for the standard benzoic acid.[3] The resulting molal heats of combustion at 25°C and 1 atmos constant pressure, expressed in terms of the *defined* kilocalorie (=4.184 absolute kilojoules), are given under the heading $-\Delta H_c°$ in the third column of Table I. Each value represents the average of six to twelve combustion measurements with a precision uncertainty of about 0.01 percent[4] for the experimental work. Making due allowance for possible impurities in the samples of material used, we then estimate the over-all uncertainty in these results as less than 0.04 percent in all cases.

The corresponding values for the heat of formation from the elements ($-\Delta H_f°$) in the last column have been computed by

TABLE I. Molal heats of combusion and formation at 25°C.

Substance and state (l=liquid; s=solid)	Mole wt.	$-\Delta H_c°$ kcal	$-\Delta H_f°$ kcal
Benzyl alcohol (l)	108.134	893.15	38.49(±0.30)
Diphenyl carbinol (s)	184.226	1607.42	25.16(±0.50)
Triphenyl carbinol (s)	260.318	2332.73	0.80(±0.60)
Phenol (s)	94.108	730.36	38.90(±0.25)
Hydroquinone (s)	110.108	682.51	86.75(±0.25)
Benzyl methyl ketone (l)	134.170	1149.09	38.96(±0.30)
Diacetyl (l)	86.088	493.56	87.60(±0.20)
Benzoquinone (s)	108.092	656.84	44.10(±0.15)
Dibenzoylethylene (s)	236.256	1887.18	27.55(±0.60)
Dibenzoylethane (s)	238.272	1921.81	61.24(±0.40)

use of −68.3174 kcal and −94.0518 kcal[5] for the $\Delta H_f°$ of H_2O (l) and CO_2 (g), respectively. In this case the estimated uncertainties are indicated parenthetically.

[1] J. W. Richardson and G. S. Parks, J. Am. Chem. Soc. **61**, 3543 (1939).
[2] Moore, Renquist, and Parks, J. Am. Chem. Soc. **62**, 1505 (1940).
[3] R. S. Jessup, J. Research Natl. Bur. Standards **36**, 421 (1946).
[4] F. D. Rossini, Chem. Revs. **18**, 233 (1936).
[5] Wagman, Kilpatrick, Taylor, Pitzer, and Rossini, J. Research Natl. Bur. Standards **34**, 143 (1945).

Initiation Processes in the Autoxidation of Fatty Acid Esters and Allied Substances*

N. A. KHAN†
Department of Scientific and Industrial Research, Karachi, Pakistan‡
(Received June 2, 1954)

FARMER'S[1] and Hilditch's[2] theories on autoxidation fail to account for the energy of the reactions involved. In particular, they inadequately explain oxidation at the double bond or at the alpha methylenic group. Similarly, they do not account for the induction periods which precede the main autoxidation reactions[3] or for the occurrence of the molecular rearrangement.[4] This paper presents a theory which both eliminates these shortcomings and also takes into consideration experimental observations.

Experimentally it was shown that the induction period is not due to impurities. Cyclohexene (cp) was chosen because of its being easily purified. It was first distilled over potassium hydroxide in a 45-cm Vigreux Column and then boiled under reflux over sodium for 18 hours. It was again fractionally distilled in an efficient Podbielniak Column at atmospheric pressure. The middle fraction was shaken with charcoal and activated alumina, filtered and redistilled. Cyclohexene, thus purified, was autoxidized by irradiation with visible light[5] at 15 to 16°C to a five percent peroxide content, noting the induction period. After reducing the peroxides with sodium bisulfite, the unoxidized cyclohexene was distilled. The distillate was purified as outlined above. This recovered and purified cyclohexene was autoxidized under the same conditions to repeat the induction period. The induction period may, thus, represent the time required for the acquisition of energy which is needed to initiate autoxidation.

Following the induction period, hydroperoxidation occurs. Monomeric monohydroperoxide has been obtained quantitatively from methyl oleate,[5] linoleate,[6] and linolenate,[7] each autoxidized to 10 percent peroxide contents. Moreover, hydroperoxidation can be carried on indefinitely at suitable temperatures below 0°C if proper precautions be taken to avoid decomposition of peroxides. The support for the formation of a monomeric monohydroperoxide at the initial stages of autoxidation of these substances has been obtained from our microdistillation data. Each type of hydroperoxide was reduced by stannous chloride and the reduced products distilled by means of a special apparatus[8] and found in all cases to consist of 98–100 percent monomers (such may not, of course, be the case for many competing reactions of initiation, propagation, and termination[9] involved in free radical mechanisms proposed by Farmer).[1,9,10]

The formation of hydroperoxide quantitatively by 3−C olefinic systems[3,6,7,11] (—CH_2—CH=CH—) in the presence of oxygen molecule[12] (:O⋮⋮O:) suggests two possible reactions. These are (a) electron transfer and (b) hydrogen atom transfer. The π or mobile electrons in 3−C systems due to hyperconjugation,[13] and the unpaired electrons in an oxygen molecule may facilitate these processes. They could act through a series of activated complexes[3] and finally through a transition state (I, Fig. 1) consisting of an electronically and energetically sound six-membered cyclic ring.[14] On rearrangement of the electrons, the transition state (I) may easily yield monomeric monohydroperoxide (II) with a compulsory shift of the double bond. This accounts for the conjugation in autoxidized linoleate[6] and linolenate.[7] The energy available in the transition state may determine the extent of *cis*, *trans*-isomerization[5,6] during autoxidation under different environmental conditions. Pro- and anti-oxidants may act by altering the energy relationships during the transition states described.

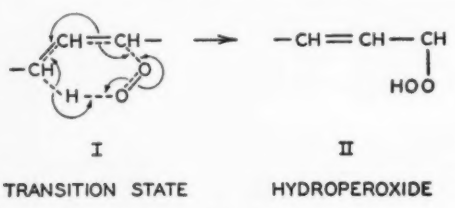

FIG. 1. Mechanism of the initiation processes in autoxidation reactions.

This theory has been placed on a firmer basis by the formation of two positional isomers of hydroperoxides (9-hydroperoxido-10-octadecenoate and 10-hydroperoxido-8-octadecenoate) by methyl oleate,[5] two (9- and 13-conjugated) by linoleate[4,6] and four (9-, 12-, 13-, and 16-conjugated) by linolenate.[7] These are not, of course, the same isomers as predicted on Farmer's free radical theory.[1,9,10,11,15] Further details on Farmer's and Hilditch's theories in relation to ours in elucidating the initiation processes of autoxidation will be published later.

* Most of the experimental work was completed through the courtesy of the different departments of The Ohio State University, Columbus, Ohio and of the University of Minnesota.
† Present address: Department of Physiology, University of Minnesota, Minneapolis, Minnesota.
‡ Supported in part by grants from this department.
[1] E. H. Farmer, Trans. Faraday Soc. **42**, 233 (1946).
[2] T. P. Hilditch, J. Oil & Colour Chemists Assoc. **30**, 1 (1947); Nature **166**, 558 (1950).
[3] N. A. Khan, J. Am. Oil Chemists' Soc. **30**, 273 (1953).
[4] N. A. Khan, J. Chem. Phys. (to be published).
[5] N. A. Khan (paper in preparation).
[6] Privette, Lundberg, and Khan, *Hormel Institute;* W. E. Tolberg and D. H. Wheeler, J. Am. Oil Chemists' Soc. **30**, 61 (1953); Khan, Tolberg, Wheeler, and Lundberg, J. Am. Oil Chemists' Soc. (to be published); Khan, Lundberg, and Holman, J. Am. Chem. Soc. **76**, 1779 (1954); N. A. Khan, Arch. Biochem. and Biophys. **44**, 247 (1953).
[7] N. A. Khan, J. Chem. Phys. **21**, 952 (1953); **22**, 764 (1954).
[8] Paschke, Kens, and Wheeler, J. Am. Oil Chemists' Soc. **31**, 5 (1954).
[9] L. Bateman, Quart. Revs. (London) **8**, 147 (1954).
[10] J. L. Bolland, and G. Gee, Trans. Faraday Soc. **46**, 236, 244 (1946).
[11] E. H. Farmer and A. Sundralingam, J. Chem. Soc. **1942**, 121; A. Robertson and W. A. Waters, Trans. Faraday Soc. **42**, 201 (1946).
[12] L. Pauling, *The Nature of the Chemical Bond* (Cornell University Press, Ithaca, 1944), p. 273.
[13] J. W. Baker, *Hyperconjugation* (Oxford University Press, London, 1952).
[14] H. Gilman, *Organic Chemistry* (John Wiley and Sons, Inc., New York, 1948), Vol. 1. p. 80. C. K. Ingold, *Structure and Mechanism in Organic Chemistry* (Cornell University Press, Ithaca, 1953), p. 44.
[15] E. H. Farmer and D. A. Sutton, J. Chem. Soc. **1943**, 119; Farmer, Koch, and Sutton, *Ibid.*, **1943**, 541.

Reply to Khan's Letter, "Initiation Processes in the Autoxidation of Fatty Acid Esters and Allied Substances"

L. BATEMAN
British Rubber Producers Research Association, 48 Tewin Road, Welwyn Garden City, Herts, England
(Received July 12, 1954)

WORK in these laboratories, with which the late Dr. E. H. Farmer was associated over the past fifteen years, has led to a comprehensive and detailed picture of olefin autoxidation which is certainly free from the interpretive inadequacies discussed by Khan. This is apparent, directly or implicitly, from a recently published review,[1] but it is perhaps useful to summarize the relevant points here in the simplest possible terms.

An extensive study[2] of the autoxidation of several highly purified olefins makes it clear that the so-called induction periods referred to by Khan are more precisely periods of immeasurably slow rates of oxygen absorption. The concentration of hydroperoxide in the olefin is extremely small; its rate of decomposition is likewise, and hence the rate of initiation of the chain reaction

responsible for autoxidation is minute. Neither Khan nor anyone else has yet measured the rate of direct interaction of the olefin and olefin under conditions remotely approximating those he describes; at observable rates of oxidation the chain mechanism is dominant, and oxygen combines solely with allylic free radicals derived from the olefin by abstraction of α-methylenic hydrogen atoms by peroxy radicals.[1,2] Accordingly, the formation of isomeric products has nothing whatever to do with direct olefin-oxygen interaction but reflects the mesomerism of allylic free radicals or intramolecular rearrangement of peroxy radicals.[1]

As regards the energetics of the reactions, these have been thoroughly analyzed and constitute some of the most intelligible and informative data pertaining to free radical reactions.[1]

[1] L. Bateman, Quart. Revs. (London) **8**, 147 (1954).
[2] A. L. Morris, Ph. D. thesis, London, 1952; Bateman, Hughes, and Morris, Discussions Faraday Soc. **14**, 190 (1953).

Electronic Absorption Spectra of the Dimethylpolyenes

P. Nayler and M. C. Whiting
Department of Chemistry, University of Manchester, Manchester, England
(Received September 27, 1954)

Recent calculations[1-3] of energy levels, and hence electronic absorption spectra, for linear polyenes have been compared with simple substances (e.g., butadiene) at one extreme, but of necessity carotenoids and their analogues have been chosen at the other. Carotenoids possess the isoprenoid repeating unit $-(CH=CH\cdot CMe=CH)_{n/2}-$, and therefore do not exactly correspond to the system $-(CH=CH)_n-$ for which the calculations were made; there are other features, e.g., the frequent occurrence of noncoplanar β-ionone terminal groupings, which make them unsuitable for such comparisons. Clearly the spectra of a simple and homogeneous series would be preferable. We now report experimental values for the dimethylpolyenes (I), $CH_3\cdot(CH=CH)_n\cdot CH_3$.

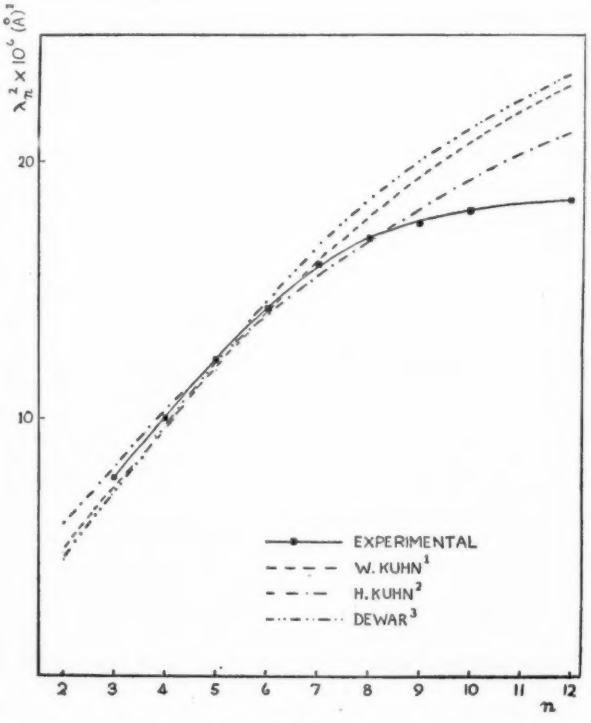

Fig. 1.

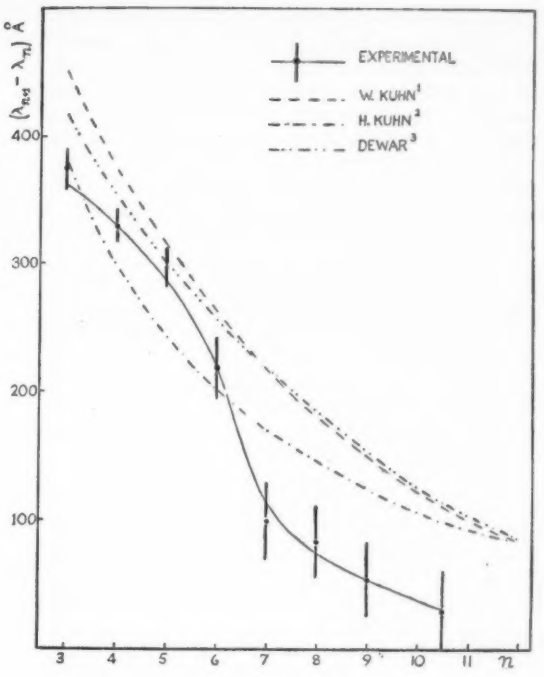

Fig. 2.

The known hydrocarbons (I), where $n=3-6$, are crystalline and sublimable solids which can be handled, albeit with increasing difficulty, in a normal manner with appropriate precautions. Where $n>7$ sublimation becomes impossible even at 10^{-5} mm, solubility falls off and sensitivity to oxygen and heat continues to increase. It is therefore necessary to handle the higher polyenes in dilute solution, relying on spectroscopic detection and assay. Since absorption spectra are also the object of interest, proof that bands measured are attributable to (I) is achieved by induction, reactions known to give (I, $n=3-6$), which can be characterized, being assumed to give higher members of the series when analogous starting materials are used provided that observed band positions vary smoothly and continuously throughout. We used the reaction

$$CH_3\cdot(CH=CH)_a\cdot CH(OH)\cdot C\equiv C\cdot CH(OH)\cdot(CH=CH)_b\cdot CH_3 \xrightarrow{LiAlH_4} CH_3(CH=CH)_{a+b+2}\cdot CH_3$$

to obtain every hydrocarbon (I) where $n=2-10$, and (I, $n=12$), which, with $n=8$ was obtained crystalline from (II, $a=b=3$), and showed five equally-spaced absorption maxima, closely resembling lower homologs. For (I, $n=7$, 9, and 10) concentrates showing the three intense, longest-wavelength bands were obtained, and a similar concentrate of (I, $n=8$) was obtained from (II, $a=5$, $b=1$), its spectrum agreeing exactly with that from (II, $a=b=3$). The best concentrate of (I, $n=12$) showed clearly only the longest-wavelength band. The λ^2 *versus* n plot[4] for the longest-wavelength band in chloroform (Fig. 1) was a smooth curve, converging as $n\to\infty$ to *ca* 4400A, i.e., much more sharply than the isoprenoid series.[5]

Without recalculation of parameters agreement of the theoretical expressions with these results could not be expected. When $(\lambda_{n+1}-\lambda_n)$ is plotted against n (Fig. 2), however, the latter give an inflexion which cannot be removed by adjusting λ_{max} values within estimated experimental errors. Of the three equations, Dewar's[3] cannot accommodate an inflexion in the differential curve: for the more complex expression of H. Kuhn and W. Kuhn, the values calculated with parameters quoted do not give an inflexion, and therefore they also probably differ qualitatively from the behavior of the actual polyenes. Both H. Kuhn[2] and

Dewar[3] have expressed surprise at the close agreement between their theoretical relationships and the values chosen from the (fairly divergent) literature on isoprenoid polyenes, in view of the "crudity" of the approximations employed. By removing this anomaly the present results may therefore help the eventual development of a more adequate theoretical treatment of this very fundamental problem.

We wish to thank Professor E. R. H. Jones, F. R. S., for his interest and advice, and the Department of Scientific and Industrial Research for a Maintenance Grant to one of us (P.N.)

[1] W. Kuhn, Helv. Chim. Acta, **31**, 1780 (1948).
[2] H. Kuhn, J. Chem. Phys., **17**, 1198 (1949).
[3] M. J. S. Dewar, J. Chem. Soc., 3544 (1952).
[4] G. N. Lewis and M. Calvin, Chem. Revs. **25**, 237 (1939).
[5] P. Karrer and C. H. Eugster, Helv. Chim. Acta **34**, 1805 (1951).

Elastic Constants of AgBr at 28°C

D. S. TANNHAUSER AND A. W. LAWSON
Institute for the Study of Metals, University of Chicago, Chicago, Illinois
(Received September 28, 1954)

USING an ultrasonic pulse technique previously described,[1] we have determined the elastic constants of AgBr at room temperature.

Two cylindrical samples about 2 cm in length and 1.5 cm in diameter were machined from crystals grown from the melt; one crystal had its axis in the ⟨100⟩ direction; the other in the ⟨110⟩ direction. After annealing at 400°C, the samples were affixed to either X-cut or Y-cut quartz crystal transducers by means of beeswax and rosin.

TABLE I. A comparison of the elastic constants of AgBr and AgCl in units of 10^{11} dyne/cm².

	AgCl[a] Ave.	AgBr 100 Xtal	AgBr 110 Xtal
C_{11}	6.05	5.622±0.014	5.62 ±0.03
C_{12}	3.64	...	3.28 ±0.03
C_{44}	0.624	0.729±0.006	0.727±0.005

[a] After Arenberg (see reference 3).

The velocity of sound in the sample was determined by observing the difference in time between the arrival of successive echoes at the transducer after the application of an initial 10.7 mc pulse. The frequency of the pulse was adjusted to obtain reflected pulses with minimum distortion and a very steep leading edge. The nominal tuned frequency of the crystals and receiver was 12 mc. To obtain the velocity of sound in the sample, the observed over-all transit time must be corrected for the transit time of the pulse in the transducer. The latter was determined by observing the change in over-all transit time when an identical transducer was affixed to the previously free end of the sample. Because the effective transducer transit time probably depends on the amount of coupling to the sample, and hence on the velocity of sound in the sample, we feel this procedure is preferable to that of Neighbors, Bratten, and Smith,[2] who used polycrystalline samples of varying lengths to determine the correction to be applied to single crystals. The correction in all cases is less than 0.5 percent of the velocity of sound in the sample.

The elastic constants were calculated from the velocity of sound measurements and the known density of AgBr of 6.473 g/cm³, using standard formulas.[1] The results are given in Table I where they are compared with the elastic constants of AgCl reported by Arenberg.[3] The only data previously reported which are directly comparable to ours are those on the isothermal compressibility, x_T. Bridgman[4] reports a value for x_T of 2.24×10^{-12} cm²/dyne, whereas Richards and Jones[5] find for the same quantity 2.60×10^{-12} cm²/dyne. Our value for x_T, calculated by the usual thermodynamic formula,[1] is 2.48×10^{-12} cm²/dyne.

It should be recorded that ten Laue photographs of each crystal indicated that they possessed a random orientation up to 2° from the ideal orientation. The effect of the random orientation on the elastic constants has been calculated approximately by perturbation methods. The calculation shows that the effect on the elastic constants is at most 0.2 percent for C_{11} and 0.5 percent for C_{12} and C_{44}. It tends to decrease the elastic anisotropy, so that the measured value of C_{11} might be too low and the values of C_{12} and C_{44} too high by the above percentages.

The most striking feature in the behavior of the elastic constants of both AgCl and AgBr is the large deviation from the Cauchy relation, $C_{12}=C_{44}$, as compared to the behavior of the alkali halides.

We are indebted to Dr. W. G. Johnston for preparing the crystals, and to the Office of Naval Research for partial support.

[1] D. Lazarus, Phys. Rev. **76**, 549 (1949).
[2] Neighbors, Bratten, and Smith, J. Appl. Phys. **23**, 389 (1952).
[3] D. L. Arenberg, J. Appl. Phys. **21**, 941 (1950).
[4] P. W. Bridgman, Phys. Rev. **57**, 237 (1940).
[5] T. W. Richards and G. Jones, J. Am. Chem. Soc. **31**, 158 (1909).

Heat of Formation of CF_3 and Some Bond Dissociation Energies for Fluorocarbons

B. S. RABINOVITCH AND J. F. REED
Department of Chemistry, University of Washington, Seattle, Washington, and Department of Chemistry, Loyola University, Chicago, Illinois
(Received September 27, 1954)

THE reaction of sodium atoms at 300°C with the series of chlorides, CH_3Cl, CH_2FCl, CHF_2Cl, and CF_3Cl, have been investigated in these laboratories by the diffusion flame method. The rate data have been corrected for subsequent reactions of the radicals produced, and activation energies for chlorine abstraction, E, have been computed using the Garvin-Kistiakowsky boundary condition for sodium concentration at the nozzle.[1] Errors in calculated rate constants resulting from neglect of further reaction between sodium and product radicals are by no means negligible even for fluorine containing radicals; while use of the Polanyi boundary conditions, rather than that of Garvin and Kistiakowsky, tends also to give low values for activation energies calculated in the conventional manner from rate data at a single temperature. This is discussed elsewhere.[2]

The E values we have obtained may, with some restrictions in principle, be related to the corresponding bond dissociation energies, D, by the familiar relation, $\Delta E=\alpha\Delta H$, of Ogg and Polanyi, where in this $\Delta H=\Delta D$; values of α are specified in the literature. For the above series of reactions the activation energies vary only slightly, the largest variation from CH_3Cl ($E=10.9$ kcal), the standard substance, being for CF_3Cl ($E=10.1$ kcal), and the values of ΔD are correspondingly insensitive to the magnitude of α or its constancy in a series. We have also been guided in the evaluation of α by results from our work on the sodium atom reaction with the corresponding bromides, values of $D(H_3C-Br)$ and $D(F_3C-Br)$ being available.[3] Based on $D(H_3C-Cl)=81.2$ kcal[4] we find that $D(F_3C-Cl)=79.5\pm2$ kcal.

Recently the heats of formation under standard conditions at 25° of CF_3Cl, CF_4, C_2F_6 and C_2F_4 have been determined as −171, −218, −303, and −162 kcal/mole, respectively, by Kirkbride and Davidson.[5a] The value for CF_4 is in excellent agreement with those reported recently,[5b] and for internal consistency we shall employ Kirkbride and Davidson's values. Using $\Delta H_f(Cl)=29$ kcal[6] we obtain $\Delta H_f(CF_3)=-120.5$ kcal, and noting the possible error in the data of Kirkbride and Davidson specified by them, this value may without further correction be taken as relating to 25°.

Two thermochemical quantities of considerable interest are $D(F_3C-F)$ and $D(F_3C-CF_3)$. The first of these has frequently

been surmised to be greater than $D(CH_3-H)$. A maximum value of 131 kcal results from combining the activation energy for the reaction of sodium atoms and CF_4[7] with $D(NaF)$.[6] Taking $D(F_2)$ as 38 kcal,[8] combination of the various data cited above yields $D(F_3C-F)=116.5$ kcal.

As remarked by Kirkbride and Davidson, their heat values suggest a low carbon bond dissociation energy in C_2F_6. The value that we calculate from the above data is $D(F_3C-CF_3)=62$ kcal. This magnitude seems difficult to reconcile with the reported thermal stability of this compound.[9] However, a possible error, estimated by Kirkbride and Davidson at less than 10 kcal, in some of their values could reconcile the discrepancy just noted; particularly if C_2F_6 decomposition reactions such as F_2 split off, the analog of H_2 split off in ethane, do not occur, and if chain propagation of decomposition is comparatively inefficient.

Finally, there seems little doubt that $D(F_2C-F)$ is less than 116 kcal. This limit results from our findings on the reaction of sodium atoms with CF_3; also the conclusion of Atkinson,[10] based on the $Hg(^3P_1)$ photosensitized reaction of C_2F_4, that the double bond dissociation energy in C_2F_4 is less than 112 kcal leads to a limit of 114 kcal in combination with values above.

Further details of this study will be forthcoming later. This work has been supported by the Office of Naval Research. We thank Professor G. H. Cady for his cooperation.

[1] D. Garvin and G. B. Kistiakowsky, J. Chem. Phys. **20**, 105 (1952).
[2] J. F. Reed and B. S. Rabinovitch (to be published).
[3] A. H. Sehon and M. Szwarc, Proc. Roy. Soc. (London) **A209**, 110 (1951).
[4] Mortimer, Pritchard, and Skinner, Trans. Faraday Soc. **48**, 220 (1952).
[5] (a) F. W. Kirkbride and F. G. Davidson, Nature **174**, 79 (1954); (b) Fluorine Chemistry Symposium, 126th Meeting American Chemical Society, New York, September 1954; CF_4: −212.7 (Duus); −220.4 (Jessup, McCosky, and Nelson); −218.3 (Scott, Good and Waddington); C_2F_4: −151.3 (Duus).
[6] Rossini, *Selected Values of Chemical Thermodynamic Constants* (National Bureau of Standards, Washington, 1952)
[7] E. Warhurst, Quart. Revs. **5**, 44 (1951).
[8] R. N. Doescher, J. Chem. Phys. **20**, 330 (1952); H. Wise, *ibid.* **20**, 927 (1952).
[9] See for example L. White and O. K. Rice, J. Am. Chem. Soc. **69**, 267 (1947); Brice, Pearlson, and Simons, *Ibid* **71**, 2499 (1949); R. K. Steuenberg and G. H. Cady, *ibid.* **74** 4165 (1952).
[10] B. Atkinson, J. Chem. Soc., 2684 (1952).

Discrepancy in the Rotational Constants of Bromoform*

GABRIEL HERRMANN
Department of Physics, College of Engineering, New York University, University Heights, New York 53, New York
(Received August 26, 1954)

IN the determination of the rotational constants of bromoform ($CHBr_3$) a large unexplained discrepancy was found between the results of Williams and Gordy[1] working in the K-band region and of Kojima *et al.*[2] in the S-band region. The latter reported 32 lines in the frequency region 2450−2650 Mc/sec which were attributed to the fine structure of the $J=0\rightarrow1$ rotational transition for the four common isotopic species of the molecule. In this investigation Kojima and his colleagues used an unmodulated spectrograph employing a double crystal circuit and oscilloscope representation. The gas pressure used was 3 mm Hg with resulting poor resolution. The authors stated that their instrument had a sensitivity of 6×10^{-8} cm^{-1} while quoting the value 2×10^{-8} cm^{-1} as the intensity of an average line. Our own calculation, however, yielded the value 4×10^{-10} cm^{-1}, for the intensity of the unsplit rotational line, or at most 1.5×10^{-11} cm^{-1} for the strongest individual fine structure component at room temperature. Part of this discrepancy may be due to the fact that we assigned to the line width the value of 20 Mc/sec per mm Hg while Kojima used the unusually small value of 1 Mc/sec per mm Hg, which enabled him in turn to claim good resolution in spite of the very high pressure. From the known line widths of similar molecules, our value seems to be the more reasonable one.

In order to verify Kojima's results a careful search was made in the region from 2200 to 2700 Mc/sec. The apparatus used consisted of a Stark modulated spectrograph described elsewhere,[3] which, owing to its very narrow band pass, we believe to be of considerably higher sensitivity than that employed by Kojima. As calculated by standard methods[4,5] this sensitivity is about 1×10^{-10} cm^{-1}, and this value was found to be consistent with observations made on other spectra with this apparatus.[3,6] In spite of the greater sensitivity no lines attributable to bromoform were observed. We must therefore assume that bromoform lines in this region are too weak to be detected by presently available techniques.

This conclusion is supported by the recent work by Sterzer[6] who, working in the same frequency region, was barely able to detect the $J=0\rightarrow1$ spectrum of CF_3I. The similarity in structure and the proximity in frequency make possible a direct comparison of expected line intensity in bromoform and CF_3I which shows that individual bromoform lines should be much weaker. This is due primarily to the great complexity of the hyperfine structure which arises from presence of three bromine nuclei of spin 3/2 and, in addition, the existence of four distinct isotopic species. In fact, more than 100 lines are predicted for the $J=0\rightarrow1$ transition. In CF_3I the corresponding line splits into only three components. Furthermore the intensity CF_3I tends to be slightly greater because its rotational constants are larger. The bromoform spectrum is therefore so much weaker that detection appears highly improbable, if we consider that the CF_3I lines themselves are so near to the limit of observation.

We conclude therefore that the results obtained by Kojima *et al.*[2] must be rejected. The lines they report are undoubtedly due to some of the spurious effects which are frequently observed in microwave spectrographs.

While the present work has not yielded any positive support to Williams and Gordy,[1] there appears no reason to doubt the validity of their work.

The writer wishes to thank Professor C. H. Townes of Columbia University and Professor Yardley Beers of New York University for helpful discussions.

* Supported by the Office of Naval Research and by the United States Air Force through the Office of Scientific Research of the Air Development Command.
[1] Q. Williams and W. Gordy, J. Chem. Phys. **20**, 1524 (1952).
[2] Kojima, Tsukada, Hagiwara, Mizushima, and Ito, J. Chem. Phys. **20**, 804 (1952).
[3] Weisbaum, Beers, and Herrmann, Phys. Rev. **90**, 338 (1953). Also, Weisbaum, Beers and Hermann, J. Chem. Phys. (to be published).
[4] W. Gordy, Revs. Modern Phys. **20**, 668 (1948).
[5] C. H. Townes and S. Geschwind, J. Appl. Phys. **19**, 795 (1948).
[6] F. Sterzer, J. Chem. Phys. (following letter).

On the Interpretation of the Spectrum of Bromoform

SHOJI KOJIMA AND KINEO TSUKADA
Department of Physics, Tokyo University of Education, Otsuka, Tokyo, Japan
(Received September 22, 1954)

PREVIOUSLY we have reported the rotational spectra of $CHBr_3$ in the frequency region from 2430 to 2650 Mc/sec.[1] Recently to verify our results, Herrmann carried out a careful search with a Stark modulation spectrograph,[2] but no lines were observed.

We have not carried out further experiment on bromoform after the publication. However, one of us (K.T.) studied the spectra of $SPCl_3$ in the frequency region from 2600 Mc to 2900 Mc with a cavity spectrometer.[3] An absorption spectrum was observed at 1.2 mm Hg, though it was not resolved into sharp lines. On the interpretation of this experiment, it was found that some lines due to the asymmetric rotors, i.e., $SPCl_2{}^{35}Cl^{37}$ and $SPCl^{35}Cl_2{}^{37}$, exhibited in this frequency region, with a considerable intensity. Itoh[4] estimated, using the theory of Cross, Hainer, and King,[5] that the transitions between the levels separated by the asymmetric K-type doubling, i.e., $\Delta J=0$, $\Delta K_{-1}=0$ and ΔK_{+1}

$=-1$, might be several times stronger, for high values of J, than that of the rotational lines of the $J=0\rightarrow1$ transition. The lines due to this transition receive smaller Stark modulation than those of the symmetric rotor. A situation similar to $SPCl_3$ can occur in bromoform of $CHBr_2^{79}Br^{81}$ and $CHBr^{79}Br_2^{81}$. Therefore some of the observed lines may be the asymmetry rotor lines.

The negative result obtained by Herrmann may indicate that the lines observed by us are not due to $J=0\rightarrow1$ transitions. If it is so, our previous assignment must be corrected. At present the rotational constant given by Williams and Gordy[6] and the quadrupole couplings given by us[7] are available. However, the asymmetry rotor lines complicate the analysis too much.

[1] Kojima, Tsukada, Hagiwara, Mizushima, and Itoh, J. Chem. Phys. **20**, 804 (1952).
[2] C. Herrmann, J. Chem. Phys. (preceding letter).
[3] K. Tsukada (to be published).
[4] T. Itoh (to be published).
[5] Cross, Hainer, and King, J. Chem. Phys. **12**, 210 (1944).
[6] Q. Williams and W. Gordy, J. Chem. Phys. **20**, 1524 (1952).
[7] Kojima, Tsukada, Ogawa, and Shimauchi, J. Chem. Phys. **21**, 1415 (1953).

$J=0\rightarrow1$ Rotational Transition of Trifluoroiodomethane*

FRED STERZER
Department of Physics, College of Engineering, New York University, University Heights, New York, New York
(Received August 26, 1954)

THE hyperfine splitting of the $J=0\rightarrow1$ transition of CF_3I has been studied at dry ice temperature with a Stark modulated spectrometer described elsewhere.[1] CF_3I represents the unusual case of a symmetric top molecule with a quadrupole coupling constant eqQ larger than the rotational constant B. For the $J=0\rightarrow1$ transition, therefore, the quadrupole interaction energy of the iodine nucleus is nearly as large as the rotational energy of the molecule. Consequently, higher-order pertubation effects become appreciable. Also because of the relatively large separation of the various lines, a study of this spectrum seems to afford a good opportunity for getting a somewhat more accurate value of the quadrupole coupling constant. Previous microwave work on this molecule[2] has employed high rotational transitions in the K-band region, where intensities are much more favorable, but where quadrupole effects are smaller. Also this work was of interest because it afforded a check upon the work on bromoform by Herrmann[3] in this laboratory.

TABLE I. The $J=0\rightarrow1$ spectrum of CF_3I.

Transition $F\rightarrow F'$	Measured frequency Mc/sec	Calculated frequency Mc/sec	2nd order correction Mc/sec	Calculated intensity cm^{-1}
$5/2\rightarrow5/2$	2715.1 ± 0.3	2715.14	11.31	5.0×10^{-10}
$5/2\rightarrow7/2$	3162.9 ± 0.25	3162.90	8.87	6.6×10^{-10}
$5/2\rightarrow3/2$	3362.9 ± 0.4	3362.94	15.97	3.3×10^{-10}

The measured frequencies of the observed lines are shown in Table I along with the values calculated on the basis of values for the rotational constant $B=1523.42\pm0.15$ Mc/sec and for the quadrupole coupling constant $eQq=-2143.8\pm2$ Mc/sec.

These values are in good agreement with the values of $B=1523.23$ Mc/sec and $eQq=-2150$ Mc/sec obtained by Sheridan and Gordy from their K-band measurements.

The calculations employed pertubation theory up to second order[4] which proved to be sufficient for getting a good fit with the observed frequencies Also shown in Table I are the relatively large second-order corrections which were used in the calculations. In addition, with reference to the work of Herrmann,[3] are listed the calculated intensities based upon an assumed line width parameter of 20 Mc/sec at 1 mm Hg at room temperature.

From the Stark splitting of the $F=5/2\rightarrow3/2$ line, a value of the dipole moment of $1.010^{-18}\pm0.1$ esu cm has been obtained.

The author wishes to thank Professor Yardley Beers for many most helpful discussions. He also wishes to thank Mr. L. J. Hals of the Minnesota Mining and Manufacturing Company for advice in the preparation of CF_3I and for a gift of some trifluoroacetic acid used in the preparation. Thanks are due Mr. William O. Meluch of the Chemistry Department, New York University, University Heights, New York for performing the actual preparation of the CF_3I used.

* Supported by the Air Force through the Office of Scientific Research of the Air Research and Development Command.
[1] Weisbaum, Beers, and Herrmann, Phys. Rev. **90**, 338 (1953). Also Weisbaum, Beers, and Herrmann (to be published).
[2] J. Sheridan and W. Gordy, J. Chem. Phys. **20**, 591 (1952).
[3] G. Herrmann, J. Chem. Phys. (preceding letter).
[4] J. H. Bardeen and C. H. Townes, Phys. Rev. **73**, 627, 1204 (1948).

Approximate Analytic Solution of the Thomas-Fermi Equation for Atoms

T. TIETZ
University Nicolas Copernicus, Torun, Poland
(Received September 13, 1954)

THE solution of the Thomas-Fermi equation for atoms is reducible[1] to the solution of the equation

$$d^2\phi/d\chi^2=\chi^{-\frac{1}{2}}\phi^{\frac{3}{2}} \quad \phi(0)=1; \quad \phi(\infty)=0. \tag{1}$$

Brinkman[2] has developed a new method of solving Eq. (1). Brinkman remarks that $\chi\phi$ equals zero for $\chi\rightarrow\infty$ as well as for $\chi=0$. For intermediate values of χ it shows a maximum, therefore, $(\chi\phi)^{\frac{1}{2}}$ is a slowly varing function in this region. Bearing this in mind Brinkman writes Eq. (1) as

$$\frac{d^2\phi}{d\chi^2}=(\chi\phi)^{\frac{1}{2}}\frac{\phi}{\chi}, \tag{2}$$

and treats $(\chi\phi)^{\frac{1}{2}}$ as if it were constant. A solution of the now linear Eq. (2) is

$$\phi=C(\chi)^{\frac{1}{2}}K_1 2[\chi(\phi)^{\frac{1}{2}}\chi^{\frac{1}{2}}], \tag{3}$$

where C is an arbitrary constant, while K_1 is a modified Bessel function of the second kind. In the approximation of Brinkman one has adjusted the constants so that $C=1.\ 73$, $(\phi\chi)^{\frac{1}{2}}=0.8$. If we assume $(\chi\phi)^{\frac{1}{2}}=a^2/\sigma$ where a is an arbitrary constant we write (2) as

$$\frac{d^2\phi}{d\chi^2}=\frac{6}{a^2}\phi^2. \tag{4}$$

A solution of the now nonlinear equation (4) is easily obtained. It is

$$\phi=a^2/(\chi+a)^2. \tag{5}$$

Using the radial momentum distribution function[3] $I(P)$ we find $a=(8/\pi)^{\frac{1}{2}}\approx1.860$. We have limited the ϕ value to two or three significant decimal places, which is sufficient for our purposes. For comparison with our approximation ϕ_{Ti} we have taken the numerical value of Bush and Caldwell's[4] ϕ_{Bn}, the Sommerfeld's[5]

TABLE I.

χ	ϕ_{Br}	ϕ_{Ti}	ϕ_{So}	ϕ_{Bn}
0.05	0.97	0.99	···	0.93
0.1	0.89	0.90	···	0.88
0.2	0.79	0.81	···	0.79
0.3	0.71	0.74	···	0.72
0.5	0.59	0.62	···	0.61
1.0	0.42	0.42	···	0.43
4.0	0.109	0.108	···	0.108
5.0	0.0783	0.0735	0.072	0.0788
10.0	0.0207	0.0242	0.0228	0.0244
20.0	0.0027	0.0072	0.0056	0.0058
40.0	···	0.00190	0.00108	···
100.0	···	0.000339	0.000103	···

approximation ϕ_{Bo} and the Brinkman's approximation ϕ_{Br} (see Table I). We conclude that Eq. (5) is simpler for practical calculation than Eq. (3) and gives no worse results than Brinkman's solution. The radial momentum distribution function $I(P)$ is normalized.

[1] E. U. Condon and G. H. Shortley, *The Theory of Atomic Spectra* (The Cambridge University Press, New York, 1935), p. 335.
[2] H. C. Brinkman, Physica **20**, 44 (1954).
[3] N. H. March, Proc. Cambridge Phil. Soc. **46**, 336 (1950); C. A. Coulson and N. H. March, Proc. Phys. Soc. (London) **A63**, 367 (1950).
[4] V. Bush and S. H. Caldwell, Phys. Rev. **38**, 1898 (1931).
[5] A. Sommerfeld, Z. Physik **78**, 283 (1932).

Decomposition of Methane in Low-Pressure Glow Discharge*

MILTON BURTON AND J. P. MANION
Department of Chemistry, University of Notre Dame, Notre Dame, Indiana
(Received September 21, 1954)

IN a modification of the Penning (ionization gauge) glow discharge[1] operated on ac, methane at 10^{-4} mm pressure was passed through the length of a cylindrical tube in the space between two electrically connected plates 2 cm long (parallel to the axis), 2.6 cm wide and 2 cm apart. Between and parallel to the two plates was a loop electrode of ~2-cm diameter.[2] With poles of an Alnico magnet of ~4600 gauss outside the tube behind each of the plates, the unit functioned as a current rectifier.[3] In the particular experiments results of which are summarized in Table I, the flow velocity of the gas was ~70 cm sec^{-1} so that, on the average, every molecule was between the plates for nearly two ac cycles.

TABLE I. Decomposition of methane in penning discharge at $\sim 10^{-4}$ mm pressure.[a]

Volts, ac	Current, dc[b] ma	i	f	h
1435	0.12±0.6	0.65	0.45	1.4
1435	0.10±0.04	0.54	0.52	1.3
2432	0.14±0.06	0.76	0.69	1.2
2432	0.20±0.11	1.08	0.63	1.3

[a] See text for explanation of symbols.
[b] There was no measurable ac component in the experiments reported. Current was erratic in the range indicated. Average current was not determined.

The value of i, the estimated fraction of molecules ionized (assuming single ionization) is given by the relation

$$i = 6.2\times10^{18}At/6\times10^{23}N,$$

where A is the current in amperes and N the number of moles of gas passed through the discharge in t seconds. The fraction of gas decomposed is represented by f and the ratio (yield of H_2)/(CH_4 decomposed) by h. At 10^{-4} mm pressure no hydrocarbon gas was produced, but a deposit of resinous and carbonaceous material appeared on the glass walls of the tubes fairly symmetrically disposed to a distance of about 2 cm entirely around, and probably also on, the plate electrodes.

It is noteworthy that more than half the molecules in the reaction zone (possibly including product molecules) are ionized and that i is greater than f. Theory of radiation chemistry indicates that the number of excited molecules probably exceeds the number of ionized molecules.[4] Apparently, under these conditions, only about half the total primary excitation and ionization yields decomposition.

In photolysis of methane at wavelengths <1500A the quantum yield is approximately unity.[5] Excited methane molecules produced in electric discharge either at atmospheric[6] or lower pressure[7] decompose with high efficiency. On the other hand, in mass spectrometry of methane, CH_4^+ appears fairly stable; its relative peak height compared to the sum of all other peaks is ~0.9.[8]

At $\sim10^{-4}$ mm pressure the mean free path of molecules is $\sim10^3$ cm; i.e., very much greater than the dimensions of the vessel. Thus, in these experiments, the excited molecules had an average life of $\sim10^{-4}$ sec before collision with the walls. This time seems adequate for the expected decomposition. Apparently the low decomposition yield is to be attributed mainly if not entirely to the behavior of ions at low pressure. For example, we may hypothesize that neutralization of positive ions at electrodes (or walls) is not accompanied by decomposition (because energy in such a locale may be dissipated in other ways) and note that all the neutralization of the ions measured took place at the electrodes.

Essex and his collaborators obtained results in alpha-particle bombardment studies on various gases in the pressure range up to 20 cm which led them to the conclusion that "ion recombination" contributed nothing to radiation-induced decomposition in the absence of a field.[9] Their results are perhaps to be ascribed to the fact that the electrons primarily produced were unable to neutralize molecules at their initial high energy,[10] but travelled to the walls. As the result of the space charge there created, ions were attracted to the walls and neutralized under conditions which did not yield a product.

* One of us (J.P.M.) performed the work herein reported as Sinclai Research Fellow. Contribution from the Radiation Project of the University of Notre Dame supported in part under U. S. Atomic Energy Commission contract AT(11-1)-38 and Navy equipment loan contract Nonr-06900.
[1] Z. M. Penning, Physica **3**, 873 (1936); **4**, 71 (1937).
[2] (a) A diagram of a somewhat similar arrangement in a gauge (i.e., *not* a reaction tube) is shown by K. M. Simpson in A. Guthrie and R. K. Wakerling *Vacuum Equipment and Techniques*, National Nuclear Energy Series (McGraw-Hill Book Company, Inc., New York, 1949), p. 129. (b) For some discussion of theory and operation see J. Backus, in A. Guthrie and R. K. Wakerling *Characteristics of Electric Discharges in Magnetic Fields*, National Nuclear Energy Series (McGraw-Hill Book Company, Inc., New York, 1949), pp. 345 ff.
[3] See reference 2(a), p. 130.
[4] See Eyring, Hirschfelder, and Taylor, J. Chem. Phys. **4**, 479, 570 (1936); M. Burton, J. Chem. Educ. **28**, 404 (1951).
[5] P. A. Leighton and A. B. Steiner, J. Am. Chem. Soc. **58**, 1823 (1936); W. Groth and H. Laudenklos, Naturwiss. **24**, 796, 828 (1936); W. Groth, Z. physik. Chem. **B38**, 366 (1937).
[6] H. Wiener and M. Burton, J. Am. Chem. Soc. **75**, 5815 (1953).
[7] L. M. Yeddanapalli, J. Chem. Phys. **10**, 249 (1942).
[8] Am. Petroleum. Inst. Research Project 44. *Mass Spectral Data*, No. 1 (1947).
[9] See H. Essex, J. Phys. Chem. **58**, 42 (1954).
[10] For discussion of conditions of neutralization in radiation chemistry, see J. L. Magee and M. Burton, J. Am. Chem. Soc. **72**, 1965 (1950).

"Threshold Potential" of the ac Electrodeless Discharge

S. R. MOHANTY
Physico-Chemical Laboratories, Banaras Hindu University, India
(Received September 15, 1954)

A SELF-MAINTAINED low-frequency electrodeless discharge is struck in a gas (vapor) confined in a tube when the applied potential V equals or exceeds the corresponding minimum "threshold potential"[1,2] V_m. The Townsend condition[3-5] for a self-maintained discharge is

$$\alpha/\beta(=1/\gamma=\alpha/\eta\theta g)=e^{\alpha\delta},$$

where α is the (first) Townsend coefficient for ionization by electron impact, β the second coefficient interpretable in terms of a γ or an $\eta\theta g$ signifying secondary liberation of electrons at the cathode by positive ion bombardment or as a photoelectric process due to photons generated in the gas, and δ the electrode separation. For each ion created in the gas by ionization by electron impact, there are created by secondary processes at the cathode enough electrons to maintain $\gamma e^{\alpha\delta}$ at its existing value. with metal electrodes immersed in the gas, the secondary electrons can be identified with the Fermi electron gas in the metal. No such simple mechanism suggests itself, in the first instance, for discharge with dielectric (e.g., glass) surfaces exposed to the gas.

Immediately below the threshold of continuous discharge, there is a narrow nonself-maintained region[6] where the field, at the peak value, is strong enough to cause ionization by electron impact. An electron introduced into the system by an external agency, e.g., cosmic and radioactive radiations, etc., initiates an avalanche which descends on the (momentary) anode. Incomplete neutralization during the half-cycle leaves a residue of loosely bound electrons on the electrode. These electrons, during the succeeding half-cycle, impart to the electrode, now the (momentary) cathode, a photoelectric activity[7] and a low work function ϕ further reduced to ϕ' by the field F, as a Schottky[8,9] consequence, according to the equation $\phi'=\phi-F^{\frac{1}{2}}$. Secondary emission occurs because of the γ and $\eta\theta g$ processes, and when at an appropriate V, *viz.*, V_m, the current in the gas, exceeds a certain minimum value, the discharge attains a self-sustained character.

[1] S. S. Joshi, Current Sci. **8**, 548 (1939); Proc. Indian Acad. Sci. **A22** 389 (1945); Current Sci. **15**, 281 (1946).
[2] S. R. Mohanty, J. Sci. Ind. Research, **B13**, 145 (1954).
[3] J. S. E. Townsend, *Electrons in Gases* (Hutchinson's Scientific and Technical Publications, London, 1947).
[4] L. B. Leob, *Fundamental Processes of Electrical Discharge in Gases* (John Wiley and Sons, Inc., New York, 1939); Proc. Phys. Soc. (London) **60**, 561 (1948).
[5] J. M. Meek and J. D. Craggs, *Electrical Breakdown of Gases* (The Clarendon Press, Oxford, 1953).
[6] S. A. Korff, *Electron and Nuclear Counters* (D. Van Nostrand Company, Inc., New York, 1949).
[7] Mohanty, Jayaraman, and Krishna Rao (private communication).
[8] W. Schottky, Z. Physik **14**, 63 (1923).
[9] I. Langmuir and K. T. Compton, Revs. Modern Phys. **2**, 124 (1930).

Infrared Spectrum and Hydrogen Bonding of Pyrrole

P. Tuomikoski
University of Helsinki, Helsinki, Finland
(Received August 26, 1954)

THE paper of Josien and Fuson[1] contains minor misunderstandings with reference to the works of the author.[2] For the most part it will suffice to refer to the originals to clear up these points. A few of them, however, may deserve a more detailed explanation.

The main point of the author's previous letter to the editor was that, in the case of pyrrole, adopting the notation of Josien and Fuson, the NH$\cdots ar$ interaction[3] may be important. Further evidence has been published elsewhere.[4] In this later work, also, an interaction of benzene and acetone molecules was shown by means of the infrared spectra, and a complicated interaction between pyrrole and acetone molecules was inferred from this.

The reference to the gradual frequency shifts of pyrrole alludes to shifts of the "unassociated" as well as the "associated" frequencies of pyrrole which ensue when the concentration of pyrrole in solution is altered and similarly in mixed solvents when the composition of the solvent is varied. Josien and Fuson present many examples of these gradual shifts.[1,5] A corresponding shift has been reported in the case of the OH frequencies of borneol and isoborneol in acetone-hexane mixtures.[6] After re-examining his own records in the fundamental region as well as in the third and second overtone regions, the author believes that these gradual shifts remain in the case of pyrrole even after the effect caused by the overlapping of the respective absorption bands has been accounted for.

There are criteria for the hydrogen bonding not related to the molecular spectra. In this connection we shall consider those concerned with the dielectric constants and dipole moments. If, in accordance with Pauling,[7] the dipole moments are plotted against the dielectric constants of the liquids, pyrrole with the dipole moment 1.8 Debye units[8] and the dielectric constant 8.0 at 25°C[9] will be found to fall into the class of nonhydrogen-bonded liquids. The empirical criterion of Kumler[10] yields the same result. For pyrrole, the Kumler function is 16 percent less than for a nonhydrogen-bonded liquid of dipole moment equal to that of pyrrole. The Onsager formula[11] for spherical molecules with the dipole in the center gives the dipole moment 1.56 Debye units in the case of pyrrole, i.e., somewhat smaller than the measured value. These last two criteria, although not convincing,[12] speak in favor of a tendency towards a dimeric head-to-head association in the case of pyrrole rather than in favor of the NH$\cdots$N bonding.

[1] M. L. Josien and N. Fuson, J. Chem. Phys. **22**, 1169 (1954).
[2] P. Tumoikoski, Suomen Kemistilehti **B23**, 44 (1950); J. Chem. Phys. **20**, 1054 (1952).
[3] The OH$\cdots ar$ interaction was first invented by R. Freymann, Compt. rend. **193**, 928 (1931); Ann. phys. (10) **20**, 242 (1933).
[4] P. Tumoikoski, J. Phys. **15**, 318 (1954). Unfortunately, this paper contains typographical errors which the intelligent reader will be able to spot.
[5] Fuson, Josien, Powell, and Utterback, J. Chem. Phys. **20**, 145 (1952).
[6] Tuomikoski, Pulkkinen, Hirsjärvi, and Toivonen, Suomen Kemistilehti **B23**, 53 (1950).
[7] L. Pauling, *The Nature of the Chemical Bond* (Oxford University Press, London, 1948), p. 293.
[8] Buckingham, Harris, and Le Fèvre, J. Chem. Soc. **1953**, 1626.
[9] Newly determined by us in Helsinki.
[10] W. D. Kumler, J. Am. Chem. Soc. **57**, 600 (1935).
[11] L. Onsager, J. Am. Chem. Soc. **58**, 1486 (1936).
[12] Compare, e.g., Fig. 2 in Kumler's paper.

Thermodynamic Temperature Scale below 90°K, the Normal Boiling Point of Normal Hydrogen*

G. W. Moessen, J. G. Aston, and R. G. Ascah
College of Chemistry and Physics, The Pennsylvania State University, State College, Pennsylvania
(Received September 13, 1954)

PREVIOUSLY[1] we have reported a new value for the oxygen boiling point. The method and accuracy of our gas thermometry between 10°K and 90°K was also mentioned at the same time.[1] It will be a few months before complete values will be available for our scale below 90°K (at ice point pressures of 1.0 m, 1.8 m, and 2.7 m). However, well spaced points between 10°K and 50°K, with a demonstration of the adequacy of the virial coefficients by a comparison of the results at 20°K at the three ice point pressures have been completely calculated. Since one of the platinum thermometers compared with our gas thermometer was a N.B.S. secondary standard, a comparison with the scale of the National Bureau of Standards is possible. As far as we are aware this is the first time agreement has been established between two independent scales below 90°K within the claimed accuracy. The extraordinary agreement and the fact that we can report a new value for the normal boiling point of normal hydrogen which also allows comparison with the Leiden scale prompts us to make available our results to date.

Table I reports the difference between our scale and that of the N.B.S.[2] The difference between our value and the value actually reported by the N.B.S. for a scale, which was believed to correspond to our chosen ice point temperature of 273.16°K, is given in column 3. However, they actually used the oxygen normal boiling point as their reference point and assigned to it the value of 90.19°K. If we accept our new value of 90.154°K for the normal boiling point of oxygen, the N.B.S. scale actually

Table I. Comparison of Penn State and N.B.S. Thermodynamic temperature scales below 90°K. March and April, 1951.

T	Ice point pressure	Δ_1 (N.B.S.$_{orig}$ − PSC)	Δ_2 (N.B.S.$_{corr}$ − PSC)
10.5	2.7	$+0.058_9 \pm 0.01$	$+0.054_8$
15.0	1.8	$+0.017_1$	$+0.011_0$
20.3	1.0	$+0.025_4$	$+0.017_3$
20.3	1.8	$+0.026_0$	$+0.017_9$
20.3	2.7	$+0.020_6$	$+0.012_5$
25.0	1.8	$+0.023_0$	$+0.012_9$
33.0	2.7	$+0.027_6$	$+0.014_3$
40.0	2.7	$+0.022_0$	$+0.005_9$
49.7	1.0	$+0.017_8$	-0.002_2

TABLE II. Temperatures corresponding to the normal boiling point of normal hydrogen on the new Penn State thermodynamic scale. Deduced from Eq. 1; 0°C = 273.16°K. March 30, 1952.

Pressure mm	Pt-G8 T°K	Pt-G12 T°K	Average T°K
735.283	20.266	20.367	20.367
748.371	20.364	20.364	20.364
773.979	20.364	20.365	20.365
Average	20.365	20.365	20.365
Interpolated	20.364	20.365	20.365

corresponds to an ice point temperature of 273.27°K. In column 4 the difference between our value and the value on the N.B.S. Scale corrected to our normal boiling point of oxygen is given. Inasmuch as Hoge and Brickwedde had only a sensitivity of about 0.015° in reading their pressures, the agreement is excellent.

Table II tabulates our values for the normal boiling point of normal hydrogen, obtained by introduction of liquid normal hydrogen directly into the gas thermometer, from readings of platinum thermometers Pt-G8 and Pt-G12 which were never removed from the original assembly. The results were corrected for *ortho-para* conversion using the data of Keesom, Bijl, and Van der Horst.[3] Correction to 760 mm was made using the equation,[3]

$$\theta = -252.754 + 0.00441(p-760) - 5.0\times10^{-6}(p-760)^2. \quad (1)$$

Columns 2 and 3 give the normal boiling points computed from the resistance of Pt-G8 and Pt-G12, respectively, and corrected to 760 mm using Eq. 1. The average for each of the thermometers is compared with a value given below which was obtained by interpolating the observed equilibrium temperatures on each thermometer to 760 mm pressure.

Table III summarizes values for the normal boiling point of normal hydrogen.

The average of all values (corrected to $T_0 = 273.16$°K) not including our own since 1913 is 20.378°K. The average of all values not including our own since 1930 is 20.379°K. The average of our two values obtained by linear interpolation (using the form log p *versus* $1/T$) is 20.365°±0.005°K. If we exclude the N.B.S. value because of the lower sensitivity but include our value, the average since 1930 is 20.374°K. It is of interest to note that if the N.B.S. value for the normal boiling point of normal hydrogen is placed on our new scale (as determined from intercomparison of the N.B.S. platinum thermometer with our gas thermometry measurements) the agreement with our recent value for this fixed point is nearly exact. It is recommended that, until our own value of 20.365°K be confirmed, that 20.37±0.01°K be used as the normal boiling point of normal hydrogen in view of the high values measured between 1917 and 1924 both at Leiden and at the Reichsanstalt. It would seem that no value as high as 20.39°K is admissable.

TABLE III. Various values reported for the normal boiling point of normal hydrogen.

Date	Investigators	Temp reported	T_0 used	Temp, °K corrected to $T_0 = 273.160$°K
1913	Onnes and Keesom[a]	20.35°K	273.09°	20.36°
1914	(PTR) Henning[b]	−252.79°C	273.10°	20.31°
1917	Cath and Onnes[c]	20.39°K	273.09°	20.40°
1922	Martinez and Onnes[d]	20.35_2°K	273.09°	20.35_7°
1924	Henning and Heuse[e]	-252.78_9°C	273.20°	20.41_4°
1927	Henning[f]	20.43°K	273.20°	20.43°
1931	Heuse and Otto[g]	−252.780°C	273.16°	20.380°
1931	Keesom, Bijl and Van der Horst[h]	−252.754°C	273.13	20.376°
1939	Hoge and Brickwedde[i]	20.39°K	273.16	20.38°[j]
1952	This research	20.365°K	273.16	20.365°

[a] H. K. Onnes and W. H. Keesom, Leiden Commun. No. 137d (1913) and later recomputed by P. G. Cath and H. K. Onnes, Leiden Commun. No. 152a (1917).
[b] Physickalisch-technische Reichsanstalt, Z. Instrumentenk. 35, 174 (1915).
[c] P. G. Cath and H. K. Onnes, Leiden Commun. No. 152a (1917).
[d] J. P. Martinez and H. K. Onnes, Leiden Commun. No. 156b (1922).
[e] F. Henning and W. Heuse, Z. Physik 23, 105 (1924).
[f] F. Henning, Z. Physik 40, 775 (1927).
[g] W. Heuse and J. Otto, Ann. Physik 9, 486 (1931).
[h] See reference 3.
[i] See reference 2.
[j] Corrected to oxygen point of 90.154°K as explained in text.

* This research was carried out under Contract N6 ONR-269 (T.O. III and X) of the Office of Naval Research.
[1] J. G. Aston and G. W. Moessen, J. Chem. Phys. 21, 948 (1953).
[2] H. G. Hoge and Ferdinand G. Brickwedde, J. Research Natl. Bur. Standards 22, 351 (1939).
[3] Keesom, Bijl, and Van der Horst, Leiden Commun. No. 217a (1931).

Force Constants of the Halides of the III and IV Group Elements

SHASHANKA SHEKHAR MITRA
Department of Physics, Allahabad University, Allahabad, India
(Received September 27, 1954)

WALSH[1] has shown that when the force constants of diatomic molecules formed between a group IV element and a group VI element are plotted against the force constants of the molecules formed between the same group IV element and the group VII element of atomic number greater by unity than that of the group VI element, a straight line passing through the origin is obtained for all the elements of the group IV. This rule has been used by Varshni[2] for the prediction of force constants of certain molecules hitherto uninvestigated experimentally. Also a straight line passing through the origin is obtained[3] by plotting the force constants of II period hydrides against those of the III period hydrides. Similarly, it has been found that the ratio of the force constant of a halide of a group IV element to that of the same halide of a group III element of atomic number less by unity, is a constant.

TABLE I. Ratio of force constant of the halides of III and IV group elements.

Molecule AX	$ke\times10^{-5}$ (dyne/cm)	Molecule BX	$ke\times10^{-5}$ (dyne/cm)	C	C(mean)
Al F	4.356	Si F	4.894	1.123	
Ga F	3.410	Ge F	3.925	1.151	1.152
In F	2.740	Sn F	3.277	1.195	
Tl F	2.310	Pb F	2.636	1.141	
B Cl	3.473	C Cl	3.767	1.084	
Al Cl	2.077	Si Cl	2.612	1.257	
Ga Cl	1.821	Ge Cl	2.322	1.276	1.196
In Cl	1.592	Sn Cl	1.976	1.242	
Tl Cl	1.454	Pb Cl	1.626	1.119	
Al Br	1.692	Si Br	2.214	1.308	
Ga Br	1.517	Ge Br	1.972	1.300	1.256
In Br	1.366	Sn Br	1.726	1.263	
Tl Br	1.259	Pb Br	1.450	1.152	

If $k(AX)$ represent the force constant of a halide of a group III element and $k(BX)$ that of the same halide of the group IV element of atomic number greater by one than that of A, it is observed that

$$k(BX)/k(AX) = C. \quad (1)$$

The validity of Eq. (1) is shown by the constancy of C, which slightly varies with the halogens.

Sufficient data for the iodides were not available. The only available data being those of Pb I and Tl I. The ωe value of the latter molecule is doubtful because of broad fluctuations in absorption and two widely different values have been given,[4] so it has not been used in Table I.

The force constant ke has been calculated from the formula $ke = 4\pi^2\mu c^2\omega e^2 5.8883\times10^{-2}\omega e^2$ dyne/cm, symbols having their usual meanings. The data for ωe and μ save those of the molecules Ga F and In F have been taken from the standard source.[5] Welti and Barrow[6] have given the required data for these two molecules.

The constant C is a linear function of the period number (n) of the halogens. C is given by (see Table II)

$$C=1.043+0.052n. \quad (2)$$

C for the iodides has been predicted from Eq. (2).

The ratio C may be used for predicting the force constant of one molecule if that of the other corresponding molecule is known. Some predicted values of force constants (marked with asterisk) are recorded in Table III. For the iodides the calculated value of C has been used.

The spectrum of C F has been investigated by Andrews and Barrow,[7] and its force constant from the experimental value of ωe is 7.41×10^5 dynes/cm which seems to be somewhat doubtful because force constants of BX molecules are always greater than those of AX molecules, whereas it is not so in the present case. Moreover, when we apply Walsh's rule, we have ke(CS)/ke(CCl) $=2.25$, and with the experimental value of ke(CF) we have

TABLE II. Observed and calculated values of C.

N	X	C calc.	C obs.
2	F	1.147	1.152
3	Cl	1.199	1.196
4	Br	1.251	1.256
5	I	1.303	···

ke(CO)/ke(CF) 2.57. The ratios are far from being equal, but with the predicted value of the latter the ratio is nearly 2.1 and is nearer to the former one.

TABLE III.

Molecule AX	$ke\times10^{-5}$ (dyne/cm)	Molecule BX	$ke\times10^{-5}$ (dyne/cm)
B F	8.044	C F	9.268*
B Br	2.666	C Br	3.349*
Al I	1.310	Si I	1.707*
Ga I	1.232	Ge I	1.605*
In I	1.114	Sn I	1.451*

The author is grateful to Dr. K. Majumdar for his guidance. He also thanks Dr. D. Sharma and Mr. Y. P. Varshni for their interest in the investigation.

[1] A. D. Walsh, Proc. Roy. Soc. (London) **207A**, 13 (1951).
[2] Y. P. Varshni, Current Sci. (India) **22**, 199 (1953).
[3] S. S. Mitra, J. Chem. Phys. **22**, 564 (1954).
[4] K. Butkow and A. Terenin, Z. Physik **49**, 865 (1928); K. Butkow, *ibid.* **58**, 232 (1929); P. T. Rao and K. R. Rao, Indian J. Phys. **23**, 185 (1949).
[5] Herzberg, *Molecular Spectra and Molecular Structure* (1951), Vol. I.
[6] D. Welti and R. F. Barrow, Proc. Phys. Soc. (London) **65A**, 629 (1952); Barrow, Jacquest, and Thompson, *Ibid.* **67A**, 528 (1954).
[7] E. B. Andrews and R. F. Barrow, Nature **165**, 850 (1950) and Proc. Phys. Soc. **64**, 481 (1951).

Note on the Branching Condition in the One-Dimensional Free Electron Gas Model

HANS KUHN
Physikal Chem. Institut der Universität Marburg, Marbacherweg 15, Marburg/L, Germany
(Received August 23, 1954)

IT has recently been shown[1] that the branching condition in the free electron gas model,

$$\left(\frac{d\psi_{s_1}}{ds_1}+\frac{d\psi_{s_2}}{ds_2}+\frac{d\psi_{s_3}}{ds_3}\right)_P=0, \quad (P=\text{branching point}) \quad (1)$$

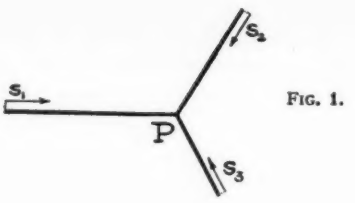

FIG. 1.

given in 1949[2] has to be exchanged for a new condition,

$$\left(\frac{d\psi_{s_1}}{ds_1}+\frac{d\psi_{s_2}}{ds_2}+\frac{d\psi_{s_3}}{ds_3}\right)_P=K\psi_P, \quad (2)$$

if the treatment is refined. $\psi_{s_1}, \psi_{s_2}, \psi_{s_3}$ is the one-dimensional wave function in the region of s_1, s_2, s_3 (see Fig. 1), respectively. Constant K approximately equals $1/l$, l being the CC-bond distance. Condition (1) has been interpreted by several authors[3] as the conservation of current. As may easily be demonstrated, (1) is indeed a sufficient condition of conservation of current, but (2) is the necessary and sufficient condition:

The probability current is zero in the case of each time independent real wave function $\psi_a, \psi_b, \cdots$, and we have thus to consider the time dependent wave function Ψ for the proof intended. For simplicity let us consider the function

$$\Psi=a\psi_a \exp[(2\pi i/h)E_a t]+b\psi_b \exp[(2\pi i/h)E_b t] \quad (3)$$

(E_a, E_b are Energies corresponding to ψ_a, ψ_b respectively; a, b are constants restricted by the normalization condition of (3); h is Planck's constant; $i=\sqrt{-1}$; $t=$time). The probability current S_1 in the region of coordinate s_1 is given by a general quantum mechanical equation:

$$S_1=\frac{h}{4\pi im}\left(\Psi_{s_1}{}^*\frac{d\Psi_{s_1}}{ds_1}-\Psi_{s_1}\frac{d\Psi_{s_1}{}^*}{ds_1}\right) \quad (4)$$

(Ψ^* conjugate complex of Ψ; m electronic mass). If (3) is introduced in (4) the expression

$$S_1=\left(\psi_{a,s_1}\frac{d\psi_{b,s_1}}{ds_1}-\psi_{b,s_1}\frac{d\psi_{a,s_1}}{ds_1}\right)C$$

results where

$$C=\frac{hab}{4\pi im}\left(\exp\left[-\frac{2\pi i}{h}(E_a-E_b)t\right]-\exp\left[\frac{2\pi i}{h}(E_a-E_b)t\right]\right).$$

Corresponding expressions are found for S_2 and S_3. In the branching point P the sum $S_1+S_2+S_3$ equals zero by the condition of conservation of current, and therefore

$$\left(\psi_{a,s_1}\frac{d\psi_{b,s_1}}{ds_1}-\psi_{b,s_1}\frac{d\psi_{a,s_1}}{ds_1}+\psi_{a,s_2}\frac{d\psi_{b,s_2}}{ds_2}-\psi_{b,s_2}\frac{d\psi_{a,s_2}}{ds_2}+\psi_{a,s_3}\frac{d\psi_{b,s_3}}{ds_3}-\psi_{b,s_3}\frac{d\psi_{a,s_3}}{ds_3}\right)_P C=0.$$

By continuity condition $\psi_{a,s_1}=\psi_{a,s_2}=\psi_{a,s_3}=\psi_{a,P}$ and $\psi_{b,s_1}=\psi_{b,s_2}=\psi_{b,s_3}=\psi_{b,P}$ in the branching point, and therefore

$$\psi_{a,P}\left(\frac{d\psi_{b,s_1}}{ds_1}+\frac{d\psi_{b,s_2}}{ds_2}+\frac{d\psi_{b,s_3}}{ds_3}\right)_P-\psi_{b,P}\left(\frac{d\psi_{a,s_1}}{ds_1}+\frac{d\psi_{a,s_2}}{ds_2}+\frac{d\psi_{a,s_3}}{ds_3}\right)_P=0,$$

if $E_a\neq E_b$ and thus $C\neq0$. By rewriting this expression it is seen that

$$\left(\frac{d\psi_{b,s_1}}{ds_1}+\frac{d\psi_{b,s_2}}{ds_2}+\frac{d\psi_{b,s_3}}{ds_3}\right)_P\frac{1}{\psi_{b,P}}=\left(\frac{d\psi_{a,s_1}}{ds_1}+\frac{d\psi_{a,s_2}}{ds_2}+\frac{d\psi_{a,s_3}}{ds_3}\right)_P\frac{1}{\psi_{a,P}} \quad (5)$$

equals a constant K. The left-hand side of Eq. (5) contains only ψ_b, the right-hand side only ψ_a. This relation holds for each pair of eigenfunctions, and thus K is a constant characteristic for the whole set of eigenfunctions. Equation (2) thus follows immediately from (5).

It is seen, that each step of the above consideration remains unchanged if applied to any branching point of a network of any

complicated structure, and it is immediately found that in this case the expression

$$\sum_k \left(\frac{d\psi_{sk}}{ds_k}\right)_P = K_P \psi_P$$

is the necessary and sufficient condition of conservation of current at a branching point P considered. The sum extends upon all branches k which meet at that joint. These considerations on conservation of current do not lead to any restrictions upon K_P (for each branching point of the network a different K_P value may be chosen). However, from considerations concerning the spatial extension of the electronic cloud, one finds[1] $K \simeq 1/l$, as mentioned previously, if three branches meet at a joint, and K_P is about twice as large if four branches meet.

[1] H. Kuhn, Z. Elektrochem. **58**, 219 (1954). For applications of the new branching condition see Kuhn, Huber, Dehnert, Knaak, and Haas, Industrie Chimique Belge, special Issue Congrès International de Chimie Industrielle, Bruxelles (1954) in print.
[2] H. Kuhn, Helv. Chim. Acta **32**, 2247 (1949).
[3] See, for example, C. A. Coulson, Proc. Phys. Soc. (London) **A67**, 608 (1954).

Erratum: Separation and Concentration of Proteins in a *p*H Field Combined with an Electric Field

[J. Chem. Phys. **22**, 1628 (1954)]
ALEXANDER KOLIN
University of Chicago, Chicago, Illinois

FIGURE 3 on page 1629 has been inverted. Rotation of the photograph through 180° establishes agreement with the legend.

Erratum: High-Temperature Equation of State by a Perturbation Method. I. Nonpolar Gases

[J. Chem. Phys. **22**, 1420 (1954)]
ROBERT W. ZWANZIG
Sterling Chemistry Laboratory, Yale University, New Haven, Connecticut

THE lower limit of integration in the integrals of Eqs. (41) and (43) should be zero and not Ox^2. The x^2 belongs in the integrands of these integrals.

CONTENTS—*Continued*

Letters to the Editor:

Note on Solutions of Linear Polyelectrolyte Molecules . Fumio Oosawa and Nobuhisa Imai 2084

Spectroscopic Evidence for Stabilized HO_2 Radicals . . . . . Paul A. Giguère 2085

Resonance Energy of Graphite . . . . . G. S. Colladay 2085

Multilayer Adsorption of Water Near Saturation Pressure on Plane Glass Surfaces . . . . . U. Garbatski and M. Folman 2086

Paramagnetic Resonance Absorption of Violanthrone and Violanthrene . . . . . Y. Yokozawa and I. Tatsuzaki 2087

Exchange Potential in the Statistical Model of Atoms . C. J. Nisteruk and H. J. Juretschke 2087

Different Ice Forms under Ordinary Conditions . . . . R. M. Vanderberg and J. W. Ellis 2088

Formation of Negative Ions in Hydrocarbon Gases . . . . . T. L. Bailey, J. M. McGuire, and E. E. Muschlitz, Jr. 2088

Heats of Combustion and Formation of Some Alcohols, Phenols, and Ketones . . . . . George S. Parks, Kenneth E. Manchester, and Leland M. Vaughan 2089

Initiation Processes in the Autoxidation of Fatty Acid Esters and Allied Substances . . . . . N. A. Khan 2090

Reply to Khan's Letter, "Initiation Processes in the Autoxidation of Fatty Acid Esters and Allied Substances" . . . . . L. Bateman 2090

Electronic Absorption Spectra of the Dimethylpolyenes . . . . P. Nayler and M. C. Whiting 2091

Elastic Constants of AgBr at 28°C . . . . . D. S. Tannhauser and A. W. Lawson 2092

Heat of Formation of CF_3 and Some Bond Dissociation Energies for Fluorocarbons . . . . . B. S. Rabinovitch and J. F. Reed 2092

Discrepancy in the Rotational Constants of Bromoform . . . . . Gabriel Herrmann 2093

On the Interpretation of the Spectrum of Bromoform . . Shoji Kojima and Kineo Tsukada 2093

$J=0\rightarrow1$ Rotational Transition of Trifluoroiodomethane . . . . . Fred Sterzer 2094

Approximate Analytic Solution of the Thomas-Fermi Equation for Atoms . . . . . T. Tietz 2094

Decomposition of Methane in Low-Pressure Glow Discharge . . . . . Milton Burton and J. P. Manion 2095

"Threshold Potential" of the ac Electrodeless Discharge . . . . . S. R. Mohanty 2095

Infrared Spectrum and Hydrogen Bonding of Pyrrole . . . . . P. Tuomikoski 2096

Thermodynamic Temperature Scale below 90°K, the Normal Boiling Point of Normal Hydrogen . . . . . G. W. Moessen, J. G. Aston, and R. G. Ascah 2096

Force Constants of the Halides of the III and IV Group Elements . . . . . Shashanka Shekhar Mitra 2097

Note on the Branching Condition in the One-Dimensional Free Electron Gas Model . . . . . Hans Kuhn 2098

Erratum: Separation and Concentration of Proteins in a *p*H Field Combined with an Electric Field . . . . . Alexander Kolin 2099

Erratum: High-Temperature Equation of State by a Perturbation Method. I. Nonpolar Gases . . . . . Robert W. Zwanzig 2099

Author Index to Volume 22 2099

Analytic Subject Index to Volume 22 2115

CONTENTS

JOURNAL OF CHEMICAL PHYSICS VOL. 22, NO. 12 DECEMBER, 1954

Force Constants for F_2CO and Thermodynamic Properties for F_2CO and FClCO . . . . . R. J. Lovell, C. V. Stephenson, and E. A. Jones 1953

Sedimentation Potential and Velocity of Solid Spherical Particles . . . . . F. Booth 1956

Statistical Interpretations of Unimolecular Reaction Rates . . Harold S. Johnston and James R. White 1969

Hybridization and Ionic Character in CH_3Cl . . . . . Paul N. Schatz 1974

Studies on a Group of Silicon Carbide Structures . . . . . Richard S. Mitchell 1977

Vibrational Spectra of $CF_2{=}CHD$ and $CF_2{=}CD_2$ . . . . . Walter F. Edgell and Casper J. Ultee 1983

Effect of Intermolecular Interactions between CH Frequencies on the Infrared Spectra of *N*-Paraffins and Polythene . . . . . R. S. Stein and G. B. B. M. Sutherland 1993

Vibrational Spectrum and Structure of Nitryl Chloride . . . . . Raymond Ryason and M. Kent Wilson 2000

Nuclear Magnetic Resonance in Liquids under High Pressure . . . . G. B. Benedek and E. M. Purcell 2003

Microwave Determination of the Structure of Pyridine . . . . . Børge Bak, Lise Hansen, and John Rastrup-Andersen 2013

Shock-Tube Measurements of Vibrational Relaxation . . . . Edward F. Smiley and Ernst H. Winkler 2018

Nuclear Quadrupole Resonances in Bromobenzene Derivatives . . . . . T. J. Bray and R. G. Barnes 2023

Chemical Effects of (d,p), $(n,2n)$, and (γ,n) Activation of Iodine . . . . . Robert H. Schuler 2026

Infrared Spectrum and Molecular Constants of C_2D_2 . . . . . Robert M. Talley and Alvin H. Nielsen 2030

Microwave Spectrum of I,1-Difluoroethane . . . . . N. Solimene and B. P. Dailey 2042

Emission Bands of NO in the Vacuum Ultraviolet Region Excited in the NO Afterglow . Yoshio Tanaka 2045

Redetermination of the Crystal Structure of Lithium Sulfate Monohydrate $Li_2SO_4 \cdot H_2O$ . . . . . Allen C. Larson and Lindsay Helmholz 2049

High-Speed Machine Computation of Ideal Gas Thermodynamic Functions. I. Isotopic Water Molecules . . . . . Abraham S. Friedman and Lester Haar 2051

Study of Carbon Monoxide, Nitrogen, Propylene, and Benzene Ionization Probability Curves near Threshold . . . . . R. E. Fox and W. M. Hickam 2059

Magnetic Moments of Some Octahedral Complexes of Iridium . . Eric N. Sloth and Clifford S. Garner 2063

Ionization of Strong Electrolytes. III. Proton Magnetic Resonance in Nitric, Perchloric, and Hydrochloric Acids . . . . . G. C. Hood, O. Redlich, and C. A. Reilly 2067

Approximate Integral Evaluations Used in the Molecular Quantum Mechanics of Nonlinear Molecules . . . . . Roland S. Barker and Henry Eyring 2072

Double-Bond Character of Conjugated Carbon-Chlorine Bonds . . . . . R. Bersohn 2078

(continued on cover three)

LANCASTER PRESS, INC., LANCASTER, PA.